



University of
Nottingham
UK | CHINA | MALAYSIA



MONASH
University

Design and evaluation of fluorescent and non-fluorescent bivalent ligands to explore their mode of action at neuropeptide Y receptors

Rachel Roseanne Richardson, BSc (Hons).

Thesis submitted to the University of Nottingham
and Monash University for the degree of Doctor of
Philosophy

September 2018

Abstract

Recent advances in understanding G protein coupled receptor (GPCR) pharmacology include accumulating evidence that GPCRs can form homo- and hetero- meric complexes, and that these complexes may affect physiological function and ligand pharmacology. However, the continuing controversy over the significance of such complexes has arisen, in part, due to a limited availability of appropriate molecular tools and ligands that would allow for a more comprehensive investigation of oligomer pharmacology. One avenue to exploit dimer selective pharmacology has been the development of bivalent ligands. However, a number of mechanisms, not all of which involve receptor dimerization, can often explain the properties of bivalent compounds.

The four cloned members of the neuropeptide Y receptor (YR) family mediate the responses to neuropeptide Y (NPY) and related peptides, pancreatic polypeptide (PP) and peptide YY (PYY), through shared $G_{i/o}$ protein coupling pathways, and facilitate the physiological roles these peptides play in appetite regulation. The bivalent anti-parallel peptide dimer GR231118 (Ile-Glu-Pro-Dap-Tyr-Arg-Leu-Arg-Tyr-NH₂; where Glu and Dap are bound to Dap and Glu, respectively, in the corresponding peptide via lactam bridges) is a Y₁R antagonist, distinguished by a much higher affinity for the Y₁R than equivalent monomer peptides based on the NPY C-terminus, such as BVD15 (Ile-Asn-Pro-Ile-Tyr-Arg-Leu-Arg-Tyr-NH₂). This thesis explores the mode of action of GR231118-based analogues at the Y₁R and the Y₄R, by using solid phase peptide synthesis (SPPS) to produce novel peptides, high content imaging assays to monitor ligand binding and function, and fluorescence correlation spectroscopy (FCS) to probe ligand-receptor complex stoichiometry.

Chapter 3 uses SPPS to create fluorescently tagged YR peptide ligands, as well as the development of novel cyclic and alanine scan GR231118 derivatives, to help elucidate structure-activity relationships (SAR) at the Y₁R and Y₄R. Chapter 4 then examines the pharmacology of fluorescent and non-fluorescent BVD15

and GR231118 based ligands in high content imaging assays. Ligand function was investigated using bimolecular fluorescence complementation (BiFC) YR β -arrestin2 recruitment assays and ligand affinities were measured using saturation or competition binding assays based on high content imaging. The resultant SARs at the Y₁R indicated that the diaminopropionic acid cyclic moiety of GR231118 is the optimal size for high affinity and Y₁R selectivity over the Y₄R. An alanine scan of GR231118, focused on a single arm of the peptide dimer, demonstrated that the second [Tyr⁵] residue in the peptide contributed significantly (10 fold) to the high Y₁R affinity of GR231118. This decrease in affinity, from [Tyr⁵] to [Ala⁵] substitution, was not observed at the Y₄R, revealing a Y₁R selective interaction.

In Chapter 5, FCS in combination with photon counting histogram (PCH) analysis investigated fluorescent ligand binding to the Y₁R and its impact on receptor oligomerisation. FCS and PCH are subcellular resolution imaging and analysis techniques that allow the concentration, diffusion co-efficient and molecular brightness of fluorescently tagged species to be measured within the defined confocal volume (~0.3 fL). Using these methods, the interactions of Cy5-labelled GR231118 dimer and BVD15 monomeric derivatives with the Y₁R were successfully quantified via the determination of slowed ligand diffusion upon binding to the larger receptor protein complexes in living cells. Molecular brightness PCH analysis provided evidence for Y₁R oligomerisation following treatment with both labelled and unlabelled GR231118 dimer, but not labelled BVD15 monomeric analogues.

In conclusion, the high Y₁R binding affinity of the bivalent ligand GR231118, in part, derives from an extended contact interface with the Y₁R binding site, involving residues in the second arm of the peptide dimer. However, these high affinity dimeric peptides are also capable of promoting Y₁R oligomerisation in living cells. Novel fluorescent GR231118 and BVD15 derivatives will provide useful tools for assessing Y₁R pharmacology in whole cells using imaging based methodologies.

Acknowledgements

Firstly, I would like to express my most sincere and heartfelt gratitude to my supervisors; Dr Nicholas Holliday for his sense of humour and unceasing use of Scottish stereotypes around Buckfast; Professor Philip Thompson for his very Australian approach to life, with the essential Hawaiian shirts and love for chicken Parma and a pint (or two) with lunch and Dr Stephen Briddon with his endless stream of truly exceptional dad jokes. I would like to thank them individually and collectively for their endless support, guidance and patience in the completion of this thesis. I feel truly grateful for the knowledge and expertise they have been able to offer me and for the endless encouragement they have provided. I would like to offer a special thanks to Nick who has had to deal with the majority of my ups and downs throughout this process, and has always had an open door and a joke at the ready to help lift my spirits. I would also like to acknowledge the School of Life Sciences at the University of Nottingham for funding my research and thesis over the last 4 years.

Secondly, I would like to thank all the members of the Institute of Cell Signalling for their continued encouragement and support in the completion of my research. I would particularly like to acknowledge the technical staff, June McCulloch, Richard Proudman, Jackie Glenn and Marleen Groenen for keeping the lab and tissue culture running smoothly, and particularly Marleen for her contribution to my experimental workload. I would like to acknowledge the SLIM team, particularly Tim Self and Seema Rajani for microscopy training and their constant restarting of the auto-run analysis computer. I would also like to extend an extra special thank you to the Post Docs and my fellow PhD students for making my time at ICS so memorable. In particular, I would like to thank Dr Lisa Stott and Penny Ensor for making me feel welcome in the Holliday lab and showing me the ropes, and thank you to Lisa and Dr Leigh Stoddart for reassuring me in my Scottish ways. I would also like to thank Dr Laura Kilpatrick for her help in all things NPY related and for her endless encouragement

through Arnie related quotes and memes, which have proved invaluable to the thesis writing process.

I would like to thank all members of Thompson lab at the Monash Institute of Pharmaceutical Sciences. In particular, I would like to acknowledge Dr Mengjie Liu and Dr Simon Mountford for their support and training in peptide synthesis techniques, along with Mitchel Silk and Dr Joanne Sampson for their support and endless banter within the peptide lab, albeit with my questionable taste in music.

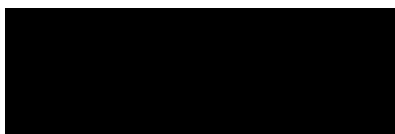
Finally, I would like to thank my family and friends for their support, particularly my mum, Sylvia Richardson, and my dad, David Richardson, who have always supported me whole-heartedly in every decision I have made and enabled me to achieve. I would like to thank my partner, Matthew Styles, for his encouragement and support; you have seen me through some very challenging times and have not faltered in your support. I would also like to thank my siblings, Jane and Steven, Jane for her ability to make me laugh at everything and for always knowing the right thing to say at the right time and Steven, for winding me up in your own special way and helping me to see the funny side of things, albeit reluctantly. I would also like to thank Jane particularly, for giving me the title of Auntie to my beautiful, chubby, dribbley, poopy niece, Isla Emily, who has provided me with endless hours of joy throughout this process.

I am not sure I have ever experienced so many highs and lows as I have during my PhD, but I do know that it has been a great adventure, and it would have been impossible without the support I have been fortunate enough to receive along the way.

“And now, Harry, let us step out into the night and pursue that flighty temptress, adventure.” - Albus Dumbledore (*Harry Potter and the Half-Blood Prince*)

Declaration

I hereby declare that this thesis, entitled “Design and evaluation of fluorescent and non-fluorescent bivalent ligands to explore their mode of action at Neuropeptide Y receptors,” is the result of my own work, which has been undertaken during my period of registration for this degree at the University of Nottingham and the Monash Institute of Pharmaceutical Sciences, under the guidance of Dr Nicholas Holliday, Professor Philip Thompson and Dr Stephen Briddon. This thesis is a presentation of my original research work, and to the best of my knowledge and belief, contains no material previously published or written by another person, except where due reference and acknowledgement has been given.



Rachel Roseanne Richardson

Student ID:



September 2018

Abbreviations

ϕ	quantum yield
1229U91	non-fluorescent dimeric Y ₁ R antagonist (amino acid sequence (IEP(Dap)YRLRY-IEP(Dap)YRLRY-CONH ₂) ₂) also known as GR231118 or 1229U91
5-HT_c	serotonin receptor
AA	amino acid
AC	adenylate cyclase
ACN	arcuate nucleus
AF	alexa fluor
AgRP	agouti and related peptides
Alloc	allyloxycarbonyl
α-MSH	α -melanocyte stimulating hormone
AOTF	acousto-optical tuneable filter
AP	alkaline phosphatase
AP-2	adaptor protein-2
aPP	avian pancreatic polypeptide
ARC	arcuate nucleus
AU	absorbance unit
β-AR	β -adrenergic receptors
BBB	blood brain barrier
BGH	bovine growth hormone
BIBO3304	Y ₁ R antagonist
BIDA81	rhodamine tagged monomeric Y ₁ R antagonist (amino acid sequence IK(RhB)PRYRLRY), also known as RhBmono
BIDA84	cyanine tagged monomeric Y ₁ R antagonist (amino acid sequence IK(Cy5)PRYRLRY), also known as Cy5mono
BIDB13	rhodamine tagged dimer Y ₁ R antagonist (amino acid sequence ((RhB)IEP(Dap)YRLRY-IEP(Dap)YRLRY-CONH ₂) ₂), also known as RhB dimer
BiFC	bimolecular fluorescence complementation
BMI	body mass index
Boc	tert-butyloxycarbonyl
BODIPY	boron-dipyrromethene
BRET	bioluminescence resonance energy transfer
BSA	bovine serum albumin
BVD15	non-fluorescent monomeric Y ₁ R antagonist (amino acid sequence INPIYRLRY) also known as BW19111U90
BW19111U90	non-fluorescent monomeric Y ₁ R antagonist (amino acid sequence INPIYRLRY) also known as BVD15
Bzl	benzyl
cAMP	cyclic adenosine monophosphate
CART	cocaine and amphetamine regulated transcript
CCK	cholecystokinin
cdNA	complementary deoxyribose nucleic acid

CFP	cyan fluorescent protein
CGPR	calcitonin gene-related peptide
CMV	cytomegavirus
CNS	central nervous system
cpm	counts per molecule
CR	concentration ratio
cryoEM	cryogenic electron microscopy
Cy5	cyanine 5 fluorophore dye
Cy5mono	Cy5 tagged monomeric Y ₁ R antagonist (amino acid sequence IK(Cy5)PRYRLRY), also known as BIDA84
Cy5dimer	Cy5 tagged dimer Y ₁ R antagonist (amino acid sequence ((Cy5)IEP(Dap)YRLRY-IEP(Dap)YRLRY-CONH ₂) ₂), also known as RR2_P037_M
Cy5dual dimer	Cy5 tagged dimer Y ₁ R antagonist (amino acid sequence ((Cy5)IEP(Dap)YRLRY-((Cy5)IEP(Dap)YRLRY-CONH ₂) ₂), also known as RR2_P037_D
CXCR	chemokine receptor
D	diffusion co-efficient
Dab	2,4-diaminobutyric acid
DAG	diacylglycerol
Dap	2,3-diaminopropionic acid
DCM	dichloromethane
ddH₂O	double distilled water
DIC	N,N-Diisopropylcarbodiimide
DIPEA	diisopropylethylamine
DMB	1,3-dimethoxybenzene
DMEM	dulbecco's modified eagles medium
DMF	dimethylformamide
DMSO	dimethyl sulphoxide
DNA	deoxyribose nucleic acid
DNP	2,4-dinitrophenol
DOTA	1,4,7,10-tetraazadodecaundecane-1,4,7,10-tetraacetic acid
DPP IV	dipeptide peptidase IV
ε	molecular brightness
ECL	extracellular loop
EDTA	ethylenediaminetetraacetic acid
EGFR	epidermal growth factor receptors
ELWD	extra-long working distance
ESCRT	endosomal sorting complexes required for transport
ESI-MS	electron spray ionisation - mass spectrometry
Et₂O	diethyl ether
ETR	endothelin receptors
FBS	foetal bovine serum
FCS	fluorescence correlation spectroscopy
Fmoc	fluorenylmethyloxycarbonyl chloride
FRET	fluorescence resonance energy transfer

GABA	γ -aminobutyric acid
GAL	galanin
GDP	guanine diphosphate
G(τ)	autocorrelation function
GFP	green fluorescent protein
GI	gastrointestinal tract
GLP-1	glucagon-like peptide 1
GPCR	G protein coupled receptor
GR231118	non-fluorescent dimeric Y ₁ R antagonist (amino acid sequence (IEP(Dap)YRLRY-IEP(Dap)YRLRY-CONH ₂) ₂) also known as 1229U91
GRAFTs	subcategory system for the GPCR superfamily
GRKs	G-protein coupled receptor kinases
GTP	guanine triphosphate
H33342	hoechst 33343 nuclear stain
HATU	1-[Bis(dimethylamino)methylene]-1H-1,2,3-triazolo[4,5-b]pyridinium 3-oxide hexafluorophosphate
HBSS	hank's balanced salt solution
HBTU	3-[Bis(dimethylamino)methyl]-3H-benzotriazol-1-oxide hexafluorophosphate
HCTU	O-(1H-6-chlorobenzotriazole-1-yl)-1,1,3,3-tetramethyluronium hexafluorophosphate
HEK293T	human embryonic kidney 293T
HEK293TR	human embryonic kidney 293T tetracycline inducible
HEL	human erythroleukaemia
HOBt	hydroxybenzotriazole
HOCT	ethyl 1-hydroxytriazole-4-carboxylate
HPLC	high performance liquid chromatography
hPP	human pancreatic polypeptide
hPYY	human peptide YY
hNPY	human neuropeptide Y
<I>	mean intensity
δI	fluctuation size
ICL	intracellular loop
IP₃	inositol trisphosphate
IQR	interquartile range
<K>	average photon counts
K_d	dissociation constant
KO	knock out
LB	luria bertani
LCMS	liquid chromatography mass spectrometry
LHA	lateral hypothalamic area
LP	laser power
LPPS	liquid phase peptide synthesis
mAChR	muscarinic acetylcholine receptors
MC	melanocortin

MCR	melanocortin receptors
MeCN	acetonitrile
MeOH	methanol
MOPs	3-(N-morpholino)propanesulfonic acid
Mr	molecular mass
mRNA	messenger ribose nucleic acid
MW	molecular weight
N	average particle number
NA	numerical aperture
NaCl	sodium chloride
NAM	negative allosteric modulator
NaOAc	sodium acetate
NaOH	sodium hydroxide
ND	not determined
NMM	N-methylmorpholine
NMR	nuclear magnetic resonance
NPY	neuropeptide Y
NTSR	neurotensin receptors
OAlI	allyl ester
Orn	ornithine
OtBu	tert-butyl ester
PAM	positive allosteric modulator
Pbf	2,2,4,6,7-pentamethyldihydrobenzofuran-5-sulfonyl
PBS	phosphate buffered saline
PCH	photon counting histogram
PCR	polymerase chain reaction
Pd(PPh₃)₄	tetrakis(triphenylphosphine)palladium(0)
PEG	polyethyleneglycol
PFA	paraformaldehyde
PhSiH₃	phenylsilane
PKA	protein kinase A
PKC	protein kinase C
pK_b	equilibrium dissociation constant
pK_d	equilibrium dissociation constant
PLC	phospholipase C
pNPY	porcine neuropeptide Y
POMC	proopiomelanocortin
PP	pancreatic polypeptide
pPP	porcine pancreatic polypeptide
PVN	paraventricular nucleus
Pyclock	6-chloro-benzotriazole-1-yloxy-tris pyrrolidinophosphonium hexafluorophosphate
pPYY	porcine peptide YY
PYY	peptide YY
R*	active receptor state
Rh6G	rhodamine 6G
RhB	rhodamine B fluorophore dye

RhBdimer	rhodamine tagged dimer Y ₁ R antagonist (amino acid sequence ((RhB)IEP(Dap)YRLRY-IEP(Dap)YRLRY-CONH ₂) ₂), also known as BIDB13
RhBmono	rhodamine tagged monomeric Y ₁ R antagonist (amino acid sequence IK(RhB)PRYRLRY), also known as BIDA81
RR2_P073_D	Cy5 tagged dimer Y ₁ R antagonist (amino acid sequence ((Cy5)IEP(Dap)YRLRY-((Cy5)IEP(Dap)YRLRY-CONH ₂) ₂), also known as Cy5 dual dimer
RR2_P073_M	Cy5 tagged dimer Y ₁ R antagonist (amino acid sequence ((Cy5)IEP(Dap)YRLRY-IEP(Dap)YRLRY-CONH ₂) ₂), also known as Cy5 dimer
Rink amide resin	4-(2,4-dimethoxyphenyl-hydroxymethyl)-phenoxyethyl-polystyrene
RP-HPLC	reverse phase - high performance liquid chromatography
rpm	revolutions per minute
R_T	retention time
RT	room temperature
S₀	electron ground state
S₁	electron relaxed singlet excitation state
S₁'	electron excited singlet excitation state
SAR	structure-activity relationship
sCy5	sulphated cyanine 5 fluorophore dye
SDS	sodium dodecyl sulphate
SEM	standard error of the mean
SME	small molecular entity
SPPS	solid phase peptide synthesis
STED	stimulated emission depletion microscopy
T75	75cm ² tissue culture flask
tBBN	truncated bombesin
tBu	tert-butyl
τD	diffusion time
TBE	tris-borate-EDTA buffer (89mM Tris-base, 89mM boric acid, 2mM EDTA; pH 7.6)
TE	tris-EDTA Buffer (10 mM Tris Base, 1 mM EDTA; pH 8)
TFA	trifluoroacetic acid
THC	tetrahydrocannabinol
TIPS	triisopropylsilane
TIRF	total internal reflection fluorescence
TM	transmembrane domain
TMP	2,4,6-Trimethylpyridine
TMR	tetramethyl-rhodamine
TNF	tumour necrosis factor
TR-FRET	time resolved-fluorescence resonance energy transfer
Trt	triphenylmethyl chloride
UR-MK299	Y ₁ R antagonist
UV	ultra violet

VEGFR	vascular endothelial growth factor receptors
VFT	venus flytrap domain
VIP	vasoactive intestinal peptide
YFP	yellow fluorescent protein
vYFP	venus yellow fluorescent protein
Y₁R	neuropeptide Y Y ₁ receptor
Y₂R	neuropeptide Y Y ₂ receptor
Y₄R	neuropeptide Y Y ₄ receptor
Y₂R	neuropeptide Y Y ₂ receptor
Y₅R	neuropeptide Y Y ₅ receptor
Yn	n-terminal fragment of venus yellow fluorescent protein
Yc	c-terminal fragment of venus yellow fluorescent protein
W₀	volume of FCS confocal volume
W₁	radius of FCS confocal volume
W₂	half height of FCS confocal volume

Table of contents

Chapter 1 – General introduction

1.1	Introduction	1
1.1.1	NPY peptide family	1
1.1.2	NPY Y receptor family	3
1.1.3	Physiological roles of the NPY family	5
1.1.4	Obesity - an unmet need for pharmacological management	6
1.1.5	The role of NPY in obesity	8
1.1.6	The role of PYY and PP in peripheral satiety	14
1.2	The GPCR superfamily	20
1.2.1	GPCR structure	20
1.2.2	GPCR ligand binding	25
1.2.3	GPCR ligand pharmacology	31
1.2.4	Y receptor ligands	36
1.2.5	GPCR activation and induction of cell signalling	39
1.2.6	GPCR life cycle	46
1.2.7	GPCR oligomerisation	51
1.2.8	Multivalent ligands	53
1.3	Aims of this thesis	56

Chapter 2 – Materials and general methods

2.1	Materials	58
2.1.1	Molecular biology materials	58
2.1.2	Cell culture materials	58
2.1.3	Cell assay materials	58
2.1.4	Peptide synthesis materials	59
2.2	Molecular biology methods	59
2.2.1	Pre-existing Y receptor and β -arrestin2 constructs	59
2.2.2	Restriction enzyme digestion	64
2.2.3	Visualisation and isolation of DNA	64
2.2.4	Alkaline phosphatase treatment and preparation of vector	65
2.2.5	Ligations	66

2.2.6	Preparation of competent cells and bacterial transformation	67
2.2.7	Miniprep isolation and purification of DNA	68
2.2.8	Maxiprep isolation and purification of DNA.....	69
2.2.9	Determination of DNA concentration and purity.....	70
2.3	Cell culture.....	73
2.3.1	Cell line maintenance	73
2.3.2	Cryogenic storage of cells	74
2.3.3	Experimental plating of cells	74
2.4	Fluorescence based pharmacological assays	75
2.4.1	Automated plate reader assays.....	76
2.4.2	Fluorescent correlation spectroscopy (FCS)	81
2.5	Solid and liquid phase peptide synthesis experimental	85
2.5.1	General methods A - preparation of linear peptides	85
2.5.2	General methods B - peptide cleavage conditions.....	86
2.5.3	General methods C – solution phase amide bond formation conditions	87
2.5.4	Reverse phase high performance liquid chromatography (RP-HPLC).	87
2.5.5	Liquid chromatography mass spectrometry (LCMS)	88
2.6	Data analysis.....	90
2.6.1	Automated plate reader analysis	90
2.6.2	Fluorescence correlation spectroscopy (FCS).....	95
2.6.3	Solid and solution phase peptide synthesis	105
Chapter 3 – Synthesis of peptide analogues of the neuropeptide Y Y₁ receptor antagonists, BVD15 and GR231118		
3.1	Introduction.....	107
3.1.1	Peptides as leads in chemical biology	107
3.2	Chemical synthesis of peptides	109
3.2.1	Solid phase peptide synthesis (SPPS)	109
3.2.2	Y ₁ R ligands.....	119
3.2.3	BVD15 monomer peptide as a Y ₁ R antagonist	119
3.2.4	GR231118 dimer peptide as a Y ₁ R antagonist.....	121

3.3	Aims	124
3.4	Results and Discussion.....	125
3.4.1	Cyclic BVD15 monomer peptide analogue design and synthesis..	125
3.4.2	GR231118 dimer peptide analogue design and synthesis	129
3.4.3	Fluorescent GR231118 dimer peptide analogue design and synthesis	136
3.5	Conclusion	138
3.6	Experimental and peptide characterisation	139
3.6.1	Cyclic BVD15 monomer analogues	139
3.6.2	GR231118 dimer analogues.....	141
3.6.3	GR231118 dimer alanine scan analogues.....	145
3.6.4	Cyclic GR231118 dimer Cy5 conjugates	151
Chapter 4 – Structure-activity relationships of novel GR231118 analogues at the neuropeptide Y Y₁ and Y₄ receptors: influence of ring size and dimer substitution on affinity and selectivity		
4.1	Introduction	152
4.1.1	Y ₁ R / Y ₄ R ligand binding, SAR and selectivity	152
4.1.2	BVD15 monomer and GR231118 dimer peptides as Y ₄ R agonists	155
4.2	Aims	156
4.3	Results.....	157
4.3.1	Cy5mono as a Y ₁ R and Y ₄ R dual fluorescent ligand	157
4.3.2	Peptide ligands used for characterisation	162
4.3.3	Pharmacological characterisation of BVD15 cyclic monomer derivatives at Y ₁ R and Y ₄ R.....	162
4.3.4	Pharmacological characterisation of GR231118 dimer cyclic variants at Y ₁ R and Y ₄ R	167
4.3.5	Pharmacological characterisation of GR231118 alanine substitution variants at Y ₁ R and Y ₄ R	173
4.4	Discussion	181
4.4.1	Summary of key findings	181
4.4.2	Cy5mono acts as a high affinity Y ₁ R antagonist and a moderate affinity Y ₄ R agonist.....	182

4.4.3 The role of cyclic moieties in monomeric peptide ligand binding at the Y ₁ R and Y ₄ R	183
4.4.4 Increasing cycle size in GR231118 dimeric peptides selectively reduced Y ₁ R binding affinity.	184
4.4.5 The selective role of the second [Tyr ⁵] in the GR231118 dimer peptide for Y ₁ R recognition	186
4.5 Final conclusions.....	188
Chapter 5 – The use of fluorescence correlation spectroscopy to investigate ligand-receptor interactions at the neuropeptide Y Y₁ receptor	
5.1 Introduction	190
5.1.1 Fluorescent ligands as tools to investigate ligand-receptor interactions.....	190
5.1.2 Evidence of YR family oligomerisation	191
5.1.3 Ligand - receptor interactions at receptor complexes	192
5.1.4 Fluorescence correlation spectroscopy (FCS).....	194
5.1.4.1 Fundamentals of FCS	194
5.1.4.2 The study of labelled receptors and oligomeric state	197
5.1.4.3 The study of ligand-receptor interaction using fluorescent ligands	198
5.1.5 Monomeric BVD15 and dimeric GR231118 ligand pharmacology...	199
5.2 Aims	201
5.3 Results.....	202
5.3.1 Fluorescent ligand pharmacological characterisation.....	202
5.3.1.1 Saturation binding	202
5.3.1.2 Analysis of Y ₁ R β-arrestin2 recruitment	206
5.3.2 Solution FCS measurements of novel fluorescent ligands	208
5.3.2.1 Solution measurement optimisation	209
5.3.2.2 FCS solution measurements.....	211
5.3.3 Optimisation of FCS for cell measurements of SNAP-Y ₁ R diffusion for SNAP surface fluorophore AF 488 and AF 647	216
5.3.4 Receptor binding of monomeric and dimeric fluorescent ligands measured by FCS	221

5.4	Discussion	227
5.4.1	Summary of key findings	227
5.4.2	Novel fluorescent peptides act as Y ₁ R antagonists	227
5.4.3	Solution FCS indicates aggregation behaviours of RhB tagged peptides.....	228
5.4.4	FCS demonstrates NPY treatment does not affect diffusion time of Y ₁ R in HEK293 cell membranes	230
5.4.5	Measurement of fluorescent ligand binding to the Y ₁ R by FCS	234
5.4.6	Providing evidence for ligand-receptor stoichiometry, and promotion of Y ₁ R oligomers by dimer ligands.....	235
5.4.7	Final conclusions.....	237
Chapter 6 – General discussion		
6.1	General Discussion	239
Chapter 7 – References		
7.1	References	251

Chapter 1

General introduction

“I’m not in the habit of embarrassing my students, but...”

Nicholas Holliday

1.1 Introduction

1.1.1 NPY peptide family

In 1980 Peptide YY (PYY) was isolated from intestinal porcine extracts using a novel method for amidated peptide extraction (Tatemoto and Mutt, 1980, 1978). This method was then used to isolate the related peptide, Neuropeptide Y (NPY), from porcine brain extracts in 1982 (Tatemoto et al., 1982). A third member of the family, Pancreatic Polypeptide (PP), was isolated and crystallised from bovine tissue in 1983 (Hoffman and Chance, 1983).

NPY has since been found to be an abundant neurotransmitter in the central nervous system (CNS), particularly within the hypothalamic and hippocampal neurons. In addition, NPY has been shown to be expressed peripherally in areas of the body such as adipose and endocrine tissue (Brothers and Wahlestedt, 2010). NPY has been shown to be a co-transmitter in postganglionic sympathetic neurons where it is released from dense core vesicles alongside nor-adrenaline (Lundberg, 1996; Lundberg et al., 1990a). This co-release has been shown to enhance the vasoconstrictor effect of nor-adrenaline, evoking potent and long lasting vasoconstriction of blood vessels, heart, spleen and the vas deferens. NPY has also been demonstrated to co-exist in perivascular nerves suggesting a role in autonomic transmission (Lundberg et al., 1990b). As well as expression in sympathetic neurons, NPY has been demonstrated to play a role in the enteric nervous system where it has been shown to be a potent anti-secretory agent, along with PYY, via Y₁R activation and subsequent inhibition of epithelial anion secretion (Tough et al, 2006; Hyland and Cox, 2004). PYY and PP have been found to be expressed mainly within the gastrointestinal (GI) tract, with PYY released from L-cells in the mucosa of the ileum and colon, and PP released from PP cells within the islets of Langerhans in the pancreas. In addition, PYY is known to have low levels of expression in bone marrow and in lymph nodes throughout the body (Ekblad and Sundler, 2002).

Studies of this family of peptides have revealed that each member consists of a 36 amino acid chain that possess an amidated C-terminal tyrosine (Figure 1.1; Babilon and Beck-sickinger, 2013). The presence of this amidated terminal group is consistent with other biologically active peptides, where the presence of the amidated C-terminus is essential to the peptides' full biological activities (Kim and Seong, 2001). Within the NPY family of peptides there is a high level of sequence homology, with porcine NPY (pNPY) showing ~70% homology with pPYY and ~50% with pPP (Tatemoto, 1982). Human derivations also express a similar level of homology between peptide subtypes (Figure 1.1), and evolutionary studies have revealed a conserved amino acid sequence throughout many species (Blomqvist et al., 1992; Larhammar, 1996; Larhammar and Salaneck, 2004; O'Hare et al., 1988). NPY has been demonstrated to be highly conserved between mammalian species such as human, rat, rabbit and guinea pig, which only differ from that of pNPY by the presence of a methionine residue, rather than a leucine, at residue 17 (O'Hare et al., 1988). PYY is the second most conserved in the peptide family, but still demonstrates a conserved amino acid sequence in mammalian species (Larhammar, 1996; Larhammar and Salaneck, 2004). PP is the least conserved within the peptide family, it has been suggested to originate from a separate lineage to NPY and PYY, and as such, shows a more divergent amino acid sequence between mammals including humans, rats and pigs (Blomqvist et al., 1992; Charlton and Vauquelin, 2010; O'Hare et al., 1988).

In addition to the primary sequence, tertiary structure analyses of these peptides have been conducted through the use of X-ray crystallography studies (Blundell et al., 1981; Wood et al., 1977). These studies revealed that avian PP (aPP; Turkey) expressed a structural PP-fold. The PP-fold consists of two helical structures; an N-terminal polyproline α -helix between residues 1-8 and a C-terminal amphiphilic α -helix between residues 14-32. These structures are linked by a type II β -turn leading to a U-shaped tertiary structure that is stabilised by hydrophobic residue interactions.

	1	11	21	31	
hNPY	YPSKPDNPGE	DAPDEDMARY	YSALRHYINL	ITRQRY	-CONH ₂
hPYY	YPIKPEAPGE	DASPEELNRY	YASLRHYLKL	VTRQRY	-CONH ₂
hPP	APLEPVYPGD	NATPEQMAQY	AADLRRYINM	LTRPRY	-CONH ₂

Figure 1.1 - Primary amino acid structure of hNPY, hPYY and hPP, demonstrating sequence homology and conserved residues within the C-terminal tail.

Through computer simulations, NPY and PYY have been shown to possess a similar hairpin-like structure (Glover et al., 1984; MacKerell, 1991), however it has been suggested from NMR studies that PP-folds are not formed under physiological conditions and the C-termini of the peptides are flexible (Bader et al., 2001; Lerch et al., 2004, 2002). As well as the primary and tertiary structures it has also been suggested that NPY may take on a dimer secondary structure in solution (Bader et al., 2001; Cowley et al., 1992).

1.1.2 NPY Y receptor family

The physiological function of these peptides is mediated through the Y family of G protein coupled receptors (GPCRs; Section 1.2). There are currently four known functional Y receptors (YR) in humans, for which NPY, PYY and PP are the endogenous ligands. The YR family includes; Y₁R, Y₂R, Y₄R and Y₅R, all of which are Class A rhodopsin-like GPCRs linked to an inhibitory G_{i/o} protein (Section 1.2.6; Brothers and Wahlestedt, 2010; Walther et al., 2011). There is a lack of molecular evidence for a putative NPY-preferring y₃R, which may have originally been suggested on the basis of non-receptor mediated actions of the peptides (e.g. mast cell degranulation; Herzog et al., 1993; Movafagh et al., 2006). Meanwhile, a y₆R is functional in some species, such as rabbit and mice, but is a non-expressed pseudogene in humans (Gregor et al., 1996; Matsumoto et al., 1996).

1.1.2.1 Y₁ receptor

Localisation of the Y₁R has been the most extensively studied through the use of immunohistochemistry methods and mRNA detection. It is mainly

expressed in the CNS, in the cerebral cortex, thalamus and amygdala (Cabrele and Beck-Sickinger, 2000; Fetissov et al., 2004). It is also found at low expression levels in the periphery, namely in the smooth muscle of the vasculature and the heart, as well as in adipose tissue (Castan et al., 1993; Lindner et al., 2008; Wahlestedt and Hakanson, 1990). In addition, the distribution of Y₁R within the body has been shown to have overlapping and non-overlapping expression across species (Dumont et al., 1998; Fetissov et al., 2004). The Y₁R is able to bind both NPY and PYY with high affinity but shows reduced affinity for PP (Cabrele and Beck-Sickinger, 2000; Gehlert et al., 1997). The endogenous truncated peptides NPY₃₋₃₆ and PYY₃₋₃₆, produced through the action of the enzyme dipeptidyl peptidase IV (DPP-IV; Grandt et al., 1993; Kushwaha et al., 2014), also demonstrate low affinity at the Y₁R (Keire et al., 2000). The rank order of potency for the endogenous ligands at the Y₁R is PYY = NPY >> PYY₃₋₃₆ = NPY₃₋₃₆ = PP.

1.1.2.2 Y₂ receptor

The Y₂R is also expressed in a number of areas within the CNS, namely the hippocampus, hypothalamus, amygdala and the cortex (Fetissov et al., 2004; Widdowson, 1993; Wood et al., 2016). As with the Y₁R, the Y₂R has also been shown to exhibit species variation in receptor localisation within the CNS (Dumont et al., 1998; Fetissov et al., 2004). In the periphery it is mainly expressed within the GI tract but is also found within the vasculature (Gehlert, 1994). The Y₂R shows similar affinities for NPY and PYY, and a lower affinity for PP (Michel et al., 1998). The Y₂R, unlike the Y₁R, is also able to bind N-terminally truncated forms of the peptides, NPY₃₋₃₆ and PYY₃₋₃₆ with high affinity (Keire et al., 2000). The rank order of potency for the endogenous ligands at the Y₂R is PYY = PYY₃₋₃₆ = NPY = NPY₃₋₃₆ >> PP.

1.1.2.3 Y₄ receptor

Unlike the Y₁R and the Y₂R, the Y₄R is largely expressed within the periphery, found in the tissue of the colon, pancreas and intestine (Schwartz, 1983). It is also found at low expressing levels within the heart and skeletal muscle, as well

as in the hypothalamus and hippocampus of the CNS (Walther et al., 2011). The Y₄R is said to be the PP selective receptor, binding PP with high affinity and showing reduced affinity for NPY and PYY (Gehlert et al., 1997, 1996a, 1996b; Tough et al., 2006). It should also be noted that the relative binding affinities of these ligands are dependent on the radioligand used in determining these parameters i.e. [¹²⁵I]-PYY versus [¹²⁵I]-PP. For example, Lundell et al., (1995) determined that hPP affinity at the hY₄R was lower ($K_i = 14$ pM) than that determined by Eriksson et al., (1998; $K_i = 39$ pM), through the use of [¹²⁵I]-PYY and [¹²⁵I]-PP, respectively. As PP is the endogenous ligand for the Y₄R the use of [¹²⁵I]-PP is more likely to give a more realistic measure of affinity in radioligand based assays. The rank order of potency for the endogenous ligands at the Y₄R is PP > PYY ≥ NPY.

1.1.2.4 Y₅ receptor

The Y₅R, in contrast to the other YR types, is almost exclusively expressed within the hypothalamus of the CNS, with no observed peripheral expression in humans (Cox et al 2001; Gerald et al., 1996). This receptor subtype binds NPY, PYY and PP. It has been shown to be relatively non selective and therefore shows affinity for NPY₃₋₃₆ and PYY₃₋₃₆ as well as the full length derivatives (Gerald et al., 1996). The rank order of potency for the endogenous ligands at the Y₅R is NPY = NPY₃₋₃₆ = PYY = PYY₃₋₃₆ ≥ PP.

1.1.3 Physiological roles of the NPY family

The NPY family has been demonstrated to possess a wide variety of physiological roles in the body, including a role in neurological processes associated with diseases such as epilepsy, schizophrenia and mood disorders (Kovac and Walker, 2013; Stålberg et al., 2014). They have also been demonstrated to play a role in peripheral processes such as bone formation and cardiovascular regulation (Horsnell and Baldock, 2016; Zhu et al., 2016). In cardiovascular regulation NPY is released as a sympathetic co-transmitter with noradrenaline to aid in vasoconstriction (McDermott et al., 1993; Wahlestedt and Hakanson, 1990). Furthermore, it has been demonstrated to play a role in

immune responses associated with inflammation and cancers, particularly in breast cancers, where overexpression in certain tumour types leads to increased proliferation and migration of cancer cells (Medeiros et al., 2011; Tilan and Kitlinska, 2016). Additionally, the NPY family has been suggested to play a role in the detection of taste (Zhao et al., 2005), and in the development of alcoholism, where NPY signalling is suggested to suppress binge drinking behaviours via increased inhibitory signalling in the amygdala (Pleil et al., 2015). Furthermore, NPY has been demonstrated to play a major role in appetite regulation and energy homeostasis. The role of the NPY family of peptides in energy homeostasis and obesity is discussed in more detail below (Sections 1.1.5 and 1.1.6).

1.1.4 Obesity - an unmet need for pharmacological management

Energy homeostasis is the process whereby energy intake is matched to energy expenditure, over time. This process promotes stability in the amount of energy stored by the body in the form of fat. When this process is unbalanced, either weight loss or weight gain occurs. Obesity is a disease state in which the body has accumulated fat to a point at which it may begin to have a negative effect on health, and is clinically defined according to the body mass index (BMI), where a BMI of >30 is classified as obese (Bhardwaj et al., 2017). Obesity has now been recognised as a disease that is on the rise and has become a growing problem throughout the world.

In 2018 the Office for National Statistics in the UK reported that 63 % of adults were classified as overweight and 26 % of adults were classified as obese. The prevalence of obesity increased from 15 % in 1993 to 27 % in 2017, making the UK the sixth most obese country in the world. It was also reported that 1 in 5 children over the age of 10 were measured as obese (Office for National Statistics, 2018). Being obese or overweight puts individuals at higher risk of developing type II diabetes, cancer (Garg et al., 2014), heart disease (Bastien et al., 2014), and depression (Ouakinin et al., 2018). In 2014-2015 it was estimated that the NHS spent £6.1 billion on overweight and obesity related

illnesses, and cost the wider UK economy £27 billion. The cost of overweight or obesity-attributed illness to the NHS is projected to rise to £9.7 billion by 2050 with the economic cost estimated to reach £50 billion a year (Office for National Statistics, 2017).

The causes of obesity are extremely complex, encompassing biology and behaviour, along with cultural, environmental and social factors. Indeed a certain level of personal responsibility plays a crucial role in obesity. However, due to the toll of obesity on the human body, along with the economic implications, it is essential to improve our understanding of the mechanisms involved in food intake and appetite regulation.

Combating obesity presents real healthcare challenges. Social engineering along with encouraging diet and lifestyle changes have not been effective in reducing the occurrence of obesity. Intestinal surgery can also promote weight loss, with bariatric surgery shown to result in greater weight loss and remission of type II diabetes compared to non-surgical intervention. This weight loss is also shown to be sustained long term (> 5 years; Maciejewski et al, 2016; Courcoulas et al, 2017). However, bariatric surgery it is a serious undertaking posing high risks to the patient with unclear long-term complications, survival, mental health outcomes and costs (Courcoulas et al, 2017). In this context, pharmacological management of body weight with drugs would be an additional asset. There is currently only one licensed drug available on the UK market, orlistat, which has demonstrated limited efficacy and undesirable side effects (Dias et al., 2018). Orlistat works through inhibition of gastric and pancreatic lipase enzymes that are responsible for the breakdown of triglycerides into absorbable fatty acids in the GI tract. The inhibition of these hydrolysing enzymes therefore leads to excretion of unprocessed triglyceride fats (Patel, 2015). Other long term weight loss management drugs that have received FDA approval include; Lorcaserin, a serotonin 2C (5-HT_{2C}) agonist that is thought to regulate energy balance and satiety through serotonin receptors in the hypothalamus (Thomsen et al., 2008). Liraglutide, a glucagon-like

peptide-1 (GLP-1) analogue that acts as an agonist at the GLP receptor family resulting in satiety and reduced food intake (Van Bloemendaal et al., 2014). In addition, combination therapies such as naltrexone/bupropion and phentermine/topiramate have also been approved by the FDA. Naltrexone is an opioid receptor antagonist that has shown weight loss effects, and bupropion is a dopamine and nor-adrenaline reuptake inhibitor, thereby mediating anorexigenic effects via pro-opiomelanocortin (POMC) signalling (Greenway et al., 2009; Section 1.1.5). Phentermine acts as a sympathomimetic amine, increasing the concentration of noradrenaline in the CNS thereby suppressing appetite, however, the mechanism by which topiramate regulates weight is not well understood (Jordan et al., 2014). It should also be noted that all of these drugs are approved in conjunction with a reduced calorie diet and increased physical activity (Patel, 2015).

Unlicensed weight loss drugs also present high risks to people seeking pharmacological interventions to aid weight loss. Unlicensed drugs are often untested and unregulated, thereby presenting a high risk of severe side effects. Additionally, the risks of these drugs may be well known, however poor information is available, resulting in incorrect administration of the drug and severe side effects (Patel and Stanford, 2018; Yen and Ewald, 2012). One such example is 2,4-dinitrophenol (DNP). DNP is reported to cause rapid weight loss and is often acquired over the internet. However, it has also been associated to significant adverse effects due to mitochondrial uncoupling and inhibition of the oxidative phosphorylation pathway. Mitochondrial uncoupling can prove fatal and the use of this drug has been linked to such fatalities (Grundlingh et al., 2011). Therefore, as the prevalence of obesity continues to rise, it is essential that the need for drug based therapies are met, ensuring safe and effective options for therapeutics.

1.1.5 The role of NPY in obesity

It has long been established that the hypothalamus is a key area that regulates homeostasis, and the regulation of appetite is no exception. The ventromedial

hypothalamus is identified as the appetite suppressing centre and the lateral hypothalamic area (LHA) the appetite increasing area (Sohn, 2015). The arcuate nucleus (ACN) is one of the most studied structures within the hypothalamus as to its role in appetite regulation. The ACN expresses two distinct populations of neurons that have been shown to have opposite effects on appetite and feeding behaviour. These consist of the POMC neurons and the NPY/agouti-related peptide (AgRP) neurons, which have been shown to act in an anorexigenic and orexigenic fashion, respectively. Due to the position of the ACN within the ventral medial part of the hypothalamus it is ideally positioned to receive information from peripheral organs and input from multiple parts of the CNS (Sohn, 2015). Therefore, NPY/AgRP and POMC neurones are ideally positioned to integrate peripheral and central inputs, modulated via multiple neurotransmitters and hormones, to centrally control feeding behaviour (Figure 1.2).

NPY was first demonstrated to play a role in energy homeostasis in 1985 (Stanley and Leibowitz, 1985), revealing NPY's role as an orexigenic agent. Central administration of NPY to the paraventricular nucleus (PVN) of the hypothalamus in rats resulted in a dose-dependent increase in food intake, with higher doses of NPY resulting in increased levels of spontaneous feeding (Stanley and Leibowitz, 1985). Studies since have reported that abolition of NPY/AgRP neurons in adult mice resulted in rapid starvation (Gropp et al., 2005). However, this was not replicated in neonate mice, where abolition of the NPY/AgRP neurons had a minimal effect, suggesting that a network-based compensatory mechanism can develop after the ablation of NPY/AgRP neurons in neonates but does not readily occur in adults, where these neurons become essential (Luquet et al., 2005). These orexigenic results in adults were supported using opto- and pharmaco- genetic methods to stimulate these neuronal pathways resulting in increased food intake (Aponte et al., 2011; Krashes et al., 2011).

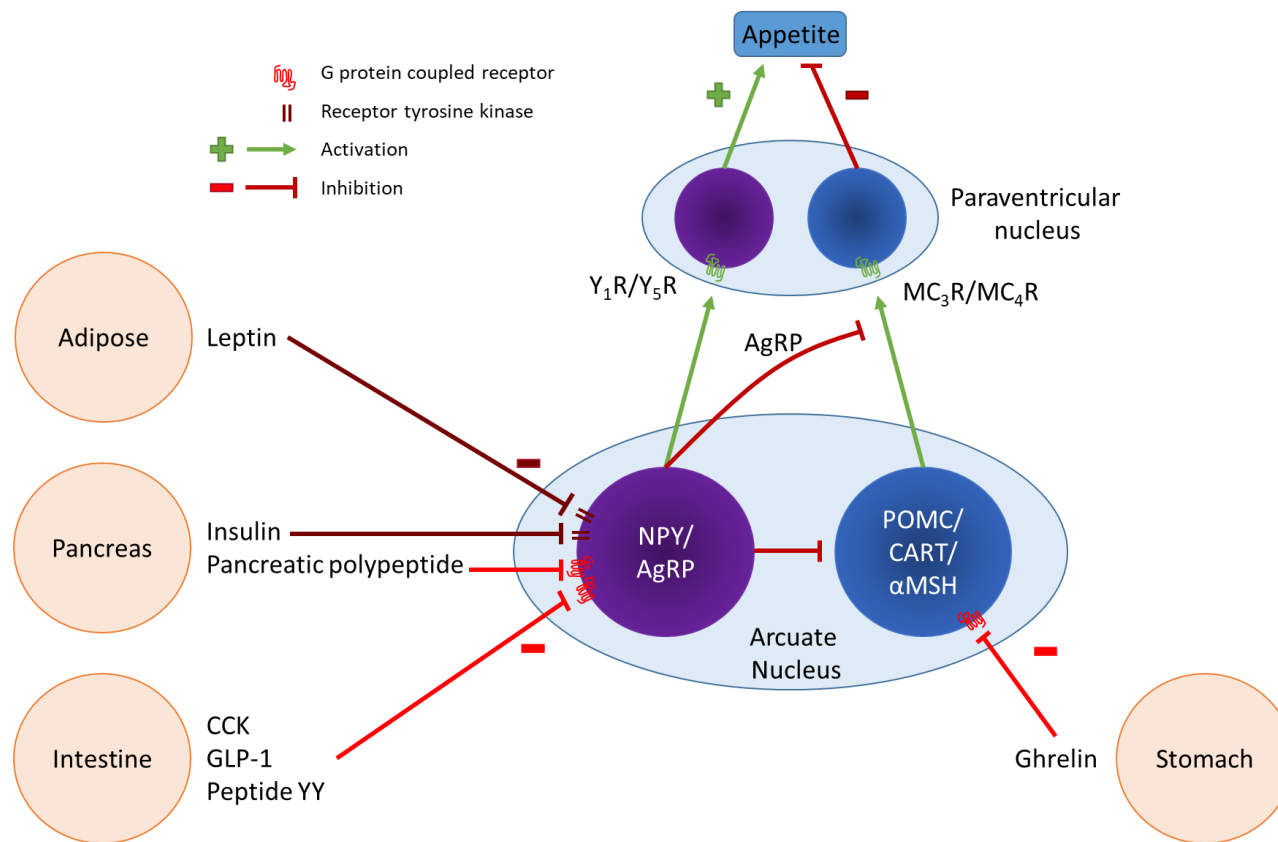


Figure 1.2 - Hypothalamic and peripheral influences on appetite signalling. NPY/AgRP neurons promote appetite via the Y_1R and Y_5R . POMC/CART neurons promote satiety via the action of peptide neurotransmitters such as α -MSH and β -MSH via the GPCRs MC_3R and MC_4R . The actions of the YRs are blocked by several peripheral satiety factors that act to inhibit NPY and promote POMC neuron signalling, where insulin and leptin act via receptor tyrosine kinases and PP, CCK, GLP-1 etc., act via GPCRs. Conversely, NPY neuron signalling is promoted through the inhibitory, GPCR mediated, action of ghrelin in POMC neurons.

As well as the regulatory role of NPY and AgRP in the mediation of this neuronal pathway, the inhibitory neurotransmitter, γ -aminobutyric acid (GABA), has also been demonstrated to be a modulator of NPY regulated signalling (Heisler and Lam, 2017). GABA is believed to mediate most of its orexigenic effects through NPY/AgRP neurons. This is supported by evidence that deletion of vascular GABA transporter genes in the AgRP neurons leads to a lean phenotype in mice (Tong et al., 2008). The role of GABA is mediated via inhibitory inputs to the anorexigenic POMC neurons within the CNS, via the NPY/AgRP neurons (Atasoy et al., 2012; Wu, 2009). As such, the NPY/AgRP neurons are well established as a major orexigenic pathway in the CNS exerting complex effects on appetite via centrally mediated signalling.

Other centrally mediated signals have also been shown to influence NPY/AgRP orexigenic signalling, including agents such as orexin and galanin (GAL; Mercer et al., 2011). The orexin family of peptides, orexin A and orexin B, exert orexigenic effects on feeding via modulation of GABAergic transmission in the hypothalamus (Kokare et al., 2006). It has been demonstrated that there is an absence of orexin induced feeding following NPY/AgRP neuron abolition in the ACN (Moreno et al., 2005), suggesting that the NPY/AgRP neurons feedback from the actions of orexins, via GABA. The galanin family of peptides, of which there are 3 members, have been shown to increase food intake via CNS signalling (Fang et al., 2011), and are believed to mediate this response through indirect activation of the NPY system, via functional interaction of GAL at the Y_1R at high doses (Parrado et al., 2007). This is supported by evidence that GAL treatment of hypothalamic neurons causes a dose dependant increase in NPY secretion, suggesting that NPY/AgRP neurons participate in a intrahypothalamic signalling pathway with galanin (Bergonzelli et al., 2001). The modulation of NPY/AgRP neurons, via these regulatory hormones, has established these signalling pathways as major orexigenic circuits within the CNS.

The anorexigenic effect of the POMC neuronal pathway is mediated through melanocortin, MC₃R and MC₄R receptors (Mountjoy, 2015; Sohn, 2015). These GPCR receptors within the POMC region of the hypothalamic PVN are activated by the release of POMC derived peptides such as cocaine and amphetamine regulated transcript (CART), adrenocorticotrophic hormone and α -melanocyte stimulating hormone (α MSH; Cone, 2015). The anorexigenic effects of the POMC pathway have been demonstrated by hyperphagia and obesity observed in POMC knock out mice (Yaswen et al., 1999). More recent studies have also employed the use of opto- and chemo- genetic stimulation methods to demonstrate that direct activation of POMC neurons leads to suppression of appetite via the release of α -MSH, which acts as an agonist at the MC₄R (Aponte et al., 2011; Zhan et al., 2013). Furthermore, it has been shown that humans expressing mutations of the MC₄R gene show hyperphagic eating behaviours and are often obese (Farooqi et al., 2003). Additionally, AgRP is a known inverse agonist of MC₄R and has been a topic of much research as it was initially considered the mode by which NPY/AgRP neurons exerted their orexigenic signalling. However the effects of NPY/AgRP neurons have been shown to be unaffected by the deletion or mutation of MC₄R (Krashes et al., 2011; Sohn, 2015). Therefore, the NPY/AgRP pathway is now considered to increase food intake independently of central MC₄R control.

Other neuronal circuits have also been demonstrated to play a role in appetite regulation via POMC and NPY/AgRP neurons, namely those involved in the reward pathways such as the 5-HT, dopamine and endocannabinoids. Some of the current and previously available drugs for weight loss are targeted to these mediators (Section 1.1.4). These brain circuits are often connected across different areas of the brain, with the hippocampus, amygdala and pre-frontal cortex all shown to be activated by food and food related cues, via the neuronal pathways associated with reward (Abdalla, 2017; Palmiter, 2007). 5-HT has been shown to express an anorexigenic effect on appetite, mediated through 5-HT_{2C} receptors expressed in POMC neurons (Berglund et al., 2013). Stimulation of these receptors increases the activity of POMC neurons through

a presumed increase of α -MSH release. Dopamine is released from neurons in the mesolimbic system and has been demonstrated to be involved in reward validation following food intake, as well as mediating emotion and pleasure (Morton et al., 2006; Nutt et al., 2015). Dopaminergic neurons have been shown, through anatomical and functional studies, to interact with the NPY/AgRP system (Decressac and Barker, 2012). More recently, it has been suggested that cerebral dopamine participates in the regulation of both NPY/AgRP and POMC mediated appetite via modulation of PI3K and NF- κ B (Hsieh et al., 2014). In this study inhibition of dopamine receptors via amphetamine resulted in an increased expression of NPY, indicating a functional role for dopamine in the suppression of NPY/AgRP signalling and appetite control. There is evidence that endocannabinoids play a role in food seeking behaviour, with studies suggesting that tetrahydrocannabinol (THC) acts via the cannabinoid 1 receptor in the hypothalamus, directly increasing appetite (Kishimoto, 2006). When mice were treated with rimonabant, an antagonist of cannabinoid receptors, they showed reduced food intake, however this drug was withdrawn from the market due to adverse effects such as the increased tendency for suicidal thoughts in patients (Di Marzo et al., 2001). It has been suggested that this response is mediated by endocannabinoids stimulating the increased production of hypothalamic orexigenic transmitters, thereby reducing the production of appetite suppressing signals (Abdalla, 2017).

This body of evidence indicates that the POMC neuronal pathway and the NPY/AgRP pathways both play a key and counteracting role in the maintenance of appetite regulation. It also demonstrates that external influences, by many different signalling pathways, are involved and aid in homeostasis of appetite, as well as highlighting the independent signalling of each system. Therefore, it is clear that NPY plays an important and complex regulatory role in hyperphagic eating behaviours, and indicates a specific and non-redundant role for NPY in orexigenic signalling in the CNS.

1.1.6 The role of PYY and PP in peripheral satiety

The promotion and inhibition of appetite is also influenced through peripheral signals, mediated by signalling peptides and hormones from four main sources; the pancreas, the GI tract, adipose tissue and the stomach, and encompass peptides and hormones such as; PP and insulin, PYY, leptin and ghrelin, respectively (Mishra et al., 2016; Figure 1.2).

PP is secreted from PP cells (also known as F cells) within the islets of Langerhans in the pancreas, along with low levels of expression in the distal gut (Neary and Batterham, 2009). Following a meal there are elevated levels of circulating PP within the blood that is sustained for roughly 30 min (Mishra et al., 2016). PP levels have been shown to remain elevated for up to 6 hours postprandially, suggesting a role in prolonged inhibition of orexigenic signalling (Adrian et al., 1976). It has been shown that the vagal nerve plays an important role in stimulating PP release, as studies have found that administration of atropine can inhibit PP release after a meal (Schwartz, 1983). This vagal parasympathetic component to the response allows PP release to start before absorption of the meal, and therefore suggests a role for PP in blood glucose homeostasis. Other factors such as exercise, gut distention and gut hormones such as CCK, ghrelin and secretin, have also been shown to play a role in PP secretion (Mishra et al., 2016). The anorexigenic effects of PP are mediated through the Y₄R, which is expressed throughout the GI tract, via the dorsal vagal complex, sending anorexigenic signals to the hypothalamic neuropeptides (Lin et al 2009; Hankir et al 2011; Section 1.1.2.3). The effects of this signalling have been demonstrated through several studies indicating that peripheral administration of PP results in reduced food intake, and overexpression of PP in mice produces a lean phenotype with reduced food intake (Mishra et al., 2016). This evidence is supported by studies that have been conducted in human subjects, where healthy volunteers demonstrated a reduction in food intake following administration of PP via injection (Batterham et al., 2003; Jesudason et al., 2007). PP has also been shown to play a role in the modulation of other peptides such as ghrelin, and in delayed

gastric emptying (Abdalla, 2017; Iwasaki et al., 2013). Therefore, PP has been shown to act as an anorexigenic regulator of appetite through suppression of food intake following a meal, and through the maintenance of blood glucose levels. In addition, it has been demonstrated that this peptide may act via central stimulation through vagal responses. The potential central signalling of this peptide is discussed in further detail towards the end of this section.

In addition to PP release, the hormone insulin is also expressed in the pancreas. Insulin is secreted from the β -cells within the islets of Langerhans after a meal and acts to maintain blood glucose homeostasis, via a co-ordinated feedback loop with glucagon (Garzilli and Itzkovitz, 2018). Insulin is released in two phases. The first phase is a rapid release following the increase of blood glucose levels minutes after food intake, and the second is a slow, sustained response that continues hours after food intake to maintain blood sugar levels (Home, 2015). It has also been shown that the level of insulin release is directly proportional to that of white adipose tissue and may reflect the important role of adiposity signalling in the hypothalamic control of energy regulation (Considine et al., 1996). Additionally, areas within the ACN that express NPY/AgRP and POMC neurons have shown a high concentration of insulin receptor expression. Deficiency of insulin has also been suggested to activate NPY/AgRP neurons (Sipols et al., 1995; Williams et al., 2010) whilst simultaneously inhibiting POMC (Hagan et al., 1999; Schwartz et al., 1997), suggesting a feedback mechanism between these signalling systems. However, the direct effects of insulin on NPY/AgRP and POMC neurons needs further clarification (Sohn, 2015; Williams et al., 2010).

Satiety factors from the GI tract include hormones such as PYY, GLP-1 and cholecystokinin (CCK; Abdalla, 2017). PYY and GLP-1 are co-released from the L-mucosal endocrine cells of the GI tract (Panaro et al., 2014), with PYY expression occurring primarily in the ileum and colon of the distal gut. A small amount of PYY expression is also found in the oesophagus, stomach and duodenum (Murphy and Bloom, 2006). There are two main forms of circulating

PYY; PYY₁₋₃₆ and PYY₃₋₃₆. The latter is produced through the cleavage of the N-terminal tyrosine-proline residues of full length PYY via the enzyme DPP-IV (Abdalla, 2017; Kushwaha et al., 2014). Through DPP-IV cleavage the predominant circulating form is PYY₃₋₃₆ (Grandt et al., 1993), and although both isoforms of PYY bind the Y₂R, PYY₃₋₃₆ shows selectivity for the Y₂R over the Y₁R (Section 1.1.2.2). PYY concentration, as with PP, increases postprandially from basal levels following a meal, with maximal levels reached 1-2 h after eating. Levels of PYY remain elevated for an extended period of time after eating, suggesting a role as a satiety factor as opposed to a feeding terminator (Chandarana et al., 2009). PYY has been demonstrated to have an anorexigenic effect on food intake mediated through the Y₂R in many systems including; rodents, humans and non-human primates, in both obese and normal models (Batterham et al., 2002; Koegler et al., 2005). It has also been shown to increase energy expenditure and delay gastric emptying (Boey et al., 2008; Talsania et al., 2005) and has been shown to be elevated during exercise and in stress (Chandarana et al., 2009). Additionally, medications such as, sitagliptin, used in the management of type II diabetes, have been developed as DPP-IV inhibitors, preventing the production of PYY₃₋₃₆. This indicates that, like PP, PYY may play a role in blood glucose homeostasis, albeit indirectly through inhibition of fat breakdown.

GLP-1 exists in pro-glucagon forms and, like PYY, is cleaved into different isoforms via convertase enzymes (Mishra et al., 2016). The main product of this cleavage produces glucagon in the pancreas and GLP-1 and GLP-2 isoforms in the intestine. GLP-1 is released following a meal and acts to promote insulin secretion, suggesting a role in satiety and blood glucose maintenance (Holst, 2004). Sitigliptin also acts to inhibit the activation of GLP-1, on the basis that GLP-1 stimulates insulin release, which is beneficial in insulin resistant diabetics. Additionally, obesity medications have included analogues of GLP-1 e.g. liraglutide (Section 1.1.4).

Leptin is a peptide hormone that is secreted by the adipose tissue. Like insulin, the levels of circulating leptin are directly correlated with the amount of body fat, with levels decreased during periods of fasting and increased after meals, thereby acting as an anorexigenic agent (Friedman, 2004; Klok et al., 2007). Leptin has been shown to cross the blood brain barrier (BBB) and exerts its anorexigenic effects directly in the hypothalamic ACN via inhibition of NPY/AgRP when leptin levels are high and activation of POMC when leptin levels are low (Williams et al., 2010), resulting in reduced food intake and increased energy expenditure (Abdalla, 2017). Leptin receptors have also been found to be expressed in NPY/AgRP and POMC neurons (Schwartz et al., 1996; Stephens et al., 1995). High levels of leptin are associated with less efficient transport across the BBB and leptin resistance (Paz-Filho et al., 2009), suggesting that leptin works via direct signalling in the brain in order to maintain adipose tissue in the body. Furthermore, leptin signalling has been suggested to be dependent on NPY signalling, as dual knockout mice models lacking leptin (i.e. -ob/-ob) and lacking NPY show reduced hyperphagia and obesity in comparison to -ob/-ob mice alone (Erickson et al., 1996), indicating that the response of leptin is synergised by NPY. It has also been demonstrated that the deletion of leptin receptors specifically expressed in POMC neurons does not increase food intake (Balthasar et al., 2004). Additionally, the reactivation of leptin receptors in the POMC neurons of leptin receptor deficient mice does not rescue hyperphagia (Berglund et al., 2012), suggesting that leptin mediated anorexigenic responses are not mediated within the POMC pathway (Scott et al., 2011).

Ghrelin is the only known orexigenic gut peptide and is released from the stomach, when empty, to promote appetite and food intake (Kojima et al., 1999; Müller et al., 2015). Ghrelin also undergoes cleavage of a precursor known as pre-pro-ghrelin following secretion, with pre-prandial levels of ghrelin shown to rise before a meal and decrease after the initiation of a meal, giving rise to the notation that ghrelin is a hunger hormone responsible for meal initiation (Abdalla, 2017). Ghrelin release occurs when fat breakdown in

adipocytes takes place and is involved in the short term regulation of food intake and long term regulation of body weight through decreased fat utilisation, thereby ghrelin is suggested to act via a feedback mechanism in response to leptin (Castañeda et al., 2010). The effects of ghrelin are mediated through growth hormone secretagogue receptor 1a, which is highly expressed within the hypothalamic ACN (Banks, 2002; Sun et al., 2004); as such ghrelin's orexigenic effects are mediated through NPY/AgRP neuronal signalling. Ghrelin is thought to have a long term effect on the regulation of body weight as obese individuals do not experience a spike in the level of ghrelin associated to the pre-prandial response in healthy individuals and levels do not drop rapidly in response to eating (Abdalla, 2017). Ghrelin has been shown to indirectly suppress POMC neurons and excite NPY/AgRP neurons via modulation of the mRNA levels of other orexigenic neuropeptides (Cowley et al., 2003; van den Pol et al., 2009). More recently, its effects have been suggested to be mediated through modulation of the endogenous cannabinoid system, specifically through hypothalamic adenosine monophosphate activated protein kinases, suggesting a role in central signalling via reward pathway stimulated appetite (Kola et al., 2008; Yang et al., 2011). In addition, the detection of ghrelin receptors on vagal afferent neurons in rats suggests that ghrelin signals from the stomach are transmitted to the brain via the vagus nerve, supporting the evidence that ghrelin has a role in mediation of central signalling (Date, 2012).

Although these signalling peptides and hormones are considered peripheral modulators of satiety, there is a large body of evidence to suggest that central and peripheral signalling pathways work in a co-ordinated fashion to regulate energy homeostasis, as alluded to above. It has been demonstrated that the Y₂R and Y₄R are expressed at low levels in the CNS, particularly in the NPY/AgRP neurons of the hypothalamic ACN (Broberger et al., 1997; Mishra et al., 2016). As such it has been suggested that PP and PYY may have a wider ranging impact on central appetite modulation, expanding the possibility of utilising these peptides as anti-obesity therapeutics (Batterham et al., 2002). It has previously been shown that peripheral i.p. injection of radiolabelled PYY₃₋₃₆ and PP can

enter the brain of rats, in low but significant quantities, in the area postrema (Dumont et al., 2007). The same study showed that i.v. injection of [¹²⁵I]PYY₃₋₃₆ and [¹²⁵I]hPP was found in the area postrema, subfornical organ, and median eminence, demonstrating that PYY₃₋₃₆ signalling could involve receptor activation out with the hypothalamus. These findings were supported by Stadlbauer et al., (2013) who found that peripheral PYY₃₋₃₆ injection in adult rats leads to reduced meal sizes. This study also found PYY₃₋₃₆ treatment resulted in an increase in the number of c-fos expressing cells (used as a measure of PYY₃₋₃₆ induced activity) in the hypothalamic ACN and PVN but not in the area postrema, contradictory to Dumont et al., (2007) but in line with the suggestion that Y₂R and Y₄R are expressed within the hypothalamus. In addition, it has been shown that PYY can cross the BBB in mice (Nonaka et al., 2003) suggesting that, in animal models at least, these peptides can cross the BBB and may induce satiation through direct action in the brain. It has been postulated that the central role of PP and PYY is mediated via YRs expressed in the ganglion of the vagus nerve (Zhang et al., 1997) via the gut-brain axis. This is demonstrated in studies where abolition of gut-brain axis pathways in rats, via vagotomy, results in a decrease of c-fos positive neurones in PYY₃₋₃₆ treated rats compared to non-vagotomised rats (Abbott et al., 2005). Furthermore, studies have demonstrated that, after delivery of PYY in fasting humans, the subjects' evaluation of food was altered, suggesting that the reward pathways role in food recognition is integrated with PYY signalling (Skibicka and Dickson, 2013). This is supported by a study conducted by Batterham et al., (2007) which demonstrated that high levels of PYY resulted in observed changes in neuronal activity within the caudolateral orbitalfrontal cortex, which is an area of the brain that predicts feeding behaviour independently of meal related sensory experiences. This study also found that low levels of PYY hypothalamic activation occurred, predicting food intake. These studies give insights into neural networks in humans that respond to a specific satiety signal in order to regulate food intake. Increased understanding of how these signals function, along with the culmination of this information provide strong evidence for the central role of PP and PYY, thereby reinforcing the possibility of utilising these

peptides as anti-obesity therapeutic targets and potentially leading to more targeted development of therapies in obesity treatment.

1.2 The GPCR superfamily

The Y receptor family are GPCRs and, as such, are members of the largest, most versatile and ubiquitous family of membrane bound receptors in the human body (Lefkowitz, 2013). GPCRs consist of ~800 different human genes, with 4% of the entire protein coding genome predicted to code for GPCRs (Benovic and Zastrow, 2014; Hu et al., 2017). As a family, GPCRs are integral to a vast number of functions and physiological processes in the body including; cell proliferation (Arakaki et al., 2018), angiogenesis (De Francesco et al., 2017), metabolism (Sebastiani et al., 2018) and neurological function (Grammatopoulos, 2017), and act to relay extracellular signals through ligand-receptor interactions, activating a multitude of intracellular pathways (Bjarnadóttir et al., 2006). It is estimated that ~700 drugs, currently available on the market, target GPCRs and GPCR-related proteins, representing ~30-35 % of therapeutic drug targets (Santos et al., 2016; Sriram and Insel, 2018), with ligands including a plethora of substances such as; photons, ions, small molecules, peptides and proteins (Stevens et al., 2013). Following activation, GPCRs traditionally couple to heterotrimeric G proteins resulting in the induction of signalling cascade that produces short-term physiological effects through the rapid production of second messenger molecules, as well as long-term effects via altered gene expression. GPCR signalling is a complex process that involves many effector proteins, such as G-proteins and β -arrestins, and involves complex signalling organisation, with evidence showing that signalling can occur both on the cell surface and within endosomes.

1.2.1 GPCR structure

Despite the size of this receptor class and its utilisation in drug targeting, the structure of GPCRs were not fully elucidated until the crystallisation of the first non-visual GPCR, β_2 -Adrenoceptor (β_2 -AR) in 2007 (Rasmussen et al., 2007), with the crystallisation of rhodopsin several years earlier (Palczewski et al.,

2000). Since the initial crystallisation of β_2 -AR, numerous other GPCRs have been crystallised. Many of the elucidated structures have emerged from mono-amine and small molecule receptors including; muscarinic receptors (Haga et al., 2012; Kruse et al., 2012; Thal et al., 2016) adenosine receptors (Doré et al., 2011; Lebon et al., 2011) and 5-HT receptors (Wacker et al., 2017; Yin et al., 2018). These structures have often been resolved in the presence of different ligands such as endogenous agonists, synthetic agonists and inverse agonists, which in themselves have provided information for the different binding modes of these ligands. More recently, successful crystallisation of GPCRs with other ligand types, such as lipids and peptides, has been achieved. Examples include; the free fatty acid receptors (Srivastava et al., 2014), Sphingosine-1-phosphate receptors (Parrill et al., 2012), chemokine receptors (Park et al., 2012), opioid receptors (Granier et al., 2012; Manglik et al., 2012; Wu et al., 2012), GLP-1 receptor (Jazayeri et al., 2017) and now the Y_1 R (Yang et al., 2018). These structures have helped to elucidate the commonalities and highlighted differences in the structure of GPCRs. It should be noted that the majority of peptide receptor structures have required crystallisation in the presence of small molecule ligands, as opposed to the endogenous ligand. However, the development of cryogenic electron microscopy (cryoEM) technology as a tool for structural characterisation, offers the opportunity for crystallisation of these receptors with their peptide ligands, as has recently been achieved for the GLP-1 receptor (Zhang et al., 2017).

All GPCRs share a common 7 transmembrane (TM) domain motif that integrates the receptor within the membrane to produce a tertiary structure resembling a barrel and spanning the membrane in an anticlockwise orientation when viewed from the extracellular surface (Figure 1.3; Lee et al., 2015). Thus, these receptors are also characterised by an extracellular N-terminus and an intracellular C-terminus joined by 3 intracellular loops (ICL1-3) and 3 extracellular loops (ECL1-3; Figure 1.3). GPCRs are sub-categorised based on sequence homology. The GRAFS system divides GPCRs into 5 distinct families; Rhodopsin (Class A), Secretin (Class B),

Glutamate (Class C), Adhesions and Frizzled/Taste 2 receptors (Fredriksson, 2003; Schiöth and Fredriksson, 2005).

Class A GPCRs are the largest family of GPCRs, with almost 700 members. It consists of 19 sub-categories including the rhodopsin, opioid, and adenosine family, as well as all four members of the YR family (Fredriksson, 2003; Pierce et al., 2002). Class A receptors typically possess a short extracellular N-terminus with ligand binding occurring at the extracellular loops or within the transmembrane helices that form a ligand binding pocket, with the exact position of binding differing between receptors and ligands (Bjarnadóttir et al., 2006). It has been demonstrated that large protein hormones, such as follicle stimulating hormone, may also interact with the N-terminal domain of the receptor (Fan and Hendrickson, 2005), whereas protease activated receptors, such as thrombin, require cleavage of the receptor N-terminus to reveal a tethered ligand that activates the receptor (Saito and Bunnett, 2005; Vu et al., 1991). In addition, Class A GPCRs also contain a number of highly conserved residues and motifs including the E/DRY motif, which spans across TM3 and TM6 (Rovati et al., 2017) and the NPxxY motif (where x represents any residue) in TM7 (Trzaskowski et al., 2012) and are discussed in further detail below (Section 1.2.5.2).

The Class B GPCR family consists of 15 receptors, all of which bind peptide endocrine hormones such as glucagon and vasoactive intestinal peptide (VIP) receptors (Bjarnadóttir et al., 2006; Schiöth and Fredriksson, 2005). These GPCRs are characterised by an N-terminal extracellular domain, forming an α -helix and four β -strands that are stabilised by six conserved cysteine residues that form disulphide bridges (Grace et al., 2004). Peptides typically bind this site of the receptor which governs peptide selectivity and high affinity (Fredriksson, 2003; Lee et al., 2015). In the case of GLP-1, the peptide makes interactions with the N-terminus of the receptor and the C-terminal residues of the peptide engage the ECL and TM regions of the receptor resulting in activation (Koole et al., 2013; Zhang et al., 2017).

The Class C GPCR family contains 22 receptors including metabotropic glutamate, γ -aminobutyric acid (GABA), calcium sensing and a number of orphan receptors (Fredriksson, 2003). Class C receptors are also characterised by a large extracellular domain. However, this domain is much larger than the Class B family, containing ~600 amino acids creating a double lobbed structure, known as the venus flytrap domain (VFT), which can assume a variety of conformations and is typically the site of orthosteric agonist binding (Brauner-Osborne et al., 2007). It has also been shown that ligands can bind out with the VFT and instead act as allosteric ligands through interactions within the TM domains, as observed with metabotropic glutamate receptors and calcium sensing receptors (Davey et al., 2012; Gregory et al., 2011).

The Adhesion GPCR family consists of 33 receptors (Schiöth and Fredriksson, 2005), and are so called because they contain motifs likely to participate in cell adhesion. They are characterised by long and highly variable N-termini that are rich in glycosylation sites (Fredriksson, 2003; Trzaskowski et al., 2012). However, these receptors consist primarily of orphan receptors and, as such, are poorly characterised. Reports of ligand identification for the orphaned receptors GPR56, GRP114 and GPR126 have recently been published (Kuffer et al., 2016; Luo et al., 2011; Stoveken et al., 2018).

The frizzled/Taste 2 GPCR family contains two groups of receptors, frizzled and Taste 2, and contains 24 receptors. These two groups are linked by the presence of consensus sequences not found in any of the other families (Fredriksson, 2003). Frizzled receptors are known to bind Wnt glycoproteins and are important in the control of cell fate, proliferation and polarity. However, as with adhesion GPCRs, these receptors are poorly understood and characterised (Zeng et al., 2018).

In the case of the Y receptor family, it is known that all four members belong to the Class A rhodopsin family of GPCRs.

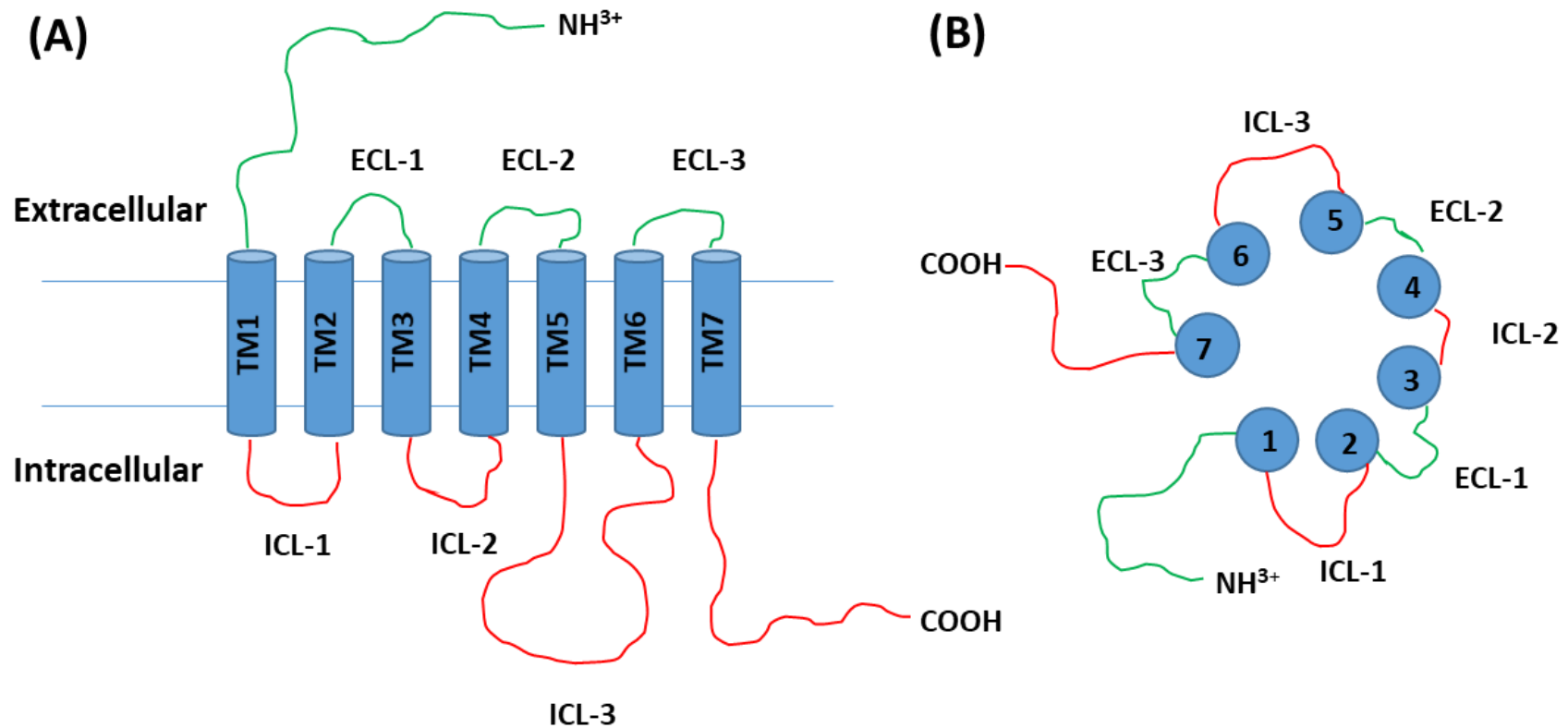


Figure 1.3 – Schematic representation of a Class A GPCR structure: (A) Represents a side view projection of a GPCR through the membrane, demonstrating the TM domains, represented by blue barrel structures, crossing the lipid bilayer, ECL1-3 and the extracellular N-terminus are represented in green and ICL1-3 and the intracellular C-terminus in red. The extracellular N-terminus and intracellular C-terminus can be seen with their respective functional groups, NH² and COO⁻, which are protonated at physiological conditions (NH³⁺ and COOH). (B) Represents an aerial view of a GPCR from above the membrane and demonstrates the barrel like conformation adopted by the TM domains.

The Y₁R is a 384 amino acid protein (Larhammar et al., 1992), Y₂R is 381 (Rose et al., 1995), Y₄R is 375 (Yan et al., 1996) and the Y₅R is 456 (Gerald et al., 1996). The Y₅R possess a large ICL3, ~100 amino acids longer than other Y receptors and a short C-terminus consisting of only 17 amino acids compared to the other subtypes which possess a C-terminus of ~60 amino acids (Walther et al., 2011). In addition, the Y₅R is known to exist in two isoforms, encoded for by two splice variant genes. These Y₅R isoforms, 455 and 445 (long and short form, respectively), differ in the N-terminus, but have been shown to display a comparable pharmacology (Rodriguez et al., 2003). The structure of the Y₁R has recently been confirmed through crystallography studies and has been shown to share the 7TM helical bundles of other known GPCR structures (Yang et al., 2018). The interactions of the receptor-ligand complex elucidated in this study are discussed in further detail below (Section 1.2.2.1).

1.2.2 GPCR ligand binding

As discussed above, many GPCR structures have been determined through crystallisation, in complex with a variety of ligands, and have elucidated the binding mode of small molecule ligands, particularly in mono-amine receptors. From these initial studies it has been determined that the TM domains play a large role in the transduction of the conformational changes that occur upon ligand binding (Unal et al., 2012). Additionally, it has been determined that the orthosteric binding site for many Class A GPCRs is generally located in the extracellular half of the GPCR, and is formed mainly by TMs 3, 6 and 7, with the specifics of residue contacts, and other important contacts made in other TMs, differing between receptor subtype (Lee et al., 2015).

Rasmussen et al., (2007) demonstrated that ligand binding at the β_2 -AR occurs within the extracellular domain of the TM bundle, with key amino acids within the binding pocket acting as contact sites for catecholamine compounds such as adrenaline and nor-adrenaline. It has been shown that TM3 plays a critical role in ligand recognition and receptor activation through interactions between [Asp¹³⁰] and the amide group of these compounds (Kobilka and

Deupi, 2007; Rasmussen et al., 1999). It has also been demonstrated that serine residues within TM5, [Ser²⁰³], [Ser²⁰⁴] and [Ser²⁰⁷], have a critical role in receptor activation through interaction with the catechol OH groups present within the ligand. This interaction has also been demonstrated to be specific for agonists (Katritch et al., 2010; Kobilka and Deupi, 2007).

Agonist binding at the β_2 -AR has been shown to promote the inward movement of the extracellular TM5 and 6 to form the ligand binding pocket and stabilise the active conformation of the receptor (Dror et al., 2011; Rasmussen et al., 2011b, 2011a). This movement of the TM domains has also been demonstrated in other mono-amine receptors, such as β_1 -AR and adenosine A_{2A} (Carpenter et al., 2017; Warne et al., 2011), and has led to the proposed “global toggle switch” model. This model suggests that agonist binding results in movement of TM6 around the highly conserved proline residue [Pro^{6.50}], and other conserved prolines present with TM5, 6 and 7. This interaction results in the formation of a kink in the TM domains that creates a pivot around the intracellular and extracellular halves of these TM domains, resulting in rotation upon ligand binding (Schwartz et al., 2006). This movement closes the extracellular part of TM6 around the ligand and opens the intracellular end of TM6, thereby facilitating G-protein interactions (Schwartz et al., 2006). This model is supported by the active crystal structures of β_2 -AR and adenosine A_{2A} which display a large outward movement of the cytoplasmic end of TM6 relative to the inactive structures (Carpenter et al., 2017; Rasmussen et al., 2011b). Additionally, the movement of TM6 has been proposed to release steric constraints within the receptor conformation, allowing the inward movement of the extracellular half of TM6 (Schwartz et al., 2006). Overall, these conformational changes result in a substantial rearrangement of the TM domains, particularly their intracellular face, which facilitates the binding of effector molecules such as G proteins.

1.2.2.1 Y₁R crystallisation and small molecule binding

The recently crystallised structure of the Y₁R was determined in the presence of two small molecule selective antagonists, UR-MK299 and BM-193885 (Yang et al., 2018; ligand structures shown in Figure 1.6; UR-MK299 binding pocket shown in Figure 1.4). Both structures exhibited inactive conformations within TM6 adopting an inward conformation similar to other inactive GPCR structures, via the [Trp^{6.48}] residue, which is recognised as the global toggle switch in various GPCRs, as discussed above (Section 1.2.2; Venkatakrishnan et al., 2013). UR-MK299 was shown to form a hydrophobic contact with this residue, potentially preventing the receptor from adopting an active confirmation and stabilising it in an inactive form. The UR-MK299 ligand bound to the Y₁R in a cavity within the helical bundle bordered by all TMs except 1 and 2. The diphenylmethyl moiety (Figure 1.4 and 1.6) was shown to interact with multiple Phe residues which form a hydrophobic cluster on TM5 and has previously been shown to be critical in the recognition of argininamide-type antagonists at the Y₁R, including ligands such as BIBO3304 and BIBP3226 (Keller et al., 2015; Figure 1.6). The hydroxyphenyl group of UR-MK299 was also shown to sit in a groove formed by TM3 and 5 of the receptor, enabling hydrophobic contacts with several residues, including [Gln^{3.32}], which is suggested to be the interaction partner for the NPY C-terminus, therefore crucial for receptor activation (Kaiser et al., 2015). This indicates that [Gln^{3.32}] is potentially blocked by UR-MK299, giving rise to its antagonist properties at the Y₁R. UR-MK299 was shown to engage with [Asn^{6.55}] in the Y₁R via the formation of two hydrogen bonds with the α -nitrogen and the carboxylic oxygen next to the hydroxybenzylamine moiety of UR-MK299. Additionally, the [Asp^{6.59}] residue was shown to create a salt bridge with the protonated guanidinyll moiety and a hydrogen bond with the carbamoyl group. As residues [Asn^{6.55}] and [Asp^{6.59}] are suggested to be important amino acids for Y₁R ligand recognition (Sautel et al., 1996), the observed interaction may further elucidate the antagonist activity of this ligand through blocking of these key residues involved in endogenous ligand binding.

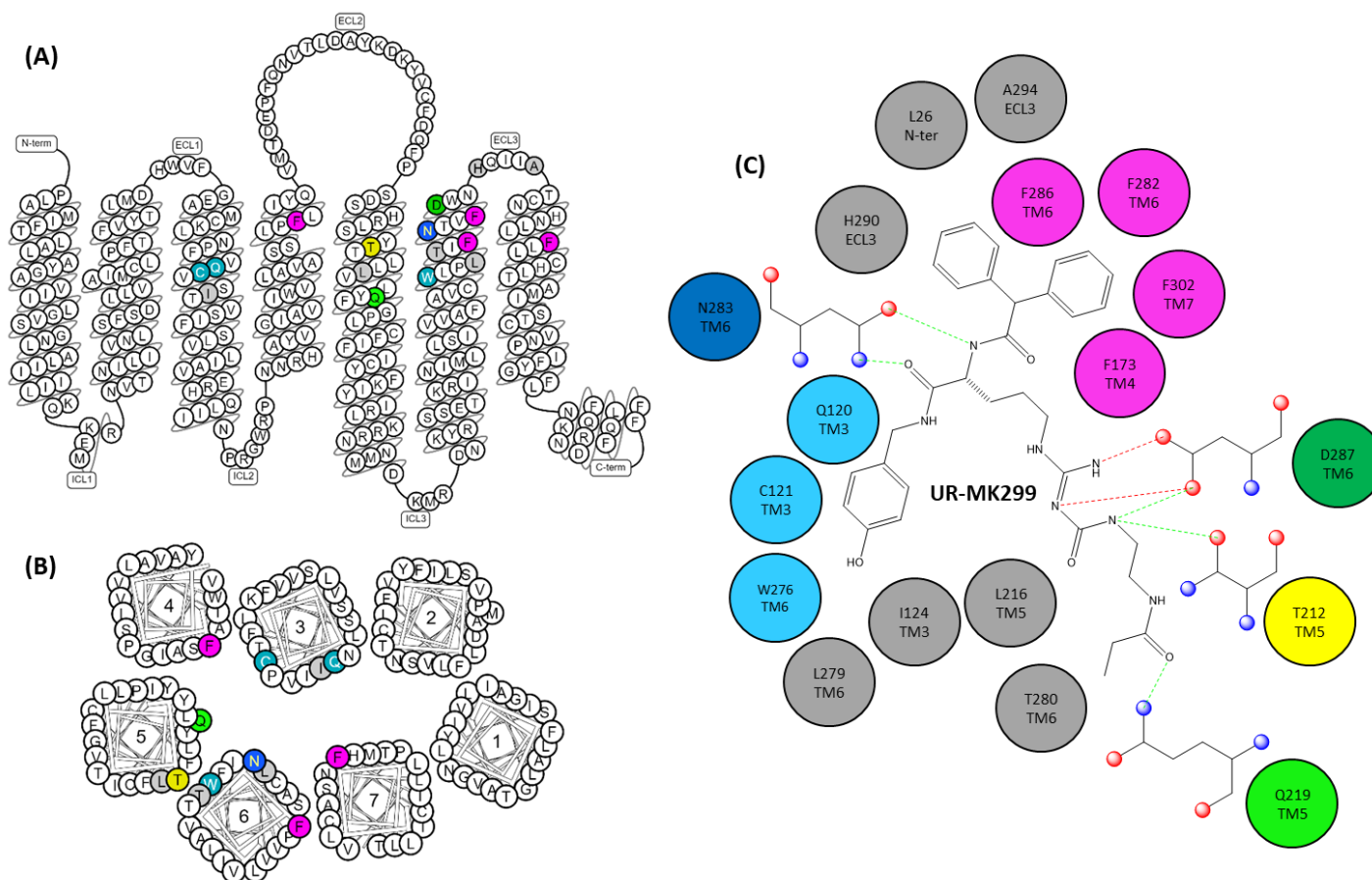


Figure 1.4 – Schematic representation of the binding pocket for UR-MK299 at the Y₁R. (A) Shows a snake-plot diagram of the Y₁R with UR-MK299 interacting residues highlighted. (B) Shows these residues from the extracellular view of the receptor and (C) shows a schematic representation of the interactions, discussed in detail in Section 1.2.2.1, between the Y₁R and UR-MK299. Salt bridges and hydrogen bonds are shown as red and green dashed lines, respectively (adapted from Yang et al., 2018).

It was also observed that BMS-193885 occupied a similar binding pocket, showing similar interaction with key residues including the [Asp^{6.59}] and the hydrophobic cluster of Phe residues in TM5. When we compare the recognition of small molecules, such as UR-MK299 and BMS-193885, to that of larger peptide ligands there are inherent differences in the way the ligand interacts with the receptor. It has been shown that peptide ligands dip into the TM bundles to activate the receptor. However, large areas of the ligand contact surface exists within the ECL loops. To date the binding of endogenous peptides have been investigated largely through mutagenesis and computational modelling and is discussed in further detail below (Section 1.2.2.2).

1.2.2.2 Peptide binding to NPY receptor subtypes

The Y₁R, Y₂R and Y₅R subtypes differ the most in sequence homology, but share high affinity binding to NPY, suggesting that a small proportion of conserved residues are important to ligand binding (Sjödín et al., 2006). The Y₁R has been shown to require the complete N-terminal domain of NPY, reflected in its lack of affinity for the N-terminal truncated forms NPY₃₋₃₆ and PYY₃₋₃₆ (Larhammar et al., 1992). However, the Y₂R and Y₅R express equal affinity for NPY, PYY, NPY₃₋₃₆ and PYY₃₋₃₆, suggesting the N-terminal portion of the peptide is not as crucial for binding at these receptor subtypes. Ligand binding to YR subtypes has been suggested to occur within the transmembrane helical bundle and involve extracellular loop residues. Extensive mutagenesis of the human Y₁R was used to characterise residues important in binding peptides (Kanno et al., 2001; Sjödín et al., 2006). Alanine substitution of the highly conserved [Tyr¹⁰⁰] in the Y₁R led to a complete loss of NPY binding (Kanno et al., 2001; Sautel et al., 1995). This residue is a tyrosine or serine in the Y₂R and Y₅R receptors, respectively, and the hydroxyl group of these amino acids have also been proposed to interact with the amidated C-terminus of the peptide ligand directly (Sjödín et al., 2006). The TM6 residues [Phe²⁸⁶] and [His²⁹⁸] within the Y₁R have also been implicated in ligand binding (Kanno et al., 2001).

In addition to receptor mutagenesis studies, alanine scans of full length NPY have been conducted (Beck-Sickinger et al., 1994). This study showed that substitution of [Pro²] and [Pro⁵] resulted in a 100 fold decrease of Y₁R affinity and revealed that [Arg³³] and [Arg³⁵] are required for binding at the Y₁R and Y₂R, where these mutations resulted in loss of binding. This loss of binding may be related to data from other studies that indicating that [Arg³⁵] of NPY and PP interact with [Asp²⁸⁶] within ECL3 of Y₁R and Y₄R, resulting in the formation of salt bridges (Lindner et al., 2008; Merten et al., 2007). A similar interaction has also been observed in Y₂R and Y₅R with [Arg³³]. In addition Y₂R and Y₅R require the presence of [Arg²⁵] in NPY for high affinity binding to occur, via interactions with [Asp¹⁹⁹] present in ECL2, whereas Y₁R and Y₄R show no sensitivity to this [Arg²⁵] mutation (Lindner et al., 2008; Söll et al., 2001). This suggests that some residues have a shared importance for ligand binding across the subtypes, but subtype specific residues are also involved. It has been suggested that the Y₁R and Y₄R subtypes may have distinct ligand binding modes to that of Y₂R and Y₅R based on these mutation studies, and may reflect the closer sequence homology of these receptor pairings (Babilon and Beck-sickinger, 2013).

Many of these findings have been further confirmed via computational modelling, NMR and mutagenesis studies based on at the recently elucidated Y₁R crystal structure (Yang et al., 2018). Modelling of NPY at this Y₁R structure suggested that NPY adopts a relatively flat NPY-Y₁R binding pose with the C-terminal tetrapeptide [Arg³³-Tyr³⁶] penetrating the binding pocket. Closer inspection of the binding pocket revealed that [Arg³⁵] of NPY adopts a similar binding pose to that of UR-MK299 with mutations of this residue resulting in a drastic decrease in activity, ~6000 fold. In addition, this study identified that [Tyr³⁶] points towards the [Gln^{3.32}] residue within TM3, forming a hydrogen bond, as well as demonstrating that the C-terminal amide may interact with [Gln^{3.32}] within the receptor. Complementary mutation of [Gln^{3.32}] resulted in a 26 fold decrease in NPY potency at the Y₁R, with loss of the C-terminal amide resulting in a 46 fold loss of activity. This study also revealed close hydrophobic

contacts of [Tyr³⁶] of NPY with [Tyr^{2,64}] of the Y₁R that was agonist specific, with loss of this residue resulting in a 284 fold decrease in potency for NPY.

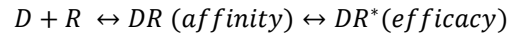
Studies such as these have aided in further elucidation of the binding mode of endogenous and exogenous ligands, and have aided and continue to direct the development of YR ligands. Further analysis of the newly revealed Y₁R structure offers the opportunity for more in depth analysis into the nature of ligand binding.

1.2.3 GPCR ligand pharmacology

GPCRs are activated through binding of ligands to the receptor (Stott et al., 2016). The binding location of these ligands determines whether the ligand is classified as orthosteric (i.e. binds to the endogenous ligand binding site) or allosteric (i.e. binds to a site on the receptor independent of the orthosteric site). The action of these ligands can then be further defined by their affinity and efficacy. The affinity is a measure of how well a ligand can bind to a receptor and the efficacy is a measure of the ligands' ability to activate the receptor, once bound, by conformational change. Furthermore, the potency of a ligand is a term that relates to the concentration of the ligand required to produce a functional response. Potency, often represented on a concentration response curve as an EC₅₀ value i.e. the agonist concentration giving 50 % response, depends on both ligand affinity and efficacy at the target receptor (Clark, 1933; Stephenson, 1956). In addition, properties of the system in question, for example receptor reserve and the extent of signal amplification between receptor and measured endpoint, can influence potency.

Basic quantification of drug receptor interactions is derived from the law of mass action, in which rates are considered to be proportional to the concentrations of the reaction participants (Hill, 1910, 1909). The scheme in Equation 1.1 represents the ability of the drug to bind the receptor (affinity), followed by a conformational change in the bound drug-receptor complex to generate an active conformation (efficacy).

Equation 1.1 - D = drug, R = receptor, * = active state.



Equations for the rates of binding and dissociation can be described based on the law of mass action, i.e. proportional to concentration (Equation 1.2 and Equation 1.3). At dynamic equilibrium, when the concentrations of both unbound and bound, D and R no longer change, these rates are equal, leading to the expression in Equation 1.4.

Equation 1.2 - k_{on} = the rate constant at which drug binds the receptor.

$$\text{Forward rate} = k_{on}[D][R]$$

Equation 1.3 - k_{off} = the rate constant at which drug dissociated from the receptor.

$$\text{Reverse rate} = k_{off}[DR]$$

Equation 1.4

$$k_{on}[D][R] = k_{off}[DR]$$

From this, a measure of affinity may be derived through the determination of the K_d (Equation 1.5) and proportional receptor occupancy (Equation 1.6). If $[D] = K_d$, $\alpha = 0.5$, leading to the alternative deviation of K_d as the concentration of ligand for 50 % receptor occupancy.

Equation 1.5 - K_d = equilibrium dissociation constant.

$$K_d = \frac{k_{off}}{k_{on}} = \frac{[D][R]}{[DR]}$$

Equation 1.6 - α = proportional occupancy.

$$\alpha = \frac{[D]}{(K_d + [D])}$$

In pharmacology, the K_d equilibrium dissociation constant is used as a fundamental measure for compound affinity at the receptor. However, increasingly the effects of drugs are considered under non-equilibrium conditions and the rates of association (k_{on}) and dissociation (k_{off}) can be important parameters to consider. This is due to k_{off} potentially influencing the duration of action of the drug at its target, where the effect is surmountable

or non-surmountable (Sykes et al., 2017; Vauquelin and Charlton, 2010; Chapter 3).

For GPCRs the concept of affinity and efficacy are further challenged by the involvement of a third partner, e.g. the G-protein or arrestin effector, which stabilises agonist-receptor complexes (Section 1.2.5.2 and 1.2.5.3). This concept is known as the ternary complex model and can lead to multiple affinity states being observed for agonists (Kenakin and Williams, 2014). For example, studies using radiolabelled agonist binding at YR, such as [¹²⁵I]PYY, often require the use of membrane preparations and assay buffer conditions that stabilise the high affinity agonist-receptor-effector ternary complex (Kilpatrick et al., 2010; Stott et al., 2016), and these conditions may differ from whole cell measurements.

Orthosteric ligands are classed into 3 groups; agonist, antagonist and inverse agonist, according to their efficacy. Agonists are ligands that bind and activate GPCRs, leading to stabilisation of the active receptor and modulation of downstream signalling. Their intrinsic efficacy is most simply defined by the relative ability to stabilise an R* active conformation (Equation 1.1). Agonists with lower receptor efficacy may be revealed as partial agonists in an assay, by being unable to produce the same maximal response compared to a full agonist (Figure 1.5A). However, whether partial agonism is observed, also depends on other factors, such as the extent of signal amplification and receptor reserve (Stott et al., 2016).

Antagonists are ligands that have no efficacy but have high binding affinity for the receptor and as such can inhibit agonist-mediated signalling without activating the receptor themselves (Kenakin and Williams, 2014). Antagonists can exhibit surmountable or non-surmountable antagonism. Surmountable or reversible competitive antagonism occurs when the antagonist competes with agonist for binding at the orthosteric site, affecting the concentration of agonist needed to produce a maximal response, but not affecting the

magnitude of the maximal response. This causes rightward shifts to occur in concentration response curves. The extent of this shift at equilibrium depends only on the antagonist concentration and its K_d (Equation 1.5), allowing the application of methods such as Gaddum (Gaddum, 1937) and Schild analysis (Schild, 1949) to calculate the affinity of the antagonist for the receptor (Chapter 2, Section 2.6.1.4). Non-surmountable or irreversible antagonism can occur through binding of antagonist to the orthosteric site resulting in a decrease in magnitude of maximal response that cannot be changed with increasing agonist concentration. This most often occurs due to irreversible or slowly reversible kinetics of the antagonist. Non-surmountable effects on concentration response curves may also arise from non-competitive antagonism in which antagonists bind at a topographically distinct allosteric site (Figure 1.5B and C).

Inverse agonists have been described more recently in systems where the spontaneous activation of receptors can be observed as constitutive activity. These ligands act as antagonists, competing for agonist binding, but also actively stabilise the receptors conformational equilibrium in the inactive conformation, thereby decreasing the basal response produced by constitutive receptor activation. An example of a constitutively active receptor is MC₄R. It has been demonstrated that a loss of this constitutive activity of the MC₄R, through receptor mutation, can result in the development of obesity (Srinivasan et al., 2004; Tao, 2008; Section 1.1.5). The endogenous inverse agonist, AgRP, is known to inhibit the activity of MC₄R in order to induce orexigenic signalling within the CNS, therefore performing a vital role in feeding behaviours.

Non-competitive antagonists are specific examples of allosteric ligands, which may be more broadly defined as positive, negative (PAMs, NAMs) or neutral allosteric modulators and offer the ability to either enhance, inhibit or have no measurable effect on ligand binding and/ or functional response of an orthosteric ligand.

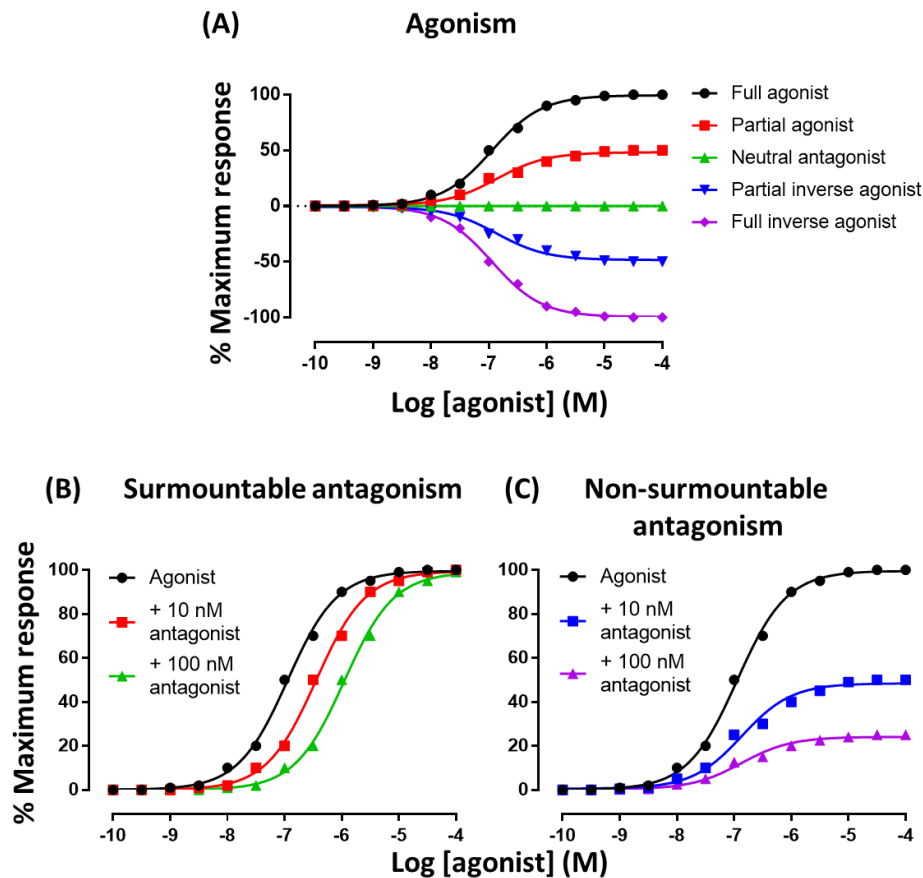


Figure 1.5 – The principles of agonist and antagonist pharmacology at GPCRs. (A) Shows model data for the action of agonists, ligands that bind and stabilise the active GPCR conformation resulting in the activation of intracellular signalling cascades. Full agonists have high efficacy and so produce the reference agonist maximal response, whereas partial agonists have lower efficacy and so induce a submaximal response. Inverse agonists bind and stabilise the receptor in an inactive conformation, thereby inhibiting constitutive activity of a receptor resulting in an apparent decrease in basal response. (B) Shows the action of surmountable competitive antagonists, ligands that are able to bind the orthosteric site but have no efficacy and so do not induce a cellular response. Therefore, ligands compete for the binding site with agonists and higher concentrations of agonist are required to induce the same maximal response, resulting in a rightward shift of the agonist induced concentration response curve. (C) Shows the actions of non-surmountable antagonists. These ligands reduce the maximal agonist response, as no amount of agonist can overcome the inhibition observed. This kind of antagonism may occur due to antagonist covalent binding to the orthosteric binding site, eliminating the possibility of competition with the agonist molecules, or due to binding at a topographically distinct (allosteric) site of the receptor.

Additionally, allosteric modulators may have efficacy in their own right and act as agonists or inverse agonists. Allosteric modulators are generally described by their cooperativity factors, which provide a measure of the degree and direction, i.e. positive or negative, of the orthosteric ligand modulation in terms of both affinity and efficacy. Allosteric modulators are receiving attention in drug discovery due to their ability to exploit different binding sites

of the receptor and elicit different signalling responses. Additionally, they can be used as tools to improve subtype selectivity of the orthosteric sites, giving properties that potentially aid in the balance between therapeutic effects versus unwanted side effects (Korczynska et al., 2018; May et al., 2007).

1.2.4 Y receptor ligands

Due to the physiological roles of the NPY family of peptides and receptors (Section 1.1.5 and 1.1.6), the development of truncated or mutated forms of the NPY peptides, as well as small molecules, has been pursued. As this receptor family shows relatively high sequence homology and overlapping recognition profiles in their binding sites for endogenous ligands, one of the major obstacles in the design of drugs has been selectivity between YR subtypes.

1.2.4.1 Y₁ receptor selective ligands

The earliest pharmacological ligands for the YRs were modified agonist peptides based on the NPY sequence. One of the first modified NPY ligands, [Leu³¹Pro³⁴]-NPY, was designed as a high affinity ligand for the Y₁R (Fuhlendorff et al., 1990), with selectivity over the Y₂R, though it has since been shown to retain some affinity for both Y₄R and Y₅R subtypes (Balasubramaniam, 1997; Gehlert et al., 1996b; Gerald et al., 1995). In addition, the substitution of [Asn⁷] to Phe ([Phe⁷,Pro³⁴]-NPY), along with other substitutions such as [Arg²⁵] to [D-Arg²⁵] and [His²⁶] to [D-His²⁶], provided Y₁R selectivity (Fuhlendorff et al., 1990; Söll et al., 2001). [Pro³⁴,Nle³¹,Bpa³²,Leu²⁴]-NPY₂₈₋₃₆ has also been identified as the first Y₁R selective peptide reduced in size compared to full length NPY (Zwanziger et al., 2009). All of these ligands, as mutations or truncated forms of NPY, act as agonists at the Y₁R. Small molecule YR agonists are lacking, however, small molecule Y₁R antagonists have been described and include, for example, BIBO3304 (Wieland et al., 1998) and BIBP3226 (Rudolf et al., 1994), both of which are argininamide derivatives that mimic the NPY peptide C-terminus. Small molecule Y₁R antagonists also include J-104870 (Kanatani et al., 1999), J-115814 (Kanatani et al., 2001), UR-MK299 (Keller et

al., 2015) and BMS-193885 (Antal-Zimanyi et al., 2008; small molecules for which the binding site of the latter two has been well described; Yang et al., 2018; Section 1.2.2.1). BIBP3226 has been shown to be potent and selective at the Y₁R over other cloned YRs, expressing nanomolar affinity. However, it has also been found to show moderate affinity for the Neuropeptide FF receptor (NFFR; Mollereau et al., 2001). BIBO3304 has also been shown to be a Y₁R selective antagonist with 10 fold higher affinity compared to BIBP3226 (Dumont and Quirion, 2000). In addition, the truncated peptide antagonist such as BVD15 and GR231118 have also been described (Daniels et al., 1995). The truncated C-terminal analogue of the NPY peptide, BVD15, displays high affinity binding and selectivity at the Y₁R, while GR231118, an anti-parallel dimer ligand based upon BVD15, has been demonstrated to display ~100 fold higher affinity at the Y₁R compared to BVD15 (Daniels et al., 1995). Both BVD15 and GR231118 analogues are also Y₄R agonists with lower affinity (Parker et al., 1998). As the principal compound series investigated in this thesis, the BVD15 and GR231118 analogues are discussed in further detail in Chapters 3 and 4.

1.2.4.2 Y₂ receptor selective ligands

In contrast to the Y₁R, C-terminal fragments of NPY and PYY, including NPY₃₋₃₆ up to NPY₂₂₋₃₆, as well as centrally truncated analogues, such as [Ahx⁵⁻²⁴]-NPY, retain affinity and agonist activity at the Y₂R (Cabrele and Beck-Sickinger, 2000; Merten et al., 2007; Michel et al., 1998). In addition, the synthetic peptide TM30338 (also known as Obinipitide), based upon full length PP and PYY, has been evaluated in clinical trials for obesity as a dual ligand for both the Y₂R and the Y₄R subtypes (Brothers and Wahlestedt, 2010). As with the Y₁R, small molecule agonists are lacking, however the non-peptide antagonist, BIIE0246, has been developed as a Y₂R selective compound (Doods et al., 1999). Additional studies have shown that BIIE0246 also binds the μ and κ opioid receptors, as well as α -1A adrenergic receptors, with sub-micromolar affinities (Brothers et al., 2010). Peptide antagonist SF-11, JNJ-5207787 and JNJ-

31020028 have also been identified as Y₂R selective antagonists (Brothers and Wahlestedt, 2010).

1.2.4.3 Y₄ receptor selective ligands

Other than the selective endogenous peptide, PP, the most potent agonist at the Y₄R that has been described is [Pro³⁴]-PYY, however this analogue binds with lower affinity at the Y₄R than PP (Bard et al., 1995; Cabrele and Beck-Sickinger, 2000; Thiele et al., 2002). The fact that these analogues retain some affinity for Y₄R is perhaps unsurprising given that original design of [Leu³¹,Pro³⁴] peptides was based on substitution of the PP residues at the relative position in NPY and PYY (Fuhlendorff et al., 1990). There have also been efforts towards the design and development of small molecule allosteric modulators at the Y₄R via fragment screening with the aim to produce PAMs (Sliwoski et al., 2016). The use of PAMs may provide the potential to increase the selectivity of the orthosteric binding for Y₄R selective ligands. Finally, few antagonists have been described for the Y₄R, and those that have been identified demonstrate low affinity (Brothers and Wahlestedt, 2010). However, studies have alluded to the possibility of producing more selective Y₄R antagonist through the application of chirality in the development of small molecule antagonist (Keller et al., 2013). Additionally, the Y₄R antagonist, BVD74-D, a truncated peptide that mimics the C-terminus of PP and expresses a similar affinity for the Y₄R, has recently been developed (Kuhn et al., 2016; Chapter 4).

1.2.4.4 Y₅ receptor selective ligands

The Y₅R subtype is relatively non-selective between the endogenous ligands, albeit binding PP at a reduced affinity compared to NPY and PYY. Selective peptide agonists [Ala³¹,Aib³²]-NPY (Cabrele et al., 2000), [D-Trp³⁴]-NPY (Parker et al., 2000) and [cPP¹⁻⁷,pNPY¹⁹⁻²³,Ala³¹,Aib³²,Gln³⁴]-PP (Cabrele and Beck-Sickinger, 2000) have been described. Small molecule antagonists MK-0557, and S-2367 (also known as velneperit; Sato et al., 2009) are both compounds that were entered into Phase II clinical trials as treatments for obesity. Studies

of MK-0577 showed modest efficacy in inducing weight loss in humans, however, although weight loss was significant, it was deemed not to be clinically meaningful, with patients showing a weight loss of 2.2kg over 52 weeks on 1mg of MK-0557 a day, in a cohort of 1661 patients (Erondur et al., 2006; Tamura et al., 2012). During initial, in vitro, characterisation of S-2367, the compound showed a surmountable binding profile in cells (Tamura et al., 2012). In vivo studies suggested that S-2367 showed statistically significant effects on weight loss in human trials where patients lost an average of 3.8kg compared to control (George et al., 2014; Tamura et al., 2013). However, when combined with a low calorie diet it was observed that over 52% of the patients receiving velneparit and 32% of patients receiving placebo lost greater than 5% body weight, suggesting a lack of significant benefit (Brothers and Wahlestedt, 2010; George et al., 2014). In addition, the use of Y₅R antagonists have been associated with severe side effects due to the CNS expression of these receptors and the role they play in epilepsy, anxiety and depression (Olesen et al., 2012).

1.2.5 GPCR activation and induction of cell signalling

1.2.5.1 The role of ECLs in receptor activation

It has been suggested that the access of ligand to the binding pocket may be regulated by the ECL2 domain. The available crystal structures of β_2 -AR show that it has a large, solvent exposed ECL2 that creates a channel to allow small, water soluble ligands access to a binding pocket within the TM helical bundle (Cherezov et al., 2007; Rasmussen et al., 2007). The crystal structure of the β_1 -AR shows that the ECL2 is also heavily involved in defining ligand access, suggesting that ECL2 plays an important role in governing the charge distribution and shape of the channel leading to the ligand-binding site and may define ligand specificity. This is demonstrated by the fact that, although β_1 -AR and β_2 -AR subtypes have a relatively high homology in the amino acids within the binding pocket, they express a marked difference in the sequence of their ECL2 regions, thereby governing ligand specificity (Rosenbaum et al., 2007).

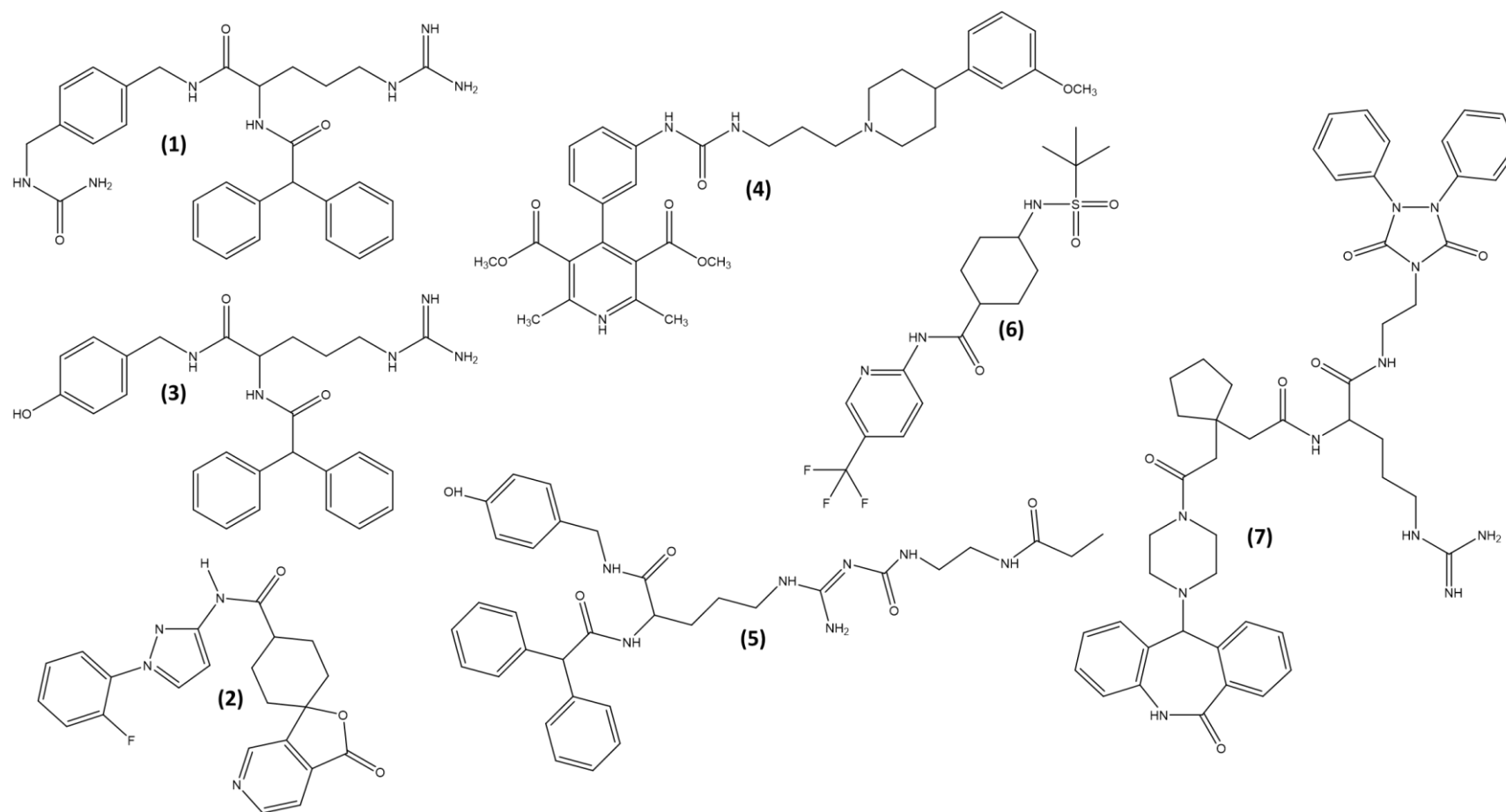


Figure 1.6 – Non-peptide ligands for the YR family – (1) Y₁R selective BIBO3304, (2) Y₅R selective MK-0557, (3) Y₁R selective BIBP3226, (4) Y₁R selective BMS-193885, (5) Y₁R selective UR-MK299, (6) Y₅R selective S-2367 or velnepatit (7) Y₂R selective BIIE0246

This governance of ligand specificity is supported by evidence obtained from the crystal structures of the spingosine-1 phosphate receptor (Hanson et al., 2012) and the GPR40 (Srivastava et al., 2014). These structures demonstrate that the ECLs sterically block the extracellular face of the receptor to diffusible ligands. In addition, direct participation of the ligand with the ECLs have been observed in some receptors, such as the interactions of [Phe^{5.29}] in ECL2 of the adenosine A_{2A} receptor (Katritch et al., 2012). This has also been observed for larger peptide ligands, such as NPY, as demonstrated through mutational studies of the highly conserved [Asp^{6.59}] within the ECL3 resulting in drastic loss of affinity in the Y₁R (Merten et al., 2007; Walker et al., 1994). The recent crystallography studies and computational modelling of the Y₁R have also confirmed ECL2 makes close contact with N-terminal region of NPY and plays an important role in the recognition of the NPY N-terminus (Yang et al., 2018). This study postulates that the Y₂R ECL2 may also interact with NPY, but via the central α -helix. Furthermore, the model revealed close contacts between [Leu³⁰] of NPY and [Ile²⁹³] in ECL3 between [Arg³³] of NPY and [Asn^{7.32}] of the Y₁R. Disulphide bridges formed between the ECLs and TMs have been suggested to contribute to stabilising the highly ordered secondary structure of the receptor (Katritch et al., 2012; Peeters et al., 2011). This is shown through the highly conserved cysteine residues of ECL2 and TM3 present in all known GPCR Class A structures, and the presence of several subtype specific disulphide bonds (Venkatakrishnan et al., 2013).

1.2.5.2 Transmembrane helices and conserved motifs in receptor activation

As discussed above, upon ligand binding of a GPCR, the receptor undergoes a conformation change via a mechanism known as the “global toggle switch” (Section 1.2.1) which allows the receptor to engage with key parts of the G-protein. This mechanism of action was deduced from the crystallisation of the first GPCRs (Palczewski et al., 2000; Rasmussen et al., 2007). Within these papers it was noted that the [Glu^{3.49}] and [Arg^{3.50}] of the highly conserved E/DRY motif were connected to [Glu^{6.30}] and [Thr^{6.34}] of the TM6, creating salt bridges. The salt bridge between [Arg^{3.50}] and [Glu^{6.30}] is known as the “ionic

lock” and has been proposed to constrain GPCRs in an inactive conformation and has been observed in crystal structures of ligand free β_1 -AR (Huang et al., 2013) and inactive dopamine D₃ receptors (Chien et al., 2011). As such, it has been postulated that abolition of this interaction between TM3 and TM6 would result in activation of the receptor. This hypothesis is supported by mutagenesis studies that indicate the absence of the E/DRY motif results in constitutive activity in β_1 -AR and β_2 -AR (Ballesteros et al., 2001; Rasmussen et al., 1999) and the A_{1B} adrenoceptor (Scheer et al., 2000). However, the role of the E/DRY motif has been the topic of much debate due to the fact that most Class A GPCRs cannot form an ionic lock. This is supported by the fact that only a small percentage of receptors contain an acidic residue at position 6.30 and the general absence of the ionic lock in the inactive state of GPCR crystal structures, suggesting that the interaction is not as essential to receptor activation as initially proposed (Tehan et al., 2014). Furthermore, some GPCRs, such as dopamine D₂ and cannabinoid receptor 2, have demonstrated a loss of G-protein dependent signalling following mutations of the [Arg^{3.50}] residue (Feng and Song, 2003; Kim et al., 2008) indicating that the E/DRY motif is involved in G-protein coupling as well as stabilising specific receptor states. This is further supported by the active crystal structure conformations of β_2 AR-G protein and adenosine A_{2A}-G protein complexes showing an interaction between [Arg^{3.50}] and the $\alpha 5$ helix of the G-protein (Carpenter et al., 2017; Rasmussen et al., 2011b).

In addition to the E/DRY motif, the NPxxY motif and the CWxP motif have also been suggested to play a role in receptor activation and are highly conserved in Class A GPCRs. The NPYxxY motif is found at the base of TM7 and is separated from the E/DRY motif by a hydrophobic barrier created by residues present in TM2 and 3, and [Trp^{6.48}] within the CWxP motif in TM6 (Balaraman et al., 2010; Bhattacharya et al., 2008). Structures of free ligand rhodopsin receptors have demonstrated that upon receptor activation the “toggle switch” residue, [Trp^{6.48}], disrupts this hydrophobic barrier resulting in conformational rearrangement of [Thr^{7.53}] within the NPxxY motif, thereby

allowing interactions between [Tyr^{5.58}] and the conserved [Phe^{6.52}] residues present within the intracellular helix 8 via its aromatic side chains (Park et al., 2008). This movement then promotes the formation of a hydrogen bonding water network from the CWxP motif to the E/DRY motif and the G-protein (Trzaskowski et al., 2012). Furthermore, mutations of the extended NPxxY motif have also been evidenced to effect receptor behaviour in terms of receptor expression, sequestration and ligand affinity (Fritze et al., 2003). These structures suggest a commonality in the activation of conformational change by ligand binding in Class A GPCRs, as well as providing insight into the selectivity of receptor coupling to different classes of G-proteins.

1.2.5.3 G-protein dependent signalling

GPCRs are able to mediate their large array of cellular responses and physiological roles through the diversity of their receptor subclasses (Section 1.2.1), intracellular signalling and tissue expression. The mainstay of GPCR signalling is mediated through interaction, activation and subsequent dissociation of the heterotrimeric G-protein. The original crystal structure studies of the β_2 AR-G protein complex allowed for further analysis into the interactions that occur between GPCRs and the G_α subunit (Rasmussen et al., 2007). Recent advancements in CryoEM are now allowing the interactions between the receptor and effectors, e.g. G-proteins and β -arrestins, to be observed more readily (Draper-Joyce et al., 2018; García-Nafría et al., 2018b, 2018a; Liang et al., 2018).

It is now generally accepted that upon agonist binding, conformational changes within a GPCR promotes receptor interaction with cytoplasmic heterotrimeric G-proteins (Duc et al., 2015; Mahoney and Sunahara, 2016; Oldham and Hamm, 2008). In the inactive state a G-protein consists of a guanosine diphosphate (GDP)-bound $G_{\alpha\beta\gamma}$ unit, with GDP bound at the G_α subunit. Upon ligand activation of the GPCR, GDP is substituted for guanosine triphosphate (GTP), resulting in the dissociation of the $G_{\alpha\beta\gamma}$ into two distinct subunits, producing a $G_{\beta\gamma}$ subunit and a GTP-bound G_α subunit. These subunits

modulate the activity of different cellular effectors such as adenylyl cyclase (AC) and phospholipase C (PLC; Wootten et al., 2018). Signalling is then terminated through the hydrolysis of GTP to GDP, performed by intrinsic GTPase activity of the G_{α} subunit, allowing for the re-association of the now GDP-bound G_{α} to the $G_{\beta\gamma}$ (Figure 1.7)

It is also important to note that the α -subunit can exist in different isoforms. These isoforms can be separated into 4 broad classes; α_s , α_q , $\alpha_{12/13}$ and α_i . $G_{\alpha s}$ proteins are positively linked to the activation of AC. The AC enzyme then catalyses the production of cyclic adenosine monophosphate (cAMP) from ATP (Steegborn, 2014). cAMP then activates protein kinase A (PKA) which phosphorylates targets such as ion channels and transcription factors. cAMP has also been demonstrated to regulate multiple processes including ion transport and vesicle trafficking through cAMP dependent mediators such as Epac and small GTPases (Fertig and Baillie, 2018). In addition, cAMP inhibits the release of Ca^{2+} from intracellular stores. The $G_{\alpha i}$ protein is negatively linked to AC (Figure 1.7). The $G_{\alpha q}$ subunit is positively linked to PLC which initiates increased levels of inositol trisphosphate (IP_3) and diacylglycerol (DAG) within the cell, resulting in calcium release and protein kinase C (PKC) activation into the intracellular environment, respectively (Kamoto et al., 2017). $G_{\alpha_{12/13}}$ interacts with the small monomeric GTPase, RhoA (Siehler, 2007) which is involved in the remodelling of the actin cytoskeleton (Narumiya and Thumkeo, 2018).

As such, receptor-G protein coupling, and subsequent intracellular signalling is dictated by the G-protein, with some receptors coupling primarily to one G-protein subtype, and others being more promiscuous and activating multiple subtypes (Premont and Gainetdinov, 2007; Tuček et al., 2002). Despite the defined role of G proteins in GPCR signal transduction it has also been suggested that GPCRs are able to signal through G-protein independent pathways, for example, β -arrestin2 mediated (Smith and Rajagopal, 2016), and mitogen-activated protein kinase mediated (Azzi et al., 2003; Luttrell, 2005).

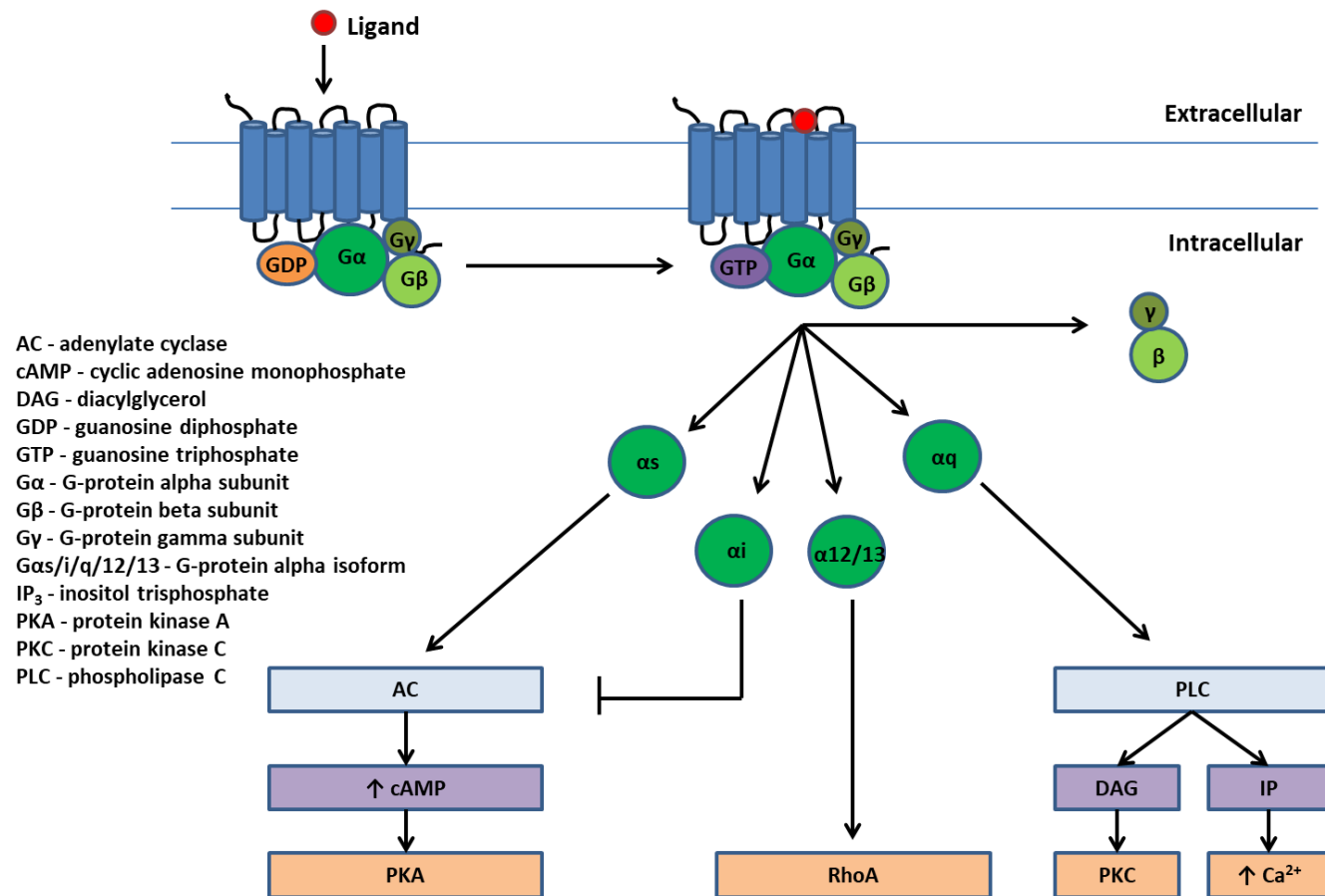


Figure 1.7 - GPCR signalling cascade through G-protein interactions, demonstrating the induction of different second messenger signals, dependent on the α subunit involved.

In the case of the Y family of receptors, all subtypes are known to couple to G_{io} proteins, resulting in decreased cAMP and second messenger signalling (Foord et al., 2005; Holliday et al., 2005). It has also been demonstrated that this signalling is largely G-protein dependant and is not known to occur through G-protein independent pathways (Kilpatrick et al., 2010).

1.2.6 GPCR life cycle

1.2.6.1 GPCR desensitisation

Following receptor activation by ligand binding and signalling through G-protein interactions, the GPCR often undergoes desensitisation, resulting in cessation of G-protein signalling. One method of desensitisation that occurs in GPCRs is through G-protein subunit uncoupling which is often mediated through a homologous method of agonist induced binding i.e. the receptor must be ligand bound and in the active conformation (Kelly et al., 2008). Heterologous desensitisation occurs through phosphorylation of unoccupied receptors via PKA or PKC and therefore occurs independently of ligand binding (Luttrell and Gesty-Palmer, 2010). After desensitisation occurs, the receptor may undergo internalisation. Internalisation is the process of internalising the receptor into the cell via early endosome vesicles (Figure 1.8).

The most commonly described mechanism for homologous desensitisation and internalisation is initiated through initial phosphorylation of the receptor at serine/threonine residues in the C-terminus or ICL3, and the subsequent recruitment of the effector protein, arrestin (Marchese et al., 2008; Moore et al., 2007). The phosphorylation step is carried out by a family of proteins known as G-protein coupled receptor kinases (GRKs; Evron et al., 2012; Rajagopal and Shenoy, 2018). GRKs were first identified through studies of β_2 -AR phosphorylation (Benovic et al., 1986). Subsequently, seven GRK isoforms have been identified, with GRK2 and GRK3 being the most widely expressed. Following GRK mediated phosphorylation of the receptor, the mediator, arrestin, binds to the agonist-activated phosphorylated GPCR and aids in the uncoupling of the GPCR and G-protein subunits, initialising

internalisation. There are three well established groups of arrestins; visual, non-visual (β -arrestins) and α -arrestins (Kang et al., 2014). The visual arrestin sub-family consists of arrestin 1 and 4, and are localised to the visual system, whereas the two members of the β -arrestin sub-family (β -arrestin1 and β -arrestin2 or arrestin-2 and arrestin-3, respectively) are ubiquitous.

1.2.6.2 GPCR clathrin mediated endocytosis

The arrestin recruitment process targets the GPCR for internalisation through a clathrin / dynamin dependent pathway. The binding of β -arrestin causes a conformational change in the arrestin protein allowing it to bind both clathrin and adaptor protein-2 (AP-2; Goodman Jr et al., 1996; Smith and Rajagopal, 2016). AP-2 then utilises arrestin as a scaffolding protein to imbed into the membrane, promoting clathrin assembly (Kang et al., 2014). Clathrin is a protein consisting of heavy and light chains that bind to one another and form a lattice-like frame work that surrounds the vesicle (Popova et al., 2013). Clathrin then binds the imbedded AP-2 causing distortion of the membrane and the formation of clathrin-coated pits. These pits are then pinched from the membrane to form a vesicle via the GTP hydrolysis action of dynamin proteins (Hinshaw, 2012). Once the vesicle is fully formed the clathrin / AP-2 complexes dissociate, and endocytosis of the receptor into the early endosome is complete (Popova et al., 2013; Figure 1.8).

The YR family has been shown to desensitise through a β -arrestin dependant mechanism. The Y_1R associates to β -arrestin2 following GRK mediated phosphorylation of clusters of serine / threonine residues in the C-terminus (Holliday et al., 2005). It has since been demonstrated that the number, not location of these phosphorylated residues are important for arrestin recruitment (Kilpatrick et al., 2010). The Y_1R has been reported to rapidly internalise following agonist exposure via a clathrin dependent mechanism (Ouedraogo et al., 2008; Pheng et al., 2003). The Y_4R has also been demonstrated to undergo the same internalisation process as the Y_1R (Berglund et al., 2003; Parker et al., 2001). However, the Y_2R has been found

to internalise at a slower rate than the Y₁R (Ouedraogo et al., 2008; Parker et al., 2001). It has recently been demonstrated that the interaction of Y₂R with β -arrestin2 is shorter lived than at the Y₁R and that the interaction is weaker at the Y₂R (Wanka et al., 2018). β -arrestin2 is also suggested to interact in a different orientation with the Y₂R compared to the Y₁R, and this has been suggested as an explanation for the slower internalisation rate of the Y₂R. These differences in β -arrestin2 association are consistent with the findings of other GPCR families (Cahill et al., 2017). However, the relative difference observed between Y₁R and Y₂R internalisation is often dependent on the agonist concentration used for comparison, and the duration of the measurement (Böhme et al., 2008; Kilpatrick et al., 2012; Lindner et al., 2009; Walther et al., 2010). The internalisation process of the Y₅R has also been suggested to occur through a clathrin dependent pathway, however, the rate of internalisation is much slower than that of other YR subtypes (Böhme et al., 2008; Parker et al., 2003). It has been suggested that the observed slow internalisation may be due to the significant structural difference of this receptor, which expresses a longer ICL3 and shorter C-terminus as discussed previously (Section 1.1.2.4).

1.2.6.3 Receptor sorting and lysosomal degradation

Once internalised into the early endosome the receptor complexes have a number of possible fates. They can either be trafficked to lysosomes for degradation, or be recycled back to the plasma membrane resulting in re-sensitisation (Marchese et al., 2008). The process of recycling involves the dissociation of agonist from the receptor. This process is aided by the acidic environment of the early endosome along with de-phosphorylation of the receptor, resulting in disassembly of the internalisation complexes. Upon entry into the endosome, GPCRs undergo sorting via ubiquitin-dependent or independent processes (Kennedy and Marchese, 2015). Ubiquitin dependent pathways involve GPCR interaction with the endosomal sorting complexes required for transport (ESCRT). There are four ESCRT machinery complexes; 0, I, II and III (Raiborg and Stenmark, 2009). Receptors that have been covalently

tagged with ubiquitin, by E3 ligases, are bound by ESCRT complexes 0-II at ubiquitin binding domains and are then sorted into multivesicular bodies. ESCRT machinery complexes work co-operatively with one another to form intraluminal vesicles within multivesicular bodies. They then direct ubiquitinated cargo to the intraluminal vesicles and the lysosome where they may be degraded (Figure 1.8).

Studies have shown rapid recycling of the Y₁R back to the membrane through expression of recycling motifs in the C-terminus (Ouedraogo et al., 2008), and when internalised, the Y₁R co-localises with markers of endosomal recycling compartments, such as transferrin (Holliday et al., 2005; Kilpatrick et al., 2010). The Y₂R has also been suggested to recycle following internalisation via the presence of similar recycling motifs in the C-terminus of the receptor (Walther et al., 2010). The Y₄R has also been demonstrated to recycle back to the membrane but does so at a much lower percentage than the Y₁R (Parker et al., 2001). As discussed above, the Y₅R has been shown to desensitise and internalise slowly, suggesting a degradative removal path (Parker et al., 2003; Section 1.2.6.2).

Although the process of desensitisation, internalisation and trafficking has traditionally been considered a regulatory process, there has been an increasing number of studies providing evidence that GPCRs can also signal from within the endosomes and that the endosomes act as GPCR signalling compartments through G-protein dependent and independent processes (Pavlos and Friedman, 2017; Tsvetanova et al., 2015). This has been evidenced through recent studies that have revealed that arrestins may act as scaffold proteins for signalling molecules such as ERK (Strungs and Luttrell, 2014), whereby β_1 -AR signalling was shown to transactivate ERK1/2 through β -arrestin and the endothelial growth factor receptor to promote cardiac myocyte growth.

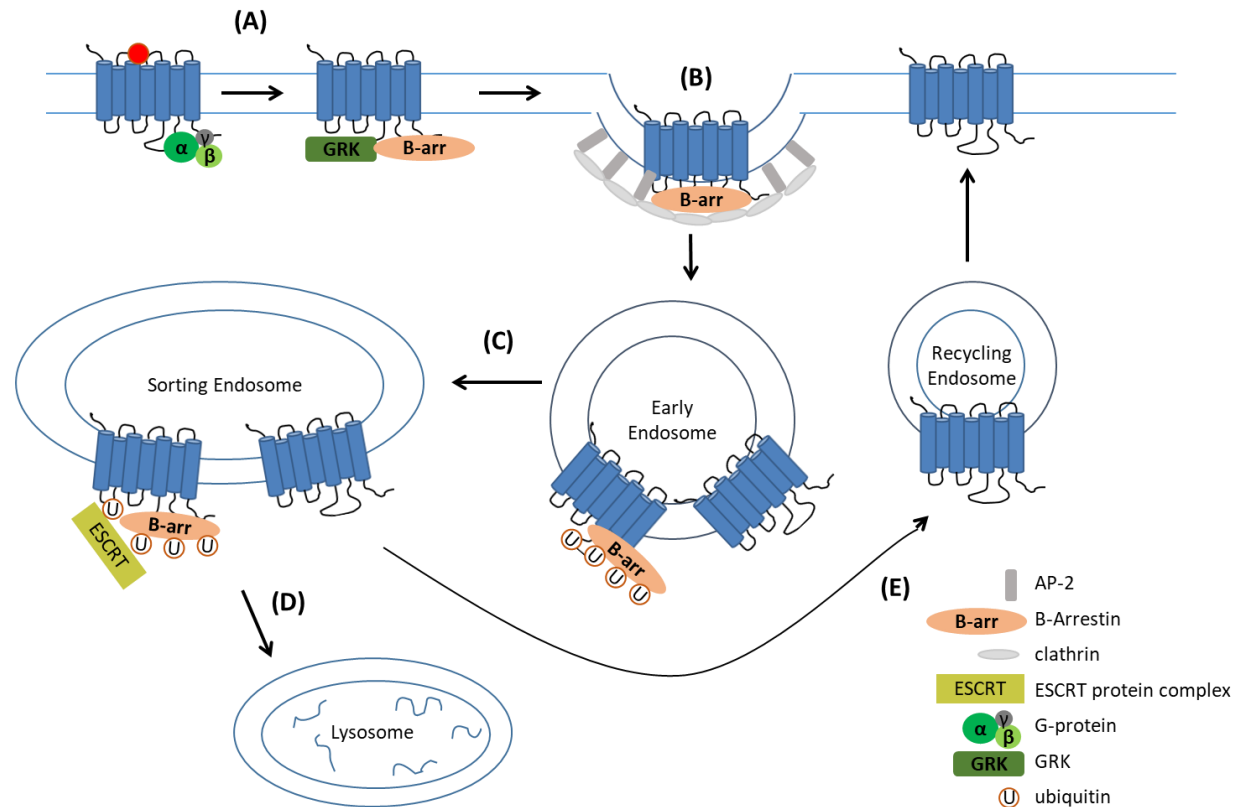


Figure 1.8 - Receptor life cycle. (A) Ligand binding results in G-protein uncoupling and signalling, resulting in the recruitment of GRK and phosphorylation of the receptor. The receptor is then bound by β -arrestin causing desensitisation of the receptor. (B) Desensitisation then leads to the recruitment of AP-2 and clathrin to the scaffold protein, β -arrestin, resulting in the formation of clathrin-coated pits. These clathrin-coated pits are then internalised into the cell to form the early endosome. (C) From the early endosome the receptors are sorted into either a (D) degradative or (E) recycling and resensitisation pathway.

Endosomal signalling of GPCRs has also been suggested because G-protein signalling complexes co-internalise with GPCRs and can regulate sustained signalling of cAMP from the endosome. This has been demonstrated in receptor subtypes such as the parathyroid hormone receptor (Feinstein et al., 2011; Gidon et al., 2014).

1.2.7 GPCR oligomerisation

GPCRs are traditionally viewed as single monomeric units, however this view has been challenged by the discovery that GPCRs can form homo- and hetero-oligomers. The formation of these distinct functional units can have potential effects on receptor functions including; signalling, ligand pharmacology, internalisation and trafficking, thereby having major implications for the physiological roles of these receptors, and their pharmacological targeting in disease (Farran, 2017). Despite the controversy surrounding this area of study, evidence of dimerisation has been demonstrated in several receptor systems. Examples include; dopamine D₂ receptors (Guo et al., 2008), β_1 -AR and β_2 -AR (Dorsch et al., 2009), adenosine A₁ and A₃ receptors (May et al., 2011), cannabinoid CB₁ and orexin OX₁ receptors (Ward et al., 2011) and chemokine CXCR₃ and CXCR₄ receptors (Watts et al., 2013).

1.2.7.1 Y receptor oligomerisation

Y₁R, Y₂R and Y₅R receptor homodimerisation has been shown, in vitro, to occur on the cell surface with the employment of fluorescence resonance energy transfer (FRET) analysis, which identifies labelled receptors in close proximity (<10 nm; Dinger et al., 2003). It has also been suggested that this homodimerisation occurs independently of ligand. Studies around Y₄R homodimerisation have suggested that ligand presence may actually cause dissociation of this receptor homodimer (Berglund et al., 2003). Contradictory studies have also suggested that dimerisation of the Y₁R is not observed in bioluminescence resonance energy transfer (BRET) assays in recombinant cell types (Felce et al., 2017). These conflicting data, which are common in GPCR dimer studies, highlight some of the limitations in FRET / BRET based analysis.

For example, resonance energy transfer signals indicating the presence of dimers are influenced strongly by expression levels of the receptors, particularly in transfected cells (Lohse et al., 2012). They also reflect numbers of receptor dimer complexes, but not the proportion of these complexes within the overall receptor population.

There is also longstanding interest in whether Y₁R and Y₅R may form heterodimers, and if so, whether this is relevant to their pharmacology or function. This interest was precipitated by the dual role of Y₁R and Y₅R in regulating NPY-mediated food intake in the hypothalamus (Section 1.1.5 and 1.1.6). The co-ordinated requirement of both receptors is suggested not only by the limited effect of Y₁R and Y₅R antagonists in inhibiting appetite (Section 1.1.4), but also by genetic evidence. For example, a study demonstrated that knockout mice lacking the Y₁R or Y₅R genes showed little to no change in eating habits, whereas those expressing a double Y₁R/Y₅R knockout demonstrated reduced food intake following a 24 h fasting period, and significantly reduced body mass (Nguyen et al., 2012). These findings suggest that the presence of both receptors is required to induce the appetite regulation observed in the central administration of NPY. Additionally, Y₁R and Y₅R are co-expressed in cells within the ARC and are located on opposite and overlapping chromosomal regions (Wraith et al., 2000), suggesting that they are co-regulated.

Several studies have been conducted in vitro to investigate the nature of this dimerisation, which was originally observed by BRET in Y₁R/Y₅R co-expressing cells (Berglund et al., 2003; Gehlert et al., 2007). This study suggested that following agonist stimulation the level of Y₅R internalisation increases when in the presence of Y₁R, supporting the previous suggestion that both subtypes may internalise as a complex (Berglund et al., 2003). This study also showed that internalisation was dependent on agonist occupancy of both receptor types. However, Böhme et al., (2008) demonstrated that the Y₁R internalises alone when co-expressed with Y₅R, which would suggest that if association between two receptors does occur, it may be transient.

Kilpatrick et al., (2015) aimed to study the impact of Y₁R/Y₅R dimer complexes on ligand pharmacology by establishing a constrained Y₁R/Y₅R dimer system using bimolecular fluorescence complementation (BiFC). Several unique pharmacological characteristics were observed in the behaviour of Y₁R/Y₅R dimers, including modified agonist pharmacology, such as the lack of effect of Y₁R antagonists, and altered action of Y₅R antagonists. In this study CGP71683, a Y₅R selective antagonist, exhibited non-surmountable antagonism at Y₁R/Y₅R dimers compared to the surmountable antagonist observed in the Y₅R population alone, and had no effect in the Y₁R population. This response was also observed in two further, structurally unrelated non-peptide Y₅R antagonists; L152804 and NPY5RA972. A similar change in surmountable to non-surmountable antagonism behaviour was also observed in Y₁R/Y₅R co-expressing cells, when the receptor partners were not linked by BiFC (Gehlert et al., 2007). These studies provide evidence that heterodimeric complexes may show allosteric communication between Y₁R and Y₅R binding sites, providing novel “heterodimer” pharmacology. However, further progress, particularly in vivo, is limited by the lack of tool ligands that can exploit these characteristics to target homo- or hetero-dimers more selectively, and therefore provide evidence for or against their relevance in native systems, such as hypothalamic neurons.

1.2.8 Multivalent ligands

In respect to this challenge of oligomerisation, a recent facet in GPCR drug discovery is the exploration of use of bitopic, or multivalent, ligands to produce enhanced affinity and selectivity for the target receptors under investigation. Most commonly, these ligands have been based on chemically linking an orthosteric and allosteric pharmacophore such that the novel bitopic ligand engages both sites within the same receptor protein simultaneously. The most common examples to date are based on acetylcholine and adenosine receptor orthosteric and allosteric agonists. For example, the novel ligand THRX-160209 was developed to simultaneously bind the orthosteric site and a known allosteric site that lie in close proximity in muscarinic M₂ acetylcholine

receptors (mAChR; Steinfeld et al., 2007). This ligand showed M₂ affinity that was several orders or magnitude higher than monovalent derivatives and a high level of selectivity over other mAChR subtypes. In addition, it showed a faster dissociation rate from the receptor when competing with monovalent ligands that are known to interact with either the orthosteric or allosteric site, suggesting coordinated binding at both sites contribute to ligand binding. All of these characteristics suggest that THRX-160209 binds the M₂ in a multivalent manner. In addition, ligands such as PD81,723 and LUF6258 were synthesised in order to investigate the location of the allosteric binding site of adenosine A_{1A} receptor (Narlawar et al., 2010). These ligands were developed with the rationale of increasing linker lengths in order to search for the exact location of the allosteric binding site in relation to the orthosteric site. It was concluded that the LUF6258 compound, with a short 9 carbon linker, showed increased efficacy compared to monovalent parent molecules, suggesting that the allosteric and orthosteric sites are in close proximity.

Furthermore, the same approach of multi- and bi-valent ligands has increasingly been used to target and exploit the novel pharmacology offered by homo- and hetero- oligomeric receptor complexes. Examples of bivalent and multivalent ligands that have been described for oligomeric receptor complexes include; dopamine D₂ / neurotensin (NTS) ₁R (Hubner et al., 2016; Kopinathan et al., 2016), cannabinoid CB₁ / CB₁ (Glass et al., 2016) and the opioid receptor systems (Bhushan et al., 2004; Vagner et al., 2008).

As D₂R and NTS₁R play major roles in the pathophysiology of neurological and psychiatric disorders such as Parkinson's disease and schizophrenia, the D₂R/NTS₁R heterodimer may be a promising pharmacological target (Binder et al., 2001). As such, bivalent ligands were developed to aid in the exploration of these heterodimers. Bivalent ligands expressing 3 different dopamine pharmacophores (antagonists, eticlopride and piperazine, and agonist aminoindane) were attached to the NTS₁R agonist, NT(8-13), via a varying length polyglycol-based linker (1-4 subunits) and a lipophilic appendage

(Hubner et al., 2016). The bivalent ligands showed picomolar affinity in cells co-expressing both D₂R and NTS₁R, and selectivity of up to three orders of magnitude when compared with cells expressing D₂R alone.

In addition, to the development of bivalent ligands as targets for known heterodimers such as the D₂R/NTS₁R, bivalent ligands have also been used to help elucidate dimeric interactions such as the heterodimer interactions of δ and κ opioid receptors (Bhushan et al., 2004). This study developed δ - κ bivalent ligands through the conjugation of δ selective antagonist, NTI, and κ selective antagonist, 5'-GNTI, with varying space lengths. It was found that the bivalent ligand KDN-21, containing a 21-atom spacer, exhibited selective antagonist activity at both the δ and the κ opioid receptors, with substantially greater affinity in co-expressing cells when compared to monovalent parent analogues. These results supported the previously suggested heterodimerisation of the δ - κ opioid receptors (Portoghese and Lunzer, 2003) and allowed for further insight and investigation of this heterodimer complex.

Bivalent ligands have also been developed to target receptors that do not dimerise, but may play a role in the same physiological functions and therefore a dual target ligand may result in increased efficacy of the drug. For example, a recent study has described the development of a chimeric peptide, EP45, targeted towards both the GLP-1 receptor and Y₂R (Chepurny et al., 2018). EP45 was designed as a monomeric agonist ligand that expresses amino acid motifs present in the blood glucose lowering agent, exendin-4, and the appetite suppressing, PYY₃₋₃₆. FRET assays showed that EP45 replicates the action of exendin-4 by stimulating cAMP production via the GLP-1 receptor, while also replicating the action of PYY₃₋₃₆ through inhibition of cAMP production via Y₂R. Such findings present a new drug development strategy, in which the co-existing metabolic disorders of type II diabetes and obesity could be treated using a single peptide ligand that lowers levels of blood glucose by GLP-1 receptor mediated effects, while simultaneously suppressing appetite via the Y₂R.

It can be challenging to interpret the mode of action of these bivalent ligands. For example, it is hard to rule out that the observed effects are not a result of independent actions of the “linked” pharmacophores on the receptors concerned, or if changes in affinity and selectivity that arise are due to a more extensive binding interface of the larger ligand. This means that a mechanism that, in systems that require bivalent ligand targeting of heterodimers or homodimeric receptors, selectivity of the compound is less easy to establish conclusively. However, the development of these bivalent ligands exemplifies the power of this approach for the development of pharmacological tools to investigate the association of different GPCRs in an oligomeric states.

Bivalent peptides have been a feature of YR ligand pharmacology for a number of years, including the dimeric Y₁R antagonist peptide GR231118 (Daniels et al., 1995) and other, more recent, examples such as the Y₄R agonist peptide series based on BVD74-D (Kuhn et al., 2017). The earliest investigations noted the dramatically increased affinity of GR231118 (10 - 100 fold) compared to its monomeric precursor BVD15 (Daniels et al., 1995), which was much more than would have been predicted from a doubling in the concentration of the linked NPY C-terminal pharmacophore. Understanding the mechanism by which dimeric ligands such as GR231118 engage YR with high affinity could open new avenues for more effective NPY ligand design, and potentially routes to selectively targeting homo- and hetero- dimer YR complexes in future.

1.3 Aims of this thesis

In this thesis we have designed, synthesised and characterised novel non-fluorescent and fluorescent derivatives of GR231118 to explore effects on YR affinity, selectivity and receptor oligomerisation, with the ultimate aim of improving our understanding of the mode of action of bivalent ligands at the YR family. Chapter 3 describes the synthesis of novel GR231118 derivatives via a novel solid phase peptide synthesis route. In Chapter 4 cycle variant and alanine scanning variants of the GR231118 analogue were employed to probe the role of the cyclic moiety and specific amino acids residues within the

GR231118 compound in Y_1R interaction, as well as selectivity over Y_4R . Finally, in Chapter 5, we use novel fluorescent derivatives of BVD15 monomer and GR231118 dimer peptides to monitor ligand-binding stoichiometry at the Y_1R and the effects on receptor oligomerisation in living cells, via the application of fluorescence correlation spectroscopy and molecular brightness analysis.

Chapter 2

Materials and general methods

"What's your PhD on? Some kind of plant cells right?"

The Richardson Clan

2.1 Materials

2.1.1 Molecular biology materials

pcDNA vectors were purchased from Invitrogen (Paisley, UK). The GenElute gel extraction and PCR purification kits were purchased from Sigma-Aldrich (Poole, UK). QIAprep spin Miniprep and Maxiprep kits were purchased from QIAGEN (Manchester, UK). Restriction enzymes, alkaline phosphatase, T4 DNA ligase and pJET cloning kits were obtained from Fermentas (St Leon-Rot, Germany). 1 Kb DNA ladder was purchased from Promega (Madison, WI, USA). Accuzyme enzyme was purchased from Bioline (London, UK). Additional general molecular biology reagents were purchased from Sigma-Aldrich (Poole, UK). TOP10F' and XL-1 chemically competent cells were purchased from Thermo-Fisher Scientific (Loughbrough, UK) or prepared by Marleen Groenen (University of Nottingham, UK), respectively, and were stored in experimental aliquots at -80°C. All materials were stored as per manufacturers' instructions unless otherwise stated.

2.1.2 Cell culture materials

HEK293T cells (ATCC number; CRL-1573), lipofectamine and the selection antibiotics; zeocin, hygromycin and blasticidin, were purchased from Invitrogen (Paisley, UK). Dulbecco's modified eagles medium (DMEM), foetal bovine serum (FBS), phosphate buffered saline (PBS), Poly-D-lysine and trypsin were purchased from Sigma-Aldrich (Poole, UK). All cell culture plastic ware and Nunc Lab-tek 8-well cover-glass plates (155411) were purchased from Thermo-Fisher Scientific (Loughborough, UK) unless otherwise stated. All items were stored as recommended by the manufacturer.

2.1.3 Cell assay materials

Neuropeptide Y (NPY), peptide YY (PYY), pancreatic polypeptide (PP), GR231118, and all other peptides were purchased from Bachem (Bubendorf, Switzerland), unless otherwise stated. BIBO3304 trifluoroacetate was obtained from Tocris Bioscience (Bristol, UK). Compounds were stored as single use aliquots at -20°C, diluted in double distilled water (ddH₂O), with the exception

of BIBO3304 which was dissolved in dimethyl sulphoxide (DMSO). Non-dissolved stock compounds were stored as instructed, either at room temperature (RT) or at -20°C. SNAP tag substrates were purchased from New England BioLabs (Ipswich, MA, USA) and stored at -20°C in DMSO. All novel peptides were synthesised as described in Chapter 3 and stored in Eppendorf tubes as single use aliquots at -20°C diluted in ddH₂O, fluorophore tagged peptides were stored in opaque Eppendorf tubes. Rhodamine 6G (Rh6G) and Cyanine 5 (Cy5) stocks for fluorescence correlation spectroscopy (FCS) calibrations were purchased from Invitrogen (Loughborough, UK) and GE healthcare (Buckingham, UK), respectively, and stored in single use experimental aliquots at -20°C in ddH₂O. All other consumables were purchased from Sigma-Aldrich (Poole, UK) or Thermo-Fisher Scientific (Loughborough, UK) unless otherwise stated and stored as per manufacturers' instructions.

2.1.4 Peptide synthesis materials

All solvents were obtained from Merck and Sigma Aldrich and were of analytical grade (Castle Hill, NSW, Australia). All Fluorenylmethyloxycarbonyl chloride (Fmoc) protected amino acids were purchased from ChemImpex (Wood Dale, IL, USA) along with Rink amide resin. All commercially obtained chemicals were used without further purification. LCMS vials and silicone liners were purchased from Adela Scientific (Thebarton, SA, Australia). All other plastic consumables were purchased from GreinerBio (Kremsmunster, Austria) unless otherwise stated.

2.2 Molecular biology methods

2.2.1 Pre-existing Y receptor and β -arrestin2 constructs

A summarised list of all constructs generated and used for this thesis can be found in Table 2.1. All constructs described were initially made by Dr. Laura Kilpatrick, Mrs Marleen Groenen or Dr. Nicholas Holliday (Kilpatrick et al., 2012; Liu et al., 2016). The strategies of DNA vector construct production and

maintenance are outlined below, with the use of specific constructs as examples.

For SNAP tagged receptors the rat Y₁ receptor or human Y₄ receptor cDNA (Y₁R and Y₄R; Genbank ref. Z11504 and NM_005972, respectively) were placed into a commercially available pcDNA3.1 (+) zeo vector containing the SNAP coding region (New England Biolabs; Hitchin, UK). This vector contains a human cytomegavirus immediate - early (CMV) promoter for high expression in mammalian cells and a bovine growth hormone (BGH) sequence for polyadenylation of mRNA (Figure 2.1). It also contains resistance genes for the antibiotics ampicillin and zeocin for selection in *E.coli* and mammalian cells, respectively. In addition, it contains the T7 promoter and BGH reverse sites for DNA sequencing. The SNAP tag was placed into the multiple cloning site of this vector between the KpnI and BamHI restriction sites with the 5-HT₃ receptor signal sequence (amino acids MRLCIPQVLLALFLSMLTGPGEGRK) placed upstream to facilitate membrane integration.

For BiFC constructs, rat Y₁R, human Y₄R or human β -arrestin2 (Genbank ref; NM_004313) cDNA was placed into commercially available pCMV FLAG vector (Clontech, Saint-Germain-en-Laye, France) or pcDNA3.1(+) vectors. The pCMV FLAG vector contains a FLAG tag epitope (MDYKDDDDK), which allows for receptor identification through antibody live labelling (Figure 2.2). This vector also contained a pCMV promoter to allow for high receptor expression and a polyadenylation signal, as with the pcDNA3.1 (+) zeo vector.

For tetracycline inducible constructs, rat Y₁R or human Y₄R was placed into a commercially available pcDNA4/TO vector (Figure 2.3; New England Biolabs; Hitchin, UK). This vector contains a pCMV promoter in conjunction with two tetracycline operator sequences inserted between the TATA box and the transcription initiation start site within the CMV promoter. This allows for binding of the tetracycline repressor protein, made independently, resulting in the suppression of the receptor DNA expression in the absence of tetracycline.

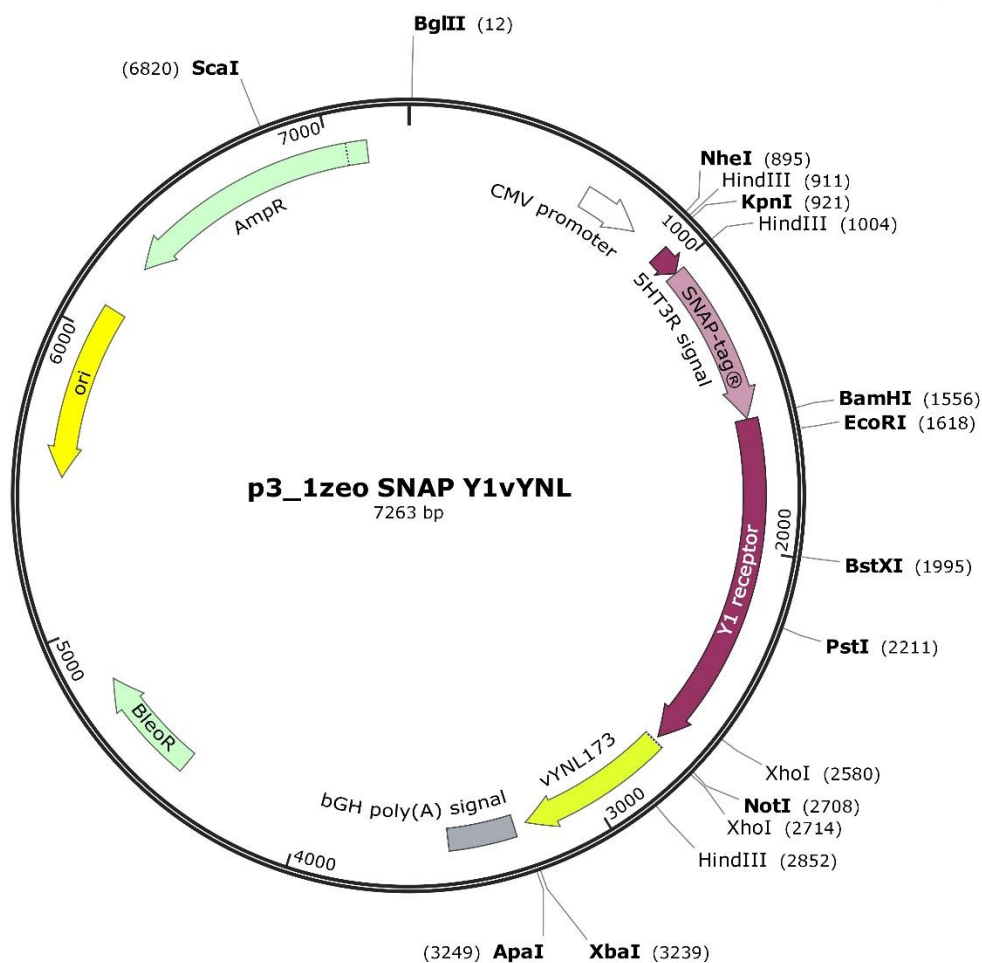


Figure 2.1 – Representative example of expression vector for pcDNA3.1 (+) zeo SNAP-Y₁R-Ynl receptor construct. This figure shows a vector map of the pcDNA3.1 zeo SNAP Y₁-Yn. The NPY Y₁R cDNA was inserted into the vector downstream of the SNAP sequence between BamHI and NotI restriction enzyme sites. A BiFC fragment tag, Yn, was inserted downstream of the receptor cDNA between XhoI and XbaI giving the linker of LRPLE, producing the SNAP-receptor-Yn in frame cDNA. Additional features in the vector, including key restriction enzyme sites and antibiotic resistance genes, are also highlighted.

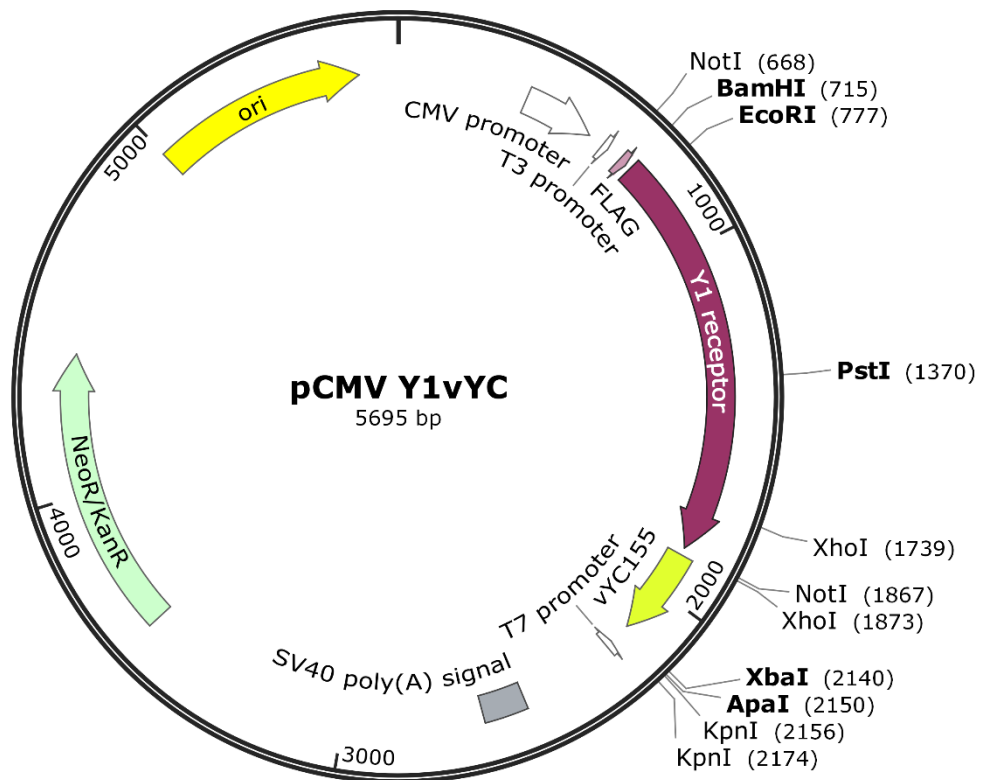


Figure 2.2 – Representative example of expression vector for pCMV-Y₁-Yc receptor construct. A vector map of the pCMV Y₁-Yc. As NotI could not be used in this vector due to an additional NotI site upstream of the FLAG tag, the receptor cDNA sequence was first inserted into a pcDNA3.1 (+) zeo vector between BamHI and NotI, as with the SNAP-Y₁R-Ynl described above, allowing for the addition of the Yc fragment between NotI and XbaI. The entire Y₁R-Yc cDNA was then inserted into the pCMV vector downstream of the FLAG tag between BamHI and ApaI restriction enzyme sites, giving the pCMV-receptor-Yc in frame cDNA. Additional features in the vector, including key restriction enzyme sites and antibiotic resistance genes, are also highlighted.

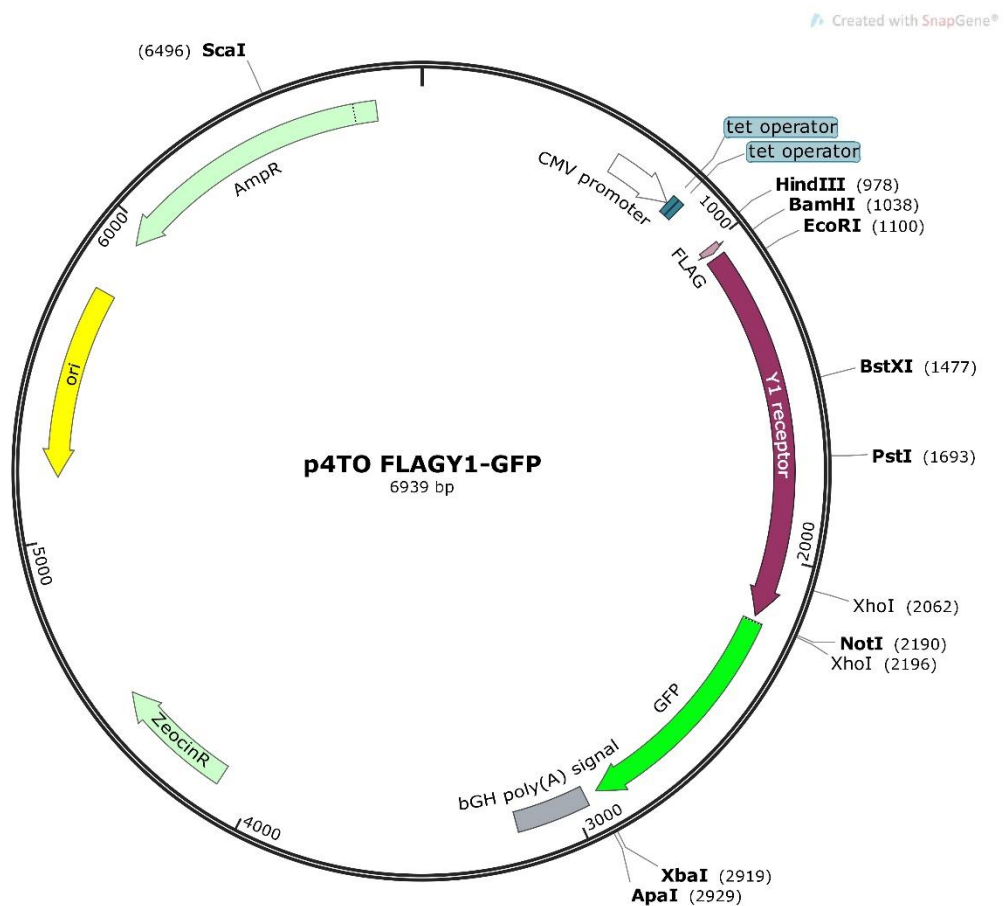


Figure 2.3 – Representative example of expression vector for pcDNA4/TO-Y₁-GFP receptor construct. A vector map of the pcDNA4/TO Y₁-GFP. As with the pCMV vector the receptor-GFP was inserted downstream of the FLAG tag epitope after construction of the receptor-GFP in the pcDNA3.1 (+) zeo vector. The receptor was inserted into the pcDNA3.1 (+) zeo vector between BamHI and NotI, and the full length super folded GFP tag was then inserted between NotI and XbaI restriction enzyme sites. The entire Y₁R-GFP cDNA was then inserted into the pcDNA4/TO vector following a BamHI and ApaI restriction enzyme digest, giving the pcDNA4/TO-receptor-GFP in frame cDNA. Additional features in the vector, including key restriction enzyme sites and antibiotic resistance genes, are also highlighted.

2.2.2 Restriction enzyme digestion

Restriction enzymes or, restriction endonucleases, are enzymes that recognise and cut DNA at particular nucleotide sequences called recognition sites. This process results in specific cleavage of the double stranded DNA to generate blunt or cohesive ends, depending on the enzyme. Restriction digests were typically performed in sterile 0.5 mL micro-centrifuge tubes using 2 µg of DNA (2 µL of a 1 µg/ µL stock), 1 µL of each appropriate restriction enzyme and 2 µL of 10x fast digestion buffer in a final volume of 20 µL ddH₂O. The reaction mixture was then incubated on a heat block (1 h; 37 °C) to allow the enzymes to digest the DNA. Restriction enzymes were then inactivated (80 °C; 5 min followed by 65 °C; 15 min) prior to cooling the reactions to 4 °C until use.

2.2.3 Visualisation and isolation of DNA

Following restriction enzyme digestion of the DNA insert (Section 2.2.2) the desired DNA fragments need to be separated and isolated from the other DNA fragments produced during the digest. This was achieved through agarose gel electrophoresis, followed by the use of the GenElute gel extraction kit (Sigma-Aldrich; Poole, UK).

For separation of the DNA fragments via electrophoresis, a 1 % agarose gel was prepared by dissolving agarose powder in TBE buffer (89 mM Tris-base, 89 mM boric acid, 2 mM EDTA; pH 7.6) facilitated through microwave heating. Once cooled to hand touch temperature, ethidium bromide was added to the agarose (0.125 µg/ mL final concentration). The gel was then poured and allowed to set for at least 30 min. Ethidium bromide intercalates with DNA and fluoresces under ultraviolet (UV) light, therefore aiding in the visualisation and excision of DNA bands from the gel. Once set, the gel was placed in an electrophoresis tank and covered with TBE buffer. The gel was then loaded with 10 µL of 1 Kb DNA ladder and 20 µL of the digested DNA insert. The samples ran at 80 mV for 45 min to allow for satisfactory separation of the DNA fragments. The gel was then placed under a UV light, and using the ladder as a guide, the appropriate DNA band was excised from the gel and placed into a

pre-weighed 1.5 mL micro-centrifuge tube. The gel was exposed to as little UV light as possible to reduce the chance of DNA damage.

DNA purification via the gel extraction kit was performed using a silica binding spin column protocol. Silica binding columns employ a solid phase extraction method that relies on nucleic acids binding to the silica. Binding of the DNA to the silica is enhanced by the presence of a chaotropic salt (normally guanidine isothiocyanate) and alcohol (ethanol or isopropanol) which strips the hydrogen bonded water shell around the DNA macromolecule to facilitate silica binding. While bound to the silica the DNA is washed to remove sample impurities. The purified DNA is then eluted in water.

Using the GenElute gel extraction kit, solubilising solution was added to the pre-weighted tube containing the gel band at 3x the weight of the gel fragment. It was then incubated for 10 min at 58 °C. 1 gel volume of isopropanol was added and the solubilised gel solution was added to a silica column prepared by centrifugation with 500 µL preparation buffer (30 s; 12000 rpm). The solubilised gel was then centrifuged (30 s; 12000 rpm) and the flow through was discarded. The column was then washed with 500 µL wash buffer containing 80 % ethanol and centrifuged (30 s; 12000 rpm) and the flow through discarded. The column was centrifuged again (1 min; 12000 rpm) to remove any remaining wash solution, and the DNA was eluted in 50 µL ddH₂O into a sterile collection tube.

2.2.4 Alkaline phosphatase treatment and preparation of vector

Following vector DNA digestion (Section 2.2.2) the vector was treated with shrimp alkaline phosphatase (AP) to de-phosphorylate the sticky ends. This helps to prevent the vector fragment from re-ligating on itself and producing a high number of antibiotic resistant background colonies, which do not contain the desired inserted DNA. After restriction enzyme digestion, 2 µL of fast AP and 2 µL of fast AP buffer (supplied with enzyme; 10x concentrations; 100 mM Tris-HCl, 50 mM MgCl₂ 1M KCl, 0.2 % Triton-X-100, 1 mg/ mL BSA;

pH 8) was added to the digestion mix and incubated for 1 h at 37 °C. The mix was then heated to 75 °C for 10 min to inactivate the fast AP enzyme.

De-phosphorylated vector DNA was purified using the GenElute PCR purification kit according to manufacturer's instructions (Sigma-Aldrich). Firstly, the digest reaction was made up to 100 µL using sterile ddH₂O, then 500 µL of binding buffer was added. In a separate collection tube a silica binding column was prepared by the addition of 500 µL column preparation buffer, centrifugation (30 s; 12000 rpm) and the flow through discarded. The binding solution, containing the vector, was then added to the column, centrifuged (30 s; 12000 rpm) and the flow through discarded. The tube was centrifuged again (1 min; 12000 rpm) to remove any residual solution from the column. The column was transferred to a fresh collection tube and the vector DNA was eluted in 40 µL ddH₂O.

2.2.5 Ligations

Following preparation of the insert and the DNA vector (Section 2.2.2, 2.2.3 and 2.2.4) they were ligated together in a 1:3 vector:insert molar ratio. The volume, in µL, of required DNA was calculated based on the number of moles required and the actual concentration of each, on the assumption of an 80 % yield from DNA extraction and purification steps, starting with 2 µg of DNA. 50 ng of vector DNA was considered optimal for use in ligations, to promote closing of the ligated plasmid rather than production of concatemeric products. Therefore;

Equation 2.1 - To calculate the amount of purified vector or insert DNA.

$$= 2 \mu\text{g DNA} \times \left(\frac{\text{size of isolated insert or vector in kbp}}{\text{total original plasmid size in kbp}} \right) \times 0.8$$

Equation 2.2 - To calculate the amount of insert required in a ligation containing 50ng vector DNA.

$$\text{Insert needed (ng)} = \left(3 \times 50 \text{ ng} \times \left(\frac{\text{insert size in kbp}}{\text{vector size in kbp}} \right) \right)$$

Positive and negative ligation reactions were carried out in sterile micro-centrifuge tubes containing the appropriate amount of both vector and insert, with the negative control containing no insert, in 10 μL of ligase buffer (final concentration; 40 mM Tris-HCl, 10 mM MgCl_2 , 10 mM dithiothreitol, 0.5 mM ATP; pH 7.8) and 1 μL of T4 DNA ligase (1 U/ μL). Ligation reactions were incubated overnight at 16 °C. Following ligation, both positive and negative reactions were transformed into chemically competent cells (Section 2.2.6).

2.2.6 Preparation of competent cells and bacterial transformation

Luria Bertani (LB) broth was prepared using 4 g LB broth powder dissolved in 200 mL ddH₂O and sterilised by autoclaving. Agar plates were prepared using 7 g LB agar powder dissolved in 200 mL ddH₂O. The LB agar was then sterilised by autoclaving and allowed to cool to hand-hot temperature before the addition of appropriate antibiotic (ampicillin; 75 $\mu\text{g}/\text{mL}$). The LB agar was then poured out into Petri dishes and allowed to set.

Chemically competent cells from the XL-1 E.coli strain were defrosted on ice and 100 μL of cell suspension, per transformation, was added to an ice chilled 1.5 mL micro-centrifuge tube. 1.5 μL β -mercaptoethanol (1.4 M), was added to each tube and left to incubate on ice for 10 min before the addition of 5 μL of ligation reaction to the appropriate tube with gentle mixing. As a reducing agent β -mercaptoethanol acts to inactivate exposed nucleases and other proteins that may adversely affect transformation efficiency. The cells were then incubated on ice for a further 30 min. Following incubation, the cells were subjected to a 45 s heat shock at 42 °C to facilitate the uptake of DNA. The tubes were then returned to ice for 2 min followed by the addition of 400 μL of previously prepared LB broth. The cells were then shaken at 225 rpm for 1 h at 37 °C. 100 μL of the transformation mix was then streaked out, using ethanol and heat sterilised apparatus, onto the previously prepared agar plates containing the appropriate selection antibiotic. The plates were then incubated at 37 °C overnight. The following day resistant colonies, derived

from competent cells that had successfully taken up the DNA and contained the antibiotic resistance gene, were identified.

Commercial chemically competent TOP10F' cells were transformed via a similar method as XL-1 cells, using 17 μ L per transformation without β -mercaptoethanol treatment, and were subject to a 30 s heat shock at 42 °C.

2.2.7 Miniprep isolation and purification of DNA

Following transformation of the DNA vector into competent cells, a small-scale isolation and purification of the cDNA was carried out. Mini suspensions or Minipreps of resistant colonies, produced through transformations (Section 2.2.6) were grown. Miniprep isolations were then performed using an alkaline sodium dodecyl sulphate (SDS) lysis, followed by a silica binding spin column protocol according to manufacturer's instructions (QIAprep spin Miniprep, QIAGEN; Manchester, UK).

Resistant colonies were picked from the agar plates using a sterile pipette tip, and were then placed in 5 mL LB broth in a 30 mL universal tube containing appropriate selection antibiotic (100 μ g/ mL ampicillin). The Miniprep cultures were then grown overnight at 37 °C, shaking at 225 rpm. The following day 3 mL of the culture suspension was centrifuged (5 min; 4000 rpm) and the supernatant was discarded. The bacterial pellet was re-suspended in 250 μ L re-suspension buffer, P1 (50 mM Tris-Cl, 10 mM EDTA, 100 μ g/ mL RNase A; pH 8.0) and vortexed to aid in re-suspension, followed by the addition of 250 μ L lysis buffer, P2 (200 mM NaOH, 1% SDS). The reaction was gently mixed by inversion and left for no longer than 5 min. The reaction was then neutralised by the addition of 350 μ L neutralisation buffer, N3 (Sodium Acetate and chaotropic salt) gently mixed through inversion, and centrifuged (10 min; 12000 rpm) to remove precipitated cell debris, proteins and genomic DNA. The clear lysate was transferred to a silica binding column, prepared by centrifugation of 500 μ L preparation buffer through the tube (1 min; 12000 rpm). The lysate was centrifuged through the prepared column (1 min;

12000 rpm) and the flow-through was discarded. The silica tube was then washed through centrifugation (1 min; 12000 rpm) of 750 µL of wash buffer, PE (containing 80 % ethanol), the flow-through was discarded and the tube centrifuged again (2 min; 12000 rpm) to remove any remaining ethanol. The silica tube was then transferred to a clean 1.5 mL micro-centrifuge tube and 100 µL of sterile ddH₂O was added to the column and centrifuged (1 min; 12000 rpm) to elute the plasmid. A small sample of this DNA was sent to the University of Nottingham sequencing laboratory to confirm the presence of the correct DNA sequence before a large-scale Maxiprep production of DNA was performed.

2.2.8 Maxiprep isolation and purification of DNA

Following confirmation of the correct sequence through DNA sequencing analysis (Section 2.2.9). A larger scale isolation and purification of the cDNA was carried out to produce a larger yield of DNA. Maxiprep isolations were performed using an alkaline-SDS lysis followed by a silica binding spin column protocol according to manufacturer's instructions (QIAprep spin Maxiprep, QIAGEN; Manchester, UK).

Maxiprep cultures were prepared based on the appropriate Miniprep clones (Section 2.2.7). 100 µL of the bacterial Miniprep culture was added to a starter culture of 5 mL LB broth containing the appropriate selection antibiotic (75 µg/ mL ampicillin). The culture was left to shake at 225 rpm at 37 °C for 4-8 h. 120 mL of LB broth was then made up in a 500 mL conical flask, sterilised through autoclaving and 75 µg/ mL ampicillin was added. This medium was inoculated with the starter culture and was left to shake at 225 rpm at 37 °C for 16 h. After overnight growth, the prepared culture was centrifuged (10 min; 4000 rpm) and the supernatant was discarded. The bacterial pellet was re-suspended in 10 mL re-suspension buffer, P1 (50 mM Tris-Cl, 10 mM EDTA, 100 µg/ mL RNase A; pH 8.0) and vortexed to aid re-suspension, followed by the addition of 10 mL Lysis buffer, P2 (200 mM NaOH, 1% SDS). The reaction was gently mixed by inversion and left for no longer than 5 min. The reaction

was then neutralised by the addition of 10 mL neutralisation buffer, P3 (3.0 potassium acetate, pH 5.5) and gently mixed through inversion. The mix was then added to a filter syringe cartridge and left to settle for 10 min, allowing the precipitate from the lysis reaction to float to the top. The clear lysate was then filtered through the syringe directly into a prepared binding column, which was prepared by the addition of 10 mL preparation buffer, QBT (750 nM NaCl, 50 mM MOPS, 15 % isopropanol, 0.15 % Triton X-100; pH 7.0), which was allowed to drain by gravity flow. Once placed into the prepared column the lysate was allowed to pass through the column and drain by gravity flow. Two column washes of 30 mL wash buffer, QC (1.0 M NaCl, 50 mM MOPS, 15% isopropanol; pH 7.0), were performed by gravity flow. The column was then transferred to a clean Falcon tube and 15 mL of elution buffer, QF (1.25 M NaCl, 50m M Tris-Cl, 15 % isopropanol; pH 8.5), was added. The eluted plasmid was collected by gravity flow. The DNA was then precipitated out of solution by the addition of 10.5 mL isopropanol and centrifuged (60 min; 4000 rpm). The supernatant was discarded and the DNA pellet was re-suspended in 300 μ L TE Buffer (10 nM Tris Base, 1 nM EDTA; pH 8) and transferred to a 1.5 mL micro-centrifuge tube, followed by the addition of 0.1 volume of 3 M sodium acetate (NaOAc; 30 μ L; pH 5) and 2.2 volumes of 100 % ethanol (660 μ L). The tube was then centrifuged (5 min; 4000 rpm), the supernatant discarded and the pellet allowed to air dry until it began to turn glassy (10-20 min). The DNA pellet was then re-suspended in 100 μ L of TE buffer and left to re-dissolve for 30 min and determination of DNA concentration was carried out (Section 2.2.9).

2.2.9 Determination of DNA concentration and purity

DNA concentration was determined by measuring sample absorbance using a UV spectrophotometer at 260 nm. At 260 nm the absorbance of 50 mg/ mL of double stranded DNA is equal to 1 absorbance unit (AU), thereby allowing for the calculation of DNA concentration. The ratio of absorbance at 260 nm and 280nm ($A_{260/280}$) provides information on sample purity.

Table 2.1 - Summary of constructs used throughout thesis. All Y₁R constructs were based on rat Y₁ cDNA whereas Y₄R and β -arrestin2 constructs were based on human cDNA. Yn-YFP fragment 1-172; Yc-YFP fragment 155-238.

Host Vector	N- terminal tag	cDNA insert	C- terminal tag	Bacterial antibiotic resistance	Mammalian antibiotic resistance	Tetracycline inducible
pcDNA3.1	SNAP	Y ₁	α	ampicillin	Zeocin	No
	α	β -arrestin 2	Yn	ampicillin	Zeocin	No
pCMV	FLAG	Y ₁	Yc	Kanamycin	Neomycin	No
	FLAG	Y ₄	Yc	Kanamycin	Neomycin	No
pcDNA4/TO	α	Y ₁	GFP	ampicillin	Zeocin	Yes
	α	Y ₄	GFP	ampicillin	Zeocin	Yes

Table 2.2 - Summary of cell lines and expressed constructs. SNAP-Y₁R was a stably transfected clonal cell line. Y₁-GFP and Y₄-GFP cells lines were mixed population stably transfected, whereas Y₁ A2 and Y₄ A2 were mixed population of the Y receptor transfected in to clonal cells of the β -arrestin2-Yn cell line. Y₁-GFP and Y₄-GFP cells lines were maintained in zeocin and blastocidin, and receptor-GFP expression was induced through tetracycline treatment (10 μ g/ mL) 16-22 h prior to experimentation.

Cell line	Parent Cell line	cDNA construct(s)	Receptor plasmid	Mammalian antibiotic resistance		Experimental use
				Selection	Maintenance	
SNAP-Y₁R	HEK293T	SNAP-Y ₁ R	pcDNA 3.1zeo	zeocin	zeocin (200 μ g/ mL)	Competition binding, FCS
Y₁ A2	HEK293T	FLAG-Y ₁ R-Yc	pCMV FLAG	neomycin	neomycin (0.8 mg/ mL)	BiFC arrestin recruitment
		β arrestin2-Yn	pcDNA 3.1zeo	zeocin	zeocin (200 μ g/ mL)	
Y₄ A2	HEK293T	FLAG-Y ₄ R-Yc	pCMV FLAG	neomycin	neomycin (0.8 mg/ mL)	BiFC arrestin recruitment
		β arrestin2-Yn	pcDNA 3.1zeo	zeocin	zeocin (200 μ g/ mL)	
Y₁ GFP	HEK293TR	Y ₁ R-GFP	pcDNA4/TO	zeocin	zeocin (200 μ g/ mL)	Competition binding
		tetracycline repressor	pcDNA6/TR	blastocidin	blastocidin (5 μ g/ mL)	
Y₄ GFP	HEK293TR	Y ₄ R-GFP	pcDNA4/TO	zeocin	zeocin (200 μ g/ mL)	Competition binding
		tetracycline repressor	pcDNA6/TR	blastocidin	blastocidin (5 μ g/ mL)	

This is due to RNA having a high absorbance at 260 nm and the aromatic amino acids in proteins having a high absorbance at 280 nm. An $A_{260/280}$ ratio of 1.7-1.9 is accepted as a sample that is relatively free from contaminants, with a ratio >1.9 indicating high RNA concentration and a ratio of <1.7 indicating high protein contamination. Once concentration and purity were determined, the volume of the DNA preparation was adjusted to give a stock concentration 1 $\mu\text{g}/\text{mL}$ in TE buffer. The stocks were then stored at $-20\text{ }^{\circ}\text{C}$ and the DNA sample was then sequenced again to ensure the correct DNA was present.

2.3 Cell culture

The base cell line used in all experiments were human embryonic kidney 293T cells (HEK293T), or the tetracycline inducible 293TR cell line (HEK293TR; Invitrogen), which stably expressed the desired receptor and / or β -arrestin2 constructs (Table 2.1). Stable cell lines produced for these studies included SNAP- $Y_1\text{R}$, $Y_1\text{-GFP}$, $Y_4\text{-GFP}$, $Y_1\text{ AR}$, and $Y_4\text{ AR}$ (Table 2.2), and were made by Dr. Laura Kilpatrick, Mrs Marleen Groenen or Dr. Nicholas Holliday.

2.3.1 Cell line maintenance

Cell lines were maintained in Dulbecco's modified Eagle's medium (DMEM) supplemented with 10 % foetal bovine serum (FBS) at $37\text{ }^{\circ}\text{C}$ in 5 % CO_2 and grown in 75 cm^2 tissue culture flasks (T75). Medium was supplemented with appropriate concentrations of selection antibiotic required for the expressed constructs in that cell line (Table 2.2). Cells were grown to 70-80 % confluency prior to passaging to prevent the detachment of the cell monolayer from the flask. Cells were passaged by removal of media, washing x1 with phosphate buffered saline (PBS) and treated with 1 mL of trypsin. Trypsin is a serine protease that facilitates cell detachment by hydrolysing proteins such as adherin, which enable the cells to adhere to the flask. Washing with PBS is an important step before the addition of trypsin, as FBS contains protease inhibitors which limit the trypsinisation reaction. Following trypsinisation the cells were left for 5 min before washing with 10 mL DMEM allowing cells to be collected. Following collection, the cells were centrifuged at 3000 rpm for

5 min, and were re-suspended in 10 mL DMEM. An appropriate volume of cell suspension was added to a T75 flask, containing 20 mL of DMEM and appropriate antibiotic, to give the required dilution ratio, typically 1:5-1:20.

2.3.2 Cryogenic storage of cells

For cryogenic storage in liquid nitrogen, cells were frozen following the same method for splitting as described above (Section 2.3.1). After cells were pelleted they were re-suspended in 2 mL FBS with 10 % DMSO (per T75). DMSO prevents the formation of ice crystals during freezing which would result in cell lysing during the thawing process. 1 mL of cell suspension was then transferred to a cryovial. The vials were then placed in a Mr Frosty freezing container containing isopropanol and left at -80 °C for 24 h. After overnight freezing the vials were then transferred to liquid nitrogen dewars for long term storage. Upon thawing, 10 mL DMEM was added to the cryocell suspension, the suspension was then pelleted and resuspended in a T75 containing 20 mL fresh DMEM and left to recover overnight. The media was then replaced the following day, and every 2nd day subsequently, until the cells were confluent and ready to be split into new T75 flasks.

2.3.3 Experimental plating of cells

All experiments used 96 well plates (Greiner 655090) or 8 well glass-bottomed plates (Lab Tek 155411). Prior to cell seeding, all wells were coated with poly-D-lysine (10 µg/ mL in PBS, filter sterilised) for 30 min at room temperature (RT). They were then aspirated and washed with DMEM before the addition of cells. 100 µL of cell suspension was loaded onto a haemocytometer and the number of cells, within a 1 mm² area and 0.1 mm depth, were counted. The average number of cells per mL was calculated (25 x 0.04 mm² squares totalling 0.1 µL) by multiplying the number of cells counted by 10 000. The cell suspension was then made up to the desired volume with DMEM to give the correct cell density. For plate reader assays, cells were seeded one day prior to experimentation at 40 000 cells/well, and for FCS assays, cells were seeded two days prior to experimentation at 20 000

cells/well, unless otherwise stated. Tetracycline inducible cells lines were seeded at 20 000 cells/well two days prior to experimentation. 16-22 h before experimentation DMEM was replaced with DMEM containing tetracycline (10 µg/ mL) and cells were incubated at 37 °C in 5 % CO₂ until experiments were conducted.

2.4 Fluorescence based pharmacological assays

Fluorescence is the result of a three stage process involving the electronic state of the fluorescent species, which include; excitation, excited-state and emission. During the excitation stage, a photon of energy is provided by an external source, e.g. a laser, and is absorbed by the fluorophore creating an excited electronic singlet state (S_1'). This excited-state has a lifetime of typically 1-10 ns depending on the fluorophore. During this time the fluorophore undergoes conformational changes, resulting in the dissipation of the S_1' phase energy, producing a relaxed singlet excitation state (S_1), from which fluorescence emission originates. During fluorescence emission, a photon of energy is emitted allowing the fluorophore to return to ground state (S_0 ; Figure 2.4). Due to the energy dissipation in the return to S_1 phase, the photon emitted is of a lower energy than the one that was initially absorbed and therefore of a longer wavelength. This difference in energy is known as the Stokes shift and is fundamental to the sensitivity of a fluorescence technique as it allows emitted photons to be detected independently of the excitation photons. From these properties the fluorescent quantum yield (ϕ) is calculated, this is a ratio of the number of fluorescent photons emitted, to the number of excitatory photon absorbed. The ϕ acts as a measure of the relative extent to which these excitatory processes occur i.e. a high quantum yield would result in a high probability of fluorescence. Molecules with a quantum yield of >0.1 are considered fluorescent.

The excitation process is cyclical unless the fluorophore is irreversibly damaged by the excitation phase. This is known as photobleaching.

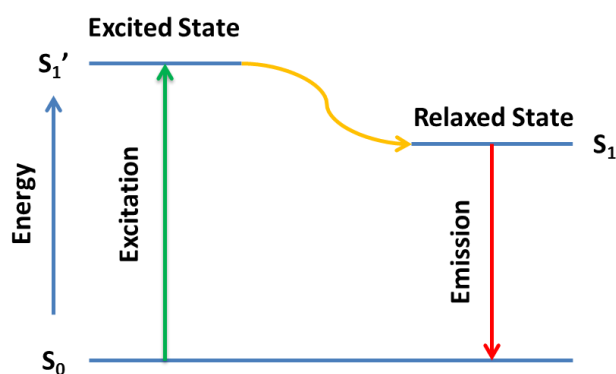


Figure 2.4 – The Jablonski Diagram shows the progression of fluorophore excitation from ground state (S_0) to the excited singlet state (S_1'). The yellow arrow represents the dissipation of energy that occurs from S_1' to the relaxed singlet state (S_1) with the difference in energies illustrating the Stoke shift of the theoretical fluorophore represented.

Another factor that should be taken into account when considering fluorophores is quenching, which is caused by a loss of fluorescence signal due to interactions between the fluorophore and the local molecular environment (Briddon and Hill, 2007). Users of fluorescent-based techniques should also be aware of other photophysical properties that their chosen fluorophores may exhibit such as triplet state, or blinking. Triplet state can be applied to any fast photophysical phenomenon that results in reversible transitions between a fluorescent and dark state in which no photons are emitted. For example, this is often observed in Cyanine dyes due to photo induced isomerisation of the fluorophore between *cis* and *trans* conformations (Eggeling et al., 1998). This causes a fast reversible change in fluorescence emission yield and is a phenomenon that results in flickering of the fluorescence intensity of a dye. Triplet state is often dependent on the excitation intensity or concentration of the dye. Blinking is also observed in many GFP mutant forms, for example in the eGFP mutants F64L and S65T, where light induced protonation of the hydroxyl group [Tyr⁶⁶] results in a dark state of ~300 μ s at pH 7 (Haupts et al., 1998; Schwille et al., 2000).

2.4.1 Automated plate reader assays

2.4.1.1 SNAP-tag system

A common approach to GPCR tagging is the employment of SNAP tag technology. SNAP tag is a 20 kDa mutant domain of the DNA repair protein

O⁶-alkylguanine-DNA alkyltransferase. This protein reacts with benzyl guanine derivatives leading to covalent binding. When treated with SNAP-tag substrate, which contains a fluorescently tagged benzyl guanine, covalent binding occurs at the SNAP tag region and results in irreversible fluorescent labelling of the SNAP tagged protein of interest (Figure 2.5). This approach is a non-invasive way of detecting membrane proteins through fluorescent imaging and allows tracking and visualisation of the receptor on the plasma membrane, or within cellular compartments, with minimal disruption to protein folding and function.

2.4.1.2 Fluorescent ligand competition binding

The range of fluorescent ligands used in cell assay studies are summarised in Table 2.3, more details on these ligands may also be found in Chapter 4 and Chapter 5 of this thesis. In fluorescent ligand binding assays, cells were seeded on 96 well black-bottomed imaging plates as previously described (Section 2.3.3). As required, cells were labelled with 0.2 μ M membrane impermeant SNAP surface Alexa Fluor (AF) 488 in complete DMEM for 30 min at 37 °C and 5 % CO₂. Cells were washed twice with Hank's balanced salt solution (HBSS; 10 mM HEPES, 1.7 mM CaCl₂, 1 mM MgSO₄, 2 mM Na pyruvate, 146 mM NaCl, 5 mM D-glucose, 5 mM KCl, 1.5 mM NaHCO₃; pH 7.4) containing 0.1 % bovine serum albumin (BSA), before the addition of ligand at the required concentrations.

5 min after ligand addition, fluorescent ligand was added to all wells at a fixed concentration as indicated, typically less than its K_d value, and cells were incubated for a further 30 min at 37 °C, 0 % CO₂ in HBSS/ 0.1 % BSA containing Hoechst 33343 (H33342 nuclear stain; 2 μ g/ mL), with a final well volume of 100 μ L. Cells were then washed and immediately imaged using the IX Ultra (Molecular devices, San Diego, CA, U.S.A.) confocal plate reader at 2 sites/well using a Plan Fluor 40x numerical aperture (NA) and 0.6 extra-long working distance (ELWD) objective.

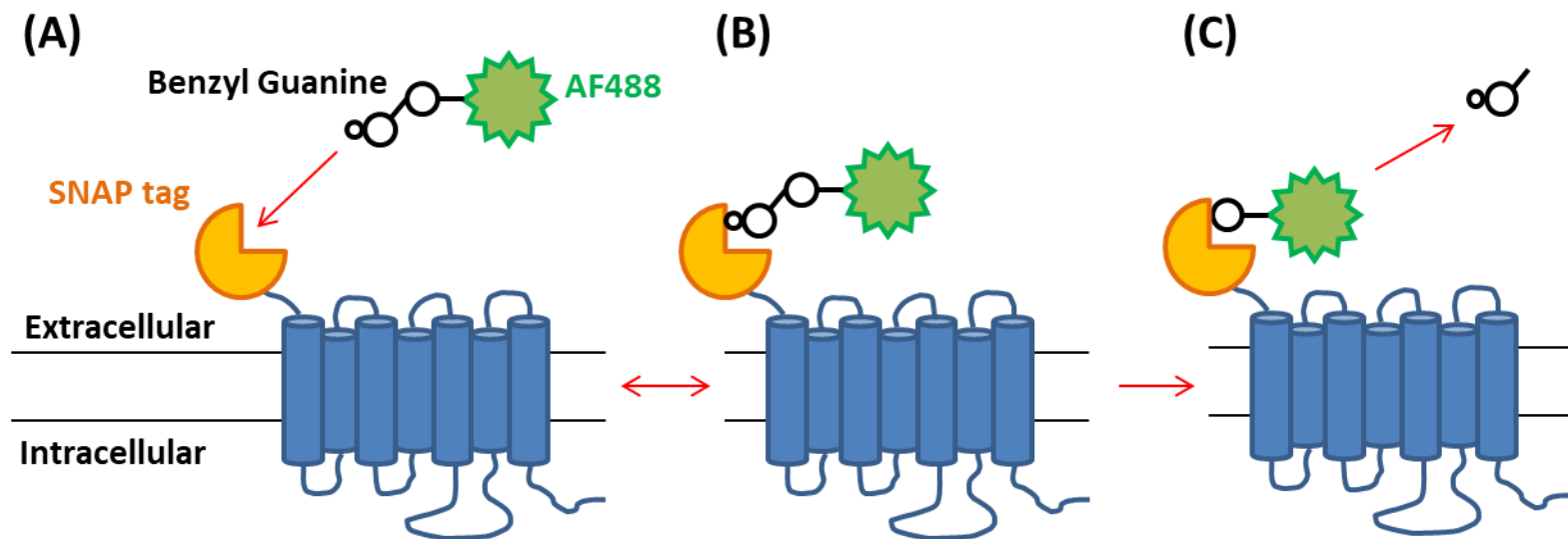


Figure 2.5 - Schematic representation of SNAP tag reaction demonstrating the SNAP tag DNA repair protein domains' action on the benzyl guanine - AF 488 reagent. With (A-C) showing the association, binding and cleavage of the benzyl guanine resulting in covalent binding of the AF 488 fluorophore to the SNAP tagged protein of interest.

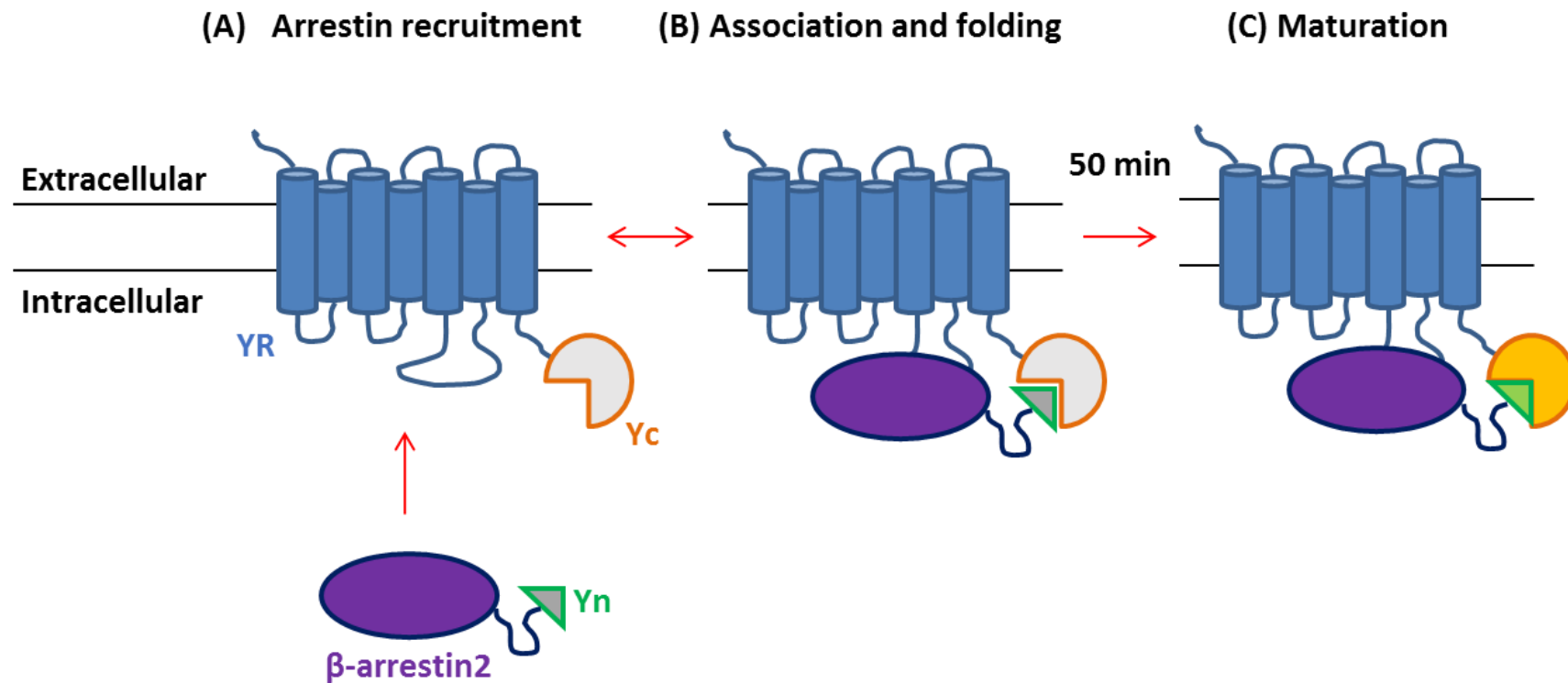


Figure 2.6 - Schematic representation of BiFC showing Y receptor (YR) tagged with Yc-vYFP fragment and β -arrestin2 tagged Yn-vYFP fragment. (A) Shows recruitment of β -arrestin2 to the receptor resulting in protein complementation and re-association of the two vYFP fragments (B). Following maturation of the complemented Yn and Yc fragments, full-length fluorescent vYFP is formed (C). Refolded vYFP fluorescence can then be used as a readout of protein-protein interaction.

Excitation and emission filters for nuclei (excitation 405nm), SNAP tag AF 488 (488nm), and Cy5 tagged fluorescent ligands (633nm) were used.

2.4.1.3 Saturation binding

In saturation binding assays, cells were seeded into 96 well black-bottomed imaging plates as previously described (Section 2.3.3). Cells were labelled with 0.2 μ M SNAP AF 488 in complete DMEM (30 min; 37 °C; 5 % CO₂). Cells were washed twice with HBSS/ 0.1 % BSA before addition of fluorescent ligands at the required concentrations. Cells were then incubated for a further 30 min (37 °C; 0 % CO₂; HBSS/ 0.1 % BSA containing H33342). To determine non-specific binding, BIBO3304 antagonist (1 μ M, Y₁R) or PP (100 nM, Y₄R) was added (30 min; 37 °C; 0 % CO₂ in HBSS/ 0.1 % BSA) prior to fluorescent ligand incubation, with a final well volume of 200 μ L. Cells were then washed and immediately imaged using the IX Ultra or IX Micro (Molecular devices, San Diego, CA, U.S.A.) confocal plate reader at 2 sites/well using a Plan Fluor 40x NA 0.6 ELWD objective or a XLS widefield objective, respectively. Excitation and emission filters for nuclei (excitation 405nm), SNAP AF 488 (488nm), Cy5 tagged fluorescent ligands (633nm; Ultra) and RhB tagged fluorescent ligands (549nm; Micro) were used.

2.4.1.4 Bimolecular fluorescence complementation (BiFC)

BiFC is a fluorescence-based technique that is used to investigate defined protein-protein interactions. In BiFC based assays a fluorescent protein is split into two non-fluorescent halves, for example in the case of venus yellow fluorescent protein (vYFP), an N-terminal fragment (Yn) and a C-terminal fragment (Yc) may be used (Figure 2.6). These fragments can then be covalently fused to proteins of interest e.g. Receptor-Yc and β -arrestin2-Yn (Kilpatrick et al., 2010). Upon interaction of the tagged proteins, the two fragment tags are brought into close proximity thereby facilitating their association and refolding into the full length vYFP. Following refolding the chromophore matures producing a fluorescent signal that acts as a readout of the interaction of the two tagged proteins (Kerppola, 2013).

Table 2.3 - Summary of fluorescent ligands used in high content imaging assays. Cy5 tagged ligands were imaged using the IX Ultra and RhB tagged ligands were imaged using the IX micro. Ligand structures are shown and discussed in more detail in Chapter 3 and 4 of this thesis.

Assay	Ligand	Concentration	Acquisition
Fluorescent ligand binding	Cy5 mono	100nM	IX Ultra
Saturation binding	RhB mono	0.5-100nM	IX Micro
	RhB dimer	0.5-100nM	IX Micro
	Cy5 mono	0.5-100nM	IX Ultra
	Cy5 dimer	1-1000nM	IX Ultra

2.4.1.5 β -arrestin2 recruitment

For BiFC assays, cells were seeded into 96 well black-bottomed imaging plates as previously described (Section 2.3.3). Cells were washed twice with HBSS/ 0.1 % BSA before addition of ligand at the required concentrations for 1 h (37 °C; 0 % CO₂; HBSS/ 0.1 % BSA). If used, antagonists were added for 30 min prior to ligand incubation, with a final well volume of 100 μ L. Incubations were terminated by fixation in 3 % paraformaldehyde (PFA) in PBS for 15 min at RT. Cell nuclei were then labelled with H33342 (2 μ g/ mL) in PBS for 15 min at RT, followed by PBS washing. Images were then acquired using the IX Ultra confocal plate reader at 4 sites/well using a Plan Fluor 40x NA 0.6 ELWD objective. Appropriate excitation and emission filters for nuclei (excitation 405nm) and vYFP (488nm) were used.

2.4.2 Fluorescent correlation spectroscopy (FCS)

2.4.2.1 FCS Calibration

FCS measurements were carried out on a Zeiss LSM 510 Meta Confocor 3 microscope, fitted with a c-Apochromat 40x NA 1.2 water immersion objective lens. Calibration was required before every experiment to ensure beam path alignment and to ensure that a Gaussian shaped detection volume was established. Dependent on the fluorescent species under investigation, calibration was performed with Rh6G (literature diffusion co-efficient $2.80 \times 10^{-10} \text{ m}^2/\text{s}$; Briddon et al., 2004) or Cy5 NHS-ester (literature diffusion co-efficient $3.16 \times 10^{-10} \text{ m}^2/\text{s}$; Briddon et al., 2004).

Solutions of Rh6G at 1 μM and 20 nM were prepared in fluorescence free high performance liquid chromatography (HPLC) water. 200 μL of each solution was added to an 8-well glass-bottomed imaging plate. With the well containing 1 μM solution positioned over the objective, the lower and upper surface of the glass bottom were detected using a reflective beam path to determine the position of the glass-solution interface. The focus was then moved 200 μm up to ensure reads were carried out with the confocal volume positioned within the solution. A beam path was selected that gave appropriate excitation for the SNAP AF 488 fluorophore using an argon laser and a pinhole diameter of 70 μm . The 1 μM solution was then used, at an optimal laser power (between 2 % - 30 %) and an Acousto-optical tuneable filter (AOTF) set at 1 %. Following manual adjustment of the correction collar an optimal count rate of 150-250 kHz was establish. The pinhole position was then automatically adjusted and optimised in both the X and Y axis. Following the beam alignment, the well containing 20 nM solution was then positioned above the objective, the AOTF and laser power was adjusted to 10 % and 60-80 %, respectively, to give an optimal count per molecule (CPM) of 100-150 kHz. An optimal CPM is essential as it is an indication of photostability and brightness of the fluorescent molecule (Widengren et al., 2007) and is required in order to produce FCS traces that can produce accurate autocorrelation and photon counting histogram (PCH) data. FCS calibration measurements of 10 x 10 s reads and a 1 x 60 s read was then taken for autocorrelation and PCH analysis, post-experiment, respectively.

For Cy5 calibration the same method was adopted as with Rh6G, with Cy5 solutions of 500 nM and 10 nM prepared in HPLC water. Using a HeNe 633 laser the correction collar was set using an optimal laser power (between 0.5 % - 8 %), a pinhole diameter of 90 μm and an AOTF of 1 %, giving a count rate of 150-250 kHz from the 500 nM solution. For calibration, reads where taken from the 10 nM solution, the AOTF was adjusted to 10 % and laser power to 50-60 %, giving an optimal CPM of 40-50 kHz. The same FCS calibration

measurements were then taken, to allow for post-experiment autocorrelation and PCH analysis.

2.4.2.2 Fluorescent ligand solution measurements

Stock solutions of fluorescent peptides were prepared at a range of concentrations (1 - 100 nM) in HBSS/ 0.1 % BSA. Following FCS calibration (Section 2.4.2.1) of appropriate beam paths, 200 μ L of each concentration was added to the chambers of an 8-well glass-bottomed imaging plate with HBSS/ 0.1 % BSA used as a control. With the objective positioned over the control well, the lower and upper surfaces of the glass-bottom were detected using a reflective beam path to determine the position of the glass-solution interface. The fine focus was then moved 200 μ m up to ensure reads were carried out with the confocal volume positioned within the solution, as was done in the calibration setup (Section 2.4.2.1). Four FCS measurements of 15 s were then taken for each concentration at varying laser powers between 10-100 % at an AOTF of 10 %.

2.4.2.3 FCS SNAP tagged receptor measurements

Y₁R expressing HEK293T cells were seeded 48 h prior to experimentation at 20 000 cells/well in 8 well glass bottomed plates as previously described above (Section 2.3.3). For NPY and GR231118 controls, cells were treated with 0.2 μ M of appropriate SNAP label, and incubated in DMEM for 30 min (37 °C; 5 % CO₂). The cells were then washed with HBSS/ 0.1 % BSA, followed by a further 30 min incubation with 1 μ M NPY, 1 μ M GR231118 or HBSS/ 0.1 % BSA alone, as a control (37 °C; 0 % CO₂). Cells were then removed from the incubator and allowed to settle to room temperature (21 °C; 15 min). The plate was then aligned for FCS measurements to be taken from the cell membrane as previously described (Kilpatrick et al., 2012).

Plate alignment was carried out through visualisation of Y₁R expressing HEK293T cells through the eyepiece using an epi-fluorescent lamp to ensure the stage was placed at the correct Z position. Cells were then visualised live,

using confocal imaging at a low laser power (5 %) in order to identify SNAP labelled cells with an intensity range suitable for FCS, and to prevent bleaching. An optimal offset and gain was set to prevent pixel saturation and a crosshair was used to identify and position the confocal volume over the cell nucleus. The stage was then adjusted using fine focus to move the confocal volume onto the upper membrane of the cell. The z position of the confocal volume was then determined by performing a z scan which produced a peak in count rate, corresponding to the upper membrane of the cell, and so the optimum position of the confocal volume. Once the confocal volume was placed at this optimum position, one FCS read/cell was taken for 30 s with a 10 s pre bleach, at 50 % laser power and AOTF of 10 %, unless otherwise stated. Measurements for RhB tagged fluorophores were taken using 561 nm laser excitation with emission collected through a LP580 filter, and Cy5 fluorophores used 633 nm HeNe laser excitation and emission collection through a LP650 filter.

2.4.2.4 FCS fluorescent ligand binding measurements

Fluorescent ligand binding experiments were conducted in a similar way, to SNAP tagged receptor measurements as described above (Section 2.4.2.3). Y₁R expressing HEK293T cells were seeded 48 h prior to experimentation at 20 000 cells/well in 8 well glass-bottomed plates as previously described (Section 2.3.3). The cells were washed with HBSS/ 0.1 % BSA, followed by the addition of fluorescent ligand at varying concentrations (1 - 100 nM). Cells were incubated for 30 min (37 °C; 0 % CO₂), then removed from the incubator and allowed to settle to room temperature (21 °C; 15 min). The cells were then washed in HBSS/ 0.1 % BSA in order to remove any unbound ligand. The plate was then aligned for FCS measurements to be taken from the cell membrane as described above (Section 2.4.2.3). One FCS read/cell was taken for 30 s with a 10 s pre bleach, at 50 % laser power and AOTF of 10 %, unless otherwise stated. All measurements were taken within 30 min of HBSS/ 0.1 % BSA washing.

Table 2.4 - Automated reaction sequence of PS3 synthesiser showing the cycle of Fmoc deprotection, amino acid activation and amino acid coupling conducted by the PS3 synthesiser, along with the reaction conditions.

Step	Reagent	Time	Repeat	Comments
1	DMF	30 s	X3	Wash resin
2	20% piperidine in DMF	5 min	X2	Removes Fmoc protection group on N-terminus
3	DMF	30 s	X6	Wash resin
4	7% DIPEA in DMF	30 s	X1	Dissolves amino acid and activating agent HCTU
5	HCTU activating agent in DMF	50 min	X1	Amino acid coupling to free N-terminus
6	DMF	30 s	X3	Wash resin

2.5 Solid and liquid phase peptide synthesis experimental

All linear peptides were produced on a 0.1 mmol or 0.3 mmol scale and were synthesised following an Fmoc-based solid phase peptide synthesis (SPPS) strategy using a PS3 automated peptide synthesiser (Protein Technologies Inc, Tucson, AZ, USA).

2.5.1 General methods A - preparation of linear peptides

A1. Rink amide resin preparation: A reaction vessel was mounted on to the PS3 automated synthesiser. Rink amide resin was then weighted at 0.1 mmol or 0.3 mmol scale and placed into the vessel. Dimethylformamide (DMF) was then added to the vessel and the resin was allowed to swell for at least 30 min. On each coupling cycle, the resin was first washed with DMF (3 x 30 s) then treated with 20 % piperidine in DMF (2 x 5 min) to remove Fmoc protecting groups, prior to amino acid coupling.

A2. Automated synthesis of linear peptide: Following resin preparation, vessels containing pre weighed amino acids and coupling reagent, O-(1*H*-6-chlorobenzotriazole-1-yl)-1,1,3,3-tetramethyluronium hexafluorophosphate (HCTU), were loaded into the PS3, with HCTU at 3 equiv. to amino acid. The automated N-terminus deprotection, amino acid activation and amino acid coupling reactions were then carried out on the PS3 (Table 2.4). Following Fmoc deprotection (general method A1), the resin was washed again with DMF (6 x 30 s; Table 2.4). After coupling of the final amino acid no further

automated Fmoc deprotection was performed giving a resin-bound peptide with an Fmoc-protected N-terminus. The resin was transferred to a filter syringe and washed with DMF (1 x 10 mL), MeOH (1 x 10 mL) and Et₂O (2 x 10 mL).

2.5.2 General methods B - peptide cleavage conditions

B1. Peptide cleavage from Rink amide resin and side chain protecting groups

(Pbf, Boc, tBu, otBu): The resin-bound linear peptide was treated with a solution of triisopropylsilane (TIPS; 5 %) and 1,3-dimethoxybenzene (DMB; 2.5 %) in trifluoroacetic acid (TFA), and then shaken for 2-3 h at RT. The resin was then filtered and washed with TFA (3 mL) and the filtrate collected. The filtrate was concentrated under nitrogen (30 min) and the peptide was precipitated out in ice cold Et₂O (up to 30 mL). The suspension was sonicated (1 min) and cooled at 0 °C (30 min), then centrifuged (3000 rpm; 5 min) and the supernatant was discarded. The residue was then washed with Et₂O and centrifuged again. The precipitate was allowed to air dry and was then re-suspended in 50:50 acetonitrile (MeCN):H₂O. A small sample was then analysed by liquid chromatography - mass spectrometry (LCMS) to confirm the desired peptide product, before lyophilisation to yield a resin cleaved, side chain deprotected, linear peptide.

B2. OAll/Alloc side chain deprotection: The OAll and Alloc protecting groups were cleaved by treating the peptide with phenylsilane (PhSiH₃; 24 equiv.) and tetrakis(triphenylphosphine)palladium(0) (Pd(PPh₃)₄; 1 equiv; dissolved in 0.5 mL DCM) in MeOH. The reaction was left to stir under nitrogen for 2 h. The reaction mixture was concentrated under vacuum and the product was washed with DCM (2-3 mL; x 1). The reaction mixture was then concentrated under vacuum again and resuspended in TFA (0.5 mL). The peptide was precipitated out in ice cold Et₂O as previously described (General method B1). A sample was analysed by LCMS to confirm the desired peptide product

B3. Manual Fmoc deprotection of peptide: In solution, the N-terminal Fmoc protected peptide was treated with 20 % piperidine in DMF, shaken for 30 min at RT. It was then immediately lyophilised. The lyophilised product was re-suspended in TFA (0.5 mL) and the peptide was precipitated out in ice cold Et₂O as previously described (General method B1). Desired Fmoc cleavage was confirmed by LCMS.

2.5.3 General methods C – solution phase amide bond formation conditions

C1. Intramolecular/intermolecular amide bond formation: Deprotected linear peptides (General method A3) were suspended in DMF containing 6-chloro-benzotriazole-1-yloxy-tris-pyrrolidinophosphonium hexafluorophosphate (Pyclock; 3 equiv.) and 2,4,6-trimethylpyridine (TMP; 10 equiv.). The reaction was stirred for 12 h at RT, then lyophilised. The lyophilised product was re-suspended in TFA (0.5 mL) and the peptide was precipitated out in ice cold Et₂O as previously described (General method B1). A sample was analysed by LCMS to confirm the desired coupling had occurred.

C2. Fluorophore tagging: Intermolecular cyclised peptides (General method C1) were suspended in DMF containing Pyclock (3 equiv.), N-Methylmorpholine (NMM; 12 equiv.) and sulphated cyanine 5 fluorophore dye (sCy5; 0.7 equiv.). The reaction was stirred for 12 h at RT, then lyophilised. The lyophilised product was re-suspended in TFA (0.5 mL) and the peptide was precipitated out in ice cold Et₂O as previously described (General method B1). A sample was analysed by LCMS to confirm successful fluorophore conjugation.

2.5.4 Reverse phase high performance liquid chromatography (RP-HPLC)

Crude peptides were purified using a Waters 600 semi-preparative RP-HPLC system fitted with a Phenomenex Luna C8 column (pore size 100 Å; particle size 10 µm; column size 250 x 21.2 mm) and a Waters 486 UV detector (Figure 2.7). The system used 0.1 % TFA in double distilled H₂O (ddH₂O) as the

aqueous buffer (buffer A) and 0.1 % TFA in MeCN as the organic buffer (buffer B). Before RP-HPLC was started, the system was flushed with 100 % buffer B for 5 min at a flow rate of 10 mL/ min, followed by 100 % buffer A for 10 min at 10 mL/min.

The crude peptide was dissolved in 10 mL or less of appropriate volumes MeCN and ddH₂O, with as little MeCN as possible, as too high a ratio of MeCN would result in the sample not binding to the column. Following the selection of a linear gradient elution profile of 0-60 % buffer B over 80 min at a flow rate of 15 mL/ min, unless otherwise stated, the sample was then taken up into a 10 mL syringe and injected into the HPLC apparatus. Absorbance of the eluent was then measured, as an indication of the elution of a sample component, using the Waters 486 UV detector with a detection wavelength set at 230 nm. All fractions with an absorbance of > 0.4 were collected with up to 3 mL eluted fraction per tube. Once all desired fractions were collected, samples of each collected fraction were submitted for LCMS testing to confirm the presence of the purified peptide and the percentage purity.

2.5.5 Liquid chromatography mass spectrometry (LCMS)

The molecular mass (Mr) of the peptides was determined by electron spray ionisation-mass spectroscopy (ESI-MS) using a Shimadzu LCMS2020 fitted with a Phenomenex Luna C8 column (Figure 2.8; pore size 100 Å; particle size 3 µm; column size 100 x 2.00 mm). The system used 0.05 % TFA in ddH₂O as the aqueous buffer, (buffer C), and 0.05 % TFA in MeCN as the organic buffer, (buffer D). 50 µL samples of 2 mg/ mL were submitted to the LCMS dissolved in 50 % MeCN and 50 % ddH₂O and the selected eluting profile was a linear gradient of 0-80% buffer D over 10 min at a flow rate of 0.2 mL/ min. Absorbance of the elute was detected at 214 nm. The resultant absorbance and MS profiles were analysed to ensure the presence of the desired product (Section 2.6.3.1).

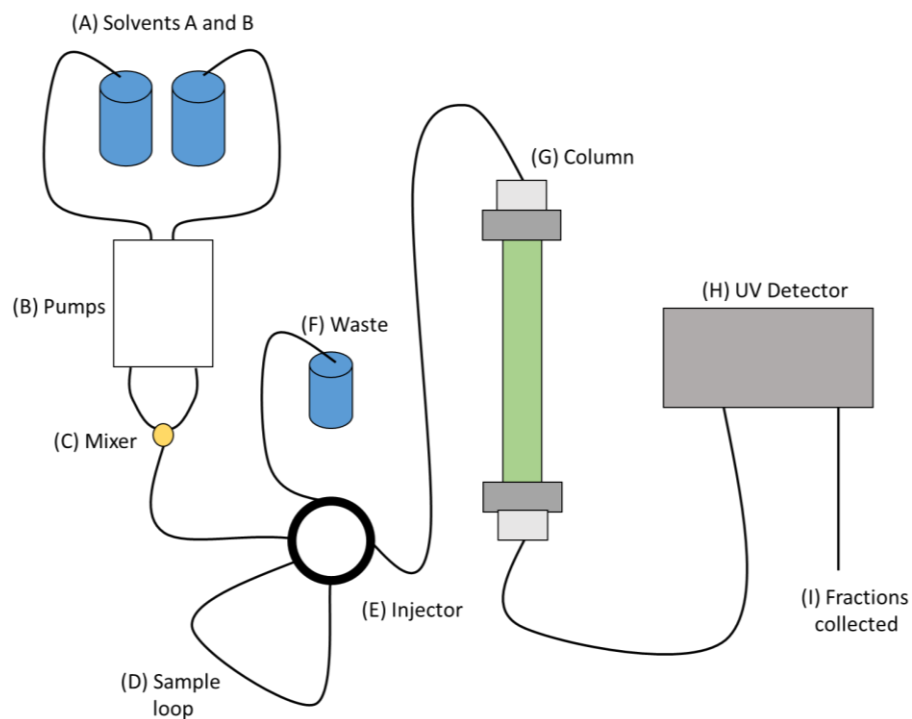


Figure 2.7 - RP - HPLC apparatus set up, where injected dissolved samples pass through the sample loop and then onto the column (E, D and G), while solvent A and B pass through the column via the pumps and mixer to create the desired gradient (A, B and C). The eluted fractions from the column pass through the UV detector to indicate when fraction collection should occur (H and I).

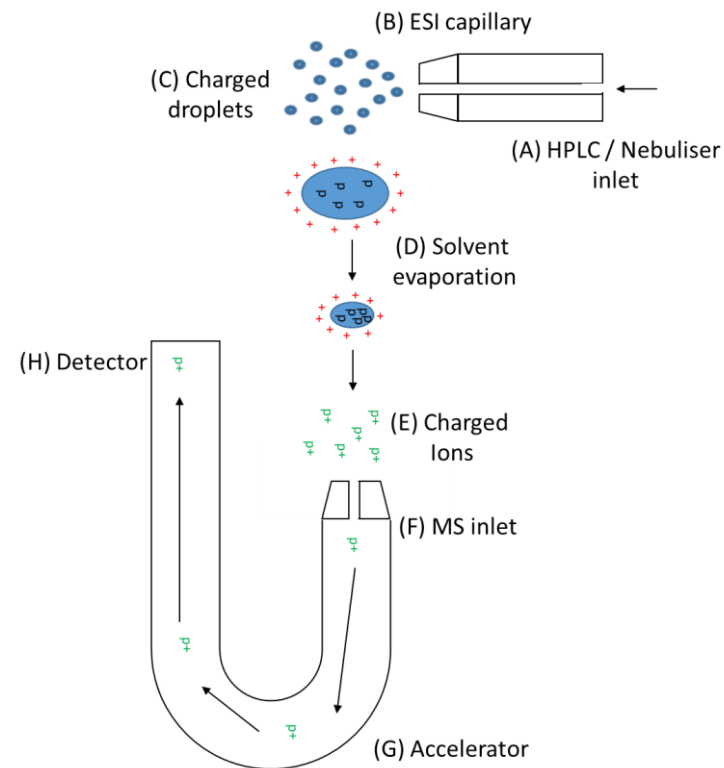


Figure 2.8 - LCMS equipment set up, where a small amount of submitted sample is injected into the nebuliser (A) to produce charged droplets (C) which then evaporate resulting in charged particles (E). The charged particles are then accelerated onto the mass detector to provide a mass read out (F, G and H).

2.6 Data analysis

2.6.1 Automated plate reader analysis

2.6.1.1 Quantification of fluorescent ligand binding and β -arrestin2 recruitment using granularity algorithm

Fluorescent ligand binding and β -arrestin2 recruitment assay images, acquired using the IX Ultra confocal plate reader (Section 2.4.1.2 and 2.4.1.5), were analysed using a granularity algorithm (MetaXpress v5.0, Molecular Devices). Granularity analysis identifies nuclei through H33342 staining and identifies spots above a set threshold intensity within the image, allowing quantification of fluorescent ligand binding or BiFC complex formation.

In fluorescent ligand competition binding, granules were defined at 2-3 μm in diameter (Figure 2.9). Quantitative data was plotted as integrated granule intensity/cell in GraphPad Prism v7 using log (inhibitor) vs. binding or log (agonist) vs response models. All values were averaged from duplicate or triplicate wells, imaged at 2 sites/well, and data was then normalised to totals (100 %) and top concentration of control ligand (NPY or PP; 0 %).

Similarly, BiFC granules were defined by a diameter of 3-8 μm , where images at 4 sites/well were acquired and data were normalised to total specific bindings (0 %) or vehicle in arrestin assays (0%), and top concentration of control ligand (NPY or PP; 100 %; Figure 2.10).

2.6.1.2 Quantification of saturation binding using transfluor algorithm

Saturation binding images, acquired using the IX Ultra and IX Micro plate reader (Section 2.4.1.3), were analysed using a transfluor algorithm (MetaXpress v5.0, Molecular Devices). Transfluor analysis measures the distribution of fluorescent species and, as with granularity analysis, this method quantifies granules through identification of pits and vesicles of differing diameters. The use of an additional “vesicle” component in saturation analysis enables exclusion of any unbound aggregates of fluorescent ligand that may be apparent in images at high ligand concentration.

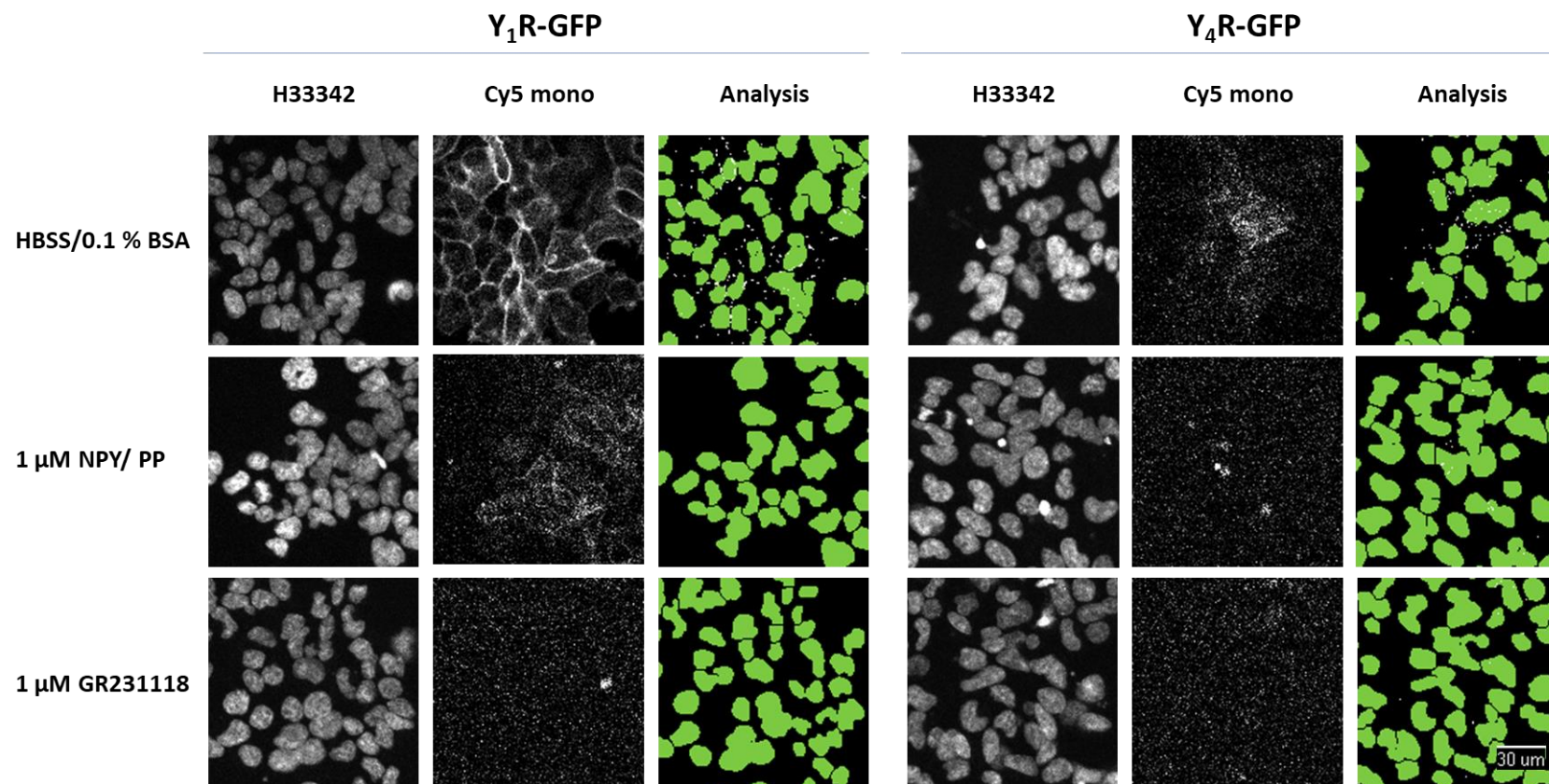


Figure 2.9 – IX Ultra acquired images of fluorescent ligand binding shown in combination with quantification via the application of granularity analysis at both the Y₁R and Y₄R. The top panel of images show control conditions of 100 nM Cy5mono treated cells. The middle panel shows images, where displacement of Cy5mono was observed following 1 μ M treatment of NPY or PP at the Y₁R and Y₄R, respectively. The bottom panel shows images of the displacement of 100 nM Cy5mono in the presence of 1 μ M high affinity ligand, GR231118. The analysis panel shows identified nuclei in green and identified granules as small white dots.

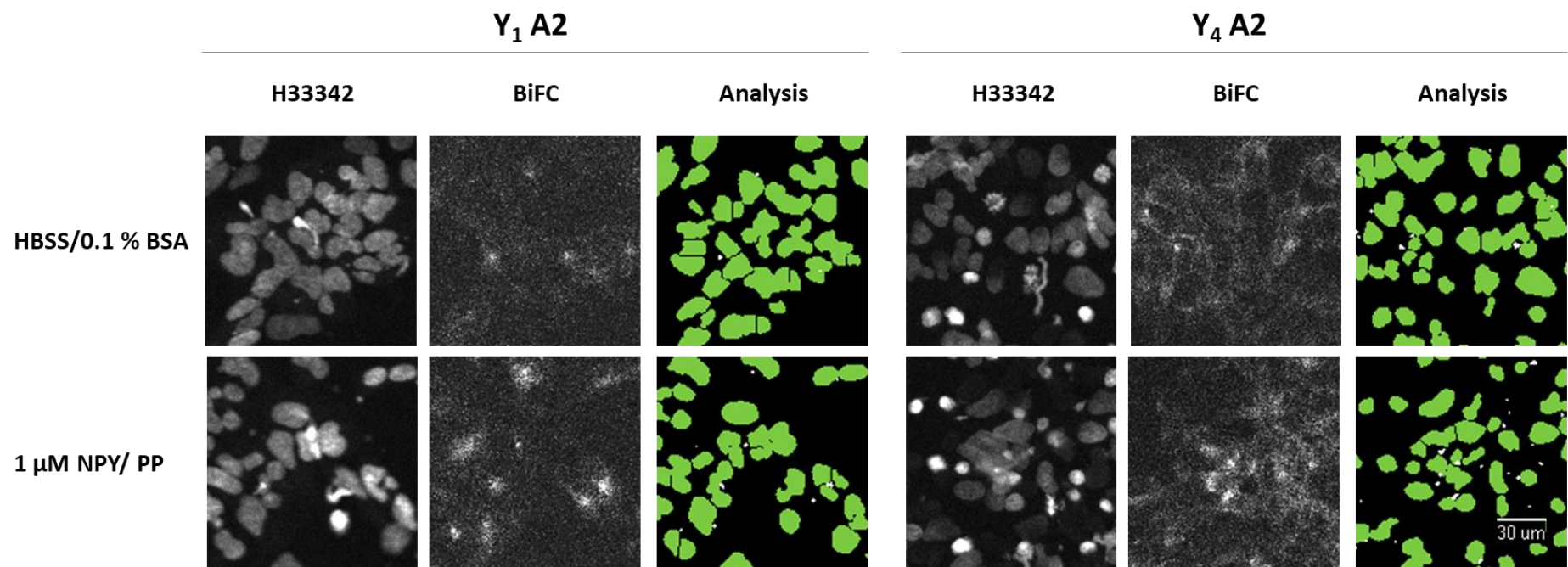


Figure 2.10– IX Ultra acquired images of β -arrestin2 recruitment shown in combination with quantification via the application of granularity analysis at both the Y₁R and Y₄R. Where the top panel of images show control conditions of HBSS/ 0.1 % BSA only and the bottom panel shows images following 1 μ M treatment of NPY or PP at the Y₁R and Y₄R, respectively. Following agonist treatment the formation of punctate BiFC granules is observed. The analysis panel shows identified nuclei in green and identified BiFC granules as small white dots.

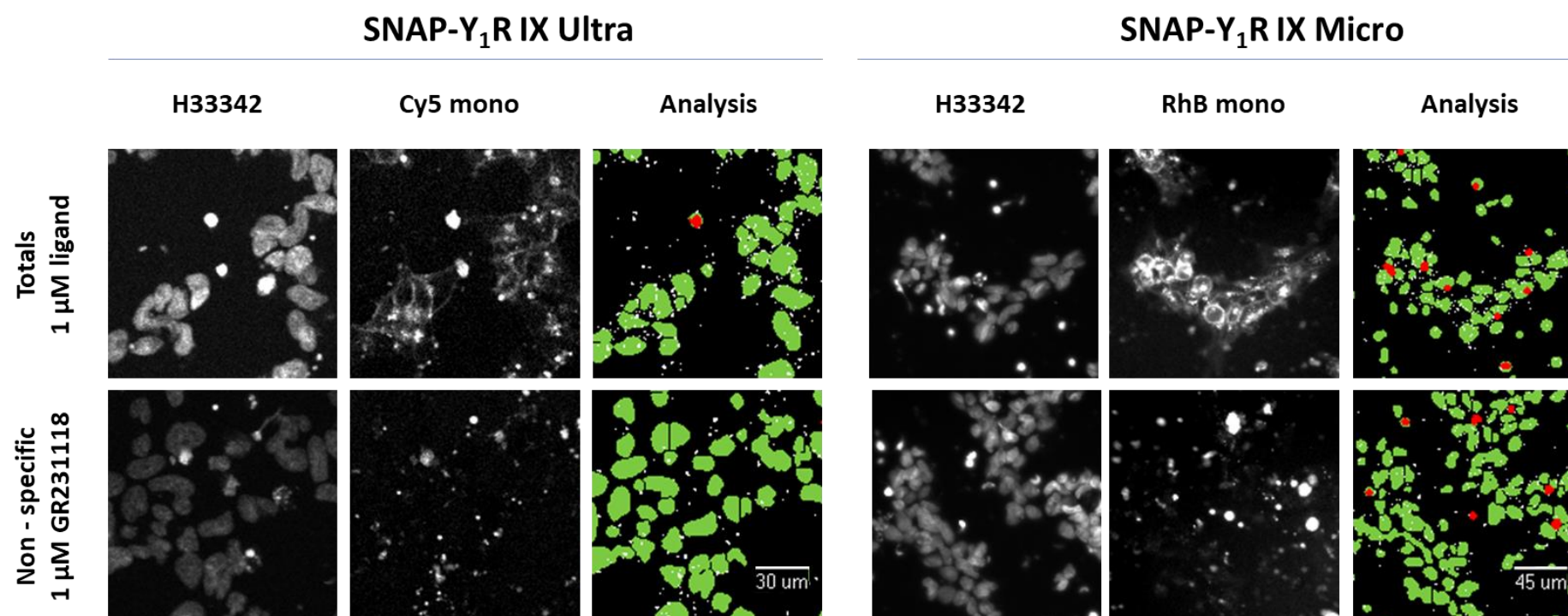


Figure 2.11 – IX Ultra and IX Micro acquired images of saturation binding shown in combination with quantification via the application of transfluor analysis at the Y₁R. The left panel shows images of Cy5mono saturation binding acquired on the IX Ultra confocal plate reader, in the absence and presence of 1 μ M high affinity ligand GR231118, where GR231118 acts to displace Cy5mono and provide a non-specific binding, background read out. The panel on the right shows images of RhBmono saturation binding acquired on the IX Micro widefield plate reader. The analysis panel shows identified nuclei in green, identified pits as small white dots and vesicles as red dots.

For images acquired on the IX Ultra, pits were defined as 2-3 μm (as for competition data) and vesicles as 10-18 μm (Figure 2.11). All values were averaged from duplicate or triplicate wells, imaged at 2 sites/well. Binding was quantified only from the pit data and was plotted as pit integrated intensity/cell in GraphPad Prism v7 using the one site - total and non-specific binding model. The calculated K_d values obtained are presented as a pooled average across individual experiments (see Chapter 4). For images acquired on the IX Micro the same approach was adopted, where pits were defined as 1-3 μm and vesicles as 12-18 μm .

2.6.1.3 Agonist concentration response analysis

When concentration response curves were produced, further analysis was conducted to determine pEC_{50} values, where applicable. If a maximal response was observed, compared to the normalised full agonist response (NPY at the $Y_1\text{R}$ or PP at the $Y_4\text{R}$), pEC_{50} values were stated as mean \pm standard error of the mean (SEM) in accordance to Equation 2.3.

Equation 2.3 - Where R_{max} is the maximal agonist response, $[A]$ is the concentration of agonist, EC_{50} is the concentration of agonist which produces half a maximal response and n is the Hill slope.

$$\text{Response} = \frac{R_{\text{max}} [A]^n}{[A]^n + \text{EC}_{50}^n}$$

2.6.1.4 Antagonist treatment analysis

Where antagonist pre-treatment was conducted the resultant data was analysed using the Gaddum equation to determine the equilibrium dissociation constant (K_d ; Equation 2.4) of the competitive antagonist used, provided the antagonism was surmountable. The K_d represents the concentration of antagonist required at equilibrium to occupy 50 % of the receptors. The concentration ratio (CR; Equation 2.5) was firstly defined as a ratio of agonist EC_{50} in the presence and absence of fixed concentration of antagonist ($[B]$). These values were then applied to the Gaddum equation to calculate the K_d . The pK_d values from each independent experiment were calculated, then pooled and expressed as mean \pm SEM. When agonist

concentration response curves were generated in the presence of multiple concentrations of antagonist, Schild analysis was used to determine the antagonist affinity (Equation 2.6).

Equation 2.4 - Gaddum equation; Where CR is the concentration ratio and [B] is the fixed concentration of antagonist present.

$$K_d = \frac{[B]}{CR - 1}$$

Equation 2.5 - Concentration ratio for Gaddam equation; Where [A1] = concentration of agonist in the absence of antagonist required to produce a 50% response, [A2] = concentration of agonist required to produce a 50% response in the presence of antagonist concentration [B].

$$CR = \frac{[A2]}{[A1]}$$

Equation 2.6 – Schild equation; Where log [B] is plotted against CR-1 and the log K_d is determined from the x-intercept of the graph.

$$pK_d = \log (CR - 1) - \log [B]$$

2.6.1.5 Competition binding analysis

Where appropriate IC_{50} values from competitive binding curves were converted to pK_i values using the Cheng-Prusoff equation (Equation 2.7; Cheng and Prusoff, 1973).

Equation 2.7 – Cheng-Prusoff correction, where K_i is the affinity of the test ligand, [FL] is the concentration of free fluorescent ligand and K_d the dissociation constant of the fluorescent ligand.

$$K_i = \frac{IC_{50}}{\left(1 + \frac{[FL]}{K_d}\right)}$$

2.6.1.6 Statistical analysis

One-way ANOVA statistical analysis was used to compare multiple data sets using GraphPad Prism v7. This was followed by Tukey's multiple comparison test to determine statistical significance. All data are expressed as mean \pm SEM.

2.6.2 Fluorescence correlation spectroscopy (FCS)

2.6.2.1 Autocorrelation analysis

The parameters for all autocorrelation analyses are summarised in (Table 2.5) below. As discussed above (Section 2.4.2) FCS measurements were acquired

from a Gaussian shaped confocal detection volume, placed on a region of interest, e.g. the cell membrane or in solution. These measurements produced time dependent fluctuation traces due to the movement of fluorescently tagged particles passing through the volume. Autocorrelation analysis was applied to these traces. This analysis compares the size of a fluctuation (δI) from the mean fluorescence intensity ($\langle I \rangle$) at a time (T), with that of subsequent fluctuations at later time points ($T+\tau$). Using a wide range of τ values the autocorrelation function ($G(\tau)$) can be derived. This is then normalised to the square mean intensity measure ($\langle I \rangle$), thus producing the autocorrelation function (Equation 2.8).

2.6.2.2 Autocorrelation analysis for calibration

A biophysical model is chosen for autocorrelation analysis, and the optimal model depends on the nature of the system. With respect to calibration analysis, the fluorescent species that was investigated was free to move within 3D space, and a 1 component 3D curve fitting model was applied, as this incorporates the movement in x, y and z dimensions. The chosen model for calibrations and free solution analysis was a 1x3D + Triplet model, shown in Equation 2.9, with the pre-exponential function to account for triplet state, A, shown in Equation 2.10.

Equation 2.8 – Autocorrelation function.

$$G(\tau) = \frac{1 + \langle \delta I(T) \cdot \delta I(T + \tau) \rangle}{\langle I \rangle^2}$$

Equation 2.9 – 1x3D autocorrelation model, where A is the pre-exponential function shown in Equation 2.10, and SP is the structural parameter that reflects the shape of the confocal volume.

$$G(\tau) = 1 + A \frac{1}{N} \cdot \left(1 + \frac{\tau}{\tau_D}\right)^{-1} \cdot \left(1 + \frac{\tau}{SP^2 \cdot \tau_D}\right)^{-0.5}$$

Equation 2.10 – Pre-exponential function accounting for triplet state in the autocorrelation model.

$$A = \left(T_r \cdot e^{\frac{\tau}{\tau_r}}\right) \cdot (1 - T_r)^{-1}$$

Following the fit of the appropriate autocorrelation decay function, parameters such as average dwell time (τD) of the particles within the confocal volume can be estimated, which is represented by the halfway point of the $G(\tau)$ decay curve. In addition, the average concentration of particles (N) within the confocal volume is inversely proportional to the amplitude of the autocorrelation function at G_0 (Figure 2.12). With respect to the calibration analysis, a fluorophore with a known diffusion coefficient (D) is used (Rh6G; $D = 2.80 \times 10^{-10} \text{ m}^2/\text{s}$ and Cy5; $D = 3.16 \times 10^{-10} \text{ m}^2/\text{s}$; Briddon et al., 2004). The dimensions of the confocal volume can then be derived, namely its radius (W_1 , in m; Equation 2.11) half height (W_2 , in m; Equation 2.12) and volume (W_0 , in litres; Equation 2.13).

Equation 2.11 - FCS confocal volume radius; Where W_1 is represented in meters.

$$W_1 = (4 \cdot D_{\text{Calibration fluorophore}} \cdot \tau D)^{0.5}$$

Equation 2.12 - FCS confocal volume half height; Where W_2 is represented in meters.

$$W_2 = W_1 \cdot SP$$

Equation 2.13 - FCS confocal volume; Where 1000 represent the conversion factor of litres to m^3 .

$$W_0 = \pi^{1.5} \cdot (W_1)^2 \cdot W_2 \cdot 1000$$

As these calibration calculations determine the dimensions of the confocal volume, these dimensions can then be applied in the calculation of diffusion times for fluorophores with unknown properties, such as those used in this study. This stage of the FCS experimental protocol is essential as it allows for accurate analysis and interpretation of any other experimental reads conducted, and as such is performed at the beginning of every experimental set-up.

2.6.2.3 Autocorrelation analysis for solution ligand reads

As these experiments were carried out in solution, a 1x3D autocorrelation fit was applied, as with calibration reads (Equation 2.9 and Equation 2.10). Using the confocal dimensions calculated through calibration analysis (Section 2.4.2.1). τD values and average concentration (N) of particles within the

detection volume can be calculated within this 3D system (in $N/\mu\text{m}^3$; Equation 2.14), along with D values (in $\mu\text{m}^2/\text{s}$; Equation 2.15).

Equation 2.14 – Average particle concentration; Where N_A = Avagadros constant, defined as the number of particles that are conatined in one mole of a sustance and is equal to $6.022 \times 10^{23} \text{ mol}^{-1}$, and W_0 is determined via Equation 2.13.

$$C = \frac{N}{W_0 \cdot N_A}$$

Equation 2.15 – Diffusion co-efficient (D); Where W_1 is determined via Equation 2.11 and τ_D represents the average diffusion time of the fluorescent species through the confocal volume determined via the autocorrelation model outline in Equation 2.8.

$$D = \frac{W_1^2}{4 \cdot \tau_D}$$

2.6.2.4 Autocorrelation analysis for SNAP labelled receptors

When we consider 2D systems, for example membrane bound receptors, we must adjust the biophysical model to incorporate the movement in x and y dimensions only. Additionally, all autocorrelation analyses of cell reads incorporated an offset (d) to allow the asymptote of the decay curve to be modelled for a value other than 1. Therefore, SNAP tagged receptors were analysed using a 1x2D + Triplet + offset model (Equation 2.16).

Equation 2.16 – 1x2D autocorrelation function; Where A is the pre-exponential function shown in Equation 2.1.

$$G(\tau) = 1 + A \frac{1}{N} \cdot \left(1 + \frac{\tau}{\tau_D}\right)^{-1}$$

2.6.2.5 Autocorrelation analysis for fluorescent ligand binding

The 1x2D model (Equation 2.16) can be also be adjusted to produce a 2 component fit that gives two τ_D values, as well as the percentage fraction (F_1 and F_2) that each component contributes to the overall amplitude of the autocorrelation curve at G_0 . The incorporation of 2 components enables separation of fluorescent species with distinctive diffusion times, for example unbound fluorescent ligands which are able to occupy both 3D space, when unbound, and 2D space, when bound to the receptor. In addition, an offset was applied, as with SNAP tagged receptors (Section 2.6.2.4). Therefore, experiments investigating fluorescent ligand bound receptors were analysed

using a 1x3D, 1x2D + Triplet + offset biophysical model. This is a 2 component model that accounts for the fast moving species of the fluorophore when free in solution (1x3D component; Equation 2.17), and the slower moving species when bound to the receptor (1x2D component; Equation 2.18). As with the solution ligand reads (Section 2.4.2.2), particle concentration (C) within the detection volume was calculated for the 2D system (in N/μm²; Equation 2.19), along with diffusion co-efficient (Equation 2.15) from the autocorrelation curve fitting.

Equation 2.17 - 1x3D, 1x2D autocorrelation model; This equation represents the 3D component attributed to fast moving, unbound fluorescent particles, of the 2 component model.

$$G(\tau) = 1 + A \frac{1}{N} \left(F_1 \left(1 + \frac{\tau}{\tau_{D1}} \right)^{-1} + F_2 \left(1 + \frac{\tau}{SP^2 \cdot \tau_{D2}} \right)^{-0.5} \right)$$

Equation 2.18 - 2x2D autocorrelation model; This equation represents the 2D component attributed to slow moving, receptor-bound fluorescent particles, of the 2 component model.

$$G(\tau) = 1 + A \frac{1}{N} \left(F_1 \left(1 + \frac{\tau}{\tau_{D1}} \right)^{-1} + F_2 \left(1 + \frac{\tau}{\tau_{D2}} \right)^{-1} \right)$$

Equation 2.19 – Particle concentration; Where $N_{\tau D}$ represents the average diffusion time for the average particle number within the detection volume, and 1×10^6 is the conversion function from m to μm.

$$C = \frac{N_{\tau D}}{(\pi \cdot W_1 \cdot 1 \times 10^6)^2}$$

2.6.2.6 Photon counting histogram analysis (PCH)

PCH analysis is an approach that uses the variation in the amplitude of fluorescence excitation in different regions of the confocal volume to model the raw fluorescence fluctuation data with respect to intensity amplitude, as opposed to autocorrelation correlation, which is concerned with the temporal behaviour of the fluorescence fluctuations. PCH analysis can provide information such as an alternative calculation of particle concentration (N) and molecular brightness (ε). The measure of brightness is proportional to the number of fluorescent molecules within a particle complex, and can therefore act as an indicator of changes in the stoichiometry of a system. For example it provides information on the oligomeric status of the molecules within the system under investigation (Chen et al., 1999; Kask et al., 1999).

When performing PCH analysis the fluorescence intensity trace is divided into bins of a specific time. The fluorescence intensity within each bin is calculated as the number of photon counts (k) and the number of bins with that number of counts (the frequency). The bin time should be optimised for every system and should ideally be less than the dwell time of the fluorescent species in the confocal volume. This eliminates fast, time-dependent fluctuations that can be attributed to photophysics of the fluorophore, whilst retaining as much information from the data set as possible.

From PCH analysis, we would expect a Poissonian distribution based on the physics of the detectors receiving information from a constant immobile source. However, the histogram produced deviates from an expected Poissonian distribution due to the movement of particles between unevenly illuminated regions of the confocal volume (Chen et al., 1999), thereby exposing the fluorescent species to higher or lower levels of light excitation. Therefore the frequency histogram generated produces a super Poissonian distribution curve (Figure 2.12C), and from this deviation, molecular brightness measurements can be derived.

Equation 2.20 – Point spread function used to determine Poissonian to super-Poissonian deviation in PCH analysis, where photon counts are represented by K , molecular brightness by ϵ and particle number by N .

$$\langle K \rangle = \epsilon \cdot N$$

This relationship from Poissonian to super-Poissonian is resolved to determine the molecular brightness (ϵ) and the particle number (N) from the average photon counts within the volume $\langle K \rangle$ (Equation 2.20). This feature is known as a non-uniform point spread function and generates a broadening of the distribution observed in the PCH super-Poissonian histogram. The extent of the deviation depends on the particle brightness and concentration. The original PCH analysis was based on two-photon excitation conditions, but is more complex for single photon excitation systems, such as the one used here, in which the shape of the confocal volume deviates from a strict Gaussian shape.

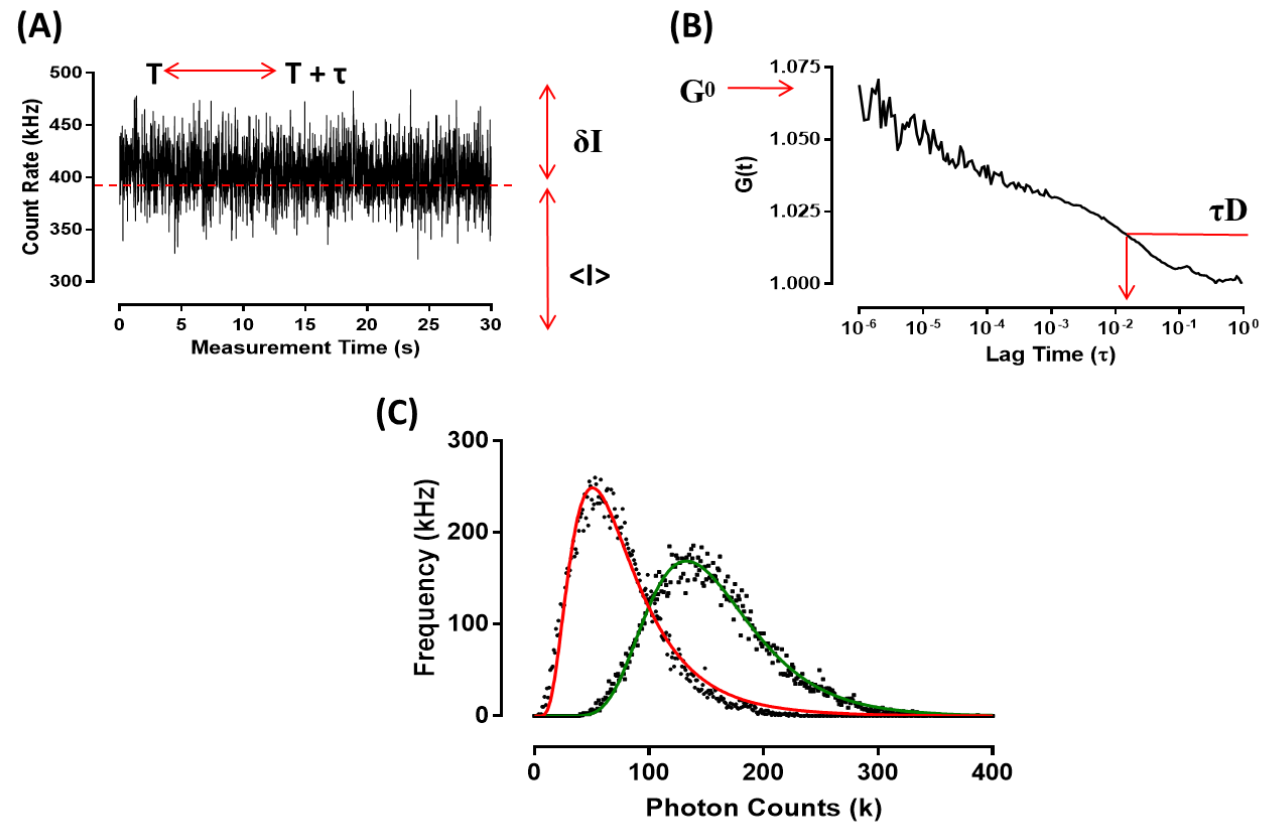


Figure 2.12 – Representative autocorrelation and PCH analysis of SNAP AF 647 labelled SNAP-Y₁R cells. (A) Shows the time dependent fluorescence fluctuations that are recorded during an FCS calibration measurement of Cy5, demonstrating the derivation of the autocorrelation function parameters. (B) Shows the production of the autocorrelation decay curve determined from these parameters and (C) shows a representative PCH trace after the application of a 1x2D component fit with a 1 ms bin time, following 1 μ M NPY treatment (green) compared to AF 647 controls (red).

Table 2.5 – Analysis parameters for autocorrelation and PCH. Analyses were performed using Zen2010 software. Measurements for AF 488 and RhB fluorophores were taken using 488 nm Argon and 594 nm laser excitation collected through a BP530-610 and LP580 filter, respectively. AF 647 and sCy5 fluorophores used 633 nm HeNe laser excitation and LP650 filter emission collection. Fixed parameters are shown as a single value and non-fixed are presented as the range of values produced during analysis.

Condition	Acquisition parameters				Autocorrelation analysis			Photon counting histogram analysis		
	Calibration fluorophore	Laser line	Pinhole	Laser power (%) / AOTF	Model	SP	Offset	Model	Bin time (μs)	F value
Calibration measurements										
Rh6G	∅	488 Argon	70	100-50/10	1x3D	∅	∅	1 Comp	20	∅
Cy5	∅	647 HeNe	90	50-70/10	1x3D	∅	∅	1 Comp	40	∅
Fluorescent ligand solution measurements										
10nM RhB mono	Rh6G	594 Argon	70	50/10	1x3D	6	∅	1 Comp	50	0.918-1.108
10nM RhB dimer	Rh6G	594 Argon	70	50/10	1x3D	6	∅	1 Comp	500	0.918-1.108
10nM Cy5 mono	Cy5	647 HeNe	90	50/10	1x3D	5.6-7.5	∅	1 Comp	50	0.568-0.637
10nM Cy5 dimer	Cy5	647 HeNe	90	50/10	1x3D	5.2-6.2	∅	1 Comp	50	0.626-0.640
10nM Cy5 dual dimer	Cy5	647 HeNe	90	50/10	1x3D	5.2-6.2	∅	1 Comp	150	0.626-0.640
SNAP labelled Y₁R +/- NPY/GR231118 treatment										
Control AF 488	Rh6G	488 Argon	70	50/10	1x2D	4.8-5.8	0.008-0.053	1 Comp	1000	0.520-0.596
AF 488 + 1μM NPY	Rh6G	488 Argon	70	50/10	1x2D	4.8-5.8	0.008-0.053	1 Comp	1000	0.520-0.596
Control AF 647	Cy5	647 HeNe	90	50/10	1x2D	4.8-5.3	0.011-0.028	1 Comp	1000	0.634-0.657
AF647 + 1μM NPY	Cy5	647 HeNe	90	50/10	1x2D	4.8-5.3	0.012-0.024	1 Comp	1000	0.634-0.657
AF 647 + 1μM GR231118	Cy5	647 HeNe	90	50/10	1x2D	4.8-5.3	0.002-0.037	1 Comp	1000	0.634-0.657
Fluorescent ligand binding at Y₁R										
10nM RhB mono	Rh6G	594 Argon	70	50/10	1x3D, 1x2D	6 (fixed)	-0.001-0.004	2 Comp	1000	0.874-2.740
10nM RhB dimer	Rh6G	594 Argon	70	50/10	1x3D, 1x2D	6 (fixed)	0.000-0.002	2 Comp	1000	0.870-1.532
10nM Cy5 mono	Cy5	647 HeNe	90	50/10	1x3D, 1x2D	5 (fixed)	-0.004-0.027	2 Comp	1000	0.603-0.670
10nM Cy5 dimer	Cy5	647 HeNe	90	50/10	1x3D, 1x2D	5 (fixed)	0.012-0.032	2 Comp	1000	0.616-0.643

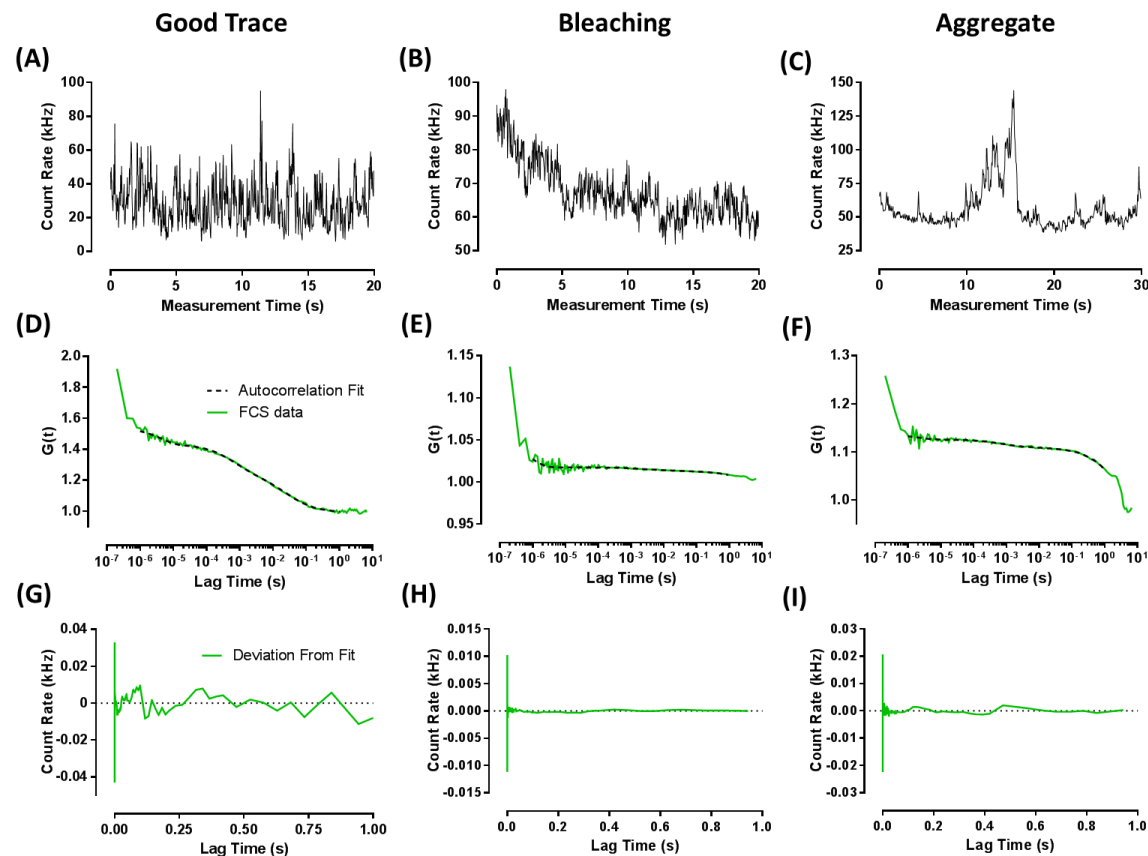


Figure 2.13 - Example FCS traces. (A, D and G) Show a representative good trace, autocorrelation decay curve and deviation from fit, measured in a Y_1 -GFP cell at 50% laser power. (B, E and H) shows a representative trace, autocorrelation decay curve and deviation from fit, where the FCS trace exhibits bleaching with a decreasing average intensity $\langle I \rangle$. (C, F and I) Shows a representative trace, autocorrelation curve and deviation from fit where initial FCS trace exhibits large transient increases in intensity that can be attributed to aggregates moving through the confocal volume.

Deviation from the strict Gaussian shape can be controlled for by calculating a first order correction (F) factor, which indicates the fraction of detected photons from the non-Gaussian part of the confocal volume. F is obtained through calibration reads (Huang et al., 2004).

As with autocorrelation analysis, a 1 or 2 component PCH model can be fitted to account for heterogeneous populations with differing brightnesses. A 1 component model was chosen for the analysis of calibration data, solution based measurements and SNAP tagged receptor measurements, while a 2 component fit was used in fluorescent ligand binding measurements. From these fits, PCH analysis offers an alternative way to calculate particle concentration (N_{PCH} in nanomolar; Equation 2.21). The parameters used in PCH analysis for each experimental condition are summarised in Table 2.5.

Equation 2.21 – PCH derived concentration, providing a measure of particle concentration in nanomolar, where N_A is Avagadro's number (6×10^{23}).

$$C = \frac{N}{W_0 \cdot N_A} \cdot 1 \times 10^9$$

2.6.2.7 FCS data exclusion criteria

Due to the nature of this technique, exclusion criteria were set to ensure consistent and non-biased exclusion and inclusion of data. For both cell based and solution based measurements, traces that showed obvious bleaching with a decline in $\langle I \rangle$ or large aggregates showing a large transient increase in intensity were excluded (Figure 2.13). If peaks in fluorescence, more than 1000% of the average count rate of the trace were present, they were cut from the trace. If more than half of the trace had to be cut due to aggregates or peaks in fluorescence they were excluded. Following autocorrelation analysis, if a clear asymptote was not reached, with or without an offset, it was excluded, and if the calculated diffusion time was longer than the length of the read time of the measurement, it was excluded. For all data points excluded due to poor traces or poor autocorrelation results, the corresponding PCH values were also excluded. These criteria allowed for a 50-70 % acceptance proportion of traces.

2.6.3 Solid and solution phase peptide synthesis

2.6.3.1 LCMS analysis

LCMS traces were analysed based on the expected mass of the product and the mass to charge ratio (m/z). The mass spectrum is a graphical display of the relative abundance of ion signals against the m/z ratios. It is common practice that the signal at the highest abundance is 100 % and all other signals are taken as a percentage of that.

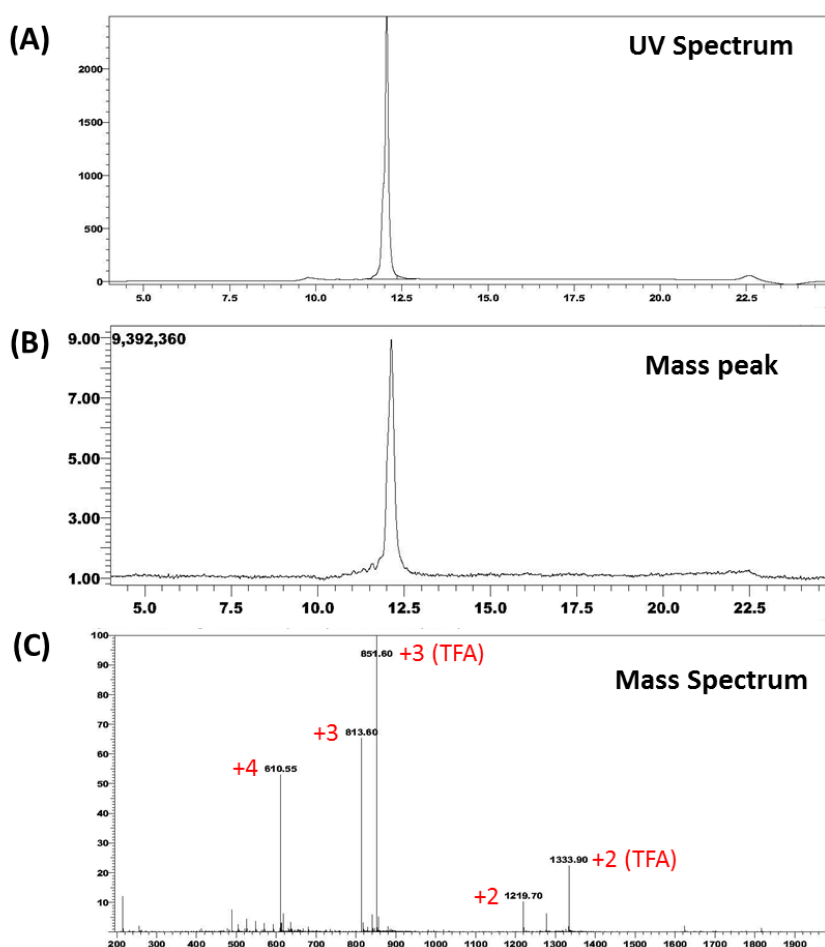


Figure 2.14 - Representative LCMS trace of analogue 2A [Dap⁴]dimer (Chapter 3). (A) Shows the UV spectra of the sample expressed in minutes and arbitrary absorbance units on the x and y-axis respectively. (B) and (C) show the mass spectra of the sample. (B) Indicates that the UV peak observed in (A) can be attributed the mass peak in (B) due to the generation of the peaks at similar times along the x-axis. (C) Shows the range of masses present within the sample that are attributed to the mass peak in (B), expressed as the mass to charge ratio (m/z) and in arbitrary units of intensity on the x and y-axis. In panel (C) several masses are observed, all of which can be attributed to the expected mass of the peptide at a different charge, where +1 +2 +3 and +4 indicate the m/z attributed to each peak. In addition, masses for the compound when complexed with TFA are also observed.

As fragmentation of peptides using ESI-MS is limited, the mass spectra can be relatively simple, however the spectra may become more complicated to analyse due to the presence of multiple-protonation states of the protein following ionisation (Figure 2.14).

Equation 2.22 - Assuming χ protonation sites;

$$MS\ peak\ mass = \frac{expected\ mass + \chi}{\chi}$$

The number of charges on a peptide is dependent on the size of the peptide and the number of accessible protonation sites. Therefore, the expected peak mass seen on the spectra can be predicted using Equation 2.22. All expected masses were determined by structures drawn in ChemBioDraw Ultra v14, and the above principles were applied in determining the correct mass peaks were present. In addition to mass spectrum analysis, the retention time (R_T), a measure of the time taken for a solute to pass through the chromatography column, was determined from analysis of the UV spectrum (Figure 2.14). R_T was calculated as the time from sample injection to detection.

Chapter 3

Synthesis of peptide analogues of the neuropeptide Y Y₁ receptor antagonists, BVD15 and GR231118

"I always said that you can't teach a biologist chemistry..."

Philip Thompson

3.1 Introduction

3.1.1 Peptides as leads in chemical biology

Since the mid 1990's, drug discovery and development has been heavily influenced by "Lipinski's Rule of 5", a set of guidelines to evaluate drug-likeness, chemical properties, pharmacological activity and likely oral activity of drugs in humans (Lipinski, 2004). The rule of 5 states that the compound should have <5 hydrogen donors, <10 hydrogen bond acceptors, a molecular mass of <500 Daltons and a partition co-efficient (measure of hydrophobicity) of <5. As such, a large number of drugs produced to target disease are small molecular entities (SME), with little work spent on the development of larger target compounds. However, drug design has seen a shift in recent years towards the use of biological compounds, such as antibodies and peptides for the treatment of disease (Li et al., 2018; Santos et al., 2016).

Biological compounds (or biologics), are considered to be macromolecules that typically require synthesis in living systems. This includes clinical antibodies, large protein hormones and some peptides. The use of these biologics have become popular, despite being more complex to design, make and deliver, as they often exhibit better specificity and lower toxicity, resulting in reduced off-target effects and increased patient compliance (Oo and Kalbag, 2016). One of the first examples of a peptide used in disease treatment was insulin, which is used to regulate glucose utilisation in the body. When insulin regulation is disrupted, blood sugar levels become uncontrolled and when these levels remain high for an extended period of time it can result in the development of the metabolic disease known as diabetes mellitus (Alam et al., 2014). As such, human insulin, composed of 51 amino acids, is used as a therapy in diabetes to maintain blood sugar levels. As insulin is administered through subcutaneous injection, many new therapies have been investigated in an attempt to develop smaller drug compounds which may be administered orally or through inhalation (Cichocka et al., 2016). However, larger peptides and proteins are often required to bind some targets with high affinity because, unlike small molecules, they replicate the binding mode and contacts

within the large binding site of the target receptor. Investigations into insulin alternatives have been unable to produce compounds that can replicate the large binding epitope of the insulin peptide for the insulin receptor. Therefore, despite the size and delivery method of insulin, it is recognised as a lifesaving treatment in diabetes (Chowdhury et al., 2014; Jin et al., 2018).

Other, more recent, examples of the use of biologics in disease treatment have come in the form of antibodies and nanobodies. The antibody infliximab, is a chimeric monoclonal antibody used for treatment of inflammatory bowel disorders through complexing with tumour necrosis factor (TNF- α) and thereby inhibiting inflammation signalling through the TNF- α receptors (Dubinsky and Fleshner, 2003; Hanauer, 2003). Antibodies have also been developed to target G protein coupled receptors (GPCRs) such as the calcitonin gene-related peptide (CGRP) and chemokine receptors (Edvinsson et al., 2018; Hutchings et al., 2017). As such, peptides, antibodies and other biologics have started to be recognised as viable targets for drug design and development.

Peptides are widely expressed in nature and they perform a wide range of essential functions in the human body. These include antimicrobial activity, such as; the role of the defensin family of peptides, which assist in pathogen phagocytosis (Fruitwala et al., 2018); Vasoactivity, such as the role of vasoactive intestinal peptide (VIP), which induces vasodilation in the intestinal tract and the heart (Moody et al., 2018; Zacharko-Siembida et al., 2013); Neuro-signalling activity, in the case of opioid peptides such as enkephalin and proopiomelanocortin (POMC; Bodnar, 2018); and regulation of metabolism through peptides such as glucagon, leptin, insulin and NPY (Abot et al., 2018). Mammalian peptides utilise 21 proteinogenic, DNA encoded amino acids, which are either synthesised in the body (non-essential) or taken into the body through diet (essential; Wu, 2009; Figure 3.1). These 21 amino acids include selenocysteine, which is unusual as it is not coded for directly in the genetic code, but is instead encoded for in mRNA by a UGA codon typically utilised as

a stop codon (Serrão et al., 2018). The sequence, and thus, arrangement of the functional groups within the side chains or 'R' groups of an amino acid, generate the unique chemical properties associated to a peptide sequence. In addition, there is a myriad of post-translational modifications that peptides may undergo, imparting a secondary level of diverse activity, such as; lipidation (Nadolski and Linder, 2007), phosphorylation (Humphrey et al., 2015) and methylation (Biggar and Li, 2015). The amino acid residues also contribute to the secondary and tertiary structure of the peptide, as is the case for the NPY family of peptides (Section 1.1.1; Chapter 1).

3.2 Chemical synthesis of peptides

Methods to produce peptides within the laboratory setting have been developed over many years. These methods include; bacterial production of peptides, solution phase peptide synthesis and solid phase peptide synthesis (SPPS). Bacterial production is limited as, in general, only natural amino acids can be incorporated into the peptide sequence. Techniques have been developed that now allow for the introduction of non-natural amino acids in prokaryotes (Uhlenbeck and Schrader, 2018) and eukaryotes (Huber and Sakmar, 2014), however these methods can present difficulties in aspects of production and purification. Due to the challenges of multi-step syntheses, SPPS is currently the mainstay of synthetic production in peptide research and the dominant approach in the production of short to medium sized peptides (Jaradat, 2018).

3.2.1 Solid phase peptide synthesis (SPPS)

SPPS was pioneered by Nobel laureate Robert Merrifield, and revolutionised the way peptides are synthesised in the laboratory (Merrifield, 1963). Now the standard method for peptide synthesis, SPPS has allowed for the fast synthesis of peptides that are difficult to express in bacteria, and has allowed for easy incorporation of non-natural amino acids, peptide backbone modifications and tertiary structure modifications (Jaradat, 2018).

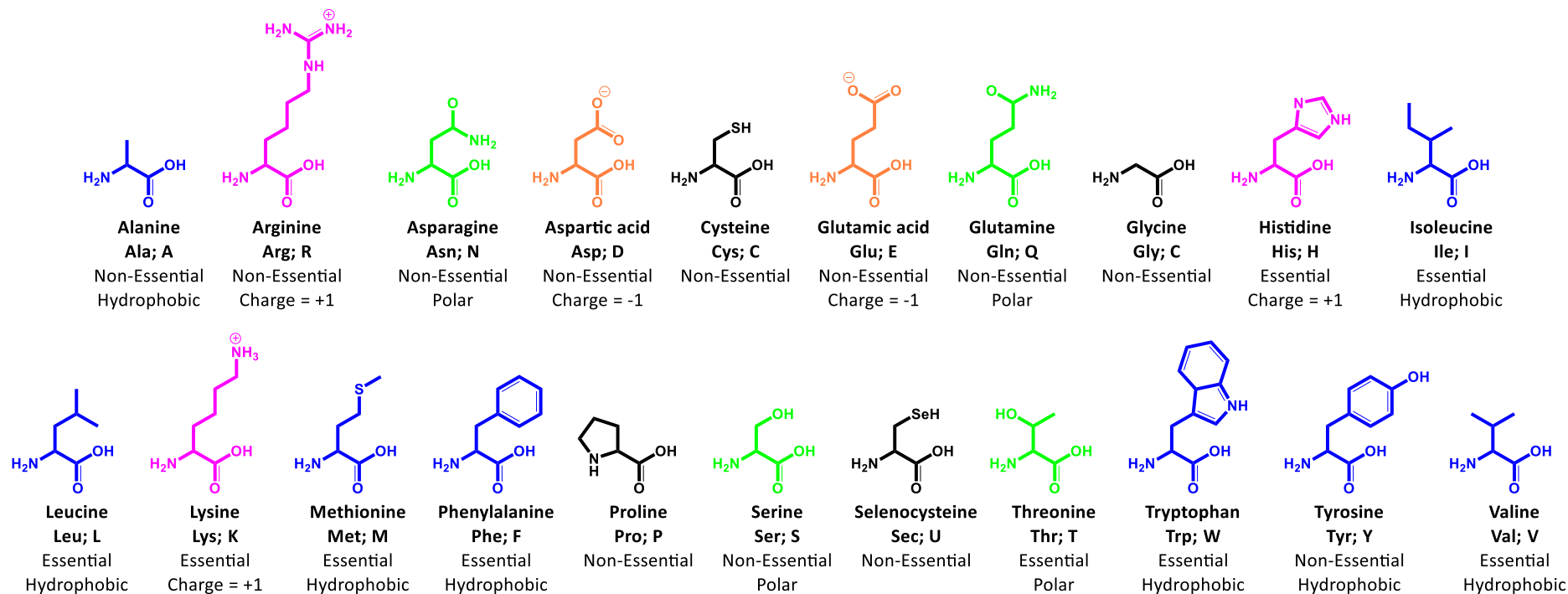


Figure 3.1 - List, in alphabetic order, of essential and non-essential 21 proteinogenic α -amino acids found in eukaryotes. Where alanine, as a representative example, demonstrates the basic amino acid structure consisting of an N-terminal amino group, a C-terminal carboxylic acid group and a side chain 'R' group. In addition, amino acids are characterised by the presence of an α -carbon and carbonyl carbon. Hydrophobic amino acids are highlighted in blue, polar in green, negatively charged in orange and positively charged in pink, annotated with; amino acid name: three letter abbreviation; one letter abbreviation; essential/non-essential; side chain properties.

Merrifield's original approach to SPPS, still fundamentally applied today, involves a sequence of reactions between N-terminally and side chain protected amino acids dissolved in an appropriate solvent, where the amino acid residue is bound to an insoluble solid support, known as a resin. Synthesis commences through the covalent coupling of the first amino acid in the peptide sequence to the solid resin support via C-terminal coupling of an N-terminal and side chain protected amino acid. The coupled amino acid is then deprotected at the N-terminus, to which the next amino acid is coupled, following carboxylate activation. This cycle is repeated through the stepwise addition of amino acids until the desired sequence is assembled (Figure 3.2). The peptide is then cleaved from the resin, usually under strong acidic conditions, whilst simultaneously cleaving side chain protecting groups, with appropriate scavenger reagents present to capture reactive cleavage adducts. Reverse phase - high performance liquid chromatography (RP-HPLC) is then generally used to purify crude products and yield homogenous pure peptides (Jaradat, 2018; Montalbetti and Falque, 2005).

The original method for SPPS used the acid sensitive tert-butyloxycarbonyl (Boc) group as a temporary N-terminal α -amino protecting group, and benzyl (Bzl) as the side chain protecting group, where the cleavage of these protecting groups was conducted via strong acid treatment such as hydrogen fluoride (Merrifield, 1963). This method has now been largely replaced with the N-terminal fluorenylmethyloxycarbonyl chloride (Fmoc) and tert-butyl (tBu) side chain protection methodology which is less hazardous and economically more viable and is discussed in more detail below (Section 3.2.1.3; Behrendt et al., 2016).

The SPPS approach has key advantages, such as the ready removal of soluble unreacted reagents and side products, through filtration and washing and thus the capacity to use large molar excesses to drive reactions to completion. It also offers advantages in speed through the automation of the stepwise reactions, particularly when combined with microwave-accelerated SPPS,

allowing full length peptides to be produced within hours (Erdélyi and Gogoll, 2002). Limiting factors in SPPS include potential for peptide length, as aggregation and poor coupling can occur with peptide lengths over 40 amino acids. In the production of complex peptides or in industrial syntheses, a mix of synthesis approaches are frequently used i.e. when tertiary modifications are required, such as cyclisation (Jaradat, 2018).

While the fundamentals of Fmoc-based SPPS have been well described (Behrendt et al., 2016; Chandrudu et al., 2013; Jaradat, 2018), there are countless variations of functionalised resins, reagents, solvents and conditions that can fall under the general approach. In what follows, the specifics of the approaches selected in this project are summarised, including the choice of functionalised resin, solvents, coupling methods and cleavage reagents.

3.2.1.1 Rink amide resin

Resins need to carry functionalisation to determine the functional group at the C-terminus following cleavage. One of the most widely used resins is 4-(2,4-dimethoxyphenyl-hydroxymethyl)-phenoxy-methyl-polystyrene, commonly known as Rink amide resin (Figure 3.3A; Rink, 1987). Rink amide resin lends itself to the synthesis of C-terminally amidated peptides due to cleavage at the acid-labile benzylic cleavage point highlighted in Figure 3.3. While studies have demonstrated the utility of Rink amide resin in synthesis, with good yields obtained from acidolytic cleavage (Behrendt et al., 2016), it is susceptible to linker decomposition during acidolytic cleavage and may even be liable during the peptide extension phase. Buffering with N,N-diisopropylethylamine (DIPEA) protects the linker through synthesis (Rink, 1987) while 1,3-dimethoxybenzene (DMB) prevents the side reactions that occurs during cleavage (Figure 3.3; Stathopoulos et al., 2006).

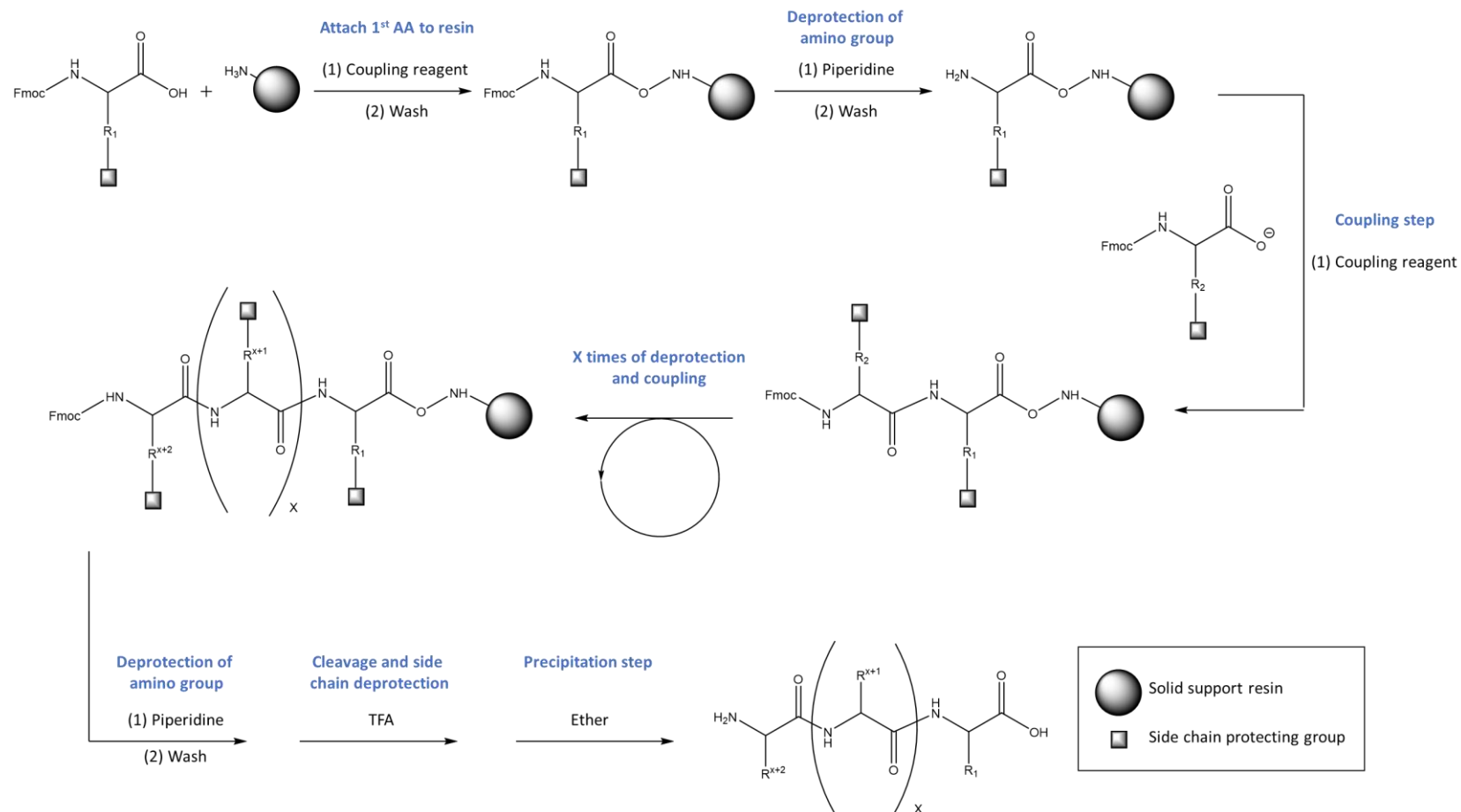


Figure 3.2 - Peptide backbone production via automated synthesis demonstrating the repeating cycle of amino acid addition for linear peptide production, with fluorenylmethyloxycarbonyl chloride (Fmoc) based synthesis as the example, where AA is used as an abbreviation for amino acid and TFA is trifluoroacetic acid.

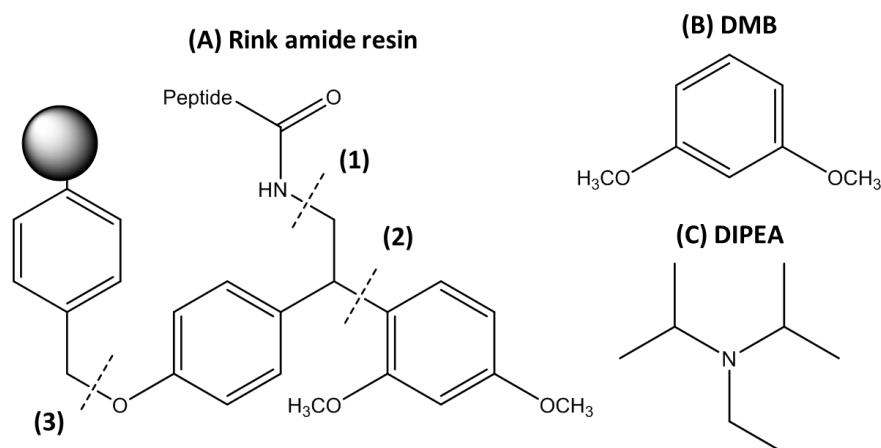


Figure 3.3 – Cleavage reaction sites on Rink amide resin. (A) Shows the structure of Rink amide resin and (1) the desired cleavage reaction site to produce an amidated C-terminus following cleavage. (2) Shows cleavage sites resulting in the production of C-terminally alkylated amide by-product and (3) shows a reaction site which can be potentiated by reaction site (2) cleavage. The addition of 1,3-dimethoxybenzene (DMB; B) to the cleavage reaction mixture results in minimising the production of undesired adducts, and (C) shows the structure of diisopropylethylamine (DIPEA) base, which is added to the reaction mixture to limit linker degradation during synthesis.

3.2.1.2 Solvents in SPPS

In SPPS, the resin must allow reactants and reagents to enter the polymer network and interact, thus an appropriate solvent, compatible with the synthesis chemistry is needed to maximise reaction rate and yield (Kent, 1988; Vaino and Janda, 2000). Polar solvents such as N,N-dimethylformamide (DMF) and dichloromethane (DCM), are utilised to enhance synthesis efficiency, as they have been found to swell polystyrene based resins 5-6x in volume (Santini et al., 1998). DMF is the favoured solvent in SPPS but it is essential to ensure that DMF of analytical grade is used during synthesis as amine-containing impurities in DMF can also result in premature cleavage of the N-terminal Fmoc group.

3.2.1.3 Fmoc deprotection and amino acid coupling reagents

As mentioned above Fmoc/tBu chemistry is widely used in SPPS (Section 3.2.1). The Fmoc/tBu strategy was initially described by Carpino and Han (1970), and utilises the base-labile Fmoc-group as an N-terminal protecting group and acid sensitive tert-butyl ether (tBu), tert-butyl ester (OtBu), triphenylmethyl chloride (Trt), and 2,2,4,6,7-pentamethyldihydrobenzofuran-5-sulfonyl (Pbf),

as side chain protecting groups depending upon the amino acid. Generally, the N-terminal Fmoc group can be quickly deprotected by treatment with either a primary or a secondary amine, e.g. piperidine, in an appropriate polar solvent. The resulting dibenzofulvene by-product is simultaneously scavenged by the amine (Carpino and Han, 1973; Carpino, 1987; Figure 3.4). The most widely used reaction conditions for N-terminal Fmoc deprotection is 20% piperidine in DMF and was the method employed throughout the work described in this Chapter (Jaradat, 2018).

In Fmoc based SPPS there are many ways of activating Fmoc-protected amino acids for amide coupling reactions. The selection of an activating agent is critical in maximising the coupling yield and minimising possible side reactions. For the work described in this thesis chapter, the coupling reagent used was O-(1H-6-chlorobenzotriazole-1-yl)-1,1,3,3-tetramethyluronium hexafluorophosphate (HCTU) in the presence of DIPEA. The HCTU/DIPEA strategy utilises HCTU as an activating agent, converting carboxyl-containing substances into 6-CLOBt esters (Figure 3.5). These reagents are more reactive than other coupling strategies owing to the production of an ethyl 1-hydroxytriazole-4-carboxylate (HOCT) intermediate (Hood et al., 2008; Sabatino et al., 2002; Figure 3.5). HCTU is a member of a series of coupling agents including, 1 [Bis(dimethylamino)methylene]-1H-1,2,3-triazolo[4,5-b]pyridinium 3-oxide-hexafluorophosphate (HATU) and 3-[Bis(dimethylamino)methylumyl]-3H-benzotriazol-1-oxide hexafluorophosphate (HBTU). HCTU is less toxic and more stable in DMF compared to HATU, and more cost effective than HBTU, giving higher purity peptides compared to other coupling reagents (Hood et al., 2008). For prolonged coupling reactions, the instability of benzotriazole-containing activating agents leads to its degradation in the extended presence of DIPEA (Albericio et al., 1998; Mountford et al., 2014). In such cases 6-chloro-benzotriazole-1-yloxy-tris-pyrrolidinophosphonium hexafluorophosphate (Pyclock) is favoured as a coupling reagent (Mountford et al., 2014; Valeur and Bradley, 2009).

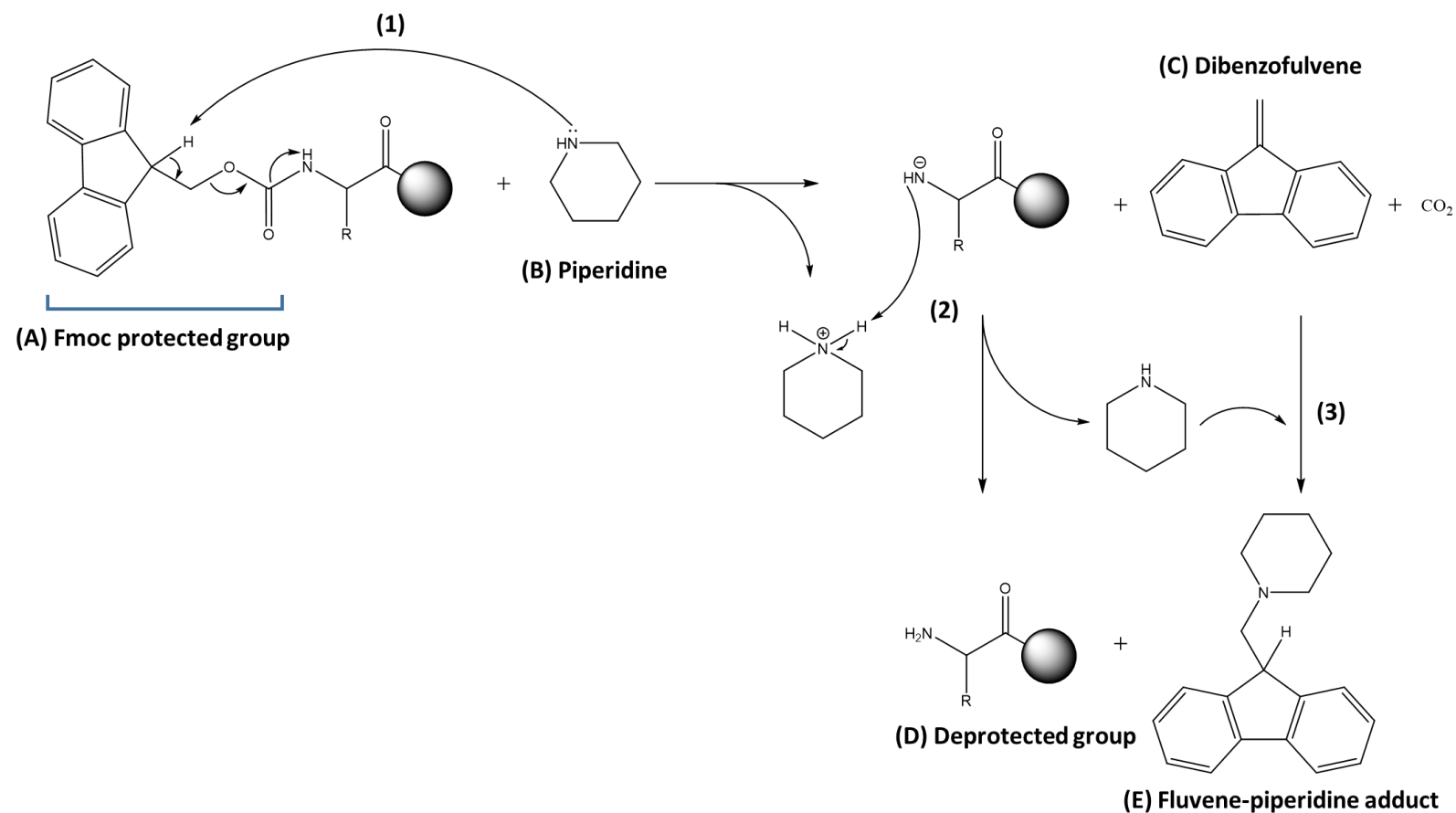


Figure 3.4 – Mechanism of Fmoc deprotection by piperidine treatment, showing an N-amino group protected by Fmoc (A) and where (B) shows the structure of mild base, piperidine. Treatment with piperidine leads to the formation of the desired free amino acid component (D) deprotected from Fmoc via (1) and (2), and the formation of a fluorene-piperidine adduct (E), via (3) between dibenzofulvene (C) where piperidine acts as a scavenger.

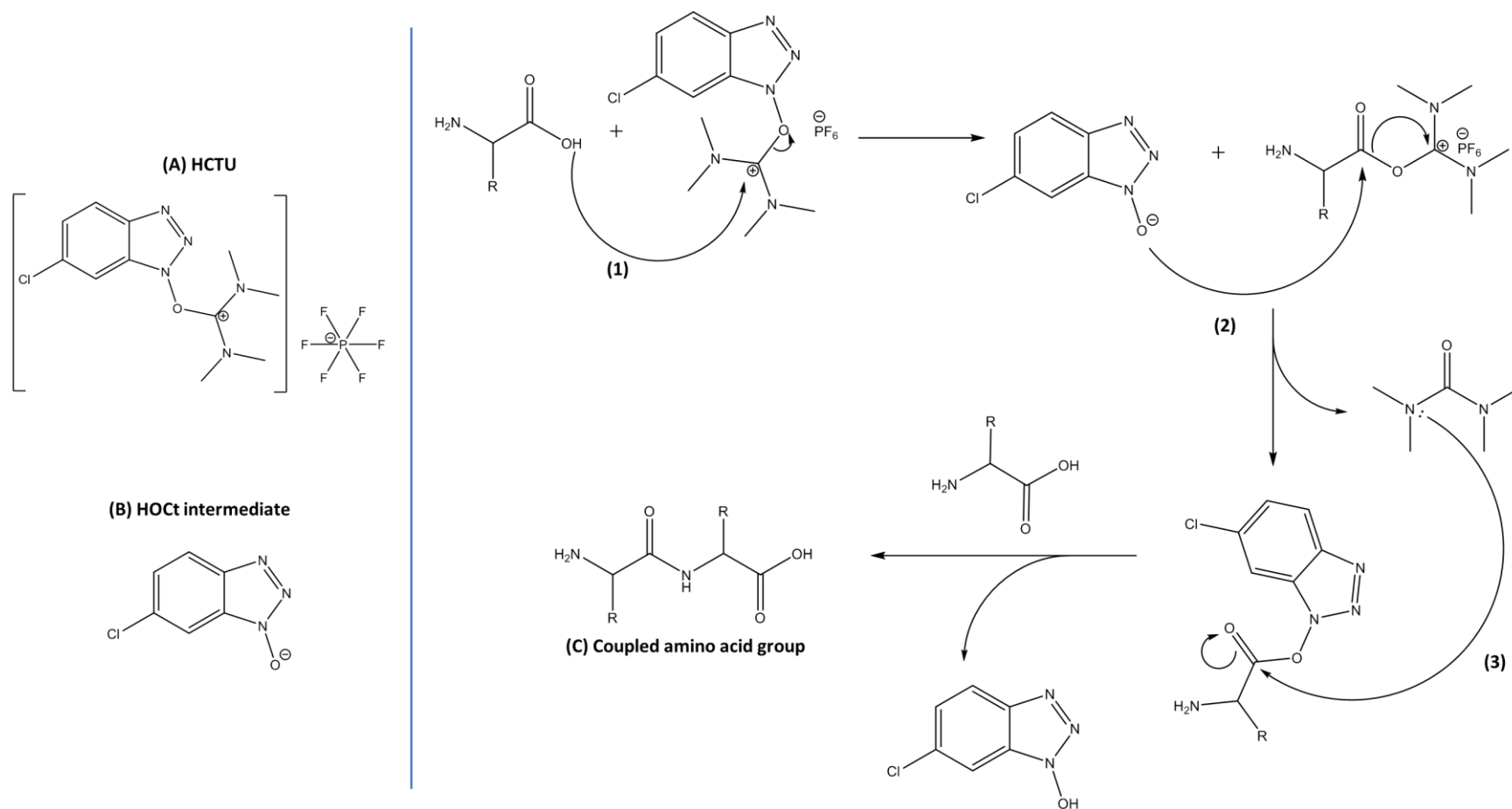


Figure 3.5 - Mechanism of HCTU coupling, showing structure of HCTU (A) and HOCT intermediate (B). Where coupling of N-amino group occurs via production of HOCT intermediate (1) result in amino acid coupling (C) via (2) and (3).

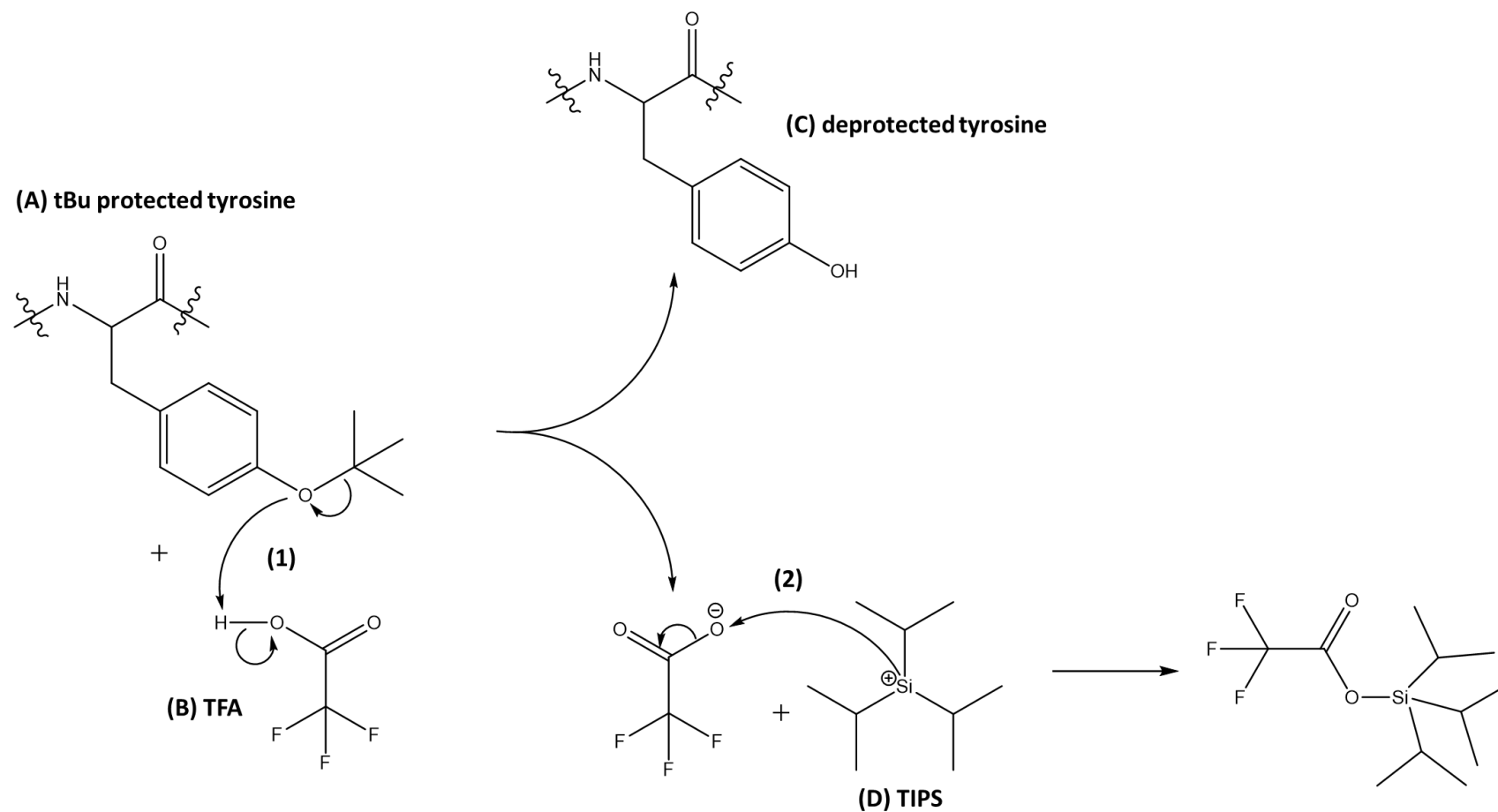


Figure 3.6 – Mechanism of tBu side chain cleavage from tyrosine, as an example, with TFA and TIPS. (A) Shows tert-butyl (tBu) cleavage from tyrosine via (1) with trifluoroacetic acid (TFA; B) to give deprotected tyrosine (C) and triisopropylsilane (TIPS; D) is shown acting as a scavenger via (2).

3.2.1.4 Side chain deprotection and resin cleavage

Upon completion of peptide chain extension, simultaneous side-chain deprotection and resin cleavage are achieved under acidolytic conditions using TFA. Chemical scavengers are often added to eliminate the reactive carbocations produced from side chain deprotection, which may otherwise cause irreversible covalent reattachment to the side-chains (Behrendt et al., 2016). Scavenger mixes of triisopropylsilane (TIPS) and DMB were utilised in this work (Figure 3.6). TIPS has been found to support efficient cleavage and TIPS scavenged side products are sufficiently volatile to be removed by a stream of nitrogen (Pearson et al., 1989). DMB was included in the scavenger mix to guard against side reactions associated with Rink amide resin cleavage, as described above (Section 3.2.1.1).

These methods summarise the fundamental methods of linear peptide synthesis employed throughout this chapter. Noting that variations employed to generate cyclic peptides through intramolecular bridging reactions and the associated specialised protection strategies are discussed below (Section 3.4).

3.2.2 Y₁R ligands

As discussed in Chapter 1 (Section 1.2.4), both peptide and non-peptide analogues have been designed and targeted towards the Y₁R. Non-peptide Y₁R analogues such as BIBO3304 (Wieland et al., 1998) and UR-MK299 (Keller et al., 2015) demonstrate high affinity competitive antagonist activity. Peptide antagonists that have been developed towards the Y₁R were designed initially from the C-terminal sequence of the NPY peptide, including BVD15 and GR231118, both of which are the basis of the chemical synthesis in this chapter.

3.2.3 BVD15 monomer peptide as a Y₁R antagonist

Leban et al., (1995) originally described a truncated decapeptide corresponding to the last 10 amino acid residues of NPY (YINLIYRLRY-CONH₂; Figure 3.7). This decapeptide was initially characterised as exhibiting modest

antagonist activity in suppressing NPY induced cytosolic calcium mobilisation in human erythroleukaemia (HEL) cells, a response mediated by the Y₁R (IC₅₀ 8.8 ± 0.5 nM). In an effort to develop further potent antagonists of the Y₁R, BVD15 (also referred to in literature as BW1911U90), was subsequently developed. BVD15 is a monomeric nonapeptide (INPIYRLRY-CONH₂) lacking the initial tyrosine of the decapeptide and where [Leu⁴] of decapeptide is replaced with [Pro³] in BVD15 (Figure 3.7). BVD15 was initially characterised as a competitive antagonist of NPY responses in HEL cell calcium assays, (IC₅₀ 8.0 ± 1.2 nM; Leban et al., 1995) and through competitive displacement of [³H]-NPY in Y₁R expressing SK-N-MC cell membranes (IC₅₀ 3.0 ± 0.7 nM; Leban et al., 1995), confirming Y₁R affinity.

More recently BVD15 has been developed further with Guérin et al., (2010) reporting that substitution of [Ile⁴] for [Lys⁴] resulted in a 5 fold increase in affinity at the Y₁R in comparison to BVD15. Additionally, Liu et al., (2016) exploited the BVD15 base structure to investigate the development of fluorescently tagged ligands as tools in the study of these receptors. This study explored a range of fluorescent rhodamine and cyanine derivatives, with different linkers and modification of BVD15 at different residues. Substitution of both position 2 and 4 for Lys in unlabelled BVD15 were well tolerated. Conjugation of [Lys²] to a sulphated cyanine 5 (sCy5) fluorophore was also found to be well tolerated, with no loss of antagonist activity at the Y₁R (pK_b 7.3 ± 0.1) when compared to [Lys⁴]-BVD15 (pK_b 7.5 ± 0.1) in β-arrestin2 recruitment assays. This fluorescent ligand, (Compound H; [sCy5-Lys²]BVD15; Cy5mono; BIDA84), is used as a tracer in our later studies (Chapters 4 and 5).

Bivalent derivatives of BVD15 have also been developed to target calcitonin gene-related peptide (CGRP) and Y₁R simultaneously, in a bid to target proliferation of tumour cells that co-express both receptors in breast cancers (Shrivastava et al., 2013). The peptide CGRP antagonist (J-G-Abz4-QWAVGHLM-NH₂), truncated bombesin (tBBN)) was conjugated to BVD15, via 1,4,7,10-tetraazadodecaundecane-1,4,7,10-tetraacetic acid (DOTA), at [Lys⁴].

This bivalent ligand (t-BBN/BVD15-DOTA) exhibited IC_{50} values of 18 ± 0.7 nM and 80 ± 11 nM at the CGRP and Y_1R , respectively, again demonstrating conjugation is well tolerated at position 4. The selectivity of BVD15 at the Y_1R , compared to other Y receptor subtypes, has also been studied through mutagenesis and modelling, and is explored in more detail in Chapter 4.

3.2.4 GR231118 dimer peptide as a Y_1R antagonist

Daniels et al., (1995) built upon BVD15 to produce GR231118 (also referred to as 1229U91 in literature). GR231118 is a homodimeric peptide where [Asn²] and [Ile⁴] of BVD15 have been substituted to [Glu²] and [Dap⁴] to form lactam bridges across the monomer peptides (IEP(Dap)YRLRY-IEP(Dap)YRLRY-CONH₂)₂) thereby creating an antiparallel dimer with a central cyclic moiety (Figure 3.7). GR231118 was initially characterised as a potent Y_1R antagonist on NPY induced cytosolic calcium in HEL cells (IC_{50} 0.5 ± 0.15 nM), with 20 fold higher potency than monomeric BVD15 (IC_{50} 8 ± 1.2 nM; Leban et al., 1995). Parker et al., (1998) demonstrated that GR231118 has a 15-100 fold higher apparent affinity at Y_1R (pK_i 10.2 ± 0.09) when compared to BVD15 (pK_i 8.3 ± 0.03) in radioligand binding.

Since its initial characterisation, GR231118 has been used, particularly in vivo, as a general Y_1R antagonist to determine the role of NPY signalling via the Y_1R in disease states. These include; the effects of ageing and long term caloric restriction on Y_1R regulation (Veyrat-Durebex et al., 2013); gastric acid secretion (Kermani and Eliassi, 2012); inhibition of μ -opioid induced fat intake (Zheng et al., 2010); hyperphagic and glycaemic responses to insulin-induced hypoglycaemia (Nedungadi and Briski, 2010) and hypothermia (Dark and Pelz, 2008). GR231118 has also been employed as a tool for in vitro characterisation of NPY at the Y_1R (Sah et al., 2005) and as a [¹²⁵I] radiolabelled analogue (Y_1R : K_d = 0.09 nM) for the characterisation of Y_1R ligands, providing rank orders of potency for previously characterised ligands e.g. NPY, PYY and [Leu³¹Pro³⁴]-NPY (Dumont and Quirion, 2000; Schober et al., 2000).

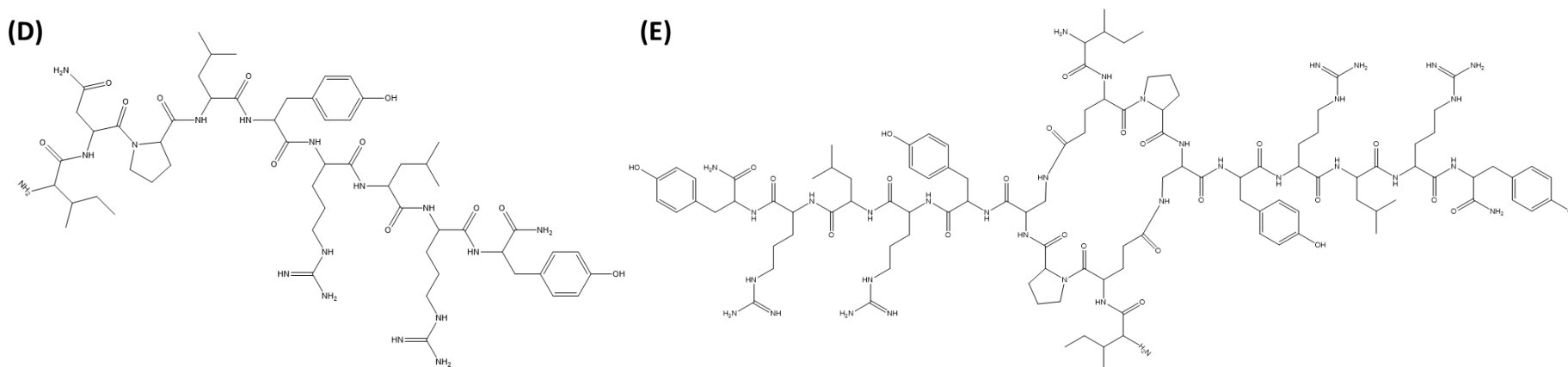
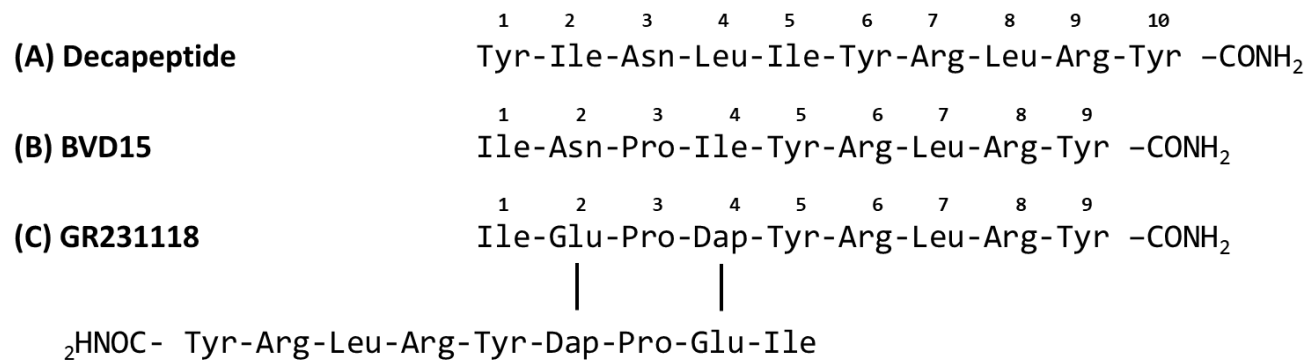


Figure 3.7 – Schematic representation of Y₁R peptide antagonists as lead compounds for chemical synthesis in this chapter. (A) Shows the original decapeptide based on the NPY C-terminus, and (B) shows BVD15 a monomeric competitive Y₁R antagonist, which exhibits nanomolar affinity, and corresponding chemical structure (D). (C) Shows GR231118 a dimeric non-surmountable Y₁R antagonist, which exhibits sub-nanomolar affinity, and corresponding chemical structure (E).

As well as radiolabelled analogues, fluorescent analogues of GR231118 have been developed for Y₁R study (Mountford et al., 2014). Rhodamine B (RhB) conjugation to the N-terminus of a single arm of the peptide was described and well tolerated (pK_i 8.5 ± 0.02) when compared to unlabelled GR231118 (pK_i 9.9 ± 0.09). This fluorescent ligand, (Compound VIII; mono[RhB]-GR231118; RhBdimer; BIDB13), is used as a tool and is further characterised in our studies (Chapter 4 and 5). In addition, GR231118 has been employed in ex vivo characterisation of NPY induced inhibition of glutamate release in cerebral cortex nerve terminals (Wang, 2005), and in the identification of Y₁R in rabbit isolated ileum (Félétou et al., 1999). GR231118 has also been shown to exhibit off-target effects, particularly at the NPFF receptors, where GR231118 has demonstrated low affinity binding (EC_{50} 3000 nM) to the NPFF₂R as an agonist of this receptor in its own right (Mollereau et al., 2002).

More recently, it has been observed that GR231118 exerts non-surmountable antagonism at the Y₁R (Mountford et al., 2014; Chapter 4 and Figure 5.6, Chapter 5) observed as a reduction in the NPY R_{max} in β -arrestin2 recruitment assays. This is in contrast to surmountable antagonism of [Lys⁴]-BVD15 in the same assay conditions (Liu et al., 2016). Given the likelihood that GR231118 competes in a competitively manner with the NPY C-terminus for the Y₁R binding site (discussed in further detail in Chapter 4), the observation of non-surmountability is most likely explained by the high apparent affinity of the peptide for the Y₁R compared to its monomeric counterparts, and as a consequence demonstrates a slow dissociation rate from the Y₁R. This would lead to apparently slowly reversible / irreversible properties of the antagonist in the β -arrestin2 recruitment assay and thus the reduction in R_{max} in a measurement with limited receptor reserve. In measuring effects in a more amplified system, e.g. Y₁R inhibition of cAMP accumulation, Parker et al., (1998) observed that the effects of a low concentration of GR231118 were surmountable. However, the calculated Y₁R binding affinities using functional data in this study were > 1000 fold greater for GR231118 (pK_b 10.5) compared to BVD15 (pK_b 7.1), consistent with potential non-equilibrium effects brought

about by slow off rates of the dimeric ligand. Mountford et al., (2014) also observed that a dimeric GR231118 analogue with lower Y₁R binding affinity, where [Dap⁴] in the cyclic moiety was substituted to [Lys⁴] (see also Chapter 4), reverted to surmountable antagonism at the concentrations tested.

Therefore, a range of studies indicate that the GR231118 dimer, relative to monomeric analogues such as BVD15, exhibits substantially higher binding affinity for the Y₁R. The dimer effect is greater than would be predicted from the effective doubling of the pharmacophore concentration through bivalency. This higher affinity is also reflected, in some functional assays, by the observation of non-surmountable antagonist properties that may be a consequence of the slow dissociation of the dimeric peptide from the receptor. Potentially the presence of two arms in the dimer might selectively alter its interaction with GPCR oligomeric complexes (Chapter 5), or the kinetics of receptor interaction by promoting rapid rebinding following dissociation (Charlton and Vauquelin, 2010). Alternatively there may be no intrinsic properties of the dimer that contribute to its pharmacology and rather, inclusion of the ring and / or second peptide arm may provide additional contacts at an extended binding site within the receptor.

3.3 Aims

The aims of this chapter were to synthesise novel derivatives of GR231118 and BVD15, via Fmoc-based SPPS, to provide insight into the binding mode of the dimeric peptide and the origins of its high Y₁R binding affinity using different approaches (Chapters 4 and 5). First, the influence of the ring structure was explored through the synthesis of a series of GR231118 dimer analogues, in which the size of the cyclic moiety was varied. This was accompanied by the synthesis of cyclic BVD15 monomeric derivatives to allow for investigation of the role of a simple intramolecular bridge at a similar position in these analogues (Chapter 4). We used targeted alanine scanning substitution analogues at key residues within only one arm of GR231118 in order to determine how positions within the second arm contribute to binding affinity

and function (Chapter 4). Finally we synthesised Cy5 labelled GR231118 analogues for direct comparison with (Cy5[Lys²])-BVD15 (Liu et al., 2016) in fluorescence correlation spectroscopy (FCS) experiments, in order to explore the stoichiometry of monomeric and dimeric ligand binding to the Y₁R (Chapter 5).

3.4 Results and discussion

The historic approaches to the synthesis of GR231118 have relied on an intermolecular dimerisation of a linear precursor peptide (Daniels et al., 1995). This reaction is typically associated with a competing intramolecular side reaction yielding a cyclic monomeric peptide. The product ratio of these competing reactions has been shown to be sequence dependant, but we were interested in examining both classes of the molecule pharmacologically. Here, the synthesis of the cyclic monomers is described first, followed by the preparation of dimeric structures, including heterodimers, by applying the novel approach to dimer synthesis first described by our group (Mountford et al., 2014).

3.4.1 Cyclic BVD15 monomer peptide analogue design and synthesis

In the production of cyclic monomer derivatives of BVD15, the synthesis strategy was to produce a linear nonapeptide, through standard SPPS methods, followed by intramolecular cyclisation in solution between [Glu²] and amine-containing residues at position 4 (Dap, Dab, Orn and Lys; Figure 3.8; Table 3.1) of the sequence. This created monomeric BVD15 derivatives containing a 2-4 cyclic moiety of varying ring sizes.

3.4.1.1 Linear monomer production (Analogue 1A)

With analogue **1A** as a representative example (Section 3.6), Fmoc-protected linear peptide was produced using the standard SPPS methods (General methods A1 and A2, Section 2.5.1, Chapter 2) on Rink amide resin.

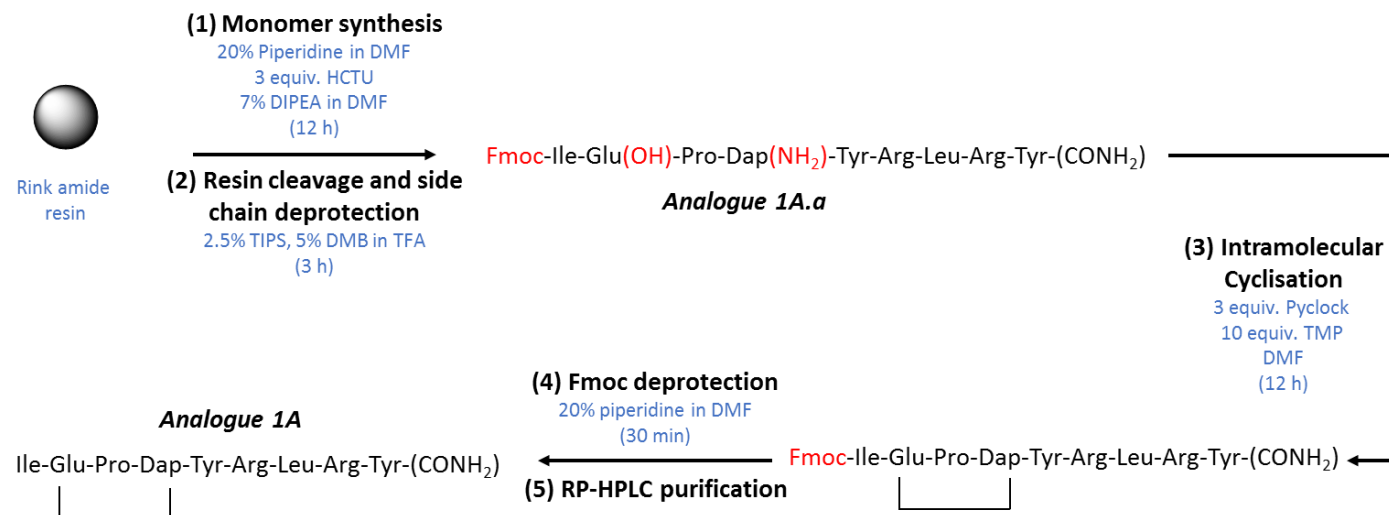


Figure 3.8 - Reaction schematic for the production of BVD15 cyclic monomers. The 5 step synthesis strategy illustrates the production of representative analogue **1A** [Dap⁴]mono, in which reaction conditions are shown in blue and important residues and functional groups in red.

Table 3.1 – Summary of cyclic BVD15 peptide derivatives synthesised. Compound name and analogue code (as referred to in the text) are listed, together with the molecular weight (MW) and electron spray ionisation-mass spectrometry (ESI-MS) ions present in liquid chromatography mass spectrometry (LCMS), providing confirmation of pure peptide product. Retention time (R_T) and purity are quoted from LCMS (0-80% over 10 min) along with the final yield of pure peptide product (Section 2.5 and 2.6.3.1, Chapter 2).

Compound name	Analogue code	MW	ESI-MS	R _T (min)	Purity (LCMS)	Yield (mg)
[Dap ⁴]mono	1A	1176.4	589.2 [M+2H] ²⁺	7.61	97%	5
[Dab ⁴]mono	1B	1190.4	596.2 [M+2H] ²⁺	7.49	>99%	11
[Orn ⁴]mono	1C	1204.5	603.3 [M+2H] ²⁺	α	99%	4
[Lys ⁴] mono	1D	1218.6	610.3 [M+2H] ²⁺	7.71	98%	6

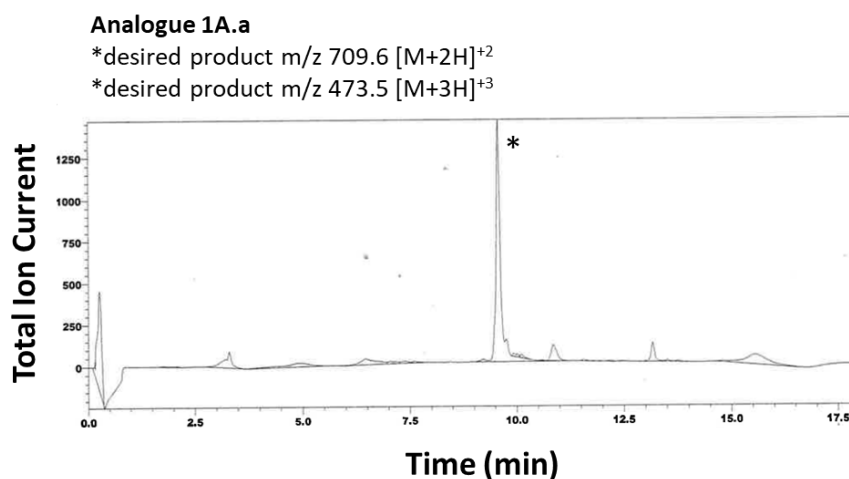


Figure 3.9 - LCMS trace of crude Fmoc protected linear peptide analogue 1A.a following automated linear peptide production, Rink amide resin cleavage and side chain deprotection, with mass ions present in the sample indicated.

The peptide (analogue **1A.a**; Figure 3.9) was found to be of high purity by liquid chromatography mass spectrometry (LCMS; analysed as described in Section 2.6.3.1, Chapter 2), and showed the desired m/z ions in electron spray ionisation-mass spectrometry (ESI-MS) indicating successful synthesis.

3.4.1.2 Intramolecular cyclisation

Intramolecular cyclisation was carried out by treatment of the Fmoc protected linear peptide. The linear peptide was dissolved in DMF with the coupling agent Pyclock for 12 h (where analogue **1A** was dissolved at 2.5 mg/ mL, **1B** at 3.75 mg/ mL and **1C** and **1D** at 7.5 mg/ mL; General method C1, Section 2.5.3, Chapter 2; 3 equiv. Pyclock, 10 equiv. TMP in DMF). The solvent was removed under vacuum, and then the peptide was dissolved in a small volume of TFA. Upon treatment with cold ether (Et₂O), the product peptide precipitated, and was isolated by centrifugation. Finally, the Fmoc-group was removed by treatment with piperidine (General method B3, Section 2.5.2, Chapter 2; 20 % piperidine in DMF). As above, the solvent was removed under vacuum and the residue dissolved in TFA and precipitated with Et₂O. The crude product was then purified by semi-preparative RP-HPLC (Section 2.5.4, Chapter 2). The presence of the desired peptide and purity was then confirmed by LCMS (Figure 3.10; Section 2.6.3.1, Chapter 2).

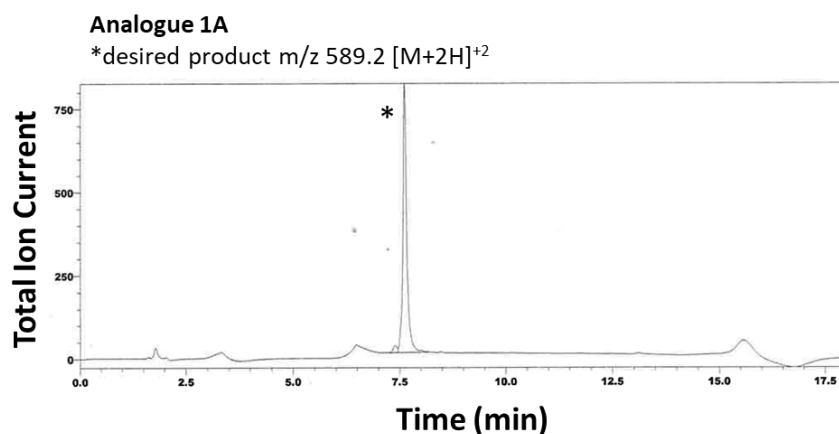


Figure 3.10 – LCMS trace of pure cyclised analogue 1A following intramolecular cyclisation of analogue **1A.a**, Fmoc deprotection and RP-HPLC purification, with mass ions present in the sample indicated.

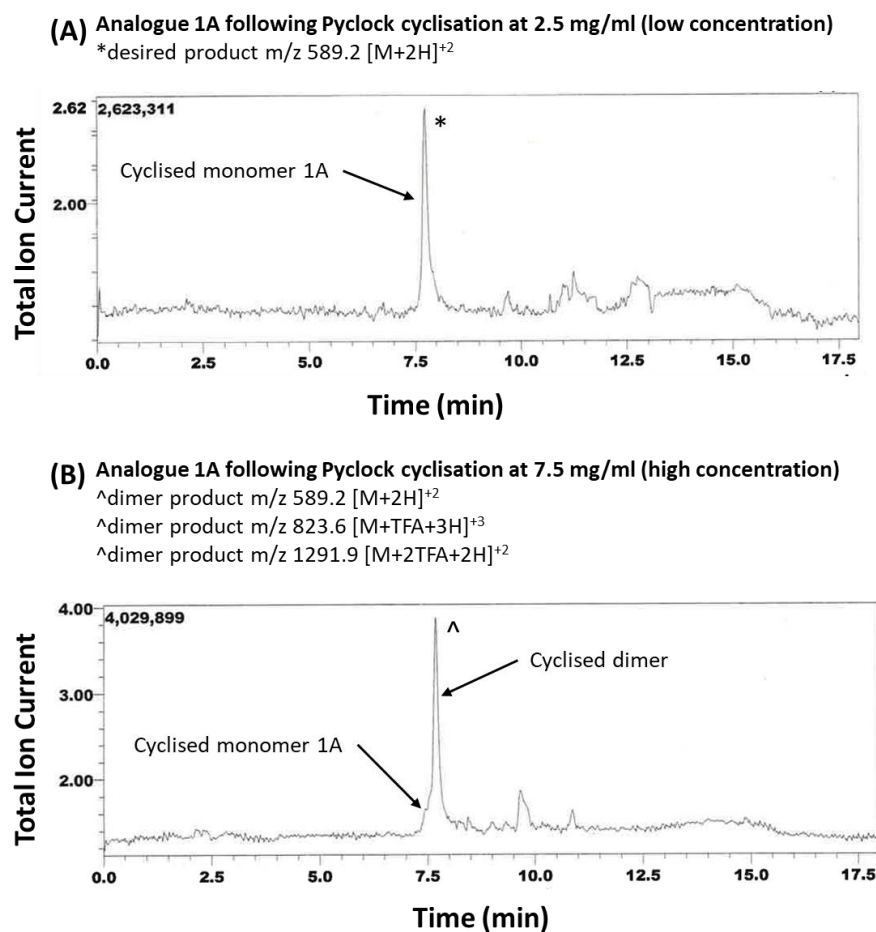


Figure 3.11 - LCMS trace of crude Fmoc de-protected linear peptide analogue 1A. (A) demonstrates the masses of the product corresponding to intramolecular cyclisation of monomer following Pyclock coupling at low concentration in DMF (2.5 mg/ mL) and (B) demonstrates the masses of the product corresponding to intermolecular dimerisation of the linear peptides following Pyclock coupling at high concentration in DMF (7.5 mg/ mL).

Note that the formation of the cyclic monomers **1A** [Dap⁴] and **1B** [Dab⁴] in this case was dependant upon the use of relatively high dilution conditions to suppress intermolecular cyclic dimer formation, while for analogues **1C** [Orn⁴] and **1D** [Lys⁴] intramolecular cyclisation was favoured at both high and low concentrations in the reaction mixture (Figure 3.11).

3.4.2 GR231118 dimer peptide analogue design and synthesis

In the synthesis of dimeric GR231118 and derivatives, the strategy was to avoid the competing intramolecular cyclisation reaction by chemoselective formation of an intermolecular bridge to make a cross-linked dimer peptide. This was done via orthogonal deprotection of corresponding linear peptides as described previously (Mountford et al., 2014). The use of orthogonal protection groups, which are stable to standard SPPS cleavage conditions, provides a powerful approach to the synthesis of non-linear peptides.

The approach using GR231118 (analogue **2A**) as an example is shown in Figure 3.12. Briefly, two partially protected linear peptides were produced by SPPS; one where [Glu²] was protected as an allyl ester (OAll) and the other where [Dap⁴] was protected as an allylocarbonyl (Alloc) carbamate. Intermolecular coupling of the two linear peptides was performed in solution to generate the first cross-link. Then OAll / Alloc deprotection was performed. Palladium catalysis was used to release the side chain groups before the intramolecular cyclisation. Finally, Fmoc-deprotection yielded GR231118. The synthesis method is described in full detail for GR231118 below, and applies to all analogues as summarised in Table 3.2.

3.4.2.1 Dimer production (Analogue **2A**)

GR231118 (**2A**) is used here as a representative example for the synthesis of derivatives **2A-D** and **3A-F** (Section 3.6.2 and 3.6.3). For the production of analogue **2A**, two Fmoc-protected linear peptides were produced by SPPS (General methods A1 and A2; Section 2.5.1, Chapter 2), one containing an OAll protected [Glu²] (analogue **2A.a**), and the other containing an Alloc protected

[Dap⁴] (analogue **2A.b**). The partially protected peptides were then purified by RP-HPLC and the structure confirmed by LCMS (Figure 3.13).

The partially protected linear peptides were synthesised on a 0.3 mmol scale cleanly and in good yield. However, careful purification of the monomers was required, as this significantly improved the outcomes of subsequent steps and allowed for ready identification of the desired peptide products. RP-HPLC conditions were carefully chosen i.e. a flow rate of 15 mL/ min, with an extended linear gradient over 80 min, allowing for separation from close running by-products. Note also, that the presence of hydrophobic protecting groups yielded products that were difficult to dissolve in elution solvents, complicating purification.

3.4.2.2 Intermolecular coupling

Intermolecular coupling was carried out using Pyclock in the presence of 2,4,6-Trimethylpyridine (TMP) to give **2A.c** (General method C1; Section 2.5.3; Chapter 2; 3 equiv. Pyclock, 10 equiv. TMP in DMF). TMP was used as Mountford et al., (2014) found that it avoided degradation of the carboxylate peptide **2A.b**, which was observed when using DIPEA. It was also found that the addition of Pyclock (1 equiv.) in three portions over the course of the 12 h reaction was preferred over a single addition of 3 equiv., resulting in higher product yield (Figure 3.14).

3.4.2.3 OAll/ Alloc deprotection

Alloc and OAll deprotection to give **2A.d** was conducted via the method outlined by Mountford et al., (2014) at high equivalencies of PhSiH₄ (24 equiv.) and Pd(PPh₃)₄ (1 equiv.; General method B2, Section 2.5.2, Chapter 2). The crude product was then purified via RP-HPLC (15 mL / min over 80 min; Figure 3.15). While successful, the removal of the reagents in work up and purification was challenging and some additional experiments were undertaken to optimise the reaction conditions.

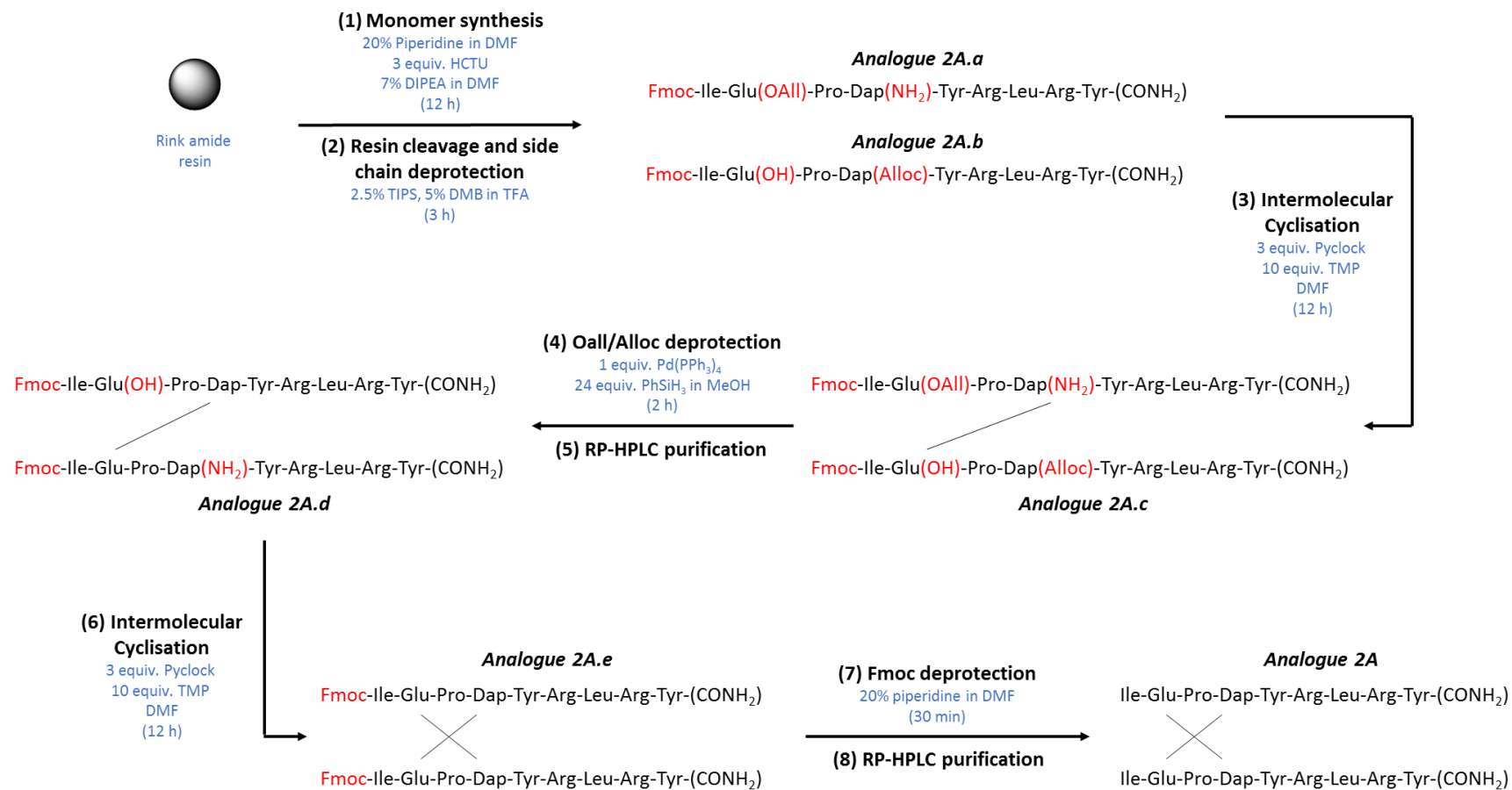


Figure 3.12 – Reaction schematic for the production of GR231118 derivatives. A representative 8 step synthesis strategy is shown for the production of GR231118 (analogue 2A) in which reaction conditions are shown in blue and important residues and functional groups in red.

Table 3.2 – Summarised list of GR231118 peptide derivatives synthesised. Compound name and code are indicated (as referred to in the text), with molecular weight (MW) and ESI-MS ions present in LCMS, providing confirmation of pure peptide product. R_T and purity is quoted from LCMS (0-80% over 10 min) along with the final yield of pure peptide product (Section 2.6.3.1, Chapter 2).

Compound name	Analogue code	MW	ESI-MS	R_T (min)	Purity (LCMS)	Yield (mg)
GR231118 linker analogues						
[Dap ⁴]dimer	2A	2353.8	1291.9 [M+2TFA+2H] ²⁺ 823.6 [M+TFA+3H] ³⁺ 785.6 [M+3H] ³⁺ 589.5 [M+4H] ⁴⁺	7.62	98%	20
[Dab ⁴]dimer	2B	2380.8	1305.4 [M+2TFA+2H] ²⁺ 834.6 [M+TFA+3H] ³⁺ 794.6 [M+3H] ³⁺ 596.2 [M+4H] ⁴⁺	7.59	99%	15
[Orn ⁴]dimer	2C	2408.9	1319.5 [M+2TFA+2H] ²⁺ 842.0 [M+TFA+3H] ³⁺ 804.0 [M+3H] ³⁺ 603.2 [M+4H] ⁴⁺	7.64	97%	3
[Lys ⁴]dimer	2D	2436.9	1333.5 [M+2TFA+2H] ²⁺ 851.3 [M+TFA+3H] ³⁺ 813.3 [M+3H] ³⁺ 610.2 [M+4H] ⁴⁺	7.71	98%	5
GR231118 alanine scan analogues						
[Ala ⁵]dimer	3A	2260.7	1245.4 [M+2TFA+2H] ²⁺ 729.6 [M+TFA+3H] ³⁺ 754.6 [M+3H] ³⁺ 566.2 [M+4H] ⁴⁺	7.44	>99%	5
[Ala ⁶]dimer	3B	2267.7	756.9 [M+3H] ³⁺	7.84	99%	18
[Ala ⁷]dimer	3C	2310.7	1270.4 [M+2TFA+2H] ²⁺ 809.2 [M+TFA+3H] ³⁺ 771.2 [M+3H] ³⁺ 578.7 [M+4H] ⁴⁺	7.28	99%	26
[Ala ⁸]dimer	3D	2267.7	756.9 [M+3H] ³⁺	7.70	99%	20
[Ala ⁹]dimer	3E	2260.7	1245.4 [M+2TFA+2H] ²⁺ 792.6 [M+TFA+3H] ³⁺ 754.6 [M+3H] ³⁺ 566.2 [M+4H] ⁴⁺	7.78	97%	12
[Ala ⁶⁻⁸]dimer	3F	2182.6	1092.3 [M+2H] ²⁺ 728.5 [M+3H] ³⁺	8.38	98%	18

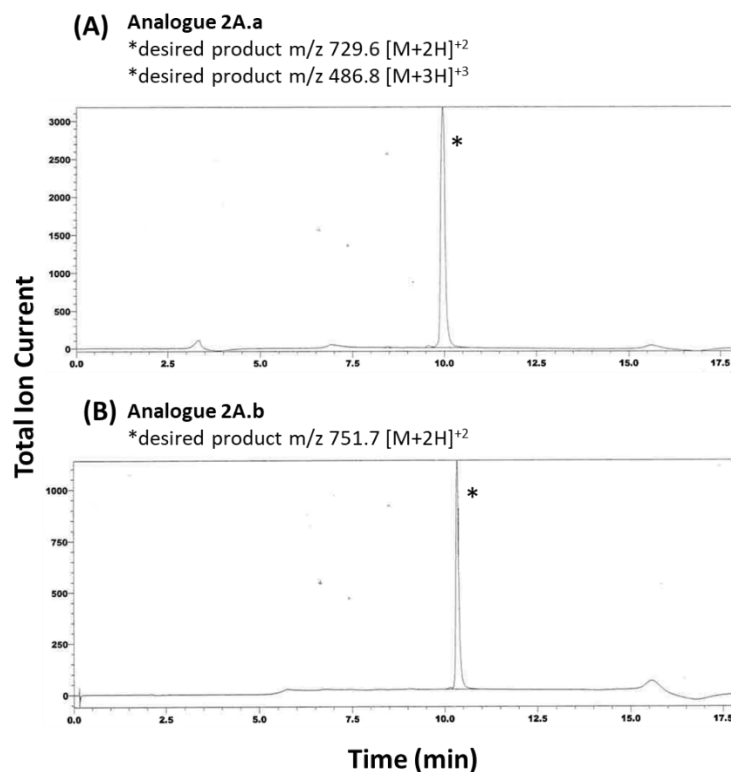


Figure 3.13 – LCMS trace of Fmoc protected pure linear peptide analogues 2A.a (A) and 2A.b (B) following automated linear peptide production, Rink amide resin cleavage, side chain deprotection, and RP-HPLC purification, with the mass ions present in the sample indicated.

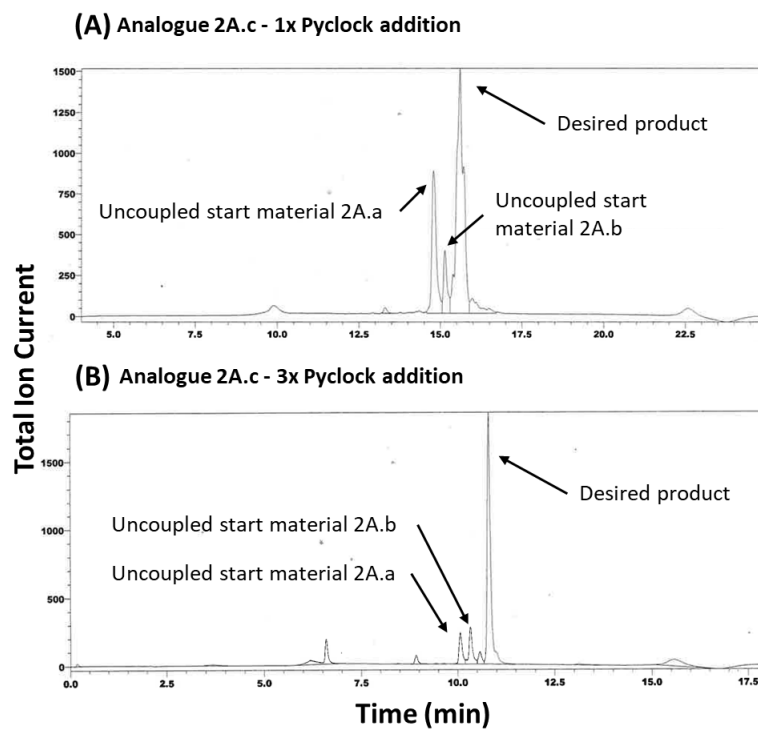


Figure 3.14 – LCMS traces of crude analogue 2A.c. (A) Shows the conversion of linear peptides 2A.a and 2A.b to the desired, coupled, product after a single addition of 3 equiv. Pyclock and (B) shows an increased conversion of liner peptide start materials to product with 1 equiv. addition of Pyclock 3x throughout the reaction.

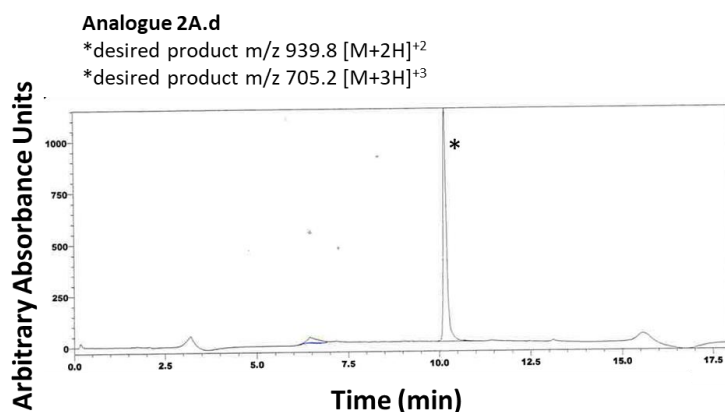


Figure 3.15 LCMS trace of pure Fmoc protected analogue **2A.d** following OAll/Alloc deprotection with the mass ions present in the sample indicated. The mass ions present confirm side chain deprotection of OAll / Alloc groups and retention of the N-terminal Fmoc protecting group in the mild basic conditions of the reaction.

Table 3.3 – Summary of tested reaction conditions for Alloc/OAll optimisation conducted on analogue **2A.b** [Dap⁴(Alloc)] monomer, with reaction carried out for 2 h at room temperature in a nitrogen environment, as describe in general method B2. Where R_T is quoted from LCMS run at 0-80% over 10 min.

Compound name	Peptide equiv.	Ph(SiH ₃) equiv.	Pd(PPh ₃) ₄ equiv.	% Purity	R _T (min)
T1.a	1	24	1	65	9.60
T1.b	1	12	1	64	9.60
T1.c	1	10	1	53	9.55
T1.d	1	8	1	62	9.54
T1.e	1	6	1	70	9.59
T1.f	1	3	1	58	9.57
T2.a	1	24	0.5	76	9.54
T2.b	1	24	0.2	79	9.59

12 equiv. of Ph(SiH₃) showed a 65% conversion rate similar to that seen at 24 equiv. (Table 3.3), similarly a reduction in the catalyst, Pd(PPh₃)₄, gave improved conversion of 79% at 0.2 equiv. In addition to equivalence, it was found that 2 h was a sufficient time for this reaction, as previous experiments indicated that after 3 h no further conversion of starting material to product was observed.

3.4.2.4 Intramolecular cyclisation and Fmoc removal

Intramolecular coupling was done using Pyclock and TMP as coupling reagents (General method C1, Section 2.5.3, Chapter 2; 3 equiv. Pyclock; 10 equiv. TMP in DMF). As with intermolecular coupling, addition of 3x 1 equiv. of Pyclock over the course of the 12 h reaction was conducted (Figure 3.16A and B).

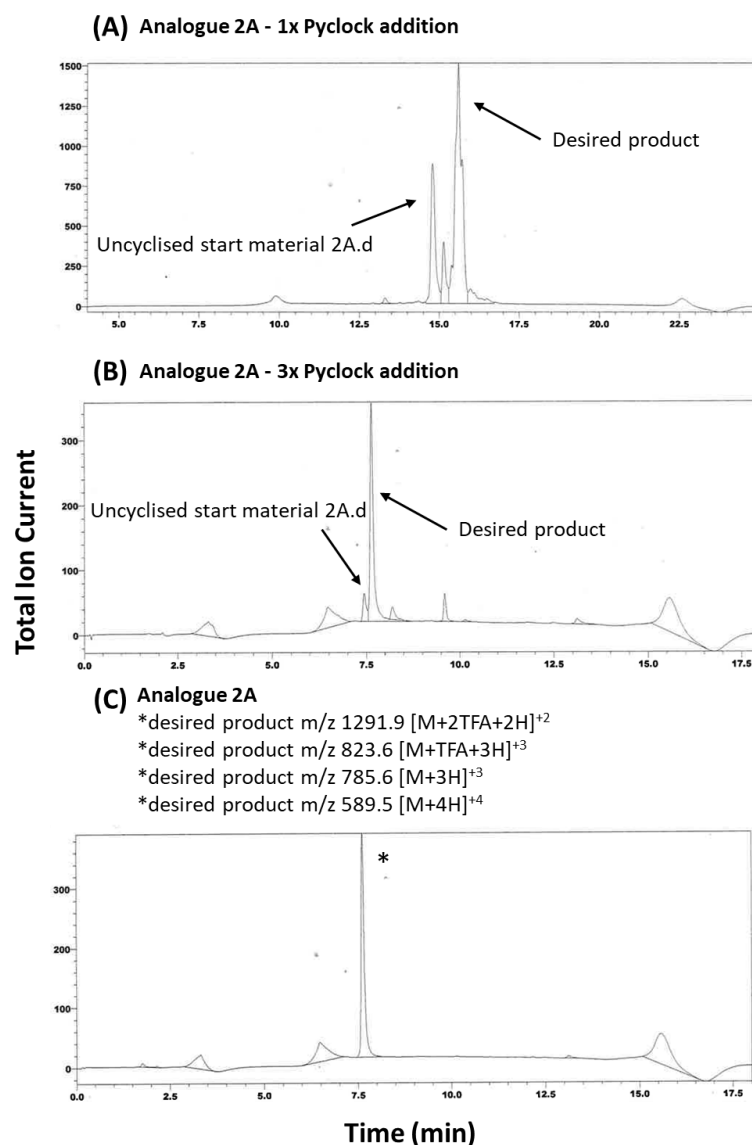


Figure 3.16 - LCMS traces of analogue 2A following intramolecular cyclisation and Fmoc deprotection. (A) Shows the conversion of start material **2A.d** to desired, cyclised, product after a single addition of 3 equiv. Pyclock. (B) Shows an increased conversion of start material **2A.d** to product with addition of 1 equiv. Pyclock 3x throughout the reaction. (C) Shows pure compound **2A** following Fmoc deprotection and RP-HPLC purification, with the mass ions present in the sample indicated.

Finally, the Fmoc-group was removed by treatment with piperidine (General method B3, Section 2.5.2, Chapter 2; 20 % piperidine in DMF). The solvent was then removed under vacuum and the residue dissolved in TFA, precipitated with Et₂O and the crude product was purified via RP-HPLC (15 mL/ min over 80 min). The presence of the desired peptide and purity was then confirmed by LCMS (Figure 3.16C; Section 2.6.3.1, Chapter 2).

The successful application of these methods allowed the synthesis of GR231118 and 9 analogues as summarized in Table 3.2. The approach gave good yields and high purity samples that allowed for a full suite of biological assays to be carried out as described in Chapters 4 and 5.

3.4.3 Fluorescent GR231118 dimer peptide analogue design and synthesis

The synthesis approach for sCy5 conjugation was to synthesise the dimer GR231118 analogue (Section 3.4.2) and then to conjugate a sCy5 moiety to the Fmoc deprotected N-terminus of one or both of the N-termini in the dimer analogue (Figure 3.17; Table 3.4)

3.4.3.1 sCy5 conjugation of GR231118 dimer.

N-terminal conjugation of sCy5 to analogue **2A** (Section 3.6.4) was achieved by treatment with sCy5, Pyclock and N-methylmorpholine (NMM) for 12 h (General method C2, Section 2.5.3, Chapter 2; 3 equiv. Pyclock, 12 equiv. NMM, 0.7 equiv. sCy5 in DMF). The solvent was removed under vacuum and then the residue was treated with TFA and precipitated with Et₂O. The products were purified by RP-HPLC (Section 2.5.4, Chapter 2). NMM was used as the base, as opposed to DIPEA or TMP as it has previously been described in the successful conjugation of sCy5 to peptides (Liu et al., 2016). The production of N-terminus mono-labelled sCy5 GR231118 also resulted in the production of a di-labelled derivative. This was due to the nature of the sCy5 coupling, with both N-termini of the now cyclised peptides exposed and able to undergo conjugation, as such the reaction was carried out for 12 h but at a low sCy5 equivalency (0.7 equiv.). Under these conditions, both mono and dual labelled products were observed at 40:60 % conversion, respectively. As these two products shared close co-elution times (Figure 3.18A), RP-HPLC conditions were optimised to ensure that products were isolated, and was achieved by extending the run time of the RP-HPLC protocol to 100 min. The use of the mono and dual labelled sCy5 derivatives in in vitro studies is discussed in further detail in Chapter 5 of this thesis.

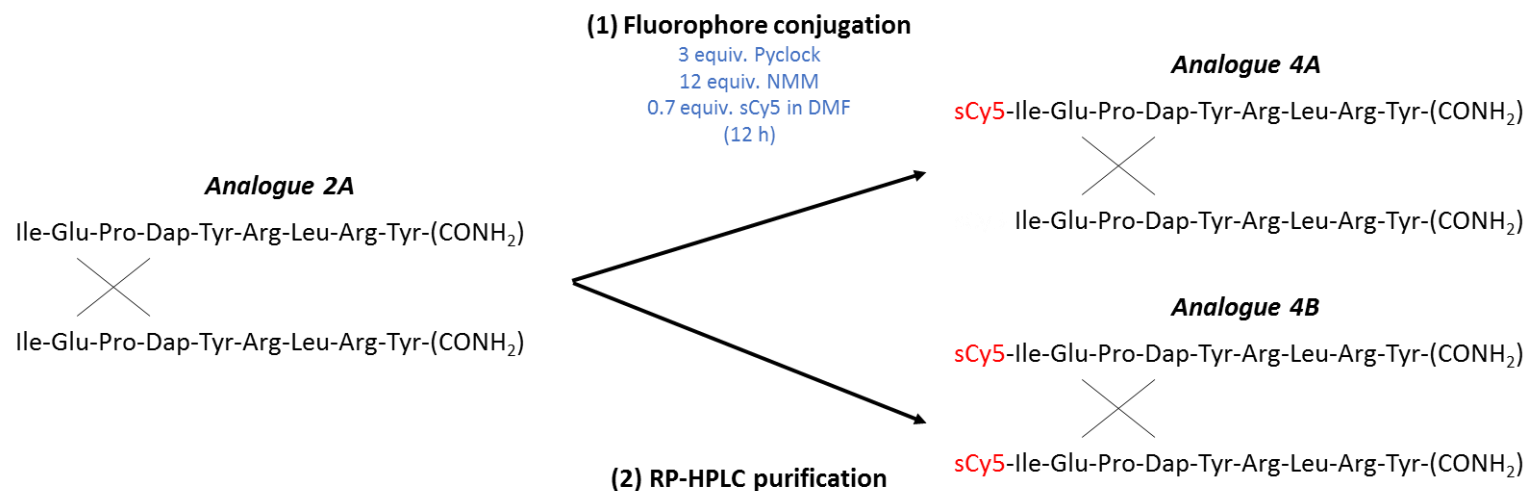


Figure 3.17– Reaction schematic for the production of GR231118 derivatives showing the representative, 2 step synthesis strategy, for the production of analogue **4A** and **4B**, following the production of analogue **2A** via an 8 step reaction synthesis (Figure 3.12), where reaction conditions are shown in blue and important residues and functional groups in red.

Table 3.4 – Summarised list of GR231118 peptide derivatives synthesised. With compound name and analogue code (the name to which they will be referred to in the text), molecular weight (MW) and ESI-MS ions present in LCMS, providing confirmation of pure peptide product. R_T and purity is quoted from LCMS (0-80% over 10 min) along with final yield of pure peptide product (Section 2.6.3.1, Chapter 2).

Compound name	Analogue code	MW	ESI-MS	R _T (min)	Purity (LCMS)	Yield (mg)
Mono sCy5	4A	2990.6	997.9 [M+3H] ³⁺	8.71	95%	1
Dual sCy5	4B	3628.4	1210.5 [M+3H] ³⁺ 908.1 [M+4H] ⁴⁺	9.25	96%	2

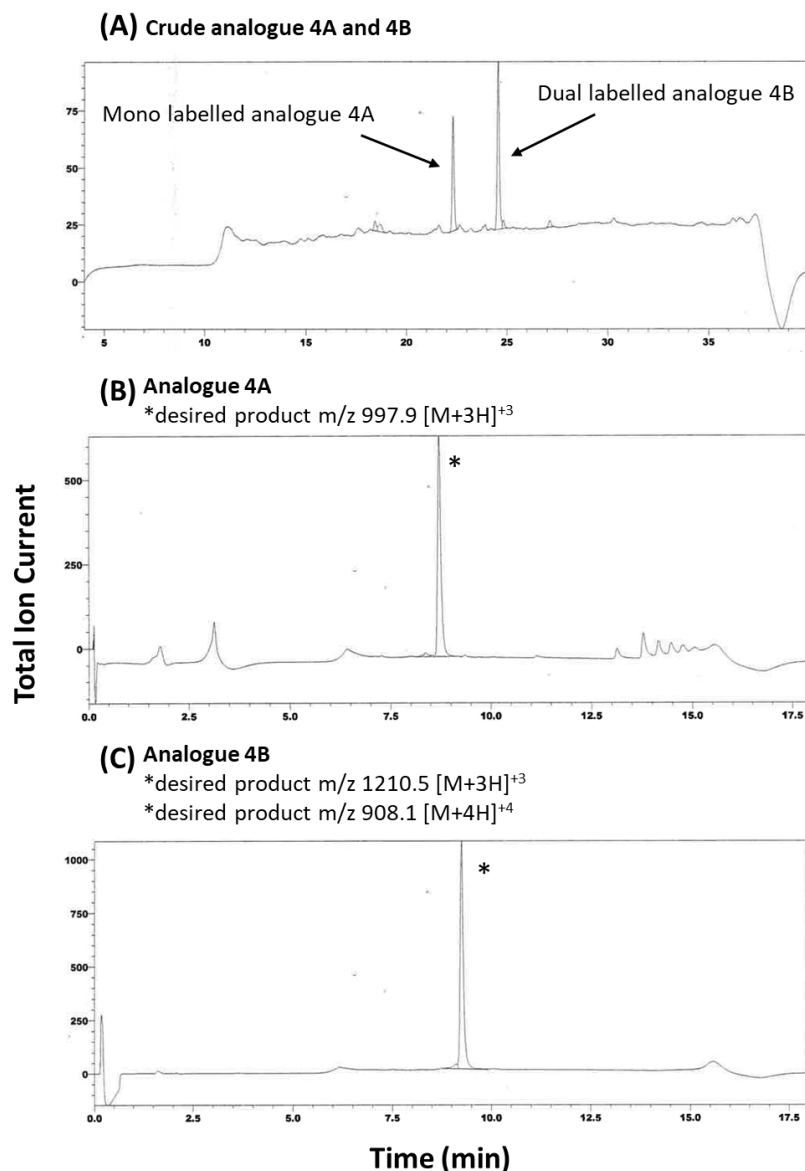


Figure 3.18 - LCMS traces of analogue 4A and 4B following sCy5 conjugation of analogue 2A. (A) Shows the conversion of start material **2A** to mono and dual labelled sCy5 analogues **4A** and **4B**, respectively. Showing complete conversion of analogue **2A** to 40 % **4A** and 60 % **4B**. (B) and (C) show pure compound **4A** and **4B**, respectively, following RP-HPLC, with mass ions present in the sample indicated.

3.5 Conclusions

In this chapter, we have described the successful use, application and optimisation of a novel dimer peptide synthesis method, resulting in the production of several novel GR231118 peptide derivatives. Although the synthesis strategies outlined here show complexity, they have also demonstrated chemoselectivity, reliability and reproducibility with this analogue series. Thus providing potential for future application in the

production of other dimer peptide analogues series. The production of these novel monomer and dimer peptides will allow for the study of structure-activity relationships of the dimer GR231118 compound at the Y₁R and Y₄R as indicated in Chapter 4.

3.6 Experimental and peptide characterisation

All peptides were synthesised via the General methods outlined in Section 2.5 (Chapter 2) of this thesis. The methods for peptide characterisation of peptide products are described in Section 2.6.3.1 (Chapter 2) of this thesis.

3.6.1 Cyclic BVD15 monomer analogues

Analogue 1A: Cyclo-[Dap⁴]BVD15:

Cyclo-[H₂N-Ile-Glu-Pro-Dap-Tyr-Arg-Leu-Arg-Tyr-CONH₂].

Analogue 1A.a: [Dap⁴] monomer: *Linear-[(Fmoc)-H₂N-Ile-Glu-Pro-Dap-Tyr-Arg-Leu-Arg-Tyr-CONH₂].* The peptide backbone was prepared via General method A2 and A3 on a 0.3 mmol scale. Cleavage was carried out via General method B1, to give peptide analogue **1A.a**. ESI-MS: m/z 709.5 [M+2H]²⁺, R_T 9.70 min, as a white solid (87 mg).

Analogue 1A: Intramolecular coupling of [Glu²(OH)] and [Dap⁴(NH₂)]: Intramolecular cyclisation of peptide **1A.a** (60 mg) was carried out via General method C1, and final Fmoc deprotection was conducted via General method B3. The crude peptide was purified using RP-HPLC over a gradient 0-60 % over 80 min at a flow rate of 15 mL/ min, to give peptide analogue **1A**. ESI-MS: m/z 589.2 [M+2H]²⁺, R_T 7.61 min, as a white solid (5 mg, 97 % purity).

Analogue 1B: Cyclo-[Dab⁴]BVD15:

Cyclo-[H₂N-Ile-Glu-Pro-Dab-Tyr-Arg-Leu-Arg-Tyr-CONH₂].

Analogue 1B.a: [Dab⁴] monomer: *Linear-[(Fmoc)-H₂N-Ile-Glu-Pro-Dab-Tyr-Arg-Leu-Arg-Tyr-CONH₂].* The peptide backbone was prepared via General methods A2 and A3 on a 0.3 mmol scale. Cleavage was carried out via General method B1, to give peptide analogue **1B.a**. ESI-MS: m/z 716.6 [M+2H]²⁺, R_T 9.65 min, as a white solid (76 mg).

Analogue 1B: Intramolecular coupling of [Glu²(OH)] and [Dap⁴(NH₂)]:

Intramolecular cyclisation of peptide **1B.a** (60 mg) was carried out via General method C1, and final Fmoc deprotection was conducted via General method B3. The crude peptide was purified using RP-HPLC over a gradient 0-60 % over 80 min at a flow rate of 15 mL/ min, to give peptide analogue **1B**. ESI-MS: m/z 596.2 [M+2H]²⁺. R_T 7.49 min, as a white solid (11 mg, >99 % purity).

Analogue 1C: Cyclo-[Orn⁴]BVD15:

Cyclo-[H₂N-Ile-Glu-Pro-Orn-Tyr-Arg-Leu-Arg-Tyr-CONH₂].

Analogue 1C.a: [Orn⁴] monomer: *Linear-[(Fmoc)-H₂N-Ile-Glu-Pro-Orn-Tyr-Arg-Leu-Arg-Tyr-CONH₂].* The peptide backbone was prepared via General methods A2 and A3 on a 0.3 mmol scale. Cleavage was carried out via General method B1, to give peptide analogue **1C.a**. ESI-MS: m/z 723.6 [M+2H]²⁺, R_T 9.68 min, as a white solid (61 mg).

Analogue 1C: Intramolecular coupling of [Glu²(OH)] and [Dap⁴(NH₂)]:

Intramolecular cyclisation of peptide **1C.a** (60 mg) was carried out via General method C1, and final Fmoc deprotection was conducted via General method B3. The crude peptide was purified using RP-HPLC over a gradient 0-60 % over 80 min at a flow rate of 15 mL/ min, to give peptide analogue **1C**. ESI-MS: m/z 603.3 [M+2H]²⁺ as a white solid (4 mg, 99 % purity).

Analogue 1D: Cyclo-[Lys⁴]BVD15:

Cyclo-[H₂N-Ile-Glu-Pro-Lys-Tyr-Arg-Leu-Arg-Tyr-CONH₂].

Analogue 1D.a: [Lys⁴] monomer: *Linear-[(Fmoc)-H₂N-Ile-Glu-Pro-Lys-Tyr-Arg-Leu-Arg-Tyr-CONH₂].* The peptide backbone was prepared via General methods A2 and A3 on a 0.3 mmol scale. Cleavage was carried out via General method B1, to give peptide analogue **1D.a**. ESI-MS: m/z 730.7 [M+2H]²⁺, R_T 9.66 min, as a white solid (63 mg).

Analogue 1D: Intramolecular coupling of [Glu²(OH)] and [Dap⁴(NH₂)]:

Intramolecular cyclisation of peptide **1D.a** (60 mg) was carried out via General method C1 with 60mg of start material, and final Fmoc deprotection was conducted via General method B3. The crude peptide was purified using RP-HPLC over a gradient 0-60 % over 80 min at a flow rate of 15 mL/ min, to give

peptide analogue **1D**. ESI-MS: m/z 610.3 $[M+2H]^{2+}$. R_T 7.71 min, as a white solid (6 mg, 98 % purity).

3.6.2 GR231118 dimer analogues

Analogue 2A: Cyclo-[Dap⁴]GR231118:

Cyclo-([H₂N-Ile-Glu-Pro-Dap-Tyr-Arg-Leu-Arg-Tyr-CONH₂])².

Analogue 2A.a: [Glu(OAll)²Dap⁴] monomer: *Linear-[(Fmoc)-H₂N-Ile-Glu(OAll)-Pro-Dap-Tyr-Arg-Leu-Arg-Tyr-CONH₂].* The peptide backbone was prepared via General methods A2 and A3 on a 0.3 mmol scale. Cleavage was carried out via General method B1. The crude peptide was purified using RP-HPLC over a gradient 0-60 % over 80 min at a flow rate of 15 mL/ min, to give peptide analogue **2A.a**. ESI-MS: m/z 729.4 $[M+2H]^{2+}$ 486.6 $[M+3H]^{3+}$ R_T 9.95 min, as a white solid (197 mg, 99 % purity).

Analogue 2A.b: [Dap⁴]Alloc monomer: *Linear-[(Fmoc)-H₂N-Ile-Glu-Pro-Dap(Alloc)-Tyr-Arg-Leu-Arg-Tyr-CONH₂].* The peptide backbone was prepared via General methods A2 and A3 on a 0.3 mmol scale. Cleavage was carried out via General method B1. The crude peptide was purified using RP-HPLC over a gradient 0-60 % over 80 min at a flow rate of 15 mL/ min, to give peptide analogue **2A.b**. ESI-MS: m/z 751.4 $[M+2H]^{2+}$ R_T 10.30 min, as a white solid (74 mg, 99 % purity).

Analogue 2A.c: Intramolecular coupling of 2A.a [Glu²(OH)] and 2A.b [Dap⁴(NH₂)]: Intermolecular cyclisation was carried out between linear peptides analogues **2A.a** and **2A.b** via General method C1 to produce crude peptide analogue **2A.c** as a white solid (187 mg).

Analogue 2A.d: [Glu²(OAll)]/[Dap⁴(Alloc)] selective deprotection of 2A.c: OAll/Alloc side chain deprotection was then carried out on peptide analogue **2A.c** via General method B2. The crude peptide was purified using RP-HPLC over a gradient 0-60 % over 80 min at a flow rate of 15 mL/min, to give peptide analogue **2A.d**. ESI-MS: m/z 939.4 $[M+3H]^{3+}$ 704.8 $[M+4H]^{4+}$ R_T 10.16 min, as a white solid (88 mg, 95 % purity).

Analogue 2A: Intermolecular coupling of 2A.d [Glu²(OH)] and [Dap⁴(NH₂)]: Intramolecular cyclisation was carried out on analogue **2A.d** via General

method C1. Finally, Fmoc deprotection of the N-termini was conducted via General method B3. The crude peptide was purified using RP-HPLC over a gradient 0-60 % over 80 min at a flow rate of 15 mL/min, to give peptide analogue **2A**. ESI-MS: m/z 1291.4 $[M+2TFA+2H]^{2+}$, 823.3 $[M+TFA+3H]^{3+}$, 785.3 $[M+3H]^{3+}$ and 589.2 $[M+4H]^{4+}$. R_T 7.62 min, as a white solid (20 mg, 98 % purity).

Analogue 2B: Cyclo-[Dab⁴]GR231118:

Cyclo-([H₂N-Ile-Glu-Pro-Dab-Tyr-Arg-Leu-Arg-Tyr-CONH₂])².

Analogue 2B.a: [Glu(OAll) 2Dab⁴] monomer: *Linear-[(Fmoc)-H₂N-Ile-Glu(OAll)-Pro-Dab-Tyr-Arg-Leu-Arg-Tyr-CONH₂]*. The peptide backbone was prepared via General methods A2 and A3 on a 0.3 mmol scale. Cleavage was carried out via General method B1. The crude peptide was purified using RP-HPLC over a gradient 0-60 % over 80 min at a flow rate of 15 mL/min, to give peptide analogue **2B.a**. ESI-MS: m/z 735.9 $[M+2H]^{2+}$ 490.9 $[M+3H]^{3+}$ R_T 9.99 min, as a white solid (98 mg, 99 % purity).

Analogue 2B.b: [Dab⁴]Alloc monomer: *Linear-[(Fmoc)-H₂N-Ile-Glu-Pro-Dab(Alloc)-Tyr-Arg-Leu-Arg-Tyr-CONH₂]*. The peptide backbone was prepared via General methods A2 and A3 on a 0.3 mmol scale. Cleavage was carried out via General method B1. The crude peptide was purified using RP-HPLC over a gradient 0-60 % over 80 min at a flow rate of 15 mL/min, to give peptide analogue **2B.b**. ESI-MS: m/z 758.4 $[M+2H]^{2+}$ R_T 10.32 min, as a white solid (105 mg, 99 % purity).

Analogue 2B.c: Intramolecular coupling of 2B.a [Glu²(OH)] and 2B.b [Dab⁴(NH₂)]: Intermolecular cyclisation was carried out between linear peptides analogues **2B.a** and **2B.b** via General method C1 to give crude peptide analogue **2B.c** as a white solid (203 mg).

Analogue 2B.d: [Glu²(OAll)]/[Dab⁴(Alloc)] selective deprotection of 2B.c: OAll/Alloc side chain deprotection was then carried out on peptide analogue **2B.c** via General method B2. The crude peptide was purified using RP-HPLC over a gradient 0-60 % over 80 min at a flow rate of 15 mL/min, to give peptide analogue **2B.d**. ESI-MS: m/z 948.8 $[M+3H]^{3+}$ 711.9 $[M+4H]^{4+}$ R_T 10.07 min, as a white solid (97 mg, 99 % purity).

Analogue 2B: Intermolecular coupling of 2B.d [Glu²(OH)] and [Dab⁴(NH₂)]:

Intramolecular cyclisation was carried out on analogue **2B.d** via General method C1. Finally, Fmoc deprotection of the N-termini was conducted via General method B3. The crude peptide was purified using RP-HPLC over a gradient 0-60 % over 80 min at a flow rate of 15 mL/ min, to give peptide analogue **2B**. ESI-MS: m/z 1305.4 [M+2TFA+2H]²⁺, 832.6 [M+TFA+3H]³⁺, 794.6 [M+3H]³⁺ and 596.2 [M+4H]⁴⁺. R_T 7.59 min, as a white solid (15 mg, 99 % purity).

Analogue 2C: Cyclo-[Orn⁴]GR231118:

Cyclo-([H₂N-Ile-Glu-Pro-Orn-Tyr-Arg-Leu-Arg-Tyr-CONH₂])².

Analogue 2C.a: [Glu(OAll)²Orn⁴] monomer: *Linear-[(Fmoc)-H₂N-Ile-Glu(OAll)-Pro-Orn-Tyr-Arg-Leu-Arg-Tyr-CONH₂]*. The peptide backbone was prepared via General methods A2 and A3 on a 0.3 mmol scale. Cleavage was carried out via General method B1. The crude peptide was purified using RP-HPLC over a gradient 0-60 % over 80 min at a flow rate of 15 mL/ min, to give peptide analogue **2C.a**. ESI-MS: m/z 743.4 [M+2H]²⁺ 495.9 [M+3H]³⁺ R_T 10.05 min, as a white solid (160 mg, 98 % purity).

Analogue 2C.b: [Orn⁴]Alloc monomer: *Linear-[(Fmoc)-H₂N-Ile-Glu-Pro-Orn(Alloc)-Tyr-Arg-Leu-Arg-Tyr-CONH₂]*. The peptide backbone was prepared via General methods A2 and A3 on a 0.3 mmol scale. Cleavage was carried out via General method B1. The crude peptide was purified using RP-HPLC over a gradient 0-60 % over 80 min at a flow rate of 15 mL/ min, to give peptide analogue **2C.b**. ESI-MS: m/z 764.9 [M+2H]²⁺ R_T 10.35 min, as a white solid (130 mg, 99 % purity).

Analogue 2C.c: Intramolecular coupling of 2C.a [Glu²(OH)] and 2C.b [Orn⁴(NH₂)]: Intermolecular cyclisation was carried out between linear peptides analogues **2C.a** and **2C.b** via General method C1 to give crude peptide analogue **2C.c** as a white solid (200 mg).

Analogue 2C.d: [Glu²(OAll)]/[Orn⁴(Alloc)] selective deprotection of 2C.c: OAll/Alloc side chain deprotection was then carried out on peptide analogue **2C.c** via General method B2. The crude peptide was purified using RP-HPLC over a gradient 0-60 % over 80 min at a flow rate of 15 mL/ min, to give peptide

analogue **2C.d**. ESI-MS: m/z 958.1 $[M+3H]^{3+}$ 718.9 $[M+4H]^{4+}$ R_T 10.05 min, as a white solid (111 mg, 97 % purity).

Analogue 2C: Intermolecular coupling of 2C.d $[Glu^2(OH)]$ and $[Orn^4(NH_2)]$:

Intramolecular cyclisation was carried out on analogue **2C.d** via General method C1. Finally, Fmoc deprotection of the N-termini was conducted via General method B3. The crude peptide was purified using RP-HPLC over a gradient 0-60 % over 80 min at a flow rate of 15 mL/ min, to give peptide analogue **2C**. ESI-MS: m/z 1319.5 $[M+2TFA+2H]^{2+}$, 842.0 $[M+TFA+3H]^{3+}$, 804.0 $[M+3H]^{3+}$ and 603.2 $[M+4H]^{4+}$. R_T 7.64 min, as a white solid (3 mg, 97 % purity).

Analogue 2D: Cyclo-[Lys⁴]GR231118:

Cyclo-([H₂N-Ile-Glu-Pro-Lys-Tyr-Arg-Leu-Arg-Tyr-CONH₂])².

Analogue 2D.a: $[Glu(OAll)]^2Lys^4$ monomer: *Linear-[(Fmoc)-H₂N-Ile-Glu(OAll)-Pro-Lys-Tyr-Arg-Leu-Arg-Tyr-CONH₂]*. The peptide backbone was prepared via General methods A2 and A3 on a 0.3 mmol scale. Cleavage was carried out via General method B1. The crude peptide was purified using RP-HPLC over a gradient 0-60 % over 80 min at a flow rate of 15 mL/ min, to give peptide analogue **2D.a**. ESI-MS: m/z 750.4 $[M+2H]^{2+}$ 500.6 $[M+3H]^{3+}$ R_T 14.45 min, as a white solid (136 mg, 98 % purity).

Analogue 2D.b: $[Lys^4]Alloc$ monomer: *Linear-[(Fmoc)-H₂N-Ile-Glu-Pro-Lys(Alloc)-Tyr-Arg-Leu-Arg-Tyr-CONH₂]*. The peptide backbone was prepared via General methods A2 and A3 on a 0.3 mmol scale. Cleavage was carried out via General method B1. The crude peptide was purified using RP-HPLC over a gradient 0-60 % over 80 min at a flow rate of 15 mL/ min, to give peptide analogue **2D.b**. ESI-MS: m/z 772.4 $[M+2H]^{2+}$ R_T 15.04 min, as a white solid (83 mg, 99 % purity).

Analogue 2D.c: Intramolecular coupling of 2D.a $[Glu^2(OH)]$ and 2D.b $[Lys^4(NH_2)]$: Intermolecular cyclisation was carried out between linear peptides analogues **2D.a** and **2D.b** via General method C1 to give crude peptide analogue **2D.c** as a white solid (182 mg).

Analogue 2D.d: $[Glu^2(OAll)]/[Lys^4(Alloc)]$ selective deprotection of 2D.c: OAll/Alloc side chain deprotection was then carried out on peptide analogue **2D.c** via General method B2. The crude peptide was purified using RP-HPLC

over a gradient 0-60 % over 80 min at a flow rate of 15 mL/ min, to give peptide analogue **2D.d**. ESI-MS: m/z 967.5 [M+3H]³⁺ 725.9 [M+4H]⁴⁺ R_T 10.01 min, as a white solid (65 mg, 99 % purity).

Analogue 2D: Intermolecular coupling of 2D.d [Glu²(OH)] and [Lys⁴(NH₂)]:

Intramolecular cyclisation was carried out on analogue **2D.d** via General method C1. Finally, Fmoc deprotection of the N-termini was conducted via General method B3. The crude peptide was purified using RP-HPLC over a gradient 0-60 % over 80 min at a flow rate of 15 mL/ min, to give peptide analogue **2D**. ESI-MS: m/z 1333.2 [M+2TFA+2H]²⁺, 851.1 [M+TFA+3H]³⁺, 813.1 [M+3H]³⁺ and 610.1 [M+4H]⁴⁺. R_T 7.71 min, as a white solid (5 mg, 98 % purity).

3.6.3 GR231118 dimer alanine scan analogues

Analogue 3A: Cyclo-[Ala⁵]GR231118:

Cyclo-[H₂N-Ile-Glu-Pro-Dap-Tyr-Arg-Leu-Arg-Tyr-CONH₂]-[H₂N-Ile-Glu-Pro-Dap-Ala-Arg-Leu-Arg-Tyr-CONH₂].

Analogue 3A.a: [Glu(OAll)²] monomer: *Linear-[(Fmoc)-H₂N-Ile-Glu(OAll)-Pro-Dap-Tyr-Arg-Leu-Arg-Tyr-CONH₂].* The peptide backbone was prepared via General methods A2 and A3 on a 0.3 mmol scale. Cleavage was carried out via General method B1. The crude peptide was purified using RP-HPLC over a gradient 0-60 % over 80 min at a flow rate of 15 mL/ min, to give peptide analogue **3A.a**. ESI-MS: m/z 729.4 [M+2H]²⁺ 486.6 [M+3H]³⁺ R_T 10.01 min, as a white solid (158 mg, 99 % purity).

Analogue 3A.b: [Dap⁴(Alloc)Ala⁵] monomer: *Linear-[(Fmoc)-H₂N-Ile-Glu-Pro-Dap(Alloc)-Ala-Arg-Leu-Arg-Tyr-CONH₂].* The peptide backbone was prepared via General methods A2 and A3 on a 0.3 mmol scale. Cleavage from the Rink amide resin and side chain protecting groups was carried out via General method B1. The crude peptide was purified using RP-HPLC over a gradient 0-60 % over 80 min at a flow rate of 15 mL/ min, to give peptide analogue **3A.b**. ESI-MS: m/z 705.32 [M+2H]²⁺ R_T 10.40 min, as a white solid (142 mg, 99 % purity).

Analogue 3A.c: Intramolecular coupling of 3A.a [Glu²(OH)] and 3A.b [Dap⁴(NH₂)]: Intermolecular cyclisation was carried out between linear

peptides analogues **3A.a** and **3A.b** via General method C1 to give crude peptide analogue **3A.c** as a white solid (106 mg).

Analogue 3A.d: [Glu²(OAll)]/[Dap⁴(Alloc)] selective deprotection of 3A.c: OAll/Alloc side chain deprotection was then carried out on peptide analogue **3A.c** via General method B2. The crude peptide was purified using RP-HPLC over a gradient 0-60 % over 80 min at a flow rate of 15 mL/ min, to give peptide analogue **3A.d**. ESI-MS: m/z 908.7 [M+3H]³⁺ 947.1 [M+TFA+3H]³⁺ 681.8 [M+4H]⁴⁺ R_T 10.10 min, as a white solid (34 mg, 98 % purity).

Analogue 3A: Intermolecular coupling of 3A.d [Glu²(OH)] and [Dap⁴(NH₂)]: Intramolecular cyclisation was carried out on analogue **3A.d** via General method. Finally, Fmoc deprotection of the N-termini was conducted via General method B3. The crude peptide was purified using RP-HPLC over a gradient 0-60 % over 80 min at a flow rate of 15 mL/ min, to give peptide analogue **3A**. ESI-MS: m/z 1245.5 [M+2TFA+2H]²⁺, 792.7 [M+TFA+3H]³⁺, 754.7 [M+3H]³⁺ and 566.2 [M+4H]⁴⁺. R_T 7.44 min, as a white solid (5 mg, 98 % purity).

Analogue 3B: Cyclo-[Ala⁶]GR231118:

Cyclo-[H₂N-Ile-Glu-Pro-Dap-Tyr-Arg-Leu-Arg-Tyr-CONH₂]-[H₂N-Ile-Glu-Pro-Dap-Tyr-Ala-Leu-Arg-Tyr-CONH₂].

Analogue 3A.a: [Glu(OAll)²] monomer: *Linear-[(Fmoc)-H₂N-Ile-Glu(OAll)-Pro-Dap-Tyr-Arg-Leu-Arg-Tyr-CONH₂].* As described above for analogue **3A.a**.

Analogue 3B.b: [Dap⁴(Alloc)Ala⁶] monomer: *Linear-[(Fmoc)-H₂N-Ile-Glu-Pro-Dap(Alloc)-Tyr-Ala-Leu-Arg-Tyr-CONH₂].* The peptide backbone was prepared via General methods A2 and A3 on a 0.3 mmol scale. Cleavage was carried out via General method B1. The crude peptide was purified using RP-HPLC over a gradient 0-60 % over 80 min at a flow rate of 15 mL/ min, to give peptide analogue **3B.b**. ESI-MS: m/z 708.8 [M+2H]²⁺ R_T 11.18 min, as a white solid (116 mg, >99 % purity).

Analogue 3B.c: Intramolecular coupling of 3A.a [Glu²(OH)] and 3B.b [Dap⁴(NH₂)]: Intermolecular cyclisation was carried out between linear peptides analogues **3A.a** and **3B.b** via General method C1 to give crude peptide analogue **3B.c** as a white solid (103 mg).

Analogue 3B.d: [Glu²(OAll)]/[Dap⁴(Alloc)] selective deprotection of 3B.c: OAll/Alloc side chain deprotection was then carried out on peptide analogue **3B.c** via General method B2. The crude peptide was purified using RP-HPLC over a gradient 0-60 % over 80 min at a flow rate of 15 mL/ min, to give peptide analogue **3B.d**. ESI-MS: m/z 1366.1 [M+2H]²⁺ 911.1 [M+3H]³⁺ 683.6 [M+4H]⁴⁺ R_T 10.38 min, as a white solid (31 mg, 99 % purity).

Analogue 3B: Intermolecular coupling of 3B.d [Glu²(OH)] and [Dap⁴(NH₂)]: Intramolecular cyclisation was carried out on analogue **3B.d** via General method C1. Finally, Fmoc deprotection of the N-termini was conducted via General method B3. The crude peptide was purified using RP-HPLC over a gradient 0-60 % over 80 min at a flow rate of 15 mL/ min, to give peptide analogue **3B**. ESI-MS: m/z 757.0 [M+3H]³⁺. R_T 7.84 min, as a white solid (18 mg, 99 % purity).

Analogue 3C: Cyclo-[Ala⁷]GR231118:

Cyclo-[H₂N-Ile-Glu-Pro-Dap-Tyr-Arg-Leu-Arg-Tyr-CONH₂]-[H₂N-Ile-Glu-Pro-Dap-Tyr-Arg-Ala-Arg-Tyr-CONH₂].

Analogue 3A.a: [Glu(OAll)²] monomer: *Linear-[(Fmoc)-H₂N-Ile-Glu(OAll)-Pro-Dap-Tyr-Arg-Leu-Arg-Tyr-CONH₂].* As described above for analogue **3A.a**.

Analogue 3C.b: [Dap⁴(Alloc)Ala⁷] monomer: *Linear-[(Fmoc)-H₂N-Ile-Glu-Pro-Dap(Alloc)-Tyr-Arg-Ala-Arg-Tyr-CONH₂].* The peptide backbone was prepared via General methods A2 and A3 on a 0.3 mmol scale. Cleavage was carried out via General method B1. The crude peptide was purified using RP-HPLC over a gradient 0-60 % over 80 min at a flow rate of 15 mL/ min, to give peptide analogue **3C.b**. ESI-MS: m/z 730.3 [M+2H]²⁺ R_T 10.24 min, as a white solid (175 mg, 99 % purity).

Analogue 3C.c: Intramolecular coupling of 3A.a [Glu²(OH)] and 3C.b [Dap⁴(NH₂)]: Intermolecular cyclisation was carried out between linear peptides analogues **3A.a** and **3C.b** via General method C1 to give crude peptide analogue **3C.c** as a white solid (106 mg).

Analogue 3C.d: [Glu²(OAll)]/[Dap⁴(Alloc)] selective deprotection of 3C.c: OAll/Alloc side chain deprotection was then carried out on peptide analogue **3C.c** via General method B2. The crude peptide was purified using RP-HPLC

over a gradient 0-60 % over 80 min at a flow rate of 15 mL/ min, to give analogue **3C.d**. ESI-MS: m/z 1366.1 $[M+2H]^{2+}$ 911.1 $[M+3H]^{3+}$ 963.4 $[M+TFA+3H]^{3+}$ 683.6 $[M+4H]^{4+}$ R_T 10.09 min, as a white solid (45 mg, 99 % purity).

Analogue 3C: Intermolecular coupling of 3C.d $[Glu^2(OH)]$ and $[Dap^4(NH_2)]$: Intramolecular cyclisation was carried out on analogue **3C.d** via General method C1. Finally, Fmoc deprotection of the N-termini was conducted via General method B3. The crude peptide was purified using RP-HPLC over a gradient 0-60 % over 80 min at a flow rate of 15 mL/ min, to give peptide analogue **3C**. ESI-MS: m/z 1270.5 $[M+2TFA+2H]^{2+}$, 809.3 $[M+TFA+3H]^{3+}$, 771.3 $[M+3H]^{3+}$ and 578.8 $[M+4H]^{4+}$. R_T 7.28 min, as a white solid (26 mg, 99 % purity).

Analogue 3D: Cyclo-[Ala⁸]GR231118:

Cyclo-[H₂N-Ile-Glu-Pro-Dap-Tyr-Arg-Leu-Arg-Tyr-CONH₂]-[H₂N-Ile-Glu-Pro-Dap-Tyr-Arg-Leu-Ala-Tyr-CONH₂].

Analogue 3A.a: $[Glu(OAll)^2]$ monomer: *Linear-[(Fmoc)-H₂N-Ile-Glu(OAll)-Pro-Dap-Tyr-Arg-Leu-Arg-Tyr-CONH₂]*. As described above for analogue **3A.a**.

Analogue 3D.b: $[Dap^4(Alloc)Ala^8]$ monomer: *Linear-[(Fmoc)-H₂N-Ile-Glu-Pro-Dap(Alloc)-Tyr-Arg-Leu-Ala-Tyr-CONH₂]*. The peptide backbone was prepared via General methods A2 and A3 on a 0.3 mmol scale. Cleavage was carried out via General method B1. The crude peptide was purified using RP-HPLC over a gradient 0-60 % over 80 min at a flow rate of 15 mL/ min, to give peptide analogue **3D.b**. ESI-MS: m/z 708.81 $[M+2H]^{2+}$ R_T 10.98 min, as a white solid (132 mg, >99 % purity).

Analogue 3D.c: Intramolecular coupling of 3A.a $[Glu^2(OH)]$ and 3D.b $[Dap^4(NH_2)]$: Intermolecular cyclisation was carried out between linear peptides analogues **3A.a** and **3D.b** via General method C1 to give crude peptide analogue **3D.c** as a white solid (102 mg).

Analogue 3D.d: $[Glu^2(OAll)]/[Dap^4(Alloc)]$ selective deprotection of 3D.c: OAll/Alloc side chain deprotection was then carried out on peptide analogue **3D.c** via General method B2. The crude peptide was purified using RP-HPLC over a gradient 0-60 % over 80 min at a flow rate of 15 mL/ min, to give peptide

analogue **3D.d**. ESI-MS: m/z 1366.1 $[M+2H]^{2+}$ 911.1 $[M+3H]^{3+}$ 683.6 $[M+4H]^{4+}$
 R_T 10.39 min, as a white solid (34 mg, 99 % purity).

Analogue 3D: Intermolecular coupling of 3D.d $[Glu^2(OH)]$ and $[Dap^4(NH_2)]$:

Intramolecular cyclisation was carried out on analogue **3D.d** via General method C1. Finally, Fmoc deprotection of the N-termini was conducted via General method B3. The crude peptide was purified using RP-HPLC over a gradient 0-60 % over 80 min at a flow rate of 15 mL/ min, to give peptide analogue **3D**. ESI-MS: m/z 757.0 $[M+3H]^{3+}$. R_T 7.70 min, as a white solid (20 mg, 99 % purity).

Analogue 3E: Cyclo-[Ala⁹]GR231118:

Cyclo-[H₂N-Ile-Glu-Pro-Dap-Tyr-Arg-Leu-Arg-Tyr-CONH₂]-[H₂N-Ile-Glu-Pro-Dap-Tyr-Arg-Leu-Arg-Ala-CONH₂].

Analogue 3A.a: $[Glu(OAll)^2]$ monomer: *Linear-[(Fmoc)-H₂N-Ile-Glu(OAll)-Pro-Dap-Tyr-Arg-Leu-Arg-Tyr-CONH₂].* As described above for analogue **3A.a**.

Analogue 3E.b: $[Dap^4(Alloc)Ala^9]$ monomer: *Linear-[(Fmoc)-H₂N-Ile-Glu-Pro-Dap(Alloc)-Tyr-Arg-Leu-Arg-Ala-CONH₂].* The peptide backbone was prepared via General methods A2 and A3 on a 0.3 mmol scale. Cleavage was carried out via General method B1. The crude peptide was purified using RP-HPLC over a gradient 0-60 % over 80 min at a flow rate of 15 mL/ min, to give peptide analogue **3E.b**. ESI-MS: m/z 705.37 $[M+2H]^{2+}$ R_T 10.37 min, as a white solid (158 mg, 98 % purity).

Analogue 3E.c: Intramolecular coupling of 3A.a $[Glu^2(OH)]$ and 3E.b $[Dap^4(NH_2)]$: Intermolecular cyclisation was carried out between linear peptides analogues **3A.a** and **3E.b** via General method C1 to give crude peptide analogue **3E.c** as a white solid (103 mg).

Analogue 3E.d: $[Glu^2(OAll)]/[Dap^4(Alloc)]$ selective deprotection of 3E.c: OAll/Alloc side chain deprotection was then carried out on peptide analogue **3E.c** via General method B2. The crude peptide was purified using RP-HPLC over a gradient 0-60 % over 80 min at a flow rate of 15 mL/ min, to give peptide analogue **3E.d**. ESI-MS: m/z 946.7 $[M+TFA+3H]^{3+}$ 908.7 $[M+3H]^{3+}$ 681.8 $[M+4H]^{4+}$ R_T 10.11 min, as a white solid (30 mg, 99 % purity).

Analogue 3E: Intermolecular coupling of 3E.d [Glu²(OH)] and [Dap⁴(NH₂)]:

Intramolecular cyclisation was carried out on analogue **3E.d** via General method C1. Finally, Fmoc deprotection of the N-termini was conducted via General method B3. The crude peptide was purified using RP-HPLC over a gradient 0-60 % over 80 min at a flow rate of 15 mL/ min, to give peptide analogue **3E**. ESI-MS: m/z 1245.5 [M+2TFA+2H]²⁺, 792.7 [M+TFA+3H]³⁺, 754.77 [M+3H]³⁺ and 566.3 [M+4H]⁴⁺. R_T 7.78 min, as a white solid (12 mg, 97 % purity).

Analogue 3F: Cyclo-[Ala^{6-8'}]GR231118:

Cyclo-[H₂N-Ile-Glu-Pro-Dap-Tyr-Ala-Leu-Arg-Tyr-CONH₂]-[H₂N-Ile-Glu-Pro-Dap-Tyr-Arg-Leu-Ala-Tyr-CONH₂].

Analogue 3F.a: [Glu(OAll)²Ala⁶] monomer: *Linear-[(Fmoc)-H₂N-Ile-Glu(OAll)-Pro-Dap-Tyr-Ala-Leu-Arg-Tyr-CONH₂]*. The peptide backbone was prepared via General methods A2 and A3 on a 0.3 mmol scale. Cleavage was carried out via General method B1, whilst [Glu²] remained OAll protected and the N-terminus remained Fmoc protected. The crude peptide was purified using RP-HPLC over a gradient 0-60 % over 80 min at a flow rate of 15 mL/ min, to give peptide analogue **3F.b**. ESI-MS: m/z 686.8 [M+2H]²⁺ R_T 10.64 min, as a white solid (117 mg, 99 % purity).

Analogue 3D.b: [Dap⁴(Alloc)Ala⁸] monomer: *Linear-[(Fmoc)-H₂N-Ile-Glu-Pro-Dap(Alloc)-Tyr-Arg-Leu-Ala-Tyr-CONH₂]*. As described above for analogue **3D.b**.

Analogue 3F.c: Intramolecular coupling of 3E.a [Glu²(OH)] and 3D.b [Dap⁴(NH₂)]: Intermolecular cyclisation was carried out between linear peptides analogues **3F.a** and **3D.b** via General method C1 to give crude peptide analogue **3F.c** as a white solid (109 mg).

Analogue 3F.d: [Glu²(OAll)]/[Dap⁴(Alloc)] selective deprotection of 3F.c: OAll/Alloc side chain deprotection was then carried out on peptide analogue **3F.c** via General method B2. The crude peptide was purified using RP-HPLC over a gradient 0-60 % over 80 min at a flow rate of 15 mL/ min, to give peptide analogue **3F.d**. ESI-MS: m/z 1323.5 [M+2H]²⁺ 882.7 [M+3H]³⁺ R_T 10.81 min, as a white solid (39 mg, 97 % purity).

Analogue 3F: Intermolecular coupling of 3F.d [Glu²(OH)] and [Dap⁴(NH₂)]: Intramolecular cyclisation was carried out on analogue **3F.d** via General method C1. Finally, Fmoc deprotection of the N-termini was conducted via General method B3. The crude peptide was purified using RP-HPLC over a gradient 0-60 % over 80 min at a flow rate of 15 mL/ min, to give peptide analogue **3F**. ESI-MS: m/z 1092.5 [M+2H]²⁺ and 728.7 [M+3H]³⁺ R_T 8.38 min, as a white solid (18 mg, 98 % purity).

3.6.4 Cyclic GR231118 dimer Cy5 conjugates

Analogue 4A: Cyclo-(Cy5) GR231118:

Cyclo--[(sCy5)-H₂N-Ile-Glu-Pro-Dap-Tyr-Arg-Leu-Arg-Ty-CONH₂]-[H₂N-Ile-Glu-Pro-Dap-Tyr-Arg-Leu-Arg-Tyr-CONH₂].

Analogue 2A: Cyclo-[Dap⁴]GR231118: *Cyclo-([H₂N-Ile-Glu-Pro-Dap-Tyr-Arg-Leu-Arg-Tyr-CONH₂])²:* As described above for analogue **2A**.

Analogue 4A: N-terminal sCy5 conjugation of analogue A2: sCy5 conjugation to the N-terminal of peptide analogue **2A** was carried out via General method C2. The crude peptide was purified using RP-HPLC over a gradient 0-60 % over 100 min at a flow rate of 15 mL/ min, to give peptide analogue **4A**. ESI-MS: m/z 764.7 [M+3H]³⁺, R_T 8.71 min, as a brilliant blue solid (1 mg, 95 % purity).

Analogue 4B: Cyclo-(Cy5)² GR231118:

Cyclo--[(sCy5)-H₂N-Ile-Glu-Pro-Dap-Tyr-Arg-Leu-Arg-Ty-CONH₂]-[(sCy5)-H₂N-Ile-Glu-Pro-Dap-Tyr-Arg-Leu-Arg-Tyr-CONH₂].

Analogue 2A: Cyclo-[Dap⁴]GR231118: *Cyclo-([H₂N-Ile-Glu-Pro-Dap-Tyr-Arg-Leu-Arg-Tyr-CONH₂])²:* As described above for analogue **2A**.

Analogue 4B: Dual N-terminal sCy5 conjugation of analogue A2: sCy5 conjugation to both N-terminals of peptide analogue **2A** was carried out via General method C2. The crude peptide was purified using RP-HPLC over a gradient 0-60 % over 100 min at a flow rate of 15 mL/ min, to give peptide analogue **4B**. ESI-MS: m/z 1815.0 [M+2H]²⁺ and 1210.3 [M+3H]³⁺ R_T 9.25 min, as a brilliant blue solid (2 mg, 96 % purity).

Chapter 4

Structure-activity relationships of novel GR231118 analogues at the neuropeptide Y Y_1 and Y_4 receptors: influence of ring size and dimer substitution on affinity and selectivity.

"Oh crumbs!"

Joanne Sampson

4.1 Introduction

As discussed in Chapter 1 (Section 1.2.2.2), the endogenous peptides of the NPY family, NPY, PYY and PP, bind to the Y receptors (YR) with varying degrees of affinity and selectivity. Y₁R and Y₂R are the primary targets of NPY and PYY, the Y₄R is selectively activated by PP while the Y₅R has affinity for all three peptides. In Chapter 3 we introduced the structure-activity relationship (SAR) of Y₁R binding by the peptide ligands BVD15 monomer and GR231118 dimer, as a rationale for the synthesis of new derivatives (Chapter 3). However, in addition to Y₁R affinity, YR selectivity should also be taken into consideration when evaluating the pharmacology of these ligands. Here we introduce current understanding of the YR selectivity of BVD15 and GR231118, prior to evaluation of their pharmacology at the Y₁R and Y₄R.

4.1.1 Y₁R / Y₄R ligand binding; SAR and selectivity

The Y₁R and Y₄R are evolutionarily the most closely related members of the YR family (Larhammar and Salaneck, 2004) arising from chromosomal doubling in early vertebrate evolution following an original duplication to create Y₁R and Y₂R genes. This similarity is somewhat surprising as the Y₄R shows selectivity for PP compared to the NPY / PYY activated Y₁R, and there was limited evidence for a separate PP receptor prior to the cloning of the Y₄R (Bard et al., 1995). Larhammar and Salaneck (2004) also concluded that the Y₄R may have originally been a receptor for NPY and PYY as well as PP, due to the chicken Y₄R variants' ability to bind NPY, PYY and PP with equal affinity. This is reinforced by the wide tissue distribution of Y₄R mRNA in shark, suggesting a more widespread functional role, compared to limited human tissue distribution. The selectivity of PP for the Y₄R is also more pronounced in mice and rats suggesting rapid co-evolution (Larhammar and Salaneck, 2004). This co-evolution is evident through a more variable PP sequence in mice and rats compared to human PP, resulting in species selectivity i.e. rat PP is selective towards the rat Y₄R (rY₄R) and human PP (hPP) is selective towards human Y₄R. This is in contrast to NPY and PYY selectivity towards the Y₁R, as these peptide sequences are highly conserved throughout species, and show little difference

in species subtype selectivity. In addition, the hY₁R and hY₄R share sequence homology, including conserved residues within the Y₁R / Y₄R binding site. Most notably [Asp^{6.59}] in both the Y₁R and Y₄R has been demonstrated to interact with [Arg³⁵] of NPY and of PP, an interaction that is specific to these YR types (Merten et al., 2007).

In the case of the Y₄R, only selective agonists are known with few antagonists described, as discussed in Chapter 1 (Section 1.2.4.3). These agonists are of particular therapeutic interest due to their ability to promote satiety (Brothers and Wahlestedt, 2010). These selective agonists are largely derived from truncated forms of the PP peptide, for example BVD74-D was developed through dimerisation, via its N-terminus, of its precursor peptide, BVD74 (YRLRY-CONH₂; Balasubramaniam et al., 2006; Kuhn et al., 2016; Liu et al., 2016). BVD74-D showed agonist binding at both the Y₁R and the Y₄R, and an increase in affinity and selectivity (~150 fold) at the Y₄R compared to the Y₁R ($pK_i Y_4R = 9.05 \pm 0.01$; $pK_i Y_1R = 7.50 \pm 0.90$). Another example of a Y₄R agonist is that of truncated NPY₂₅₋₃₆ where [Gln³⁴] mutation to cyclopentane-based amino acid (β Cpe) resulted in Y₄R selectivity (Berlicki et al., 2013). This study found that the [β Cpe³⁴]-NPY₂₅₋₃₆ analogue displayed partial agonism ($EC_{50} = 41 \pm 6$ nM; $E_{max} = 71\%$ of PP, $K_i = 10 \pm 2$ nM) at the Y₄R, and 50-100 fold selectivity compared to the Y₁R, Y₂R and Y₅R. This study also showed that the substitution of [Thr³²] to Tyr ([Tyr³² β Cpe³⁴]-NPY₃₂₋₃₆) resulted in an analogue that expressed selective binding at the Y₄R ($EC_{50} = 94 \pm 21$ nM; $E_{max} = 73\%$; $K_i = 105 \pm 42$ nM) with 100 fold selectivity compared to the Y₁R, Y₂R and Y₅R. In addition, selective small molecule positive allosteric modulators (PAMs) have also been identified and described for the Y₄R (Schubert et al., 2017).

The pursuit of Y₄R antagonists, for which there are currently very limited selective peptide or non-peptide compounds, has also proven challenging. For example, in a SAR study based on aza- and D-amino acid derivatives of BVD74-D, analogues with moderate Y₄R antagonist like properties and affinity were identified (Kuhn et al., 2017). However, within this series of analogues,

achieving high selectivity over the Y₁R in particular remained problematic. Thus, Y₄R antagonists with appropriate high affinity and selectivity remain a key goal as pharmacological tools to evaluate the physiological function and relative importance of this receptor system, for example in diabetes and obesity.

As discussed in Chapter 1 (Section 1.2.2.2), NPY and PYY also display equivalent affinities for the Y₁R and Y₂R, with Y₂R agonist selectivity being achieved by truncated peptide analogues such as NPY₃₋₃₆, NPY₁₃₋₃₆ and PYY₃₋₃₆ (Bard et al., 1995; Gerald et al., 1995; Rose et al., 1995). As such, it could be speculated that the Y₁R and the Y₂R may express a similar evolutionary root as the Y₁R and the Y₄R. However, it has been shown that the Y₁R only shares a 31% overall amino acid identity with the Y₂R, compared to the 53% shared with the Y₄R (Larhammar et al., 2001). Recent modelling studies have investigated the binding of truncated C-terminal peptides at the Y₂R, which have highlighted the importance of the interaction pattern between [³²TRQRY³⁶]-amide in the C-terminus of the peptides and the Y₂R, in optimising selective ligands (Xu et al., 2018). This study is in agreement with previous mutational studies that have identified key residues within the NPY peptide required for YR binding, with the loss of [Arg³³] and [Arg³⁵] resulting in a loss of binding at the Y₁R and the Y₄R, and the substitution of [Arg³⁵] and [Tyr³⁶] being the most susceptible in the Y₂R (Beck-Sickinger et al., 1994). It has also been demonstrated through NMR and molecular modelling studies that [Arg³⁵] of NPY is equally important in Y₂R binding as it is in Y₁R and Y₄R binding (Kaiser et al., 2015). However, the peptide makes a different set of interactions at the Y₂R, with aromatic residues [Trp^{5,26}] and [Tyr^{5,39}], compared to the interaction observed at [Asp^{6,59}] in the Y₁R and the Y₄R. In addition, [Pro³⁴]-NPY analogues result in Y₁R and Y₄R selectivity over the Y₂R (Fuhlendorff et al., 1990; Gehlert et al., 1997). It has been demonstrated that [Gln³⁴] plays a key role in NPY binding at the Y₂R and [Pro³⁴] substitution results in disruption of binding site conformation of the peptide (Kaiser et al., 2015). Current structural pharmacological studies therefore suggest that ligand selectivity between the more distinct Y₁R and Y₂R

binding sites is easier to achieve than for Y₁R and Y₄R. This is further demonstrated by the known selectivity of BVD15 and GR231118 ligands, discussed below.

4.1.2 BVD15 monomer and GR231118 dimer peptides as Y₄R agonists

When BVD15 was developed, it was initially shown to exhibit potent agonist activity at the Y₄R, along with its Y₁R antagonist activity (Balasubramaniam et al., 2001; Leban et al., 1995; Parker et al., 1998). Parker et al., (1998) demonstrated high affinity binding of BVD15 at the Y₁R and Y₄R ($pK_i = 8.3 \pm 0.03$ and 8.3 ± 0.08 , respectively) and low affinity at the Y₂R ($pK_i < 6$) in radioligand binding assays. In addition, this study demonstrated antagonist activity at the Y₁R ($pA_2 = 7.1 \pm 0.05$) and agonist activity at the Y₄R ($pEC_{50} = 6.8 \pm 0.03$) in cAMP accumulation assays.

Guérin et al., (2010) built upon the BVD15 analogues through modification with Lys(DOTA) at position 2 or 4 of the BVD15 peptide, to generate compounds with potential for tumour imaging. The [Lys⁴(DOTA)]-BVD15 derivative showed no binding to the Y₂R and Y₄R up to 10 μ M, compared to the Y₁R in radioligand binding assays (K_i Y₁R = 63 ± 25 nM), suggesting that these modifications generated at least 100 fold Y₁R selectivity. [Lys⁴(Pip-Ga-DOTA), Bip⁵]-BVD15 was also found to exhibit low affinity ($K_i > 1000$ nM) binding at both the Y₂R and Y₄R compared to K_i 20 - 30 nM at the Y₁R (Zhang et al., 2016). However, other modifications at [Lys²] for BVD15 did not achieve the same degree of selectivity. For example, Liu et al. (2016) generated sCy5 fluorophore [Lys²] conjugated derivatives of BVD15 that retained Y₁R affinity and antagonist activity (e.g. [Lys²(sCy5), Arg⁴]-BVD15; $pK_d = 7.2 \pm 0.1$ in whole cell saturation binding; known as Cy5mono in this thesis). However Cy5mono also acted as a partial agonist at the Y₄R ($pEC_{50} = 7.10 \pm 0.19$; 1 μ M response 59.0 % of maximal PP), with a Y₄R binding affinity ($pK_d = 6.26 \pm 0.11$) that indicated ~8 fold selectivity for the Y₁R. Liu et al., (2016) also confirmed a lack of Cy5mono binding to Y₂R expressing cells up to 1 μ M.

Studies around the GR231118 dimer ligand show similar trends of high Y₁R selectivity over the Y₂R, combined with agonist activity at the Y₄R. Parker et al., (1998) showed GR231118 was a weak, low potency agonist at the Y₂R ($pEC_{50} = 6.0 \pm 0.1$) and a higher potency agonist at the Y₄R ($pEC_{50} = 8.6 \pm 0.1$) in cAMP production assays. Parker et al (1998) also demonstrated that GR231118 acted as a high potency antagonist at the Y₁R ($pA_2 = 10.5 \pm 0.2$) in cAMP production assays. The same study showed that GR231118 displayed highest affinity at the Y₁R ($pK_i = 10.2 \pm >0.1$), followed by the Y₄R ($pK_i = 9.6 \pm 0.2$) and finally the Y₂R ($pK_i = 7.2 \pm >0.1$), in radioligand binding studies. These findings were in agreement with later studies by Balasubramaniam et al. (2001). In addition, Beck-Sickinger et al. (1994) determined that the [Arg³⁵] residue within NPY was important for NPY binding at both the Y₁R and the Y₄R, as discussed above (Section 4.1.1) indicating a similar binding mode at these receptors.

Therefore, BVD15 and GR231118 compounds show selectivity for Y₁R, but also show affinity and partial agonism at the Y₄R. Increasing Y₁R versus Y₄R selectivity, for either receptor type, would be desirable in the development of new candidate ligands. Equally it is possible that dual Y₁R antagonists / Y₄R agonists might have favourable properties in mimicking both PP-mediated satiety and inhibiting the central appetite promoting effects of NPY. As such, the action of the ligands synthesised for this study should also be investigated at the Y₄R, in order to determine if these analogues can better discriminate between the Y₁R and the Y₄R.

4.2 Aims

Chapter 3 explained the synthesis of a series of BVD15 monomer and GR231118 dimer analogues, via Fmoc-based solid phase peptide synthesis (SPPS), to investigate the roles of the cyclic moiety and key residues, in one of the GR231118 arms, in binding to the Y₁R. The primary purpose of these derivatives was to explore different mechanisms that may be attributable to the much higher GR231118 dimer affinity for the Y₁R, compared to monomeric

BVD15-like peptides. In this chapter I have introduced the concept that parent BVD15 and GR231118 compounds are also Y₄R agonists, and thus determining the selectivity between the Y₁R and Y₄R for novel derivatives is an important factor in characterisation. Therefore, the aims of this chapter were to study the SAR of the novel BVD15 and GR231118 peptides at both the Y₁R and the Y₄R. This was done through the application of plate reader based competition binding assays and β -arrestin2 recruitment functional assays, to provide estimates of affinity and agonist efficacy where appropriate. In this way, the contributions of the ring cycle present in the GR231118 dimer, and amino acid side chains within a single dimer arm, could be explored for their impact on Y₁R and Y₄R affinity and selectivity.

4.3 Results

4.3.1 Cy5mono as a Y₁R and Y₄R dual fluorescent ligand

Previously published data describes the characterisation of the Cy5 monomer, compound H, called Cy5mono in this thesis (Liu et al., 2016). This published data describes the characterisation of Cy5mono functionality and affinity at the Y₁R and Y₄R through the use of β -arrestin2 recruitment, saturation and competition binding assays, via imaging and radioligand based studies. The key data performed as part of this work are reproduced here.

β -arrestin2 recruitment assays were performed in Y₁ A2 and Y₄ A2 cells, expressing the BiFC fragment tagged YR-Yc and β -arrestin2-Yn constructs, as described in Chapter 2 (Section 2.2.1 and Table 2.2; Kilpatrick et al., 2010). Antagonist effects in β -arrestin2 recruitment assays were assessed by Schild analysis, carried out as described in Chapter 2 (Section 2.4.1.5 and 2.6.1.4). Saturation binding and competition binding studies were conducted in Y₁R-GFP and Y₄R-GFP expressing cells as described in Chapter 2 (Section 2.2.1 and Table 2.2) using high content imaging as laid out in Section 2.4.1.3 and 2.4.1.2, respectively.

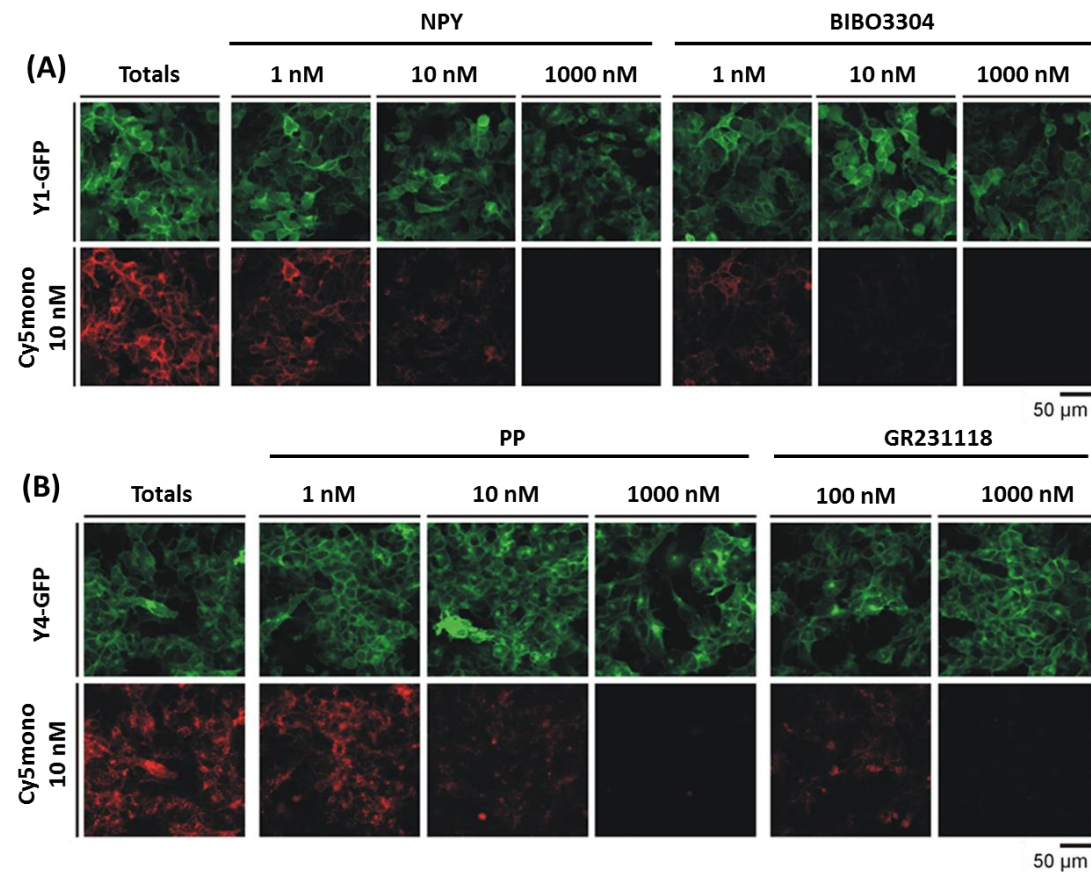


Figure 4.1 - IX Ultra acquired images of Cy5mono fluorescent ligand binding at both the Y₁R and Y₄R. Totals show control cells exposed to 10 nM Cy5mono only, followed by increasing concentrations of competing unlabelled ligand. Full displacement of Cy5mono was observed following 1 μ M treatment of NPY or PP at the (A) Y₁R and (B) Y₄R, respectively, and the in the presence of BIBO3304 or GR231118. Images are replicated from Liu et al., (2016).

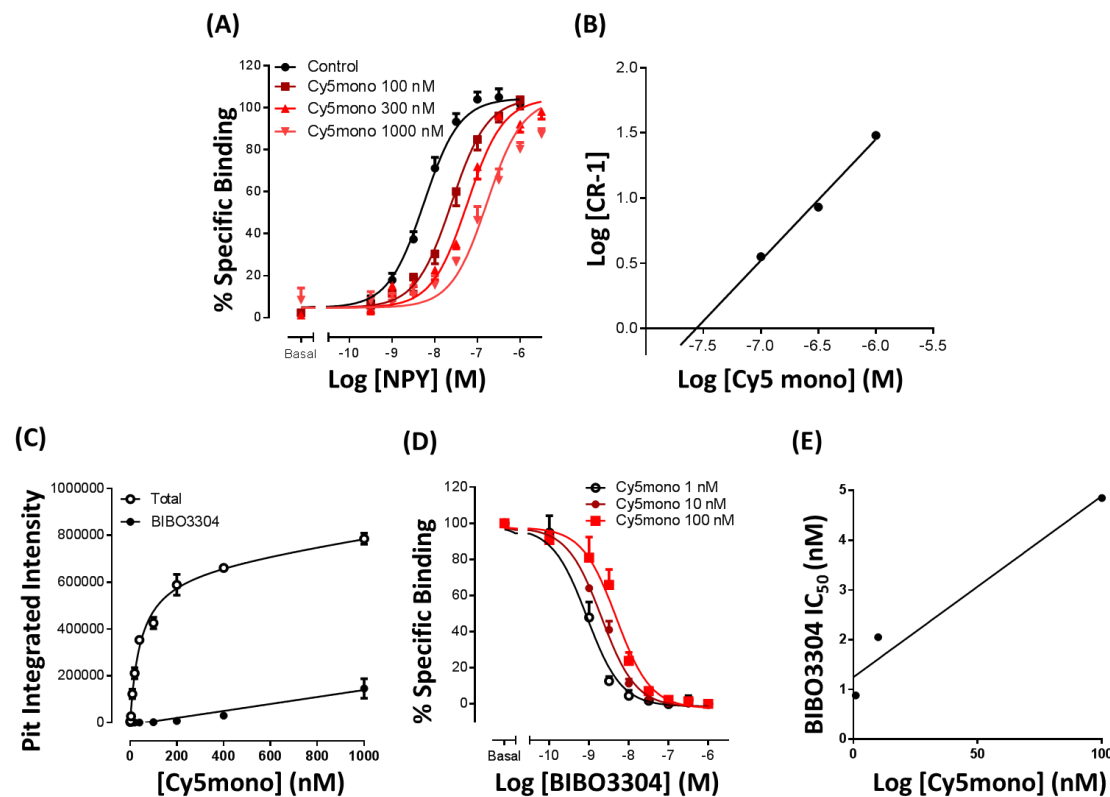


Figure 4.2 – Functional characterisation of Cy5mono fluorescent ligand at the Y₁R. (A) Shows NPY induced Y₁R β-arrestin2 recruitment in Y₁ A2 cells, following treatment with increasing concentrations of Cy5mono as indicated and (B) shows Schild analysis of β-arrestin2 recruitment, calculated from NPY pEC₅₀ estimates, with a calculated pA₂ of 7.5 ± 0.1. (C) Shows a representative saturation binding profile in Y₁-GFP cells of Cy5mono, normalised to total specific binding (100%) from which a derived pK_b of 7.2 ± 0.1 was calculated. (D) Shows BIBO3304 competition binding curves in Y₁-GFP cells in the presence of increasing concentrations of Cy5mono as indicated and (E) shows the plot of BIBO3304 IC₅₀ versus ligand concentration from competition binding, providing a pK_i affinity estimate for Cy5mono of 7.3 ± 0.1. Data were pooled from at least 4 individual experiments, are presented as mean ± SEM and are replicated from Liu et al., (2016).

At the Y₁R, Cy5mono behaved as a surmountable antagonist of NPY induced β -arrestin2 recruitment (Figure 4.2A), sharing the characteristics of [Lys⁴]-BVD15 (data shown in Liu et al., 2016). Cy5mono had no effect on β -arrestin2 recruitment alone (up to 1 μ M), and from its effects as an antagonist, Schild analysis calculated a pA₂ of 7.5 ± 0.1 (Figure 4.2B and Figure 5.6D and E; Section 2.6.1.4). This was somewhat lower than the affinity of Cy5mono measured by [¹²⁵I]-PYY competition binding in Y₁R-GFP containing membranes (pK_i 9.4; Liu et al., 2016).

Binding assays using Cy5mono, performed by high content imaging, of living Y₁-GFP expressing cells, demonstrated saturable binding to the Y₁R, consistent with single site binding and derived a Cy5mono pK_d value of 7.2 ± 0.1 . This whole cell estimate of Y₁R affinity was not significantly different to that observed in functional assays (Figure 4.2C). Equally, competition binding analysis, using 10 nM Cy5mono, demonstrated specific and predominantly plasma membrane labelling of the Y₁R that could be fully inhibited by NPY and BIBO3304 (Figure 4.1A; Liu et al., 2016). BIBO3304 competition curves were constructed where the Cy5mono concentration was varied to obtain a set of BIBO3304 IC₅₀ values (Figure 4.2D and E). BIBO3304 IC₅₀ values varied in a manner predicted by Cheng-Prusoff analysis (Section 2.6.1.5) and from this linear relationship, a final Cy5mono pK_i estimate of 7.3 ± 0.1 was calculated, consistent with previous affinity estimates.

The Cy5mono ligand also displayed a moderate affinity for the Y₄R (Figure 4.3; Liu et al., 2016). Whole cell saturation binding analysis, through imaging of the Y₄-GFP cells, provided a pK_d of 6.3 ± 0.1 (~8 fold lower than at the Y₁R), and binding was displaced by unlabelled PP. In contrast to the labelling observed in Y₁-GFP cells, Cy5mono labelling of Y₄-GFP cells demonstrated a predominately intracellular distribution (Figure 4.1B; Liu et al., 2016), suggesting that Cy5mono co-internalised with this receptor as a result of agonist stimulation.

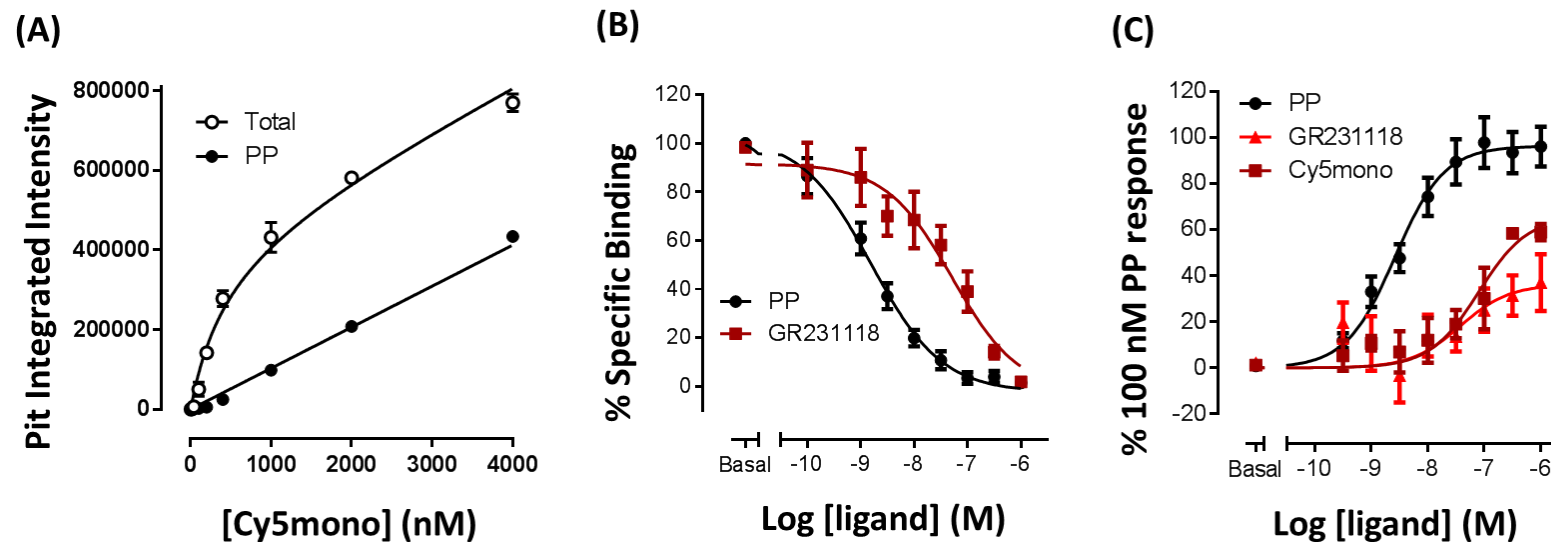


Figure 4.3 – Characterisation of Cy5mono fluorescent ligand at the Y₄R. (A) Shows a representative saturation binding profile in Y₄-GFP cells of Cy5mono, from which a derived pK_d of 6.3 ± 0.1 was calculated. Non-specific binding was assessed in the presence of 1 μ M PP. (B) Shows competition binding curves in Y₄-GFP cells with increasing concentrations of PP and GR231118 as indicated, from which pK_i values of 8.7 ± 0.1 and 7.2 ± 0.1 were estimated for PP and GR231118, respectively, in the presence of 100 nM Cy5mono. (C) Shows Y₄R β -arrestin2 recruitment in Y₄ A2 cells, following treatment with increasing concentrations of ligand, as indicated, where Cy5mono was shown to act as a partial agonist at the Y₄R compared to PP, but of higher efficacy compared to GR231118. Data were pooled from at least 4 individual experiments and are shown as mean \pm SEM. Data are replicated from Liu et al., (2016).

This was confirmed in Y₄R β -arrestin2 recruitment assays (Figure 4.3C), in which Cy5mono was an agonist, in contrast to its antagonist actions at the Y₁R. Cy5mono stimulated β -arrestin2 recruitment by the Y₄R, with an estimated pEC₅₀ of 7.1 ± 0.2 and a reduced R_{max} response of 59 % compared to PP controls (pEC₅₀ = 8.77 ± 0.07 , R_{max} = 100 %).

These data combined show that the Cy5mono compound is a high affinity Y₁R antagonist with a K_d of ~30 nM and a low affinity Y₄R agonist with a K_d of ~300 nM. Thus, it is a suitable ligand for conducting competition binding and functional assays against the Y₁R and the Y₄R, and as such was employed as a tool in the future experiments for the determination of Y₁R and Y₄R affinities of the novel compounds investigated in this chapter.

4.3.2 Peptide ligands used for characterisation

Peptides produced for this study were made via the General methods laid out in Chapter 2 (Section 2.5) and a more detailed analysis of their design, production and purification is discussed in Chapter 3. A summary list of the peptides investigated in this study can be found in Table 4.1, Table 4.4 and Table 4.7 below.

4.3.3 Pharmacological characterisation of BVD15 cyclic monomer derivatives at Y₁R and Y₄R

As discussed for Cy5mono above, β -arrestin2 recruitment assays were first performed in order to establish ligand pharmacology. Due to the initial expectation that BVD15 related compounds would be antagonists at the Y₁R and agonists at the Y₄R, we examined the inhibitory effect of cyclic derivatives on Y₁R β -arrestin2 recruitment. This was achieved through pre incubation with 300 nM antagonist for 30 min at 37 °C in HBSS/ 0.1 % BSA, prior to NPY treatment, followed by a further 60 min incubation (Figure 4.4A).

Table 4.1 - BVD15 derived monomeric cyclic peptides investigated throughout this chapter. Peptide name indicates the reference name used in the text, and the sequence shows the 3 letter code amino acid sequence of each peptide. All monomer peptides contain an intramolecular cyclic moiety between [Glu²] and the position 4 amino acid: 2,3-diaminopropionic acid (Dap), 2,4-diaminobutyric acid (Dab), Ornithine (Orn) or Lysine (Lys), and the molecular weight is quoted (MW). Changes to the original BVD15 sequence are highlighted in green.

Peptide name	Analogue code (Chapter 3)	Sequence	MW
[Dap ⁴]mono	1A	Ile- <u>Glu</u> -Pro- <u>Dap</u> -Tyr-Arg-Leu-Arg-Tyr-(CONH ₂) 	1174
[Dab ⁴]mono	1B	Ile- <u>Glu</u> -Pro- <u>Dab</u> -Tyr-Arg-Leu-Arg-Tyr-(CONH ₂) 	1189
[Orn ⁴]mono	1C	Ile- <u>Glu</u> -Pro- <u>Orn</u> -Tyr-Arg-Leu-Arg-Tyr-(CONH ₂) 	1205
[Lys ⁴]mono	1D	Ile- <u>Glu</u> -Pro- <u>Lys</u> -Tyr-Arg-Leu-Arg-Tyr-(CONH ₂) 	1219

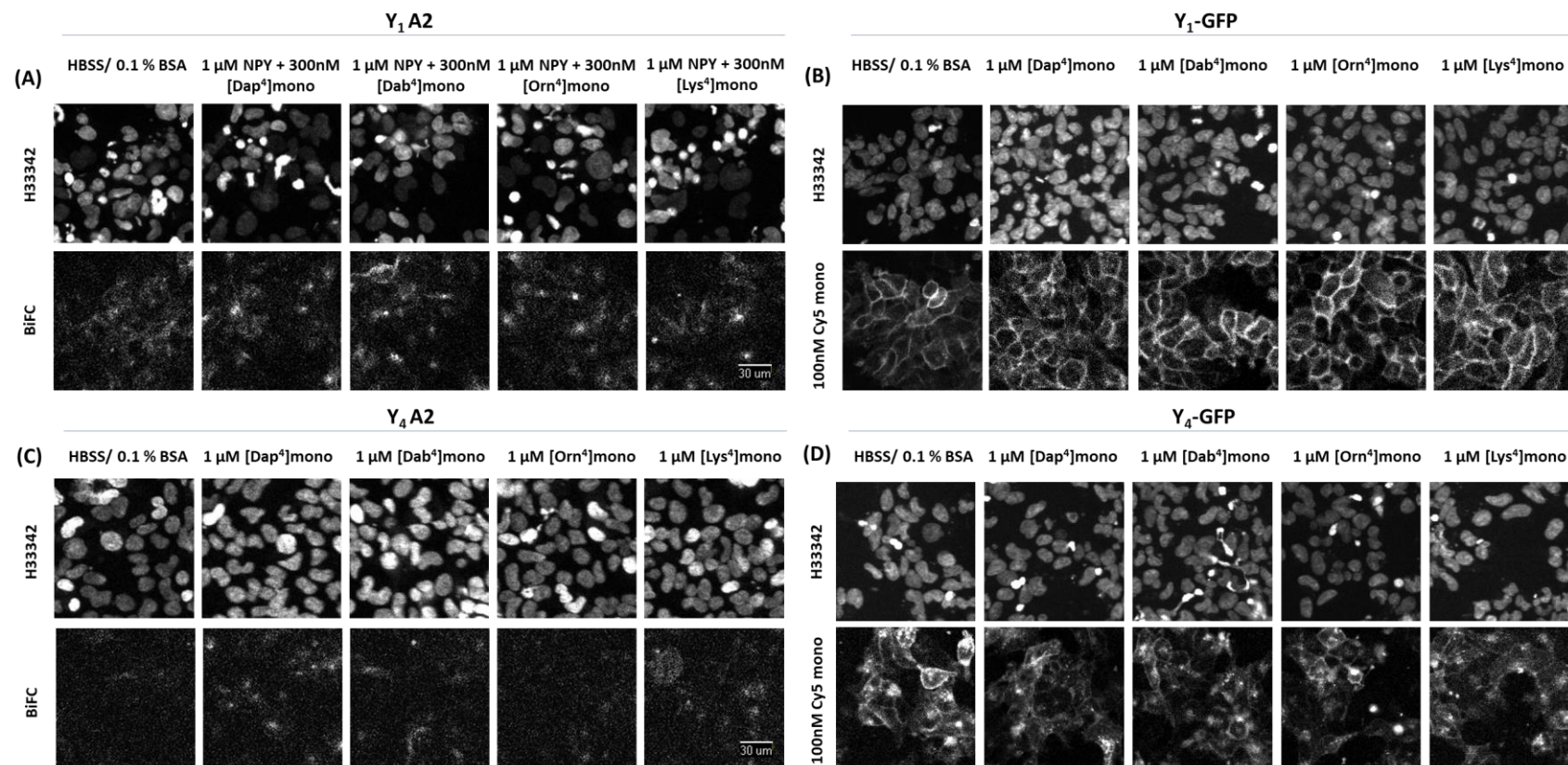


Figure 4.4 -- IX Ultra acquired images of BVD15 cyclic monomer variants at the Y₁R and Y₄R. (A) Shows 1 μM NPY induced β-arrestin2 recruitment complexes (BiFC) in the presence of 300 nM cyclic monomers in Y₁ A2 cells. (B) Shows Cy5mono competition binding in the presence of 1 μM cyclic monomer in Y₁-GFP cells. (C) Shows β-arrestin2 recruitment complexes (BiFC) in Y₄ A2 cells in the presence of 1 μM BVD15 monomers. (D) Shows 100 nM Cy5mono competition binding in the presence of 1 μM cyclic monomers in Y₄-GFP. All images were acquired on the IX Ultra and analysed using the MetaXpress granularity algorithm as previously described (Chapter 2, Section 2.4.1.2, 2.4.1.5 and 2.6.1.1) to produce the graphs shown in Figure 4.5.

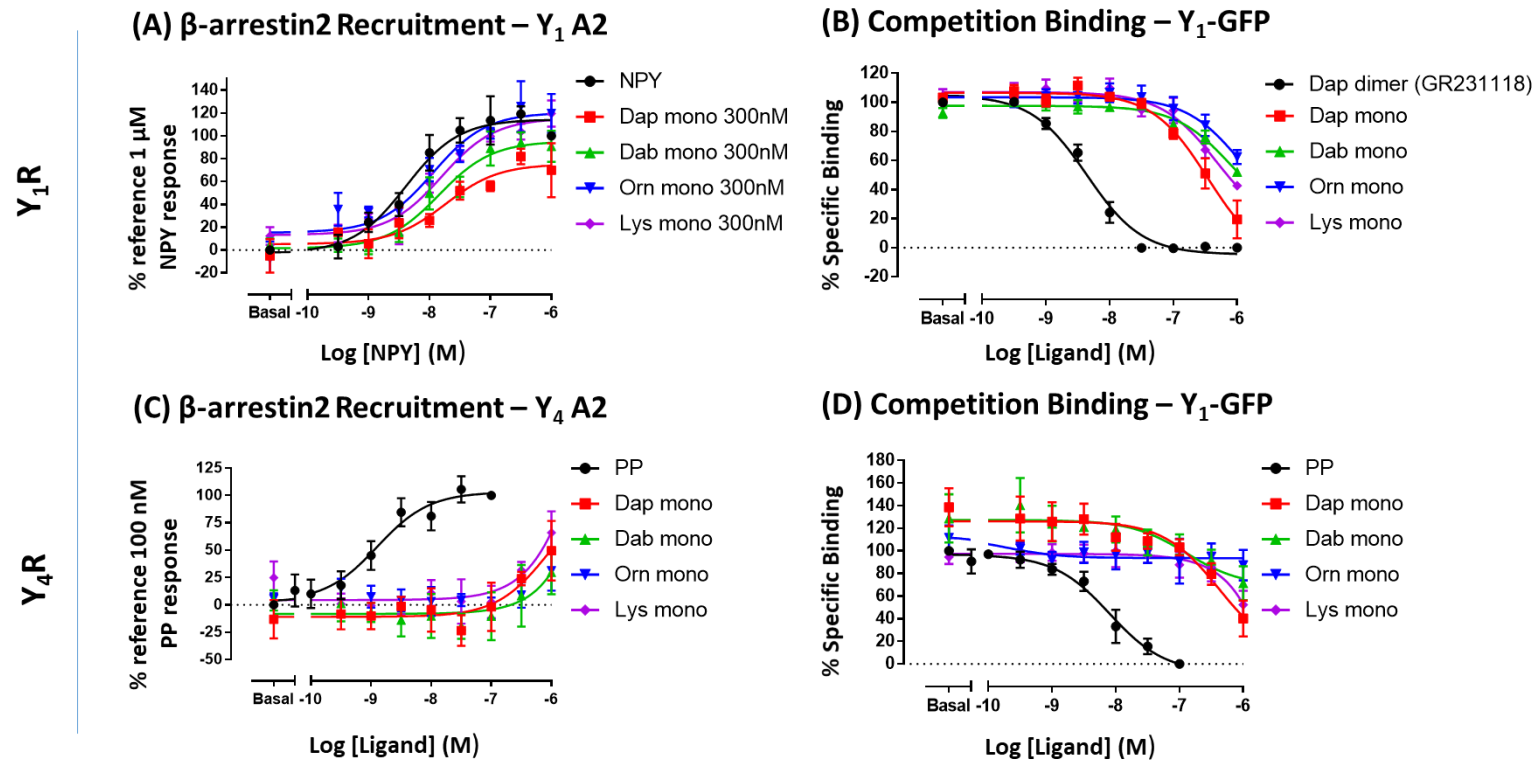


Figure 4.5 – Pharmacological characterisation of BVD15 cyclic monomer variants at the Y_1 R and Y_4 R. (A) Shows the effect of cyclic derivatives as antagonists on NPY stimulated β -arrestin2 recruitment at the Y_1 R and (B) shows the Cy5mono competition binding profiles at the Y_1 R. (C) Shows the effect of BVD15 cyclic derivatives as agonists on β -arrestin2 recruitment at the Y_4 R and (D) shows Cy5mono competition binding profiles at the Y_4 R. All images were acquired on the IX Ultra (Figure 4.4) and analysed using the MetaXpress granularity algorithm. Graphs were plotted from pooled data (n of 3 or more individual experiments) and are represented as mean \pm SEM using the average granule intensity / cell in GraphPad Prism v7. Data was normalised to 1 μ M NPY response in β -arrestin2 assays and Cy5mono specific binding was defined by 1 μ M [Dap⁴]dimer (GR231118) at the Y_1 R or normalised to 100 nM PP for the Y_4 R.

Table 4.2 - Summarised table of pharmacological parameters for BVD15 derived cyclic monomer peptides at the Y₁R. Values were determined in β -arrestin2 recruitment and competition binding assays (Figure 4.5A and B). For β -arrestin2 recruitment, NPY pEC₅₀ was measured in presence of 300 nM ligand and pK_b values were estimated using the Gaddum equation ($K_b = [B] / (CR - 1)$; Section 2.6.1.4). For competition binding, pK_i values were estimated using the Cheng-Prusoff correction (Section 2.6.1.5), in the presence of 100 nM Cy5mono, where Cy5mono K_d was stated as 30 nM for the Y₁R (Figure 4.2; Liu et al., 2016). All values are represented as mean \pm SEM.

Y ₁ R		β -arrestin2 recruitment				Competition binding			
Peptide name	Analogue code	n	NPY pEC ₅₀	NPY R _{max} (% 1 μ M NPY)	pK _b	n	pIC ₅₀	% competition by 1 μ M ligand	pK _i
NPY	⌀	4	8.34 \pm 0.17	115.72 \pm 3.52	⌀	⌀	⌀	⌀	⌀
[Dap ⁴]dimer (GR23118)	2A	⌀	⌀	⌀	⌀	3	8.35 \pm 0.10	⌀	8.99 \pm 0.10
[Dap ⁴]mono	1A	4	7.36 \pm 0.50	84.98 \pm 14.36	7.41 \pm 0.37	3	6.43 \pm 0.13	80.57 \pm 12.99	7.06 \pm 0.13
[Dab ⁴]mono	1B	4	7.65 \pm 0.27	99.79 \pm 7.09	7.07 \pm 0.22	3	<6.5	47.81 \pm 1.46	⌀
[Orn ⁴]mono	1C	4	7.84 \pm 0.35	124.55 \pm 16.86	7.28 \pm 0.68	3	<6.5	37.60 \pm 4.83	⌀
[Lys ⁴]mono	1D	4	7.80 \pm 0.17	114.93 \pm 7.06	7.24 \pm 0.27	3	<6.5	57.39 \pm 3.01	⌀

Table 4.3 - Summarised table of pharmacological parameters for BVD15 derived cyclic monomer peptides at the Y₄R. Values were determined in β -arrestin2 recruitment and competition binding assays (Figure 4.5C and D). For β -arrestin2 recruitment assays * indicates that R_{max} was not established and 1 μ M agonist response is quoted. From competition binding, pK_i values were estimated using the Cheng-Prusoff correction, in the presence of 100 nM Cy5mono, where Cy5mono K_d was stated as 300 nM for Y₄R (Figure 4.3; Liu et al., 2016). All values are represented as mean \pm SEM.

Y4R		β-Arrestin2 recruitment			Competition binding			
Peptide name	Analogue code	n	Analogue pEC ₅₀	Analogue 1 μM R _{max} (% 100 nM PP)	n	pIC ₅₀	% competition by 1 μM ligand	pK _i
PP	∅	4	7.90 ± 0.21	103.99 ± 5.67	4	8.06 ± 0.13	∅	8.19 ± 0.13
[Dap ⁴]mono	1A	3	<6.5	64.29 ± 22.76*	3	6.76 ± 0.62	40.17 ± 15.99	6.32 ± 0.36
[Dab ⁴]mono	1B	3	<6.5	49.39 ± 16.09*	3	<6.5	71.34 ± 15.01	∅
[Orn ⁴]mono	1C	3	<6.5	58.89 ± 8.26*	3	<6.5	87.36 ± 13.58	∅
[Lys ⁴]mono	1D	3	<6.5	65.61 ± 17.53*	3	<6.5	52.46 ± 12.45	∅

The cyclic monomers showed no agonist activity at 300 nM, measured by no effect on Y₁R β-arrestin2 recruitment, consistent with a lack of agonism (Figure 4.4A and 4.5A; Table 4.2). However NPY concentration response curves (control pEC₅₀ = 8.34 ± 0.17) were shifted to the right following pre-treatment (Figure 4.4A and 4.5A; Table 4.2). The antagonist effects was observed in the cyclic [Dap⁴]mono and [Dab⁴]mono derivatives which also slightly suppressed the maximal NPY response, however this suppression was not significant (one-way ANOVA followed by Tukey's post-test). Approximate pK_b values calculated from the concentration response curve shifts ranged from 7.07 ± 0.22 to 7.41 ± 0.37 (Table 4.2). To confirm the affinities of the cyclic monomers for the Y₁R, whole cell competition binding assays were performed in Y₁-GFP cells using 100 nM Cy5mono as the fluorescent ligand (Section 2.4.1.2). Compared to the reference GR231118 ligand ([Dap⁴]dimer; pIC₅₀ = 8.35 ± 0.10; Figure 4.4B and 4.5B), the cyclic monomers displayed modest affinity in this assay. Using a maximal competing ligand concentration of 1 μM, only the [Dap⁴]mono cyclic monomer fully competed for the fluorescent ligand with a calculated pK_i of 7.06 ± 0.13 (Table 4.2; Figure 4.4B and 4.5B).

In the Y₄R β-arrestin-2 recruitment assay, the effects of 60 min ligand pre-treatment were explored, in comparison to the endogenous agonist PP (Figure 4.4C and 4.5C; Table 4.3). All four derivatives were weak Y₄R agonists, with limited stimulation of β-arrestin2 association at 1 μM ligand. Similarly, the cyclic ligands were unable to fully compete with Cy5mono for the Y₄R-GFP in whole cell binding assays, at concentrations up to 1 μM (Figure 4.4D and 4.5D; Table 4.3).

4.3.4 Pharmacological characterisation of GR231118 dimer cyclic variants at Y₁R and Y₄R

As GR231118 has previously been characterised as a Y₄R agonist and Y₁R antagonist (Section 4.1) these analogues were examined as agonists at the Y₄R and as antagonists at the Y₁R in β-arrestin2 recruitment assays. β-arrestin2

recruitment assays were performed in Y₁ A2 and Y₄ A2 cells (Figure 4.6A and 4.6C; Table 4.4), in which Y₁R cells were pre incubated with 30 nM antagonist for 30 min at 37 °C in HBSS/ 0.1 % BSA prior to NPY treatment in order to assess their action as antagonists. Competition binding was performed in Y₁-GFP and Y₄-GFP tetracycline inducible cells and assays were conducted according to the general method laid out in Section 2.4.1.2, in the presence of 100 nM Cy5mono (Figure 4.6B and 4.6D). At the Y₁R, β -arrestin2 recruitment showed that these compounds acted as antagonists through a right shifted NPY concentration response curve, without altering the baseline β -arrestin2 recruitment at 30 nM ligand. Previous studies in our group demonstrated non-surmountable antagonism in this assay by GR231118 ([Dap⁴]dimer; Figure 4.7A). This was replicated in the current set of experiments comparing the different dimer bridge derivatives (Figure 4.7B). A reduction in the NPY R_{max} was observed for all compounds except [Lys⁴]dimer, at a pre-treatment concentration of 30 nM. GR231118 ([Dap⁴]dimer) produced the largest depression of NPY, R_{max} 45.2 ± 12.1 %, compared to NPY control of 100 % (p<0.01; following one-way ANOVA and Tukey's post-test), and an NPY R_{max} of 92.2 ± 14.3 % after 30 nM [Lys⁴]dimer derivative, showing no significant difference. The shift in apparent potency was also greatest for the GR231118 [Dap⁴]dimer, compared to the three other bridge compounds (Figure 4.7B; Table 4.5; Mountford et al., 2014). Competition binding at the Y₁R reinforced the apparent order of affinity for the 4 derivatives, with a reduction in pK_i as ring size increased. The order of affinity in this binding assay was [Dap⁴] (GR231118) > [Dab⁴] = [Orn⁴] > [Lys⁴] (with [Lys⁴]dimer showing ~30 fold lower affinity than [Dap⁴]dimer; Figure 4.7D; Table 4.5).

At the Y₄R, β -arrestin2 recruitment demonstrated that the compounds acted as agonists, as previously reported for GR231118 (Balasubramaniam et al., 2001; Mountford et al., 2014; Parker et al., 1998). In this study, the [Dap⁴]dimer (GR231118) stimulated Y₄R β -arrestin2 recruitment with a pEC₅₀ of 7.95 ± 0.25, but was a weak partial agonist compared to PP (producing 22 % of the 100 nM PP maximal response; Figure 4.7D; Table 4.6).

Table 4.4 – GR231118 derived cyclic dimer peptides investigated throughout this chapter. All dimer peptides contain an intermolecular cyclic moiety between [Glu²] and the position 4 amino acid (Dap, Dab, Orn or Lys) of the corresponding dimer peptide arm. Changes to the original GR231118 ([Dap⁴]dimer) sequence are highlighted in green.

Peptide name	Analogue code (Chapter 3)	Sequence	MW
[Dap ⁴]dimer (GR231118)	2A	(H ₂ NOC)-Tyr-Arg-Leu-Arg-Tyr-Dap-Pro-Glu-Ile Ile-Glu-Pro-Dap-Tyr-Arg-Leu-Arg-Tyr-(CONH ₂)	2353
[Dab ⁴]dimer	2B	(H ₂ NOC)-Tyr-Arg-Leu-Arg-Tyr-Dab-Pro-Glu-Ile Ile-Glu-Pro-Dab-Tyr-Arg-Leu-Arg-Tyr-(CONH ₂)	2381
[Orn ⁴]dimer	2C	(H ₂ NOC)-Tyr-Arg-Leu-Arg-Tyr-Orn-Pro-Glu-Ile Ile-Glu-Pro-Orn-Tyr-Arg-Leu-Arg-Tyr-(CONH ₂)	2409
[Lys ⁴]dimer	2D	(H ₂ NOC)-Tyr-Arg-Leu-Arg-Tyr-Lys-Pro-Glu-Ile Ile-Glu-Pro-Lys-Tyr-Arg-Leu-Arg-Tyr-(CONH ₂)	2436

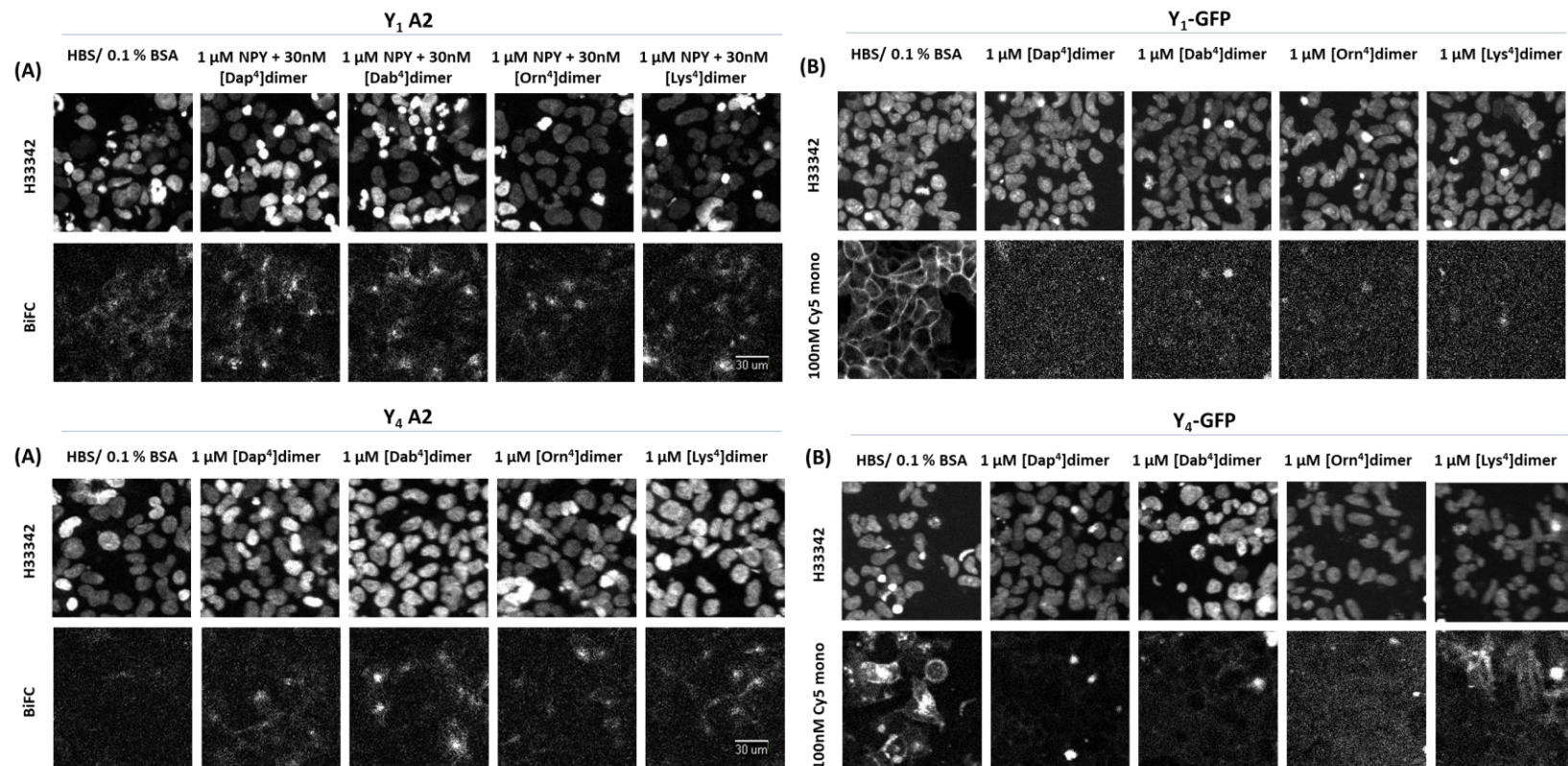


Figure 4.6 - IX Ultra acquired images of GR231118 dimer cycle variants at the Y₁R and Y₄R. (A) Shows NPY induced β -arrestin2 recruitment complexes (BiFC) in Y₁ A2 cells in the presence of 30 nM GR231118 cyclic derivatives. (B) Shows the extent of displacement of 100 nM Cy5mono following 1 μ M treatment of GR231118 cyclic dimer derivatives in Y₁-GFP cells. (C) Shows β -arrestin2 recruitment complexes (BiFC) in Y₄ A2 cells in the presence of 1 μ M GR231118 cyclic variants. (D) Shows the extent of displacement of 100 nM Cy5mono following 1 μ M treatment of GR231118 cyclic dimer derivatives in Y₄-GFP cells. All images were acquired on the IX Ultra and analysed using the MetaXpress granularity algorithm as previously described (Chapter 2, Section 2.4.1.2, 2.4.1.5 and 2.6.1.1) to produce the graphs shown in Figure 4.7.

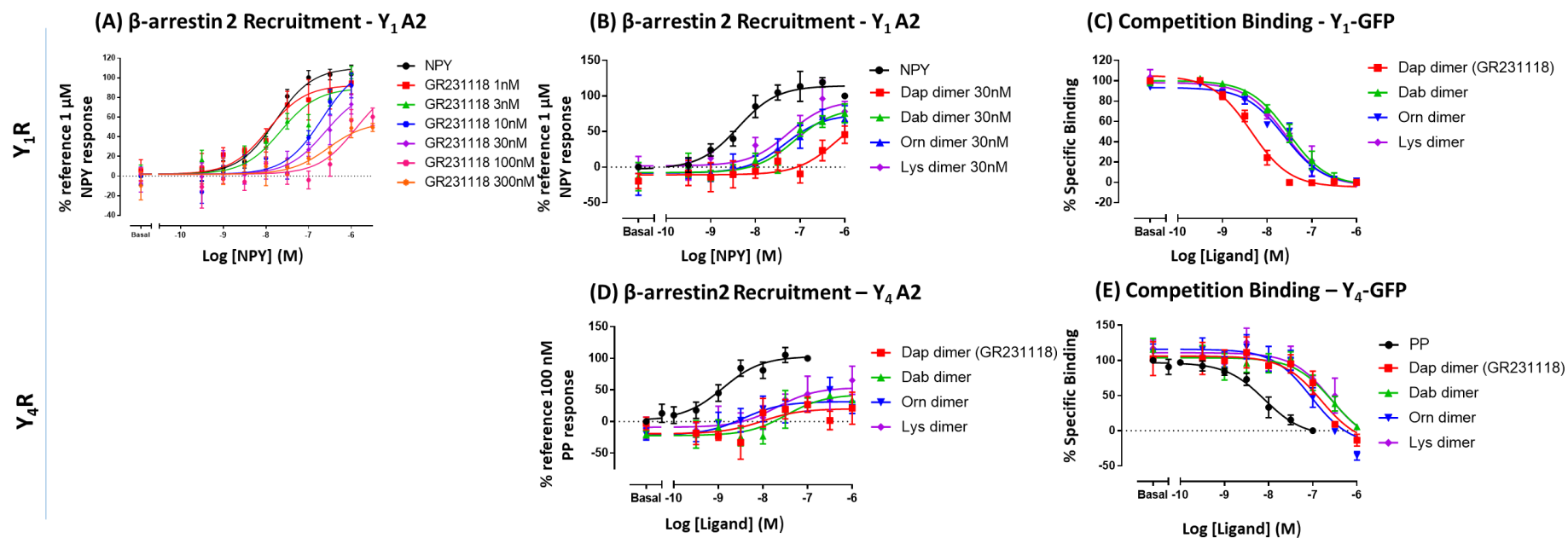


Figure 4.7 - Pharmacological characterisation of GR231118 dimer cycle variants at the Y_1R and Y_4R . (A) Demonstrates the non-surmountable antagonism of GR231118 in β -arrestin2 recruitment assays (data provided by M Tempone). (B) Shows the effect of cyclic derivatives as antagonists on NPY stimulated β -arrestin2 recruitment at the Y_1R , and (C) shows the Cy5mono competition binding profiles at the Y_1R . (D) Shows the effect of cyclic derivatives on β -arrestin2 recruitment at the Y_4R , and (E) shows the Cy5mono competition binding profiles at the Y_4R . All images were acquired on the IX Ultra (Figure 4.6) and analysed using the MetaXpress granularity algorithm. Graphs were plotted from pooled data (n of 3 or more individual experiments) and represented as mean \pm SEM using the average granule intensity / cell in GraphPad Prism v7. Data was normalised to 1 μM NPY response in β -arrestin2 assays and Cy5mono specific binding was defined by 1 μM [Dap⁴]dimer (GR231118) at the Y_1R or normalised to 100 nM PP for the Y_4R .

Table 4.5 - Summary of pharmacological parameters for GR231118 cyclic dimer variants at the Y₁R. Values were determined in β -arrestin2 recruitment and competition binding assays (Figure 4.7B and C). For β -arrestin2 recruitment, NPY pEC₅₀ was measured in presence of 30 nM ligand; when there was no significant change in R_{max}, pK_b values were also estimated for guidance using the Gaddum equation ($K_b = [B] / (CR - 1)$), excluding GR231118 which was not determined (ND). For competition binding pK_i values were estimated using the Cheng-Prusoff correction, in the presence of 100 nM Cy5mono, where Cy5mono K_d was stated as 30 nM for Y₁R (Figure 4.2). All values are represented as mean \pm SEM. **p<0.01 following one-way ANOVA and Tukey's test compared to NPY control.

Y ₁ R			β -arrestin2 recruitment			Competition binding			
Peptide name	Analogue code	n	NPY pEC ₅₀	NPY R _{max} (% 1 μ M NPY)	pK _b	n	pIC ₅₀	% competition by 1 μ M ligand	pK _i
NPY	α	4	8.34 \pm 0.17	115.72 \pm 3.52	α	5	α	α	α
[Dap ⁴]dimer (GR231118)	2A	4	6.47 \pm 0.29	45.16 \pm 12.07**	ND	5	8.35 \pm 0.10	α	8.99 \pm 0.10
[Dab ⁴]dimer	2B	4	6.95 \pm 0.25	79.22 \pm 9.08	8.89 \pm 0.08	5	7.46 \pm 0.14	99.76 \pm 0.97	8.09 \pm 0.14
[Orn ⁴]dimer	2C	4	7.36 \pm 0.31	71.94 \pm 14.30	8.45 \pm 0.15	5	7.26 \pm 0.24	98.59 \pm 1.00	7.89 \pm 0.24
[Lys ⁴]dimer	2D	4	7.08 \pm 0.24	92.16 \pm 14.28	8.75 \pm 0.11	3	6.97 \pm 0.97	100.85 \pm 1.92	7.60 \pm 0.60

Table 4.6 - Summarised table of pharmacological parameters for GR231118 derived cyclic dimer variants at the Y₄R. Values were determined in β -arrestin2 recruitment and competition binding assays (Figure 4.7D and E). For competition binding pK_i values were estimated from curves where baseline was shared at -20 % (compared to 100 nM PP competition), using the Cheng-Prusoff correction, in the presence of 100 nM Cy5mono, where Cy5mono K_d was stated as 300 nM for Y₄R (Figure 4.3). All values are represented as mean \pm SEM. *p<0.05, **p<0.01 following one-way ANOVA and Tukey's test compared to PP control.

Y ₄ R			β -Arrestin2 recruitment		Competition binding			
Peptide name	Analogue code	n	Analogue pEC ₅₀	Analogue R _{max} (% 100 nM PP)	n	pIC ₅₀	% competition by 1 μ M ligand	pK _i
PP		4	7.90 \pm 0.21	103.99 \pm 5.67	4	8.06 \pm 0.13	α	8.19 \pm 0.13
[Dap ⁴]dimer (GR231118)	2A	3	7.95 \pm 0.25	21.82 \pm 16.63**	3	6.93 \pm 0.11	113.41 \pm 8.40	7.05 \pm 0.11
[Dab ⁴]dimer	2B	3	7.52 \pm 0.23	43.78 \pm 1.42*	3	6.69 \pm 0.10	94.29 \pm 0.36	6.81 \pm 0.10
[Orn ⁴]dimer	2C	3	8.37 \pm 0.43	33.04 \pm 11.57*	3	7.08 \pm 0.10	135.71 \pm 6.19	7.20 \pm 0.10
[Lys ⁴]dimer	2D	3	7.63 \pm 0.31	56.38 \pm 21.95	4	6.67 \pm 0.18	111.28 \pm 2.39	6.80 \pm 0.18

In comparison to [Dap⁴]dimer, the three other dimer derivatives were of similar overall potency (Figure 4.7D; Table 4.6). However the [Lys⁴]dimer was of higher partial agonist efficacy compared to [Dap⁴]dimer, with an R_{max} of 56 % of the 100 nM PP response (Figure 4.7D; Table 4.6). Competition binding studies at the Y₄R demonstrated all derivatives had modest affinity for the Y₄R (approximately 30 fold lower than PP), with an approximate order of affinity of [Lys⁴]dimer = [Dab⁴]dimer > [Orn⁴]dimer = [Dap⁴]dimer (Figure 4.7E; Table 4.6).

4.3.5 Pharmacological characterisation of GR231118 alanine substitution variants at Y₁R and Y₄R

The final series of GR231118 analogues were designed to explore the contribution of individual arms, and key residues within each arm of the peptide dimer, to the higher affinity and non-surmountable pharmacology observed when compared to the BVD15 monomeric peptides. Alanine substitutions were made at different positions within just one arm of the GR231118 dimer, and we also examined the effect of one double alanine mutant, [Ala^{6-8'}]dimer, with point [Ala⁶] and [Ala^{8'}] mutations in different arms (Table 4.7). Y₁R and Y₄R affinity and pharmacology were assessed in the same manner as the cyclic monomers and dimer derivatives (Section 4.3.3 and 4.3.4 above). Y₁ A2 β -arrestin2 recruitment assays used pre incubation with 3 nM or 30 nM dimer peptide, as indicated, for 30min at 37°C in HBSS/ 0.1 % BSA prior to NPY treatment and 60min incubation.

In Y₁R competition binding assays using Cy5mono, alanine substitutions at most positions within the GR231118 ligand had no detrimental effect on binding affinity (Figure 4.8B; Figure 4.10C; Table 4.8). However [Ala⁵]dimer, in which the most proximal tyrosine to the cyclic linker has been substituted in one dimer arm, exhibited ~10 fold loss in affinity at the Y₁R (Figure 4.10C; Table 4.8). [Ala^{6-8'}]dimer, with the alanine substitutions in different dimer arms, showed a dramatic loss of affinity, ~100 fold loss compared to GR231118 (Figure 4.10C; Table 4.8). The calculated pK_i for [Ala^{6-8'}]dimer (pK_i = 7.50 ± 0.06)

was equivalent to that of the NPY affinity measured in whole cell assays ($pK_i = 7.78 \pm 0.09$; Table 4.8).

As stated above, previous studies have demonstrated GR231118 acts as a non-surmountable antagonist at the Y_1R in the β -arrestin2 recruitment assay (Figure 4.8A; Figure 4.10B). The non-surmountable activity of the GR231118 was reinforced for alanine scan GR231118 derivatives, which at 30 nM induced a substantial reduction in the NPY R_{max} for all of the compounds (Figure 4.10A). The effects of these ligands were therefore also studied in the assay at a lower concentration (3 nM). This reinforced the effect of substituting tyrosine 5 in the second dimer arm (Figure 4.10B). In the presence of a low concentration of antagonist (3 nM), non-surmountable antagonism of the NPY response to GR231118 continued to be observed, with a rightward shift in the NPY pEC_{50} and a significant reduction in R_{max} ($p < 0.05$ following one-way ANOVA and Tukey's post-test; Figure 4.10B; Table 4.8). Similar antagonist effects in the assay were largely preserved in the presence of 3 nM alanine GR231118 analogues substituted at positions 6, 7, 8, and 9, with a trend to decline in the NPY maximum response. However, the NPY curve shift and reduction in NPY R_{max} by [Ala⁵]dimer (3 nM) was reduced (Table 4.8), and there was no change in antagonist effect with the combination [Ala^{6-8'}]dimer derivative at this same concentration (Figure 4.10B; Table 4.8).

In the Y_4R competition binding assays, all single site alanine substitutions had no detrimental effect on ligand affinity for the receptor compared to GR231118 (Figure 4.9B; Figure 4.10E; Table 4.9). However [Ala^{6-8'}]dimer displayed incomplete competition of the Cy5mono binding to the Y_4R in this assay, at a maximum concentration of 1 μM (Figure 4.10E; Table 4.9). Y_4R β -arrestin2 recruitment assays, assessing the analogues as partial agonists, also reinforced this data, as the single substituted analogues showed similar agonist potency and maximum response in comparison to the GR231118 control ($pEC_{50} = 7.38 \pm 0.13$; Figure 4.9A; Figure 4.10D; Table 4.9).

Table 4.7 – GR231118 derived dimer peptides with alanine scan substitutions. All dimer peptides contained an intermolecular cyclic moiety between [Glu²] and [Dap⁴] of the corresponding dimer peptide arm, and the alanine (Ala) substitution positions are highlighted in green, with ' indicating substitution on the second arm of the peptide.

Peptide name	Analogue code (Chapter 3)	Sequence	MW
[Ala ⁵]dimer	3A	(H ₂ NOC)-Tyr-Arg-Leu-Arg-Tyr-Dap-Pro-Glu-Ile Ile-Glu-Pro-Dap- Ala -Arg-Leu-Arg-Tyr-(CONH ₂)	2261
[Ala ⁶]dimer	3B	(H ₂ NOC)-Tyr-Arg-Leu-Arg-Tyr-Dap-Pro-Glu-Ile Ile-Glu-Pro-Lys-Tyr- Ala -Leu-Arg-Tyr-(CONH ₂)	2268
[Ala ⁷]dimer	3C	(H ₂ NOC)-Tyr-Arg-Leu-Arg-Tyr-Dap-Pro-Glu-Ile Ile-Glu-Pro-Dap-Tyr-Arg- Ala -Arg-Tyr-(CONH ₂)	2311
[Ala ⁸]dimer	3D	(H ₂ NOC)-Tyr-Arg-Leu-Arg-Tyr-Dap-Pro-Glu-Ile Ile-Glu-Pro-Dap-Tyr-Arg-Leu- Ala -Tyr-(CONH ₂)	2268
[Ala ⁹]dimer	3E	(H ₂ NOC)-Tyr-Arg-Leu-Arg-Tyr-Dap-Pro-Glu-Ile Ile-Glu-Pro-Dap-Tyr-Arg-Leu-Arg- Ala -(CONH ₂)	2261
[Ala ^{6,8'}]dimer	3F	(H ₂ NOC)-Tyr- Ala -Leu-Arg-Tyr-Dap-Pro-Glu-Ile Ile-Glu-Pro-Dap-Tyr- Ala -Leu-Arg-Tyr-(CONH ₂)	2183

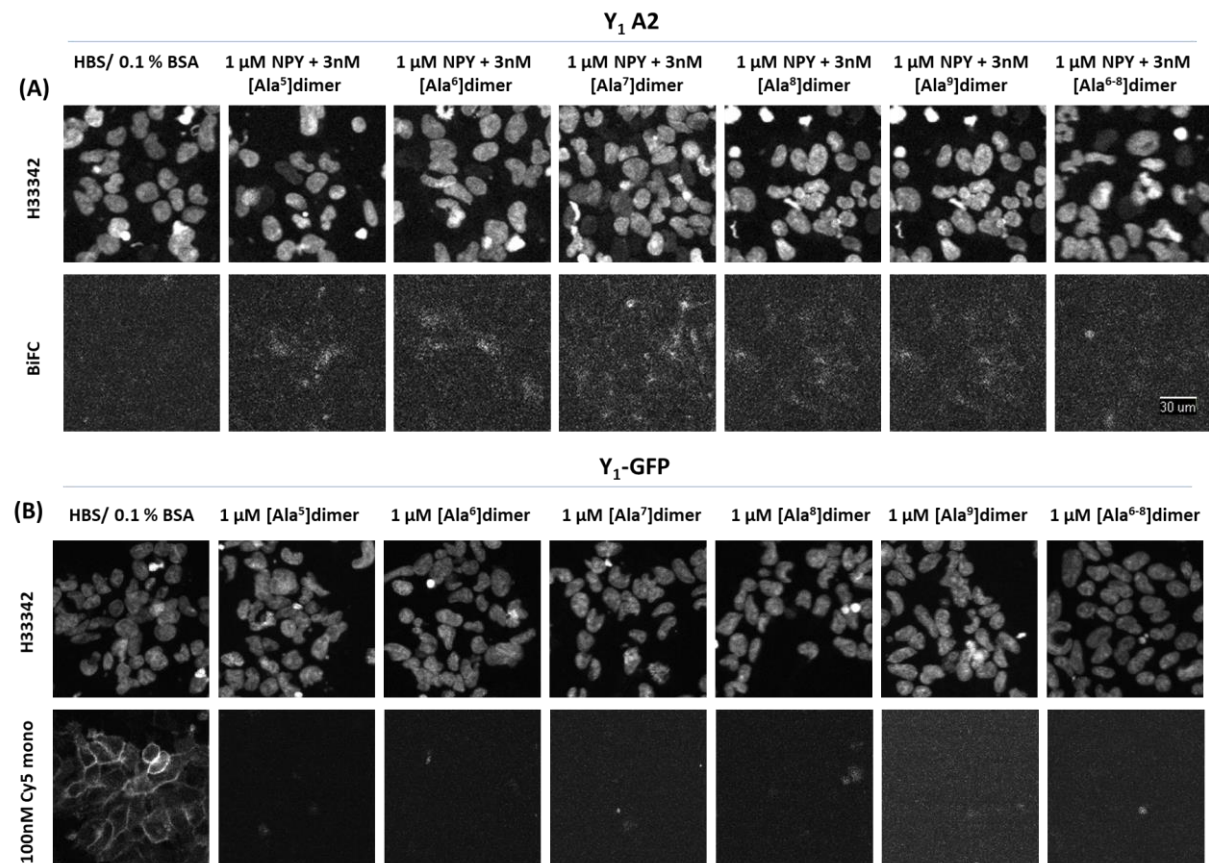


Figure 4.8 – IX Ultra acquired images of GR231118 alanine scan variants at the Y₁R. (A) Shows 1 μ M NPY induced β -arrestin recruitment complexes (BiFC) in Y₁ A2 cells in the presence of 3 nM GR231118 Ala scan derivatives. (B) Shows the extent of displacement of 100 nM Cy5mono following 1 μ M treatment of GR231118 alanine scan derivatives in Y₁-GFP cells. All images were acquired on the IX Ultra plate reader as previously described (Chapter 2, Section 2.4.1.2, 2.4.1.5 and 2.6.1.1) to produce the graphs shown in Figure 4.10.

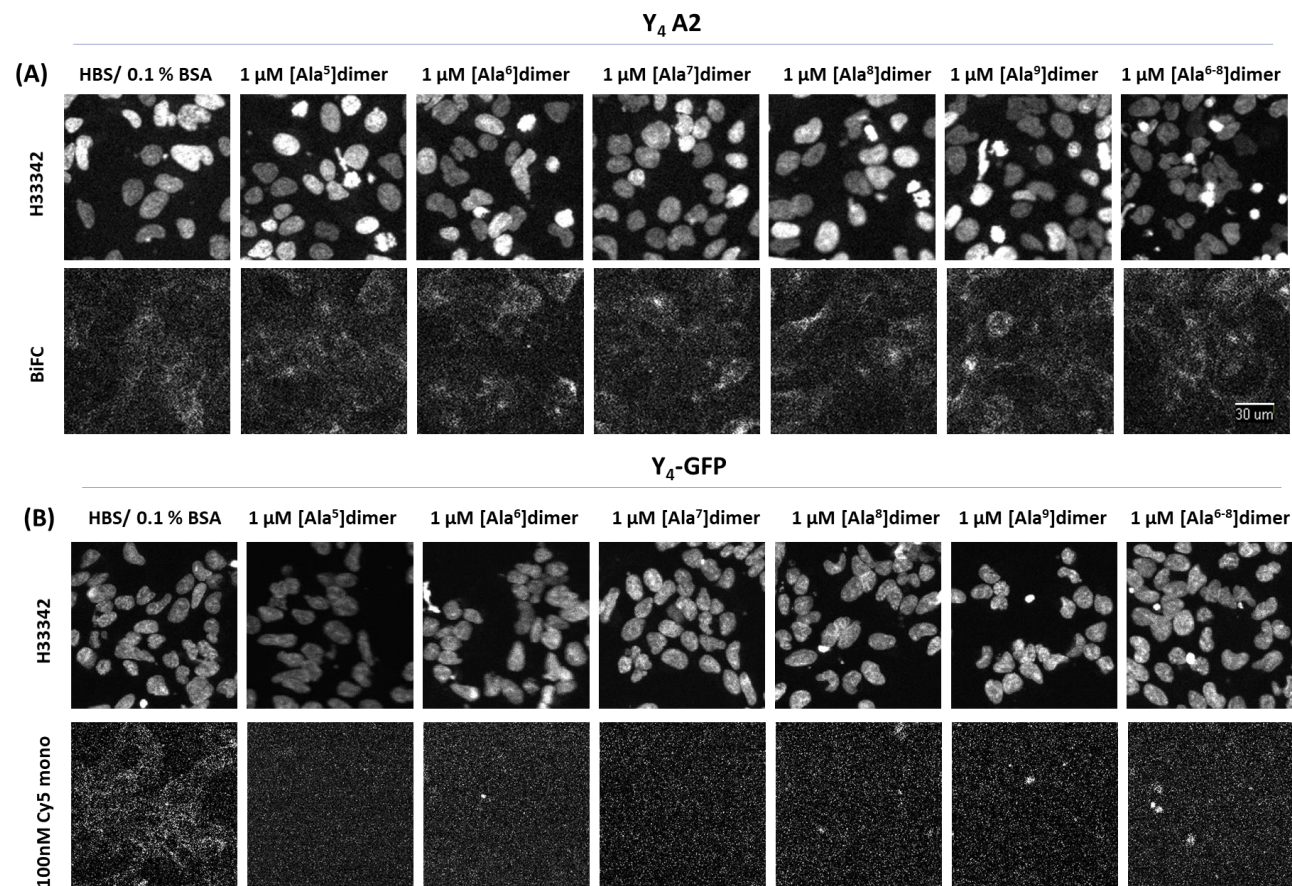


Figure 4.9 – IX Ultra acquired images of GR231118 alanine scan variants at the Y₄R. (A) Shows β -arrestin recruitment complexes (BiFC) in Y₄ A2 cells in the presence of 1 μ M GR231118 alanine scan derivatives. (B) Shows the extent of displacement of 100 nM Cy5mono following 1 μ M treatment of ligand in Y₄-GFP cells. All images were acquired on the IX Ultra plate reader as previously described (Chapter 2, Section 2.4.1.2, 2.4.1.5 and 2.6.1.1) to produce the graphs shown in Figure 4.10.

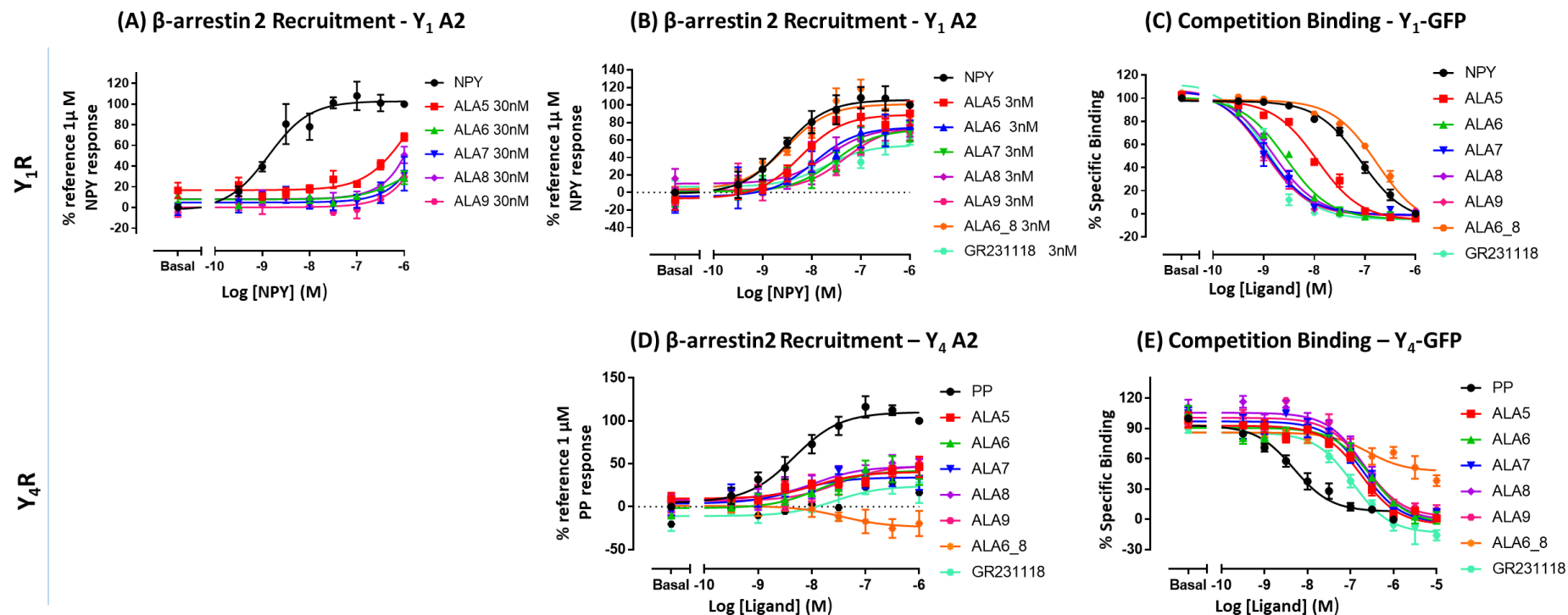


Figure 4.10 - Pharmacological characterisation of GR231118 alanine scan variants at the Y_1 R and Y_4 R. (A) and (B) show the effect of alanine scan derivatives as antagonists on NPY stimulated β -arrestin2 recruitment at the Y_1 R at 30 nM and 3 nM, respectively. (C) Shows the competition binding profiles at the Y_1 R of all derivatives at varying concentrations indicated in the presence of 100 nM Cy5mono. (D) Shows the effect of GR231118 alanine scan derivatives as agonists on β -arrestin2 recruitment at the Y_4 R. (E) Shows the 100 nM Cy5mono competition binding profiles at the Y_4 R in the presence of varying concentration of GR231118 alanine scan derivative as indicated. All images were acquired on the IX Ultra (Figure 4.8 and 4.9) and analysed using the MetaXpress granularity algorithm. Graphs were plotted from pooled data (n of 3 or more individual experiments) and are represented a mean \pm SEM using the average granule intensity / cell in GraphPad Prism v7. Data was normalised to 1 μ M NPY or 1 μ M PP response at the Y_1 R and Y_4 R, respectively.

Table 4.8 - Summarised table of pharmacological parameters for GR231118 alanine scan peptides at the Y₁R. Values were determined in β -arrestin2 recruitment and competition binding assays (Figure 4.10B and C). For β -arrestin2 recruitment, NPY pEC₅₀ was measured in presence of 3 nM ligand. For competition binding pK_i values were estimated using the Cheng-Prusoff correction, in the presence of 100 nM Cy5mono, where Cy5mono K_d was stated as 30 nM for Y₁R (Figure 4.2). All values are represented as mean \pm SEM. *p<0.05 following one-way ANOVA and Tukey's test compared to NPY control.

Y ₁ R		β -arrestin2 recruitment			Competition binding			
Peptide name	Analogue code	n	NPY pEC ₅₀	NPY R _{max} (% 1 μ M NPY)	n	pIC ₅₀	% competition by 1 μ M ligand	pK _i
NPY	α	4	8.43 \pm 0.28	105.48 \pm 8.61	7	7.14 \pm 0.09	α	7.78 \pm 0.09
GR231118	3A	3	7.82 \pm 0.12	62.88 \pm 7.33*	4	8.89 \pm 0.04	98.74 \pm 0.72	9.53 \pm 0.04
[Ala ⁵] dimer	3B	4	8.24 \pm 0.17	90.56 \pm 10.00	4	8.00 \pm 0.07	96.07 \pm 1.80	8.63 \pm 0.07
[Ala ⁶] dimer	3C	4	7.85 \pm 0.30	77.26 \pm 9.89	4	8.60 \pm 0.03	96.03 \pm 1.54	9.24 \pm 0.03
[Ala ⁷] dimer	3D	4	7.46 \pm 0.16	71.93 \pm 9.90	4	8.92 \pm 0.10	99.53 \pm 0.47	9.56 \pm 0.10
[Ala ⁸] dimer	3E	4	7.61 \pm 0.38	77.03 \pm 8.25	4	8.80 \pm 0.03	98.58 \pm 1.14	9.44 \pm 0.03
[Ala ⁹] dimer	3F	4	7.36 \pm 0.18	73.05 \pm 8.28	4	8.95 \pm 0.05	97.55 \pm 2.22	9.59 \pm 0.05
[Ala ⁶⁻⁸] dimer	3G	3	8.61 \pm 0.08	102.02 \pm 10.85	4	6.86 \pm 0.06	97.64 \pm 0.40	7.50 \pm 0.06

Table 4.9 - Summarised table of pharmacological parameters for GR231118 alanine scan peptides at the Y₄R. Values were determined in β -arrestin2 recruitment and competition binding assays (Figure 4.10D and E). For competition binding pK_i values were estimated using the Cheng-Prusoff correction, in the presence of 100 nM Cy5mono, where Cy5mono K_d was stated as 300 nM for Y₄R (Figure 4.3). All values are represented as mean \pm SEM. **p<0.01 ***p<0.001 following one-way ANOVA and Tukeys test compared to GR231118 control.

Y ₄ R		β -arrestin2 recruitment			Competition binding			
Peptide name	Analogue code	n	pEC ₅₀	R _{max}	n	pIC ₅₀	% competition by 1 μ M ligand	pK _i
NPY	α	6	8.47 \pm 0.27	112.10 \pm 5.40***	10	8.29 \pm 0.18	α	8.41 \pm 0.18
GR231118	3A	4	7.43 \pm 0.24	36.12 \pm 5.64	5	7.25 \pm 0.13	108.36 \pm 4.58	7.38 \pm 0.13
[Ala ⁵]dimer	3B	4	7.43 \pm 0.81	52.33 \pm 12.91	4	6.84 \pm 0.08	95.50 \pm 1.46	6.20 \pm 0.08
[Ala ⁶]dimer	3C	3	8.12 \pm 0.61	49.07 \pm 12.99	4	6.49 \pm 0.18	92.16 \pm 4.49	6.61 \pm 0.18
[Ala ⁷]dimer	3D	3	7.89 \pm 0.20	48.15 \pm 6.91	5	6.76 \pm 0.14	94.67 \pm 0.86	6.89 \pm 0.14
[Ala ⁸]dimer	3E	5	8.29 \pm 0.72	50.21 \pm 7.99	5	6.64 \pm 0.12	94.85 \pm 2.45	6.77 \pm 0.12
[Ala ⁹]dimer	3F	4	8.17 \pm 0.81	55.23 \pm 6.81	5	6.60 \pm 0.09	91.17 \pm 2.67	6.76 \pm 0.11
[Ala ⁶⁻⁸]dimer	3G	3	α	-9.51 \pm 17.98*	4	5.92 \pm 0.46	55.52 \pm 6.92	6.04 \pm 0.46

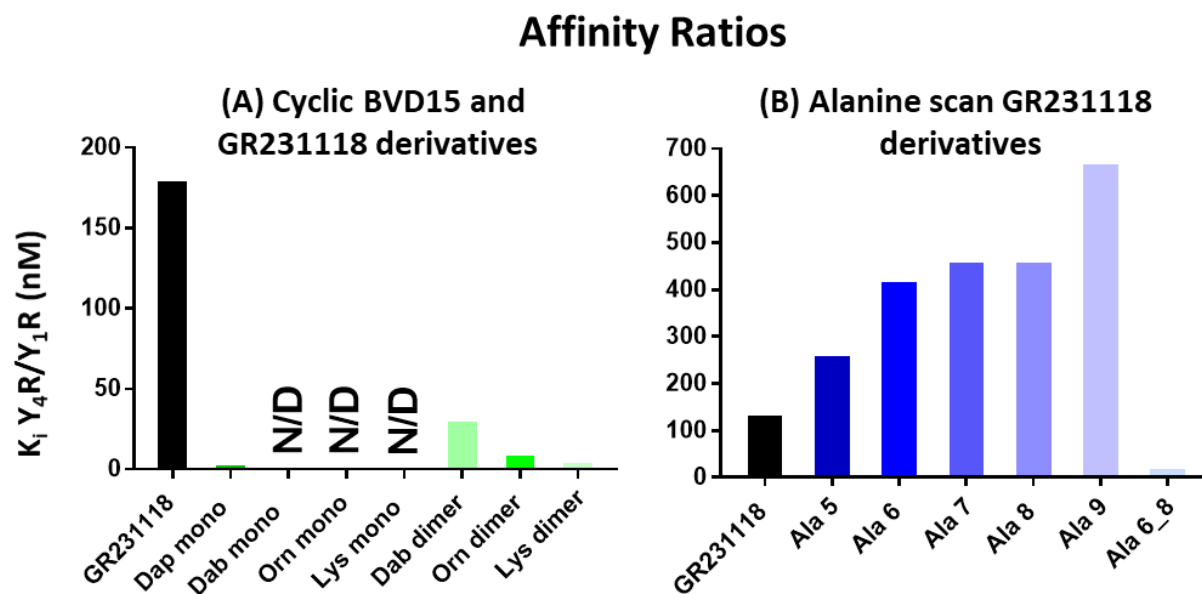


Figure 4.11 - Y_4R/Y_1R selectivity ratios for BVD15 monomer and GR231118 dimer derivatives. Values are expressed as a ratio of Y_4R/Y_1R K_i (nM) from previously calculated pK_i values (Table 4.2, 4.3, 4.5, 4.6, 4.8 and 4.9). (A) Shows the relative selectivity of the BVD15 cyclic monomer and GR231118 cyclic dimer derivatives and (B) shows the relative selectivity of alanine substitution GR231118 dimer analogues, where GR231118 ([Dap⁴] dimer) is used for comparison.

However, the [Ala^{6-8'}]dimer derivative displayed no agonist activity at the Y₄R in this assay at up to 1 µM (Figure 4.9A; Figure 4.10D; Table 4.9).

Figure 4.11 summarises the effects of varying the cyclic linker and alanine substitution on the selectivity of the analogues for Y₄R over Y₁R, measured as a ratio of the calculated K_i values. The affinity ratios for competition binding suggest increased selectivity for alanine substituted dimers at the Y₁R compared to Y₄R. In contrast, cycle variant GR231118 analogues all displayed reduced selectivity between the two receptor subtypes.

4.4 Discussion

4.4.1 Summary of key findings

GR231118 is an example of a dimeric, bivalent GPCR ligand which generates much higher affinity for the Y₁R than its constituent monomers, BVD15 and BVD15 derived analogues. The main aim of this study was first to explore the contributions made by individual dimer arms and the cyclic structure, within the GR231118 derivative, to the high Y₁R binding affinity. Using a series of novel cyclic peptide analogues, we have been able to demonstrate that larger cycles within the GR231118 dimer resulted in lower affinity at the Y₁R and the introduction of cycles in a similar position within the monomer did not increase the affinity of BVD15 analogues. This indicates that the presence of the cycle contributes to the high Y₁R affinity of GR231118, with the [Dap⁴]dimer analogue ring size being optimal. Using a series of novel single alanine substituted peptides we have determined a key role for [Tyr⁵] in the second GR231118 arm in extending the dimer contact surface with the receptor and increasing affinity. In addition, we considered the impact of these analogue substitutions on the related Y₄R activity, demonstrating that alterations in ring structure were better tolerated at the Y₄R binding site, preserving Y₄R agonism, and led to analogues that were less selective at the Y₁R compared to the Y₄R. Equally, [Tyr⁵] in the second dimer arm was not a contributor to the observed Y₄R affinity of these analogues, and substitution of the other residues with

alanine had no effect. However, at least one intact arm was required in order to retain binding at the Y₄R, as shown with [Ala⁶⁻⁸].

4.4.2 Cy5mono acts as a high affinity Y₁R antagonist and a moderate affinity Y₄R agonist.

The data presented in Section 4.3.1 (Figure 4.1 - Figure 4.3) demonstrate our previously published characterisation of the Cy5mono fluorescent ligand (Liu et al., 2016), which was used as the basis for the competition binding assays in this work. Following confirmation of its properties as a Y₁R high affinity antagonist and Y₄R moderate affinity agonist, the Cy5mono compound was selected for use in the development of a whole cell, plate reader based, imaging assay. Cy5mono was employed successfully in Y₁R and Y₄R receptor binding studies, displaying low non-specific binding, albeit with an 8 fold lower level of affinity at the Y₄R and the capacity to stimulate Y₄R internalisation as an agonist at this receptor.

The development of this fluorescent ligand for use in receptor binding studies offers advantages over traditional radioligand binding assays. The main advantage of whole cell binding assays is that they are performed in the presence of physiological buffer (HBSS/ 0.1 % BSA) used in functional experiments, as opposed to the membrane buffer conditions used in routine YR membrane binding assays. Membrane buffers often have low sodium and an absence of guanine nucleotides, designed to promote the high affinity ternary receptor complex also containing the effector (e.g. G protein, AR*G) to maximise radiolabelled agonist peptide binding, for example [¹²⁵I]-NPY and [¹²⁵I]-PYY (Stott et al., 2016). This can lead to discrepancies in affinity measurements made using different binding and functional assays. For example, Cy5mono pK_i using [¹²⁵I]-PYY radioligand binding in Y₁-GFP membranes appeared almost 100 fold higher than in either whole cell saturation binding in the same cells, or functional affinity determination from antagonist shifts reproduced in Figure 4.2 (Liu et al., 2016). In addition to the influence of assay buffer and receptor state, it is possible that BVD15 based

peptides may also have direct disruptive effects on the receptor-G protein interaction when intracellular access is possible in isolated membranes, thereby leading to more potent inhibition of radiolabelled agonist binding (as reported for NPY C-terminal fragments; Mousli et al., 1995). Radiolabelled agonists such as [125 I]-PYY etc. need the high affinity R* state promoted by isolated membranes and membrane assay buffer, therefore radiolabelled derivative binding can be difficult to detect in whole cells. Thus, the use of fluorescent derivatives, particularly antagonists, allows measurement of ligand binding in whole cells to produce more physiologically relevant affinity estimates. For Cy5mono these closely match the functional pEC₅₀ values (Y₄R; with limited receptor reserve) and the pK_b estimates (Y₁R; Kilpatrick et al., 2010; Liu et al., 2016) determined through β -arrestin2 recruitment.

4.4.3 The role of cyclic moieties in monomeric peptide ligand binding at the Y₁R and Y₄R

The cyclic BVD15 monomers showed consistently lower affinity values at the Y₁R (~10-15 fold less) in whole cell binding, compared to our report of [Lys⁴]-BVD15 (pK_i = 8.6) or of BVD15 itself (pK_i = 8.3) using [125 I]-PYY competition binding in Y₁R expressing membranes (Liu et al., 2016; Parker et al., 1998). This apparent reduction in affinity may be overestimated by comparing non-equivalent membrane versus whole cell conditions (Section 4.4.2). Quantifying the functional effects of [Lys⁴]-BVD15 or BVD15 as antagonists leads to lower affinity estimates in both previous studies (pK_b=7.5 for [Lys⁴]-BVD15 in β -arrestin2 recruitment assay; Liu et al., 2016; and pK_b = 7.1 for BVD15 in cAMP assay; Parker et al., 1998). Broadly, the estimates of cyclic BVD15 monomer binding affinity aligned with their moderate potency as Y₁R antagonists in the β -arrestin2 recruitment assay. Clearly, however, these data indicate that introduction of a cyclic moiety at a similar position in the BVD15 monomer to its bivalent derivatives does not lead to the 10 - 100 fold gain in Y₁R binding affinity observed for GR231118. This suggests that a 2 - 4 position cyclic ring is not, in itself, a key determinant promoting Y₁R binding. Other bulky substitutions at a similar position in BVD15 such as the [Lys⁴(DOTA)]

derivative of BVD15 (Guérin et al., 2010b; Zhang et al., 2016) or indeed fluorescent BVD15 derivatives modified at the 2 and 4 positions (Liu et al., 2016; Mountford et al., 2014), have been shown to be tolerated with modest (up to 5 fold) increases in affinity at the Y₁R when compared to BVD15.

At the Y₄R, the cyclic monomer compounds acted as agonists but exhibited very low potency and affinity. Therefore, it is difficult to quantify the impact of the cycle insertion on monomer selectivity for the Y₁R versus the Y₄R. In some respects our data are similar to those of Guérin et al., (2010) and Zhang et al., (2016) for [Lys⁴] substituted BVD15 derivatives, who claimed increased Y₁R:Y₄R selectivity, based on the failure of these compounds to displace radiolabelled PP binding at the Y₄R. As the competing concentration of ligand used was not stated in these studies, it is not easy to distinguish the impact of [Lys⁴] modification on Y₁R:Y₄R selectivity, compared to an overall change in affinity for both receptors.

4.4.4 Increasing cycle size in GR231118 dimeric peptides selectively reduced Y₁R binding affinity.

The novel GR231118 dimer cyclic derivatives represented a systematic increase in the cyclic ring size at the heart of the dimer from [Dap⁴] (GR231118) to [Dab⁴] to [Orn⁴] to [Lys⁴]. At the Y₁R these changes were accompanied by a progressive loss of binding affinity (up to 30 fold). There was an equivalent reduction in the ability of these ligands (at 30 nM) to act as antagonists of NPY induced Y₁R β-arrestin2 recruitment, with a transition from non-surmountable to a more surmountable profile. This change in the nature of antagonism would be expected if, as assumed, the non-surmountable characteristics of GR231118 in this assay derive from its high affinity and slowly reversible nature at the Y₁R.

In the original study reporting GR231118 (Daniels et al., 1995), a dimer derivative linked only by short Cys-Cys disulphide bonds at the 2 and 4 positions (383U91) displayed a modest 3 fold higher Y₁R affinity than BVD15,

compared to > 100 fold for GR231118 in this study. A second diaminopropionic acid (Dap) dimer linked only at position 4 (1120W91), without the cyclic constraint, had an intermediate effect on Y₁R affinity, increasing ~20 fold compared to BVD15. Together with the SAR of the novel cyclic analogues described here, it appears that the [Dap⁴] cycle in GR231118 represents the optimum cycle size for Y₁R activity. It is possible that larger cycles sterically hinder analogue interaction to the Y₁R binding site. Additionally, the presence of [Pro³], which is a conformational constrained amino acid, may express conformational constraints on the ring, with the smaller ring size being relatively rigid in comparison to the larger ring size analogues and may provide an important feature for binding. Equally the [Dap⁴] cycle, replicated in the Dap linked dimers, but not in dimers with larger or smaller linkers e.g. Cys-Cys bridges, may allow better positioning of residues within the second arm of the GR231118 dimer for additional Y₁R contacts, thereby contributing to Y₁R high affinity (Section 4.4.5 below).

Conversely, the cyclic variants had no significant impact on the affinity of GR231118 for the Y₄R, or its action as a partial agonist compared to PP in β -arrestin2 recruitment assays. Indeed dimer derivatives with larger cycles, e.g. [Lys⁴]dimer, demonstrated a potential for a somewhat higher maximum response than GR231118 itself, while still below that of PP. Although some previous investigations have highlighted full agonist effects of GR231118 compared to PP, for example in the inhibition of cAMP accumulation (Parker et al., 1998), the efficacy of such ligands can be overestimated due to the signal amplification inherent in such assays (Stott et al., 2016). With more limited receptor reserve, β -arrestin2 recruitment can provide a better guide to intrinsic ligand efficacy as changes in R_{max} . Nevertheless, given the possibility of ligand bias between signalling pathways (Stott et al., 2016), it would be useful in future to confirm agonist properties of the Y₄R in G_i protein coupling assay. Overall the synthesised cyclic variants represent a class of compounds with reduced selectivity between the Y₁R and Y₄R, while retaining antagonist and agonist properties at each subtype. As Y₄R agonists, including PP and

BVD74-D, have been shown to have a regulatory effect on food intake in mice (Li et al., 2010), and Y₁R antagonists, such as GR231118 and BIBO3304, have been shown to inhibit food intake in animal models (Veyrat-Durebex et al., 2013; Yulyaningsih et al., 2011; Zheng et al., 2010), these less selective cyclic GR231118 derivatives may represent potential for the development of dual pharmacology ligands that could be desirable as starting points in anti-obesity agents.

4.4.5 The selective role of the second [Tyr⁵] in the GR231118 dimer peptide for Y₁R recognition

The alanine scan derivatives of GR231118 were designed to explore the contribution of the second arm of the dimer to Y₁R binding affinity. Both monomer and dimer peptides are assumed to engage a similar core binding site to the NPY C-terminus on the Y₁R (Beck-Sickinger et al., 1994; Fuhlendorff et al., 1990; Gehlert et al., 1997; Kaiser et al., 2015; Leban et al., 1995; Merten et al., 2007; Pedragosa-Badia et al., 2014) and in particular, require key contacts for this affinity including; [Arg⁶], [Arg⁸], and the [Tyr⁹] amide. In the full length NPY peptide, single alanine substitution of the equivalent residues ([Arg³³], [Arg³⁵] or [Tyr³⁶]) is sufficient for a dramatic loss in Y₁R binding affinity (Beck-Sickinger and Jung, 1995). However using the chemical synthesis route outlined in Chapter 3, heterodimer GR231118 analogues were able to be constructed in which alanine substitutions could be placed within defined arms of the dimer. This enabled one peptide arm to be preserved intact for engagement with the core Y₁R binding site, while investigating the effects on the second arm interactions and contribution to Y₁R binding affinity. Confirmation of the overall effects of [Arg⁶] and [Arg⁸] substitution in the dimeric ligands was achieved by their alanine substitution in separate arms of the [Ala⁶⁻⁸]dimer analogue. This analogue displayed substantial loss of both Y₁R affinity (100 fold) and antagonist action, as predicted from the inability of either arm to engage with the core Y₁R binding site.

Generally, the single alanine scan derivatives, at positions 6 to 9, showed only a modest reduction in Y₁R binding affinity, no more than would be predicted from the loss of bivalency and halving the effective concentration of the ligand required to engage the core Y₁R binding site. The exception was [Tyr⁵] substitution in one arm of GR231118, which resulted in ~10 fold loss of binding affinity, suggesting that this residue in the second arm of a bound dimer plays a key role in Y₁R recognition. Our data therefore provides evidence to suggest that the high affinity of the GR231118 dimer, in part, results from an extended Y₁R binding interface. In addition to the core C-terminus binding site, common to monomers and NPY itself, GR231118 may make use of the [Tyr⁵] amino acid side chain in the second arm to make additional contacts with the Y₁R. Molecular modelling studies are underway to identify possible contact residues, for example in the extracellular loops that might contribute to this interaction. One speculative possibility was first highlighted by Leban et al., (1995). In their original derivation of the BVD15 monomer peptide, the substitution of [Thr⁵], the native residue in NPY, for [Tyr⁵] was performed to increase affinity on the basis that this might replicate the necessary contribution of NPY [Tyr¹] to its high Y₁R binding affinity. Potentially the positioning of the second [Tyr⁵] in GR231118, combined with the optimal constraints of the Dap cycle, provides an optimal structure to replicate the NPY [Tyr¹] interaction in addition to its C-terminus contacts. The implication is that high affinity analogues equivalent to GR231118 could be obtained without including a full dimer structure, preserving [Tyr⁵], but not the remaining amino acids 6 - 9, in the second arm. This possibility could be tested in future.

Previous studies have suggested that the Y₄R shares many of the same key residue interactions with ligands in its core binding site as the Y₁R. For example, modelling studies by Jois et al., (2006) proposed that [Arg⁶], [Arg⁸] and [Tyr⁵] were involved in hydrogen bonding interactions between BVD15 at both the Y₁R and the Y₄R. However, these simulations were conducted in homology models and were not experimentally tested, e.g. by alanine scan peptides. Additionally, studies have confirmed direct ionic interactions of [Arg³⁵] in NPY

and PP at [Asp^{6,59}] in the Y₁R and Y₄R, respectively (Merten et al., 2007). The loss of Y₄R agonism in [Ala^{6-8'}]dimer, and lack of its full competition for binding at high concentrations, is consistent with these proposed interactions. However, in contrast to its effect in reducing Y₁R affinity, single alanine substitution of [Tyr⁵] in the second arm of the peptide had no significant effect on Y₄R affinity or agonist properties, in common with the single alanine substitutions at other positions. This implies that the additional Y₁R interactions proposed for this second arm [Tyr⁵] are not replicated in the Y₄R GR231118 binding site. Given the hypothesis that this residue might mimic NPY [Tyr¹] in Y₁R binding, it is worth noting that this Tyr residue is not preserved in the hPP sequence, but is an alanine in hPP, and is therefore unlikely to be recognised by the Y₄R. Future modelling studies should enable greater molecular understanding of the differences in Y₁R and Y₄R interaction implied by the [Ala⁵] and cyclic variant GR231118 analogues.

4.5 Final conclusions

In this chapter we have characterised a series of cyclic BVD15 monomeric and cyclic GR231118 dimeric derived peptides at the Y₁R and the Y₄R in order to investigate the role of the cyclic structure in receptor recognition and selectivity. Our studies have shown that the cyclic moiety within the dimer compounds plays a role in Y₁R recognition, with the original [Dap⁴] based cycles in GR231118 being optimal. Larger cycles may have a more limited impact in enhancing agonist activity at the Y₄R. In addition to the role of the cyclic moiety, we have successfully investigated the role of the single dimer arm residues in Y₁R and Y₄R activity, through the generation and characterisation of GR231118 dimer alanine substitution derivatives. These compounds revealed a new role for [Tyr⁵] in the second arm of GR231118 in contributing to high Y₁R, but not Y₄R affinity. This suggests that [Tyr⁵] interacts with the receptor at a different site from its position on the first arm, mimicking the NPY C-terminus binding mode, potentially replicating the role of NPY [Tyr¹]. Overall, this identifies a structural basis for explaining, in part, the higher affinity of dimeric versus monomeric peptide derivatives for the Y₁R.

With the advent of the first YR crystal structure (Yang et al., 2018), molecular modelling studies should be undertaken to support the hypotheses implied by our SAR studies, and to identify new YR contact residues which could then be explored by receptor mutagenesis. Alanine scanning studies of the BVD15 monomer would also confirm the roles of [Arg⁶], [Arg⁸], and [Tyr⁹] residues in Y₁R and Y₄R binding implied by studies on full length NPY.

The data in this chapter provides evidence for an extended GR231118 binding site which contributes to its high affinity, implying distinct interactions for the two arms of the dimer in Y₁R binding that are not replicated by monomer peptides. As outlined in the aims to Chapter 3, other mechanisms have been proposed to explain the properties of dimeric GPCR ligands, in which oligomeric receptor complexes may influence bivalent ligand interaction or binding kinetics. Chapter 5 explores this possibility for the GR231118 related compounds, using fluorescent monomeric and dimeric derivatives to investigate ligand - YR stoichiometry by fluorescence correlation spectroscopy (FCS) and related approaches.

Chapter 5

The use of fluorescence correlation spectroscopy to investigate ligand-receptor interactions at the neuropeptide Y Y_1 receptor.

"It's the variation of biology that's the issue..."

Stephen Briddon

5.1 Introduction

5.1.1 Fluorescent ligands as tools to investigate ligand-receptor interactions

Since the discovery, isolation and purification of naturally occurring fluorescent proteins, such as green fluorescent protein (GFP) in the 1960-1970s, fluorescence microscopy has become an invaluable tool in the biological sciences. Due to improvements in detectors, dyes and methods of image acquisition and analysis, along with advantages over biochemical and radioactive techniques, the use of fluorescence based techniques have been at the forefront of GPCR research.

Historically, techniques such as co-immunoprecipitation, western blotting and radiolabelling have been used to investigate GPCRs. However, unlike the biochemical methods, fluorescence has the advantage that it can be used in live cells, and poses a much lower safety risk in comparison to radiolabelling, providing a non-invasive way of tracking and tracing biological molecules. Fluorescence can be used in a range of techniques, from whole cell fluorescence resonance energy transfer (FRET) or bimolecular fluorescence complementation (BiFC); which can be employed to investigate protein interactions across a cell population (Ni et al., 2017); to single molecule techniques such as fluorescence correlation spectroscopy (FCS), which has single molecule sensitivity, or total internal reflection fluorescence (TIRF), which traces the movement of fluorescent particles in a small area of cell membranes (Shashkova and Leake, 2017).

The application of fluorescence, in most techniques, requires simple genetic modification of GPCRs or other proteins of interest, to produce proteins that express the desired constructs and allow for the implementation of your chosen technique i.e. the addition of GFP / YFP or BiFC fragments. Thereby allowing for the tracking and visualisation of the proteins on the plasma membrane or within cellular compartments, with minimal disruption to protein folding and function.

In addition to genetic modification of the receptor, the use of fluorescently tagged ligands may also be employed, allowing for further study of ligand-receptor interactions, including receptor oligomeric stoichiometry and structure-activity relationships (SARs). The use of fluorescent ligands have previously been demonstrated in a number of GPCR families, across a range of ligand types and fluorescent moieties. Examples include; the development of a fluorescent peptide for Vasopressin V_{1B} receptor which incorporated an Alexa 647 fluorophore (Corbani et al., 2018); a fluorescent small molecule expressing a KK114 fluorophore, targeted to the β -adrenergic receptors (β -AR; Mitronova et al., 2017); a fluorescent peptide expressing a tetramethyl-rhodamine (TMR) fluorophore, targeted to the VEGFR₂ (Kilpatrick et al., 2017) and fluorescent small molecules expressing BODIPY fluorophores, targeted to the adenosine A₃ receptor (Stoddart et al., 2015). The implementation and use of these fluorescent ligands range from establishing the distribution and function of receptor in native tissue, to providing tools for receptor pharmacology determination, across many different techniques including; time resolved fluorescence resonance energy transfer (TR-FRET), stimulated emission depletion microscopy (STED) and FCS, demonstrating the versatility of fluorescent ligands in GPCR research.

5.1.2 Evidence of YR family oligomerisation

As discussed in Chapter 1 (Section 1.2.7), oligomerisation of GPCRs may influence receptor localisation and trafficking, receptor signalling, and ligand pharmacology through allosteric interactions between binding sites. While still controversial, there have been many indications within the literature suggesting that GPCRs can form homodimers, heterodimers and oligomers in living cells (Dijkman et al., 2018; Ferré et al., 2014; Gomes et al., 2016; Smith and Milligan, 2010). Evidence of dimerisation has been demonstrated in several receptor systems, for example; opioid receptors (Ferré et al., 2014; Rogacki et al., 2018; Yang et al., 2018), dopamine D₂ receptors (Guo et al., 2008), β_1 -AR and β_2 -AR (Dorsch et al., 2009), adenosine A₁ and A₃ receptors

(May et al., 2011) and chemokine CXCR₃ and CXCR₄ receptors (Watts et al., 2013).

There has been evidence for the formation of dimeric structures in the YR family in multiple combinations including; Y₁R/Y₁R (Dinger et al., 2003), Y₅R/Y₅R (Dinger et al., 2003), Y₁R/Y₅R (Gehlert et al., 2007; Kilpatrick et al., 2015), Y₄R/Y₄R (Estes et al., 2008); and Y₂/Y₂ (Dinger et al., 2003; Estes et al., 2008). Evidence of Y₁R, Y₂R and Y₅R homodimerisation has been obtained via FRET studies (Dinger et al., 2003), where receptor-GFP fusion proteins were created along with complementary receptor constructs tagged with cyan fluorescent protein (CFP) to be used as a FRET pair. FRET was then seen in both fluorescence microscopy and fluorescence spectroscopy approaches. Y₂R and Y₄R homodimers have also been demonstrated in rabbit kidney through GTP-γS binding stoichiometry (Estes et al., 2008). Y₁R/Y₅R heterodimerisation has been indicated through co-expression and localisation of the receptors in many brain regions and through the application of co-immunoprecipitation techniques (Gehlert et al., 2007). In addition, antagonist pharmacology has been suggested to be altered in cells co-expressing Y₁R and Y₅R using FRET (Dinger et al., 2003) and BiFC approaches (Kilpatrick et al., 2015). Kilpatrick et al., (2015) showed that BiFC complexes of Y₁R/Y₅R altered the mode of CGP71683 antagonism from surmountable to non-surmountable, suggesting an influence of dimerisation on ligand pharmacology in Y₁R/Y₅R heterodimers through cooperative binding. It has also been demonstrated that these Y₁R/Y₅R heterodimers may play a role in appetite regulation and the development of obesity through the use of Y₁R/Y₅R receptor knock out mice models (Nguyen et al., 2012). This study showed that Y₁R/Y₅R knock out mice expressed a much larger decrease in appetite stimulated eating when compare to single Y₁R and Y₅R knockouts and wild type controls.

5.1.3 Ligand - receptor interactions at receptor complexes

There is evidence that ligands may influence the dimerisation of receptors in the GPCR family. Several studies have discussed to what extent the absence

and presence of a ligand can influence the dynamics of dimerisation in GPCRs. This has been explored previously for D_{2L} receptors through TIRF microscopy, in which the formation of dimer complexes was increased through receptor-ligand interaction. However this study found that only agonists had this affect and that antagonist treatment showed no change in receptor complex formation (Tabor et al., 2016). Another study suggested that the muscarinic receptor family may express ligand selective dimerisation, whereby treatment with clozapine resulted in homo- and hetero- dimerisation of the M₂ and M₃ receptors. However, it was observed that treatment with agonists of the M₂ resulted in a decrease of M₂-M₃ interaction, and conversely M₃ agonists did not affect homo- or hetero- dimerisation of these receptors (Aslanoglou et al., 2015). The concept of ligand-induced dimerisation has also been described and well documented in other receptor families. Particularly in the tyrosine kinase family of receptors where receptor dimerization is required for activation and is often induced by endogenous ligand binding, which is the case for VEGFR and EGFR (Kozer et al., 2013; Simons et al., 2016).

As well as having a potential influence on dimerisation, ligands may also interact differently with monomeric receptors compared to dimeric receptor complexes. Examples of this can be found in the numerous dimeric bivalent ligands that have been described, such as those targeted towards the dopamine D_{2R}-NT_{1R} heterodimers (Hubner et al., 2016), where the bivalent ligand showed an increased affinity and selectivity for the dimer in co-expressing cells compared to cells that only expressed D_{2R}. This increased affinity was also observed in CXCR₄ bivalent ligands when compared to monovalent ligands (Nomura et al., 2015; Tanaka et al., 2017). This difference in monomer and dimer interactions is also apparent in D₂-like receptor homodimers, where the ability of bivalent ligands to bridge two neighbouring receptors were tested in comparison to the monomeric analogues. The Hill slope analysis indicated a bivalent binding mode in the presence of dimers, indicating simultaneous occupancy of two neighbouring binding sites (Salama et al., 2014). However, despite the suggestion that dimer bridging has

occurred, one of the major issues with the standard pharmacological analysis is that it is difficult to distinguish a true bridging dimer mechanism from other binding events, such as the pharmacophores binding different sites in the receptor independently, to give a bivalent binding profile. Therefore, a more refined and sensitive technique is required to tackle this question.

5.1.4 Fluorescence correlation spectroscopy (FCS)

The investigation of receptor dimers has led to the development and use of more sensitive fluorescence techniques that incorporate biophysical analysis models, such as FCS. In combination with autocorrelation and photon counting histogram (PCH; Chapter 2, Section 2.6.2), FCS allows for a more rigorous study of receptor oligomerisation and the effects of ligand binding on receptor stoichiometry. The FCS technique has previously been applied in fluorescent ligand characterisation, and in the investigation of ligand-receptor and receptor-receptor complexes, which are discussed in more detail below.

5.1.4.1 Fundamentals of FCS

FCS is an established confocal technique that is used to measure the diffusion of fluorescent particles, in solution or within living cells, as they pass through a defined confocal volume (Briddon et al., 2018; Diekmann and Hoischen, 2014). It was first described by Magde et al., (1972) in an application to investigate the diffusion and binding kinetics of ethidium bromide intercalation with DNA. However, the early systems suffered from low signal to noise ratios and the true potential of FCS was not realised until it was combined with confocal detection (Elson, 2004; Magde et al., 1974).

The power of FCS, in part, derives from its small detection volume. This is created by focusing a laser to a diffraction limited spot using a microscope objective lens with a high numerical aperture (NA). The size of the volume is thus related to Abbé's limit, which states that the fundamental maximum resolution of the system due to diffraction is based on the wavelength and the

NA of the optical imaging system (Equation 5.1), as opposed to other factors that may affect resolution such as lens impurities and misalignment.

Equation 5.1 – Abbé's limit.

$$\text{Diffraction limit} = \frac{\lambda}{2 \cdot NA}$$

The positioning of a pinhole in the confocal setup limits the size of the detection volume in the axial plane, thereby blocking light that is not coming from the confocal source. This creates a Gaussian-shaped detection volume of 0.2 - 0.3 fl (Figure 5.1). It follows that the size of a confocal volume created in this manner can differ, dependent on the wavelength of light used, as determined by the Abbé equation (Equation 5.1).

As the fluorescent moieties pass through the confocal volume they are excited and the emitted photons are then detected by a single photon counting device in a time-dependent manner (Figure 5.1). Autocorrelation analysis, can then be applied, providing quantitative data about the nature of the fluorescent species including the average particle number (N) and the average dwell time of the species within the volume (τ_D) during the data collection window as described in Chapter 2 (Section 2.6.2.1). These data thereby give an indication of the particles' mobility. An additional analysis of the same fluctuation data, PCH, can also be applied and is concerned with the amplitude of fluorescence as opposed to temporal behaviours. PCH provides quantitative data about the nature of the fluorescent species including; average particle number (N) and molecular brightness (ϵ). These data thereby give an indication of the brightness and stoichiometry of the molecules (Section 2.6.2.6).

One of the main principles of FCS is that the number of observed molecules is low enough that each of them contributes substantially to the measured signal, thereby increasing signal to noise. For example, autocorrelation analysis looks at the fluctuations from the mean intensity ($\langle I \rangle$) over time, and the relative size of these fluctuations are greatest with lower numbers of particles.

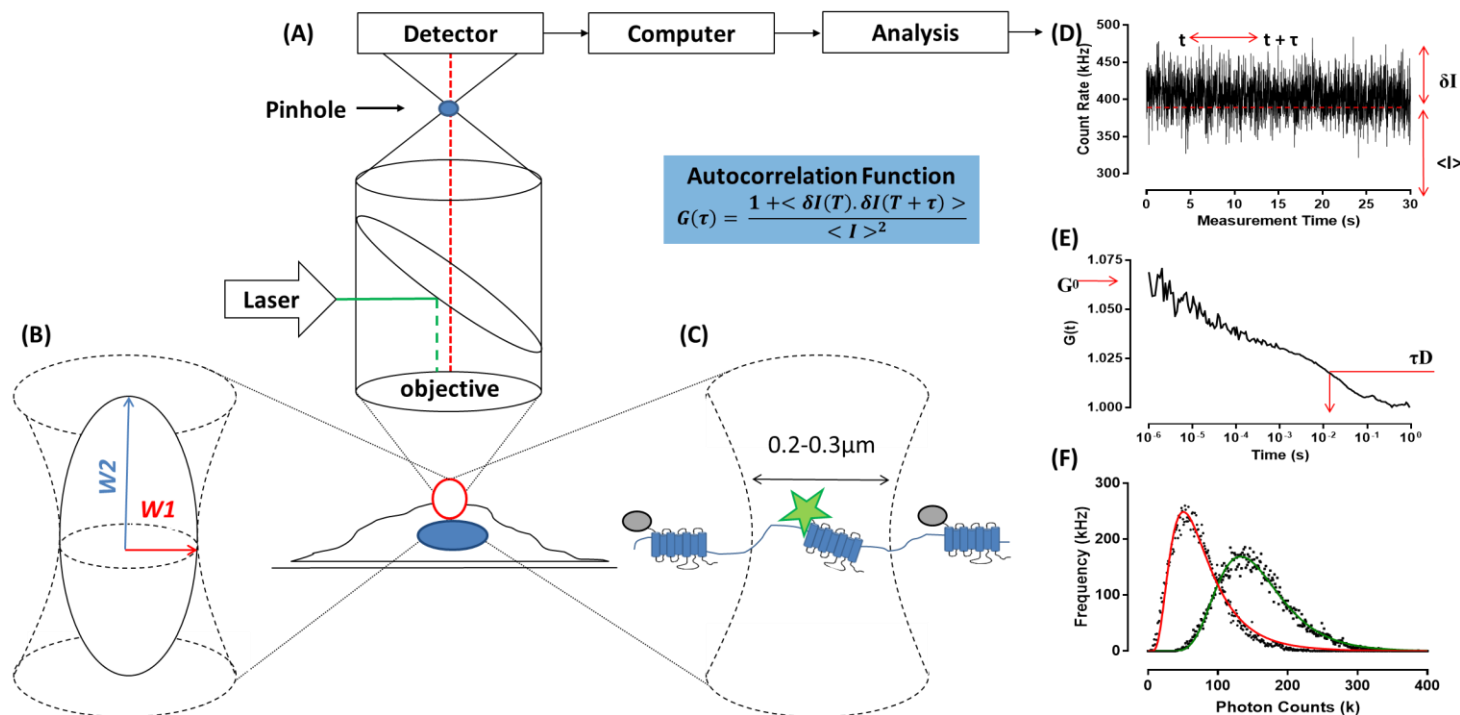


Figure 5.1 - Confocal setup of FCS system with detection volume parameters and resultant analysis. (A) Shows the basic FCS experimental setup. Light from a laser is focused by a dichroic mirror and an objective to form a small confocal detection volume (0.2-0.3 fL; shown in red). Photons are then emitted from the sample due to excitation of fluorophores present within the confocal volume (e.g. SNAP tagged receptors expressed within the membrane, represented schematically in (C)) and are received by the detectors after passing through the appropriate filters and the pinhole. (B) Shows the derivation of the confocal volume dimensions. The resultant intensity fluctuation trace (D) is then analysed using the autocorrelation function (shown in the blue box) to produce the autocorrelation decay curve in (E) from which τ_D and particle number is derived. PCH analysis (F) is also applied to the FCS fluctuation data, providing the super-Poissonian histogram from which molecular brightness can be derived. (E) Shows representative autocorrelation of AF 488 SNAP tagged Y_1R following application of a 1x2D model to the FCS fluctuation trace (D). (F) Shows representative PCH trace following a 1 component fit and 1 ms bin time, demonstrating the deviation of brightness following 1 μM NPY treatment (green) compared to AF 488 controls (red).

It is also important to note that the information obtained by FCS is extracted from cellular regions containing only $\sim 0.1 \mu\text{m}^2$ of plasma membrane consisting of typically 1-100 fluorescent particles, therefore FCS works ideally at nanomolar concentrations (Kilpatrick and Hill, 2016; Schwille and Haustein, 2001). FCS is therefore a very sensitive technique that allows for single cell study and measurement in a non-invasive manner. In combination with autocorrelation and PCH analysis, it provides information on the diffusion characteristics and molecular composition of fluorescently tagged complexes.

5.1.4.2 The study of labelled receptors and oligomeric state

FCS has been used to study receptor oligomerisation states in many systems, largely using GFP or YFP tagged receptors that have employed resonance energy transfer techniques, in conjunction with FCS and PCH analysis, in order to investigate protein-protein interactions.

The application of PCH as a measure of receptor oligomerisation is used instead of changes in diffusion time due to the hydrodynamic radius or Stokes' radius principle, which is a cubic relationship that dictates that diffusion co-efficient halves as molecular mass increases 6 fold (Latunde-Dada et al., 2016). Therefore, there must be a 6 fold increase in mass before there is a measurable change in receptor diffusion. However molecular brightness is a stoichiometric measurement i.e. the brightness of a fluorescent protein is directly proportional to the number of fluorescent proteins travelling together within the protein complex (Figure 5.15). Therefore, the predicted effect of this is that if receptors form oligomeric complexes the molecular brightness will increase in reflection of that.

This use of PCH analysis has been employed to investigate oligomerisation in many receptor systems such as the serotonin 5-HT_{2C} receptors (Herrick-Davis et al., 2012). In these studies, PCH analysis was applied in order to determine the extent of oligomerisation through changes in molecular brightness, along with complementary techniques such as BiFC and FRET. Similar approaches

were employed in the investigation of β_2 -AR, where the extent of dimerisation was investigated through the mutations of key amino acid residues in the dimer interface. This resulted in the disruption of β_2 -AR self-association at the plasma membrane, which was reflected in PCH analysis as a halving of the molecular brightness in comparison to wild type receptors (Parmar et al., 2017). Similar techniques and observations were made at the μ -opioid receptor and Y_1 R (Golebiewska et al., 2011; Kilpatrick et al., 2012, respectively). In the study of Y_1 R, it was observed that the addition of 100 nM endogenous ligand, NPY, resulted in an increase in diffusion time compared to untreated receptor, this was not observed in μ -opioid after 1 μ M treatment of morphine and was attributed to clustering of the Y_1 R in clathrin coated pits during endocytosis.

FCS has also been employed to study receptor-receptor interactions out with the Class A group of GPCRs, such as EGF receptor tyrosine kinases (Saffarian et al., 2007). Again, through the application of complementary PCH analysis, this study showed that the EGF receptor exists in a complex equilibrium of single molecules and clusters of two or more receptors through changes in molecular brightness.

5.1.4.3 The study of ligand-receptor interaction using fluorescent ligands

FCS has also been used to study ligand-receptor interactions in many systems. FCS can be employed to study these interactions using a wide range of fluorophore tagged ligands, across a range of spectra and ligand type. The study of ligand-receptor interactions is possible due to the application of the hydrodynamic radius, as discussed above. This is applicable in the case of ligand-receptor binding because, as fluorescent ligand binds the receptor its relative molecular mass increases substantially, and its diffusion co-efficient decreases. The distinct properties of the bound and unbound populations can then be determined through the application of a 2 component autocorrelation model as discussed in Chapter 2 (Section 2.6.2.5). This allows for a distinction between fast-diffusing free fluorescent ligand and slow-diffusing receptor-

bound fluorescent ligand, through the production of two D values, where $D1$ can be attributed to the first component of the autocorrelation fit i.e. free ligand, and $D2$ can be attributed to the second component of the autocorrelation fit i.e. bound ligand (Figure 5.2).

The application of this FCS principle has been employed in the study of ligand-receptor binding in many receptor systems. One example includes serotonin 5-HT_{3A} receptors (Wohland et al., 1999), where a Cy5-labelled receptor antagonist was used in FCS competition binding assays to determine ligand affinity. It has also been employed to study endothelin A receptors (ET_AR) and the binding of TMR-tagged endothelin-1 to membrane bound ET_AR (Zemanová et al., 2004). Autocorrelation analysis was used to confirm TMR-ligand concentration. PCH analysis was then employed to determine the fraction of receptor bound ligand following titration experiments, allowing for the determination of ligand K_d . Similar techniques and observations were made at the A₁ and A₃ receptors (Cordeaux et al., 2008; Corriden et al., 2014; Middleton et al., 2007) and the histamine H₁ receptor (Rose et al., 2012). Ligand-receptor interactions using FCS have also been employed in the receptor tyrosine kinase family to determine receptor-ligand interactions at the VEGFR₂ (Kilpatrick et al., 2017). Thereby, demonstrating the versatility and application of this technique.

5.1.5 Monomeric BVD15 and dimeric GR231118 ligand pharmacology

As discussed in Chapter 3 and Chapter 4 we have utilised fluorescent labelling of NPY YR ligands for the study of the YR family, with the development of fluorescently tagged monomeric and dimeric ligands based on the parent compounds BVD15 (Figure 5.3; Daniels et al., 1995; Liu et al., 2016) and GR231118 (Figure 5.3; Daniels et al., 1995; Mountford et al., 2014). The BVD15 monomeric and GR231118 dimeric ligands have previously been investigated in order to establish their pharmacological profiles. GR231118 exhibits a 30-100 fold higher affinity for the Y₁R than BVD15 (Daniels et al., 1995).

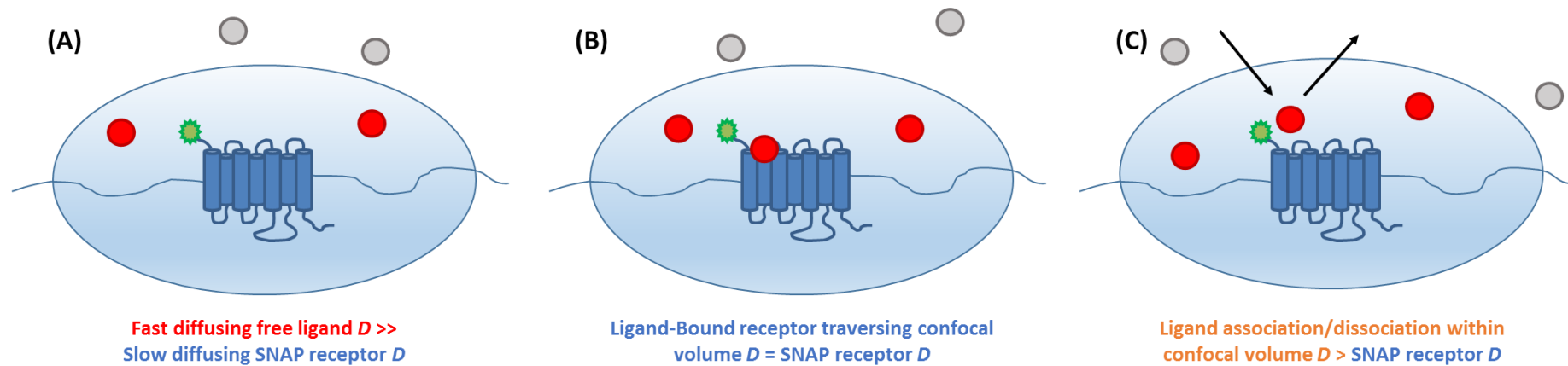


Figure 5.2 – Schematic representation of the detection of different diffusion co-efficients (D) observed at GPCRs in the presence of fluorescent ligand. Where blue volumes represent the membrane area within the confocal volume. (A) Shows the fast diffusing, unbound fluorescent ligand, with a substantially faster D than that of SNAP-tagged receptor, due to the much larger molecular mass and limited mobility of the membrane bound receptor. (B) Shows the traversing of a bound fluorescent ligand-receptor complex, where the ligand will adopt a slower D , comparable to that of the SNAP-tagged receptor, due to the ligand now being restrained to the 2D diffusion of the receptor and an increased relative mass through receptor association. (C) Shows the association and/or dissociation of fluorescent ligand from the receptor within the confocal volume, resulting in an artificially fast D . The D value of this fluorescent species would not be as fast as that of free ligand due to its limited association with the receptor. However, it would be substantially faster than that of the SNAP-tagged receptor, due to the faster diffusion time it would have expressed when not associated with the receptor.

In addition BVD15 has been shown to be a competitive antagonist at the Y₁R whereas GR231118 has shown to be non-surmountable (Chapter 4; Mountford et al., 2014). These distinct pharmacological profiles, in combination with evidence that the YR family may exist in homodimer, heterodimer or oligomeric complexes (Section 1.2.7), allows for speculation into the mechanism of action of drug binding at the Y₁R.

The increased affinity of GR231118 dimer derivatives might be attributed to the interactions of an oligomeric complex when bound. For example, one possible mechanism of binding maybe a flip-flop motion of the dimeric ligand being able to disassociate and re-bind more rapidly at an oligomeric receptor complex, due to its larger size, when compared to the BVD15 monomeric derivatives. This rebinding might be an explanation for the much higher apparent affinity and the non-surmountable pharmacological profile that is observed (Sykes et al., 2017; Vauquelin and Charlton, 2010). It is also possible that the size and structure of the dimeric ligand aids binding through residue interactions with the Y₁R extracellular domains in a way that is not feasible with a smaller monomeric peptide, thereby producing the non-surmountable pharmacology profile through slow ligand dissociation kinetics.

5.2 Aims

The aims of this chapter were to firstly characterise and determine the pharmacological binding profiles, at the Y₁R, of the novel monomer and dimer fluorescent peptides; RhBmono, RhBdimer and Cy5dimer (Figure 5.3; Chapter 3; Liu et al., 2016; Mountford et al., 2014) in comparison to Cy5mono (Figure 5.3; Chapter 4; Liu et al., 2016). This was conducted through the application of plate reader based saturation binding and β -arrestin2 recruitment assays in order to assess their suitability as high affinity Y₁R selective ligands in further FCS based measurements. Secondly, this chapter aims to use the FCS technique to provide evidence for the stoichiometry of Y₁R complexes. The suitability of the fluorescent ligands for use in FCS based measurements was first assessed through solution based measurements in order to assess the

behaviour and properties of the free ligand in solution. The fluorescent ligands were then employed in cell based FCS measurement, and subsequent autocorrelation and PCH analysis, to compare the effects of monomeric and dimeric ligand occupation of the Y₁R on oligomeric complex formation. Thereby determining if monomeric or dimeric Y₁R peptides have a direct effect on Y₁R complex stoichiometry.

5.3 Results

5.3.1 Fluorescent ligand pharmacological characterisation

The structure of the fluorescent ligands synthesised for this study can be seen in Figure 5.3, and a more detailed analysis of their design rationale and synthesis is available in Chapter 3.

5.3.1.1 Saturation binding

Saturation binding was carried out in living SNAP-Y₁R HEK293 cells to establish Y₁R affinities of RhBmono, RhBdimer, Cy5dimer and the Cy5 dual labelled dimer in comparison to Cy5mono (data shown previously in Chapter 4, Figure 4.2). Saturation binding was performed on imaging plate readers as described in Chapter 2 (Section 2.4.1.3). Assays were carried out at 37°C for 30 min as this has previously been established as an appropriate equilibration time (Liu et al., 2016). Cells were treated with SNAP AF 488 in DMEM (0.2 µM, 30 min, 37 °C) and then pre-treated with 1 µM of antagonist BIBO3304 or GR231118 for 30 min in HBSS/ 0.1 % BSA before the addition of fluorescent peptide, to determine non-specific binding. Pre-treatment with antagonist was found to increase signal to noise for the GR231118 compound only. A final well volume of 200 µL was also implemented in this assay to prevent ligand depletion, particularly for the high affinity Cy5dimer. Due to the excitation-emission spectra of the chosen RhB and Cy5 fluorophores, RhB tagged derivatives were read on the IX Micro, and Cy5 derivatives were read on the IX Ultra (Figure 5.4). For RhB tagged peptides, background fluorescence from free ligand resulted in a limited maximal free concentration of 100 nM.

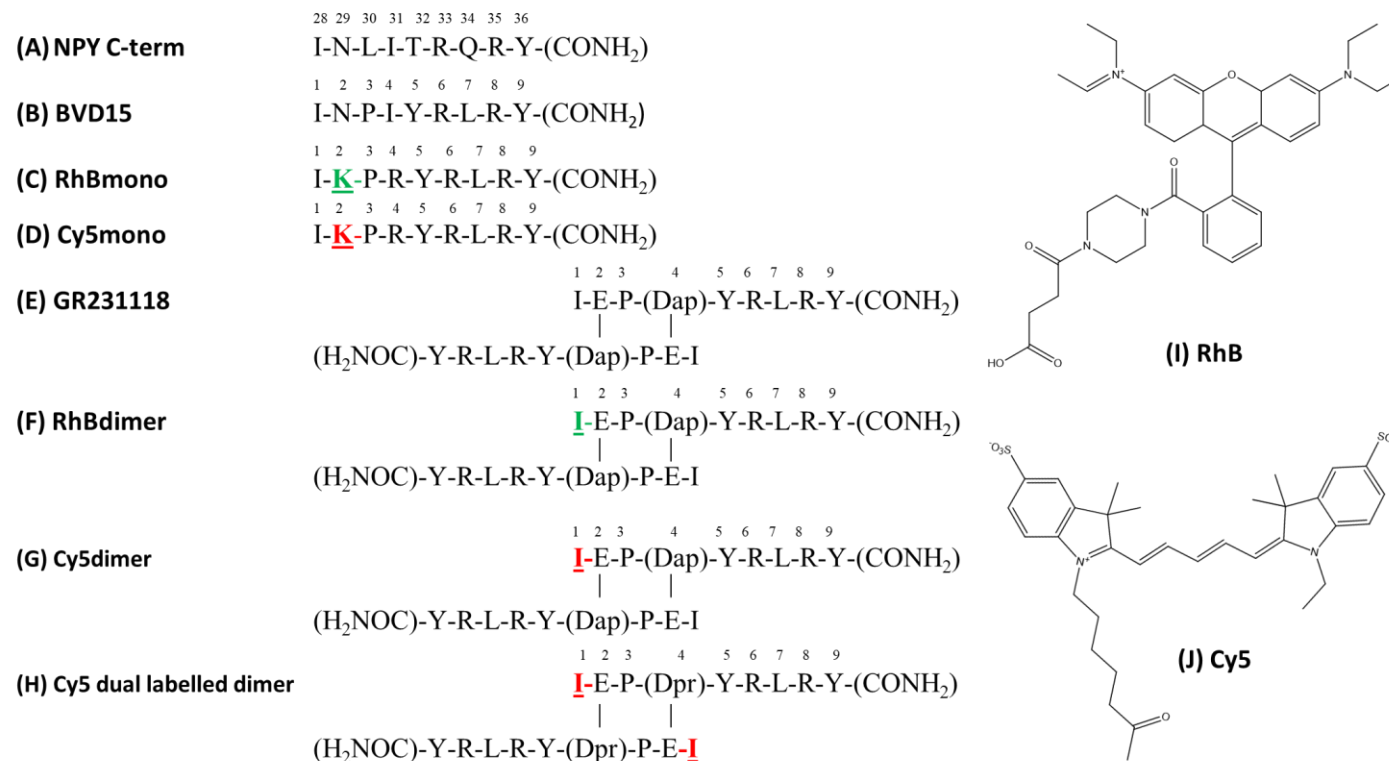


Figure 5.3 - Novel fluorescent Y₁R peptide antagonists. A schematic representation of the amino acid sequence for a series of truncated peptides based on (A) the C-terminus of NPY, annotated with wild type amino acid number. (B) Shows BVD15, a monomeric non-fluorescent Y₁R antagonist, and (C) and (D) show RhBmono and Cy5mono, monomeric fluorescent Y₁R antagonists. Both are based on BVD15 and conjugated at [Lys²] with (I) a RhB and (J) a Cy5 moiety, highlighted in green and red, respectively. (E) Shows the non-fluorescent anti-parallel dimer peptide, GR231118, where non-natural amino acid, Dap, forms lactam bridges with glutamate found on the adjacent peptide strand. (F) and (G) show fluorescent analogues of GR231118 tagged at the N-terminal of one peptide strand with a RhB or Cy5 moiety, known as RhBdimer and Cy5dimer, respectively. (H) Is a dual tagged dimeric ligand conjugated to both N-terminals of the antiparallel dimer strands, known as Cy5 dual labelled dimer.

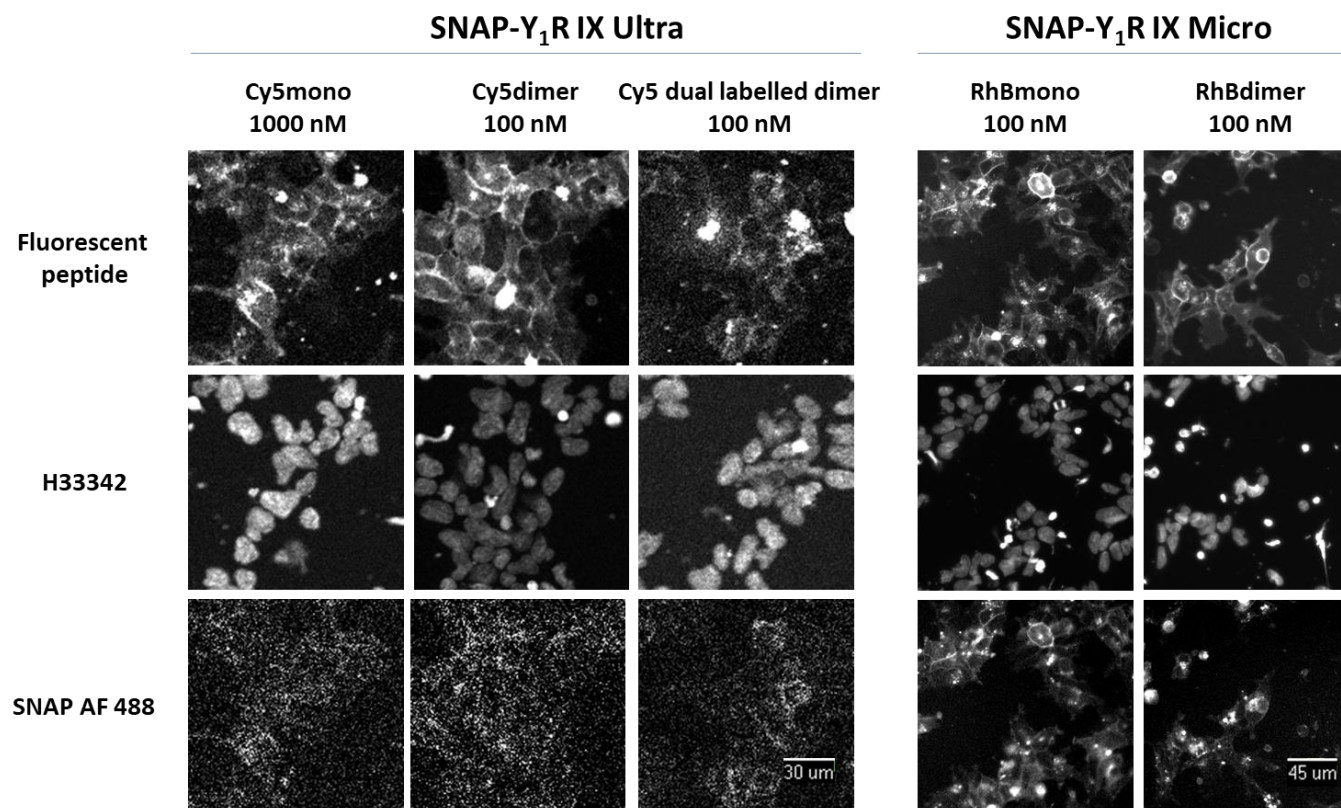


Figure 5.4 - Representative images of saturation binding acquired on the IX Ultra and IX Micro. The left panel shows images of Cy5 tagged peptide saturation binding acquired on the IX Ultra confocal plate reader and the right panel shows images of RhB tagged peptide saturation binding acquired on the IX Micro widefield plate reader. With the top row of images acquired in the Cy5 (IX Ultra) or Tritc (IX Micro) channel showing plasma membrane distribution of fluorescent peptides at 100 nM for all, except Cy5mono which was used at 1000 nM. The middle row of images show H33342 staining of cell nuclei and the bottom row shows SNAP AF 488 binding, demonstrating the presence of SNAP-Y₁R.

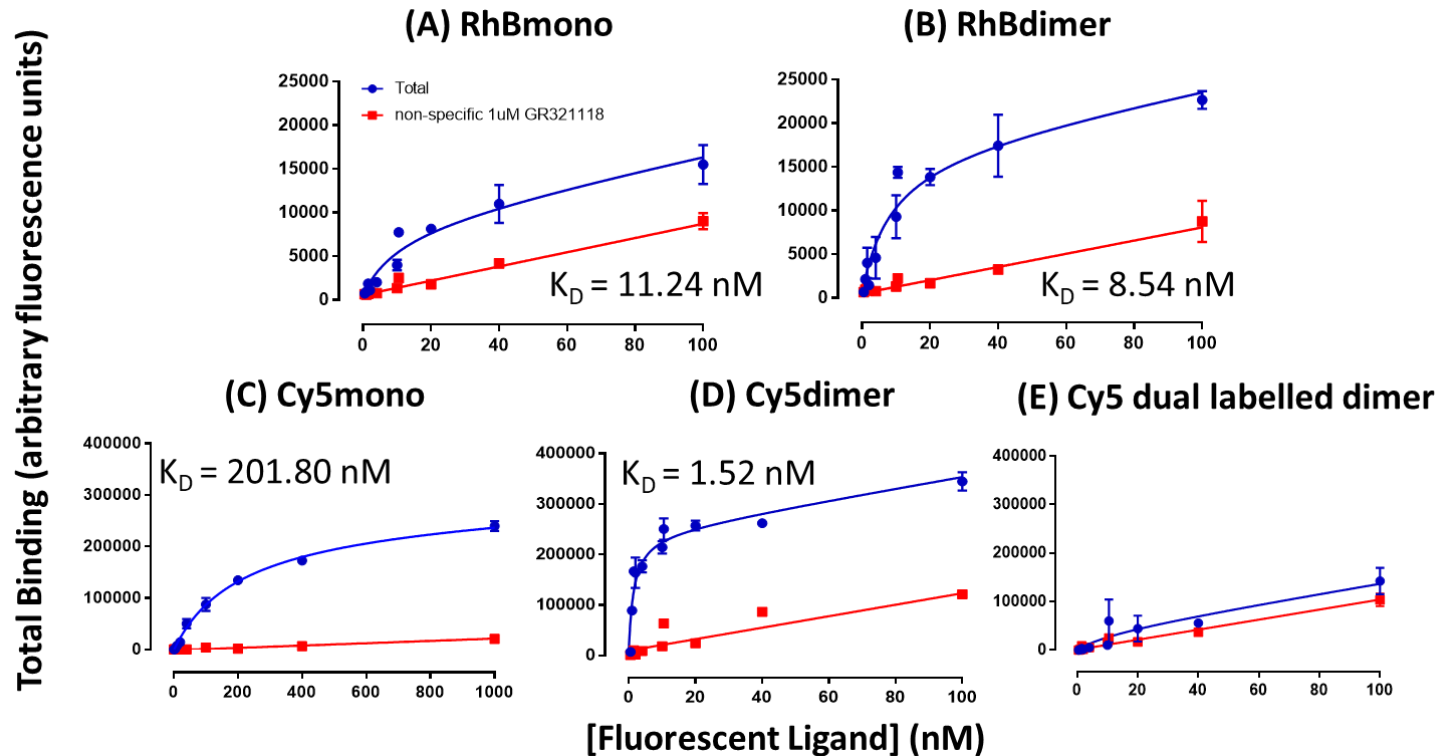


Figure 5.5 – Representative saturation binding profiles for monomeric and dimeric Y₁R fluorescent ligand derivatives in SNAP-Y₁R cells. Following a 30 min pre-treatment with HBSS/ 0.1 % BSA as control or 1 μ M GR231118 in HBSS/ 0.1 % BSA at 37 °C. SNAP-Y₁R expressing cells were treated with fluorescent ligand, [0.1-100nM] for RhB compounds and for Cy5 dimers, except Cy5 mono, which was treated at a larger concentration range [0.1-1000nM], for 30 min at 37 °C in HBSS/ 0.1 % BSA containing H33342 nuclear dye. They were then washed with HBSS/ 0.1 % BSA before imaging live on the IX Micro or IX Ultra for RhB and Cy5 compounds, respectively. Images were analysed using Transfluor analysis to identify fluorescent ligand binding, and the integrated intensity/cell was plotted against concentration. Curves were fitted in GraphPad prism v7 using a one site - total and non-specific saturation model producing the above saturation curves. K_d values were calculated in GraphPad Prism v7.

Following acquisition, images were analysed using transfluor analysis as previously described in Chapter 2 (Section 2.6.1.2). From saturation binding experiments (Figure 5.5) an order of affinity was established for the fluorescent ligands, with Cy5dimer showing the highest affinity ($pK_i = 8.95 \pm 0.05$; $n = 4$), followed by RhBdimer ($pK_i = 7.90 \pm 0.09$; $n = 3$), RhBmono ($pK_i = 7.97 \pm 0.16$; $n = 3$) and finally Cy5mono ($pK_i = 6.70 \pm 0.11$; $n = 4$) showing the lowest affinity. Cy5 compounds showed a 100 fold change in pK_i between monomeric and dimeric ligands. The Cy5dimer expresses a 10 fold decrease in pK_i when compared to all RhB derivatives and a 100 fold decrease when compared to Cy5mono.

Although a pK_i value for the Cy5dual labelled dimer was established ($pK_i = 7.80 \pm 0.05$; $n = 2$), it was found that the assay had a low signal to noise ratio for total verses non-specific binding for this compound. It was also observed that Cy5mono expressed a lower pK_i of 6.70 compared to the previously published value of 7.5 (Liu et al., 2016). This difference may be attributed to adaptations to the assay protocol (i.e. increased antagonist pre-treatment time and increased final well volume). In the interest of consistency, the previously published pK_i value of 7.5 was used in all future calculations.

5.3.1.2 Analysis of Y₁R β -arrestin2 recruitment

β -arrestin2 recruitment assays were performed in order to establish the mode of action of the novel fluorescent derivatives as Y₁R antagonists. These were performed in Y₁ A2 cells, co-expressing the BiFC fragment tagged Y₁R-Yc and β -arrestin2-Yn constructs, as described in Chapter 2 (Section 2.2.1; Table 2.2; Kilpatrick et al., 2010). Cells were treated with varying concentrations of NPY for 1 h at 37 °C, following 30 min pre-treatment with fixed concentrations of peptide as indicated (Figure 5.6). Incubations were terminated through PFA fixation. Under control conditions, NPY stimulated β -arrestin2 recruitment to the Y₁R, produced a pEC_{50} of 8.11 ± 0.13 (Figure 5.6A; $n=16$).

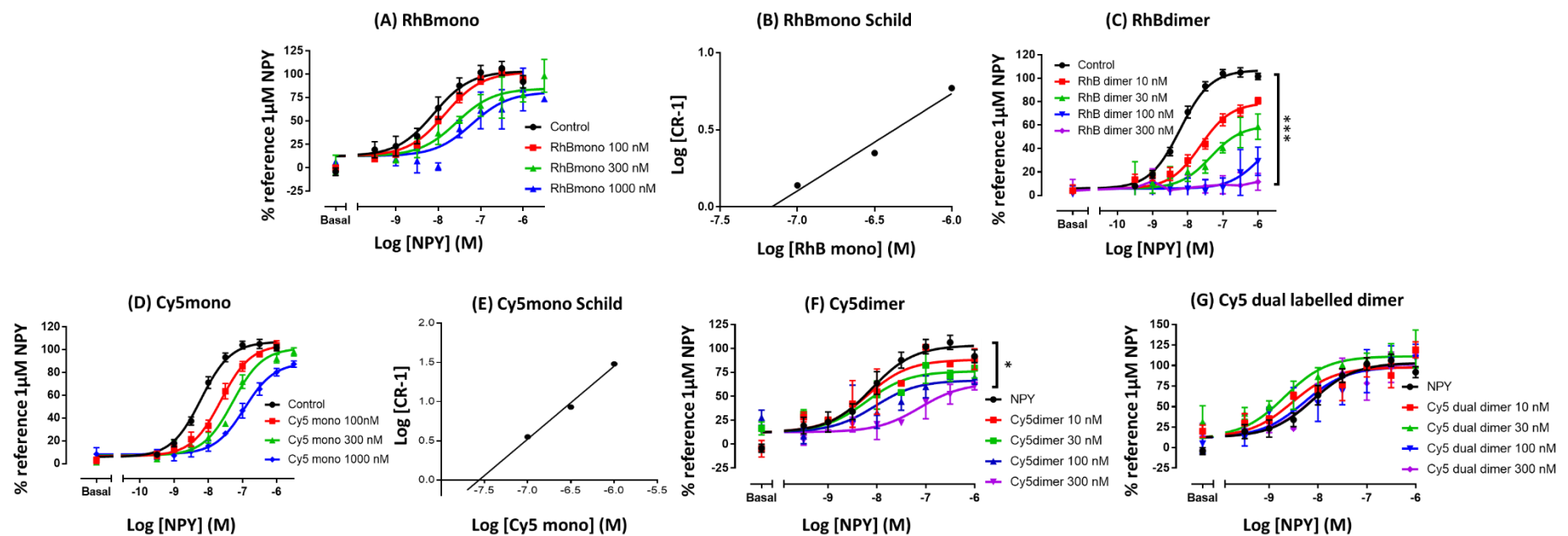


Figure 5.6 – Effect of the novel Y₁R fluorescent ligands on NPY-stimulated β-arrestin2 recruitment. Y₁R β-arrestin2 recruitment was measured in response to NPY following treatment with novel Y₁R fluorescent ligands RhBmono (A) RhBdimer (C) Cy5mono (D) Cy5dimer (F) and Cy5 dual labelled dimer (G). Cells were pre-treated with ligand at the concentrations indicated in HBSS/ 0.1 % BSA, with HBSS/ 0.1 % BSA only as a control, for 30 min at 37 °C. Cells were then treated with NPY at the concentrations indicated for 1 h at 37 °C in HBSS/ 0.1 % BSA. Images were then acquired on the IX Ultra plate reader and analysed using the MetaXpress granularity algorithm. The average granule intensity was then plotted and normalised to 1 μM NPY control, producing the above graphs using GraphPad prism v7. Data was pooled from at least 4 individual experiments. Significant differences are indicated by *p<0.05 ***p<0.001 following one-way ANOVA and Tukey's post-test.

30 min pre-treatment with 1 μ M RhBmono resulted in a rightward shift of the NPY concentration response curve, pEC_{50} 7.21 ± 0.26 (Figure 5.6A; $n=4$), with no significant change in R_{max} . A similar effect was observed with NPY in the presence of 1 μ M Cy5mono with a pEC_{50} of 6.94 ± 0.09 (Figure 5.6D; $n=4$). Multiple antagonist concentrations allowed for Schild analysis (Figure 5.6B and E) and a calculated pA_2 of 6.7 ± 0.1 and 7.5 ± 0.1 was established for RhBmono and Cy5mono, respectively. Conversely, in the presence of RhBdimer and Cy5dimer, β -arrestin2 recruitment assays showed a significant decrease in R_{max} ($p<0.001$ and $p<0.05$, respectively, following one-way ANOVA and Tukey's post-test) suggesting non-surmountable antagonism of NPY responses, as previously described for other GR231118 derivatives (Mountford et al., 2014).

5.3.2 Solution FCS measurements of novel fluorescent ligands

The novel monomeric and dimeric fluorescent peptides demonstrate competitive and non-surmountable antagonist profiles, respectively, that have previously been demonstrated for their unlabelled counterparts (Chapter 3 and Chapter 4; Section 5.3.1; Liu et al., 2016). These observed differences in pharmacology maybe due to differences in peptide conformation or stoichiometry when binding to the Y_1R . As discussed above, FCS analysis of fluorescent ligand binding provides an opportunity to probe any differences in stoichiometry.

However, interpretation first requires accurate determination of the free ligand concentration in these experiments, as this might be affected by aggregation of the peptide in solution, or non-specific binding to chamber surfaces; this can be achieved through FCS measurements. Therefore, initial FCS measurements of the novel peptides were conducted, to first establish their behaviour in solution including observed particle concentration, diffusion co-efficient and molecular brightness, as well as the potential contribution of the different fluorophores, RhB and Cy5, to these behaviours.

5.3.2.1 Solution measurement optimisation

Initial optimisations were conducted for solution based experiments in order to establish optimum laser powers (LP) and concentrations (Figure 5.7). Measurements were taken at varying LP from 10-100 % across a 0.1 nM-100 nM concentration range. This was conducted for RhBmono, RhBdimer, Cy5mono, Cy5dimer and Cy5dual labelled dimer according to the general method laid out in Chapter 2 (Section 2.4.2.2).

Calibration of the appropriate beam paths was conducted before measurements were taken (RhB = 561 nm argon laser excitation and LP580 emission collection; Cy5 = 633 nm HeNe laser excitation and LP650 filter emission collection). Measurements were then taken at room temperature (RT; 21°C) with the confocal volume positioned within the solution, 200 μ m above the coverslip, with a final well volume of 200 μ L. Four FCS measurements of 15 s were then taken for each concentration at varying LP between 10-100 %.

From FCS optimisation (Figure 5.7) it was observed that as laser power increased the measured dwell time (τ_D) remained relatively constant. The apparent dwell time may decrease with increasing laser power as a result of increased photo bleaching, resulting in an artificially fast diffusion time. This phenomenon is not observed in these data, indicating no spot or photo bleaching is occurring, therefore these data are consistent with the expectation that free ligand diffusion time should not be affected by LP, providing an accurate estimate of D .

It was also observed that between 0.1 nM and 30 nM the FCS calculated particle number does not increase with LP but does change with increasing concentration. As increasing concentration results in increased particles present in the system this is consistent with expected behaviour of the compounds.

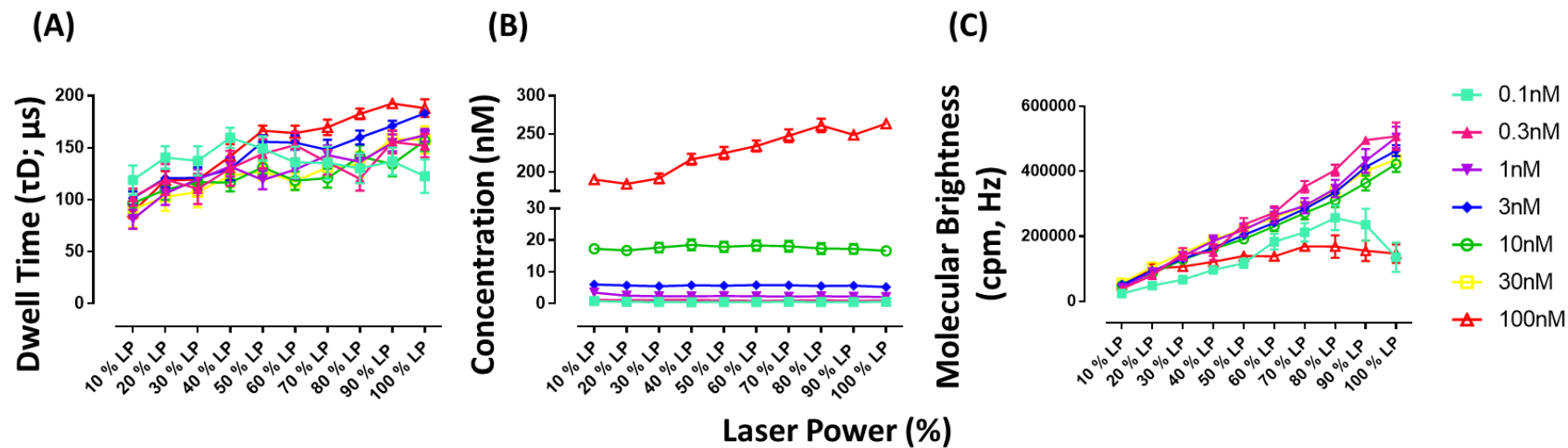


Figure 5.7 – Cy5mono representative data of FCS solution optimisation. Where novel fluorescent peptides were subjected to FCS solution measurements at concentrations ranging from 0.1 nM to 100 nM and varying laser powers (LP), as indicated. Data is pooled from 4 individual experiments, where 4 x 15 s FCS reads were taken per condition per experiment. Data was analysed using a 1x3D autocorrelation analysis and a 1 component PCH analysis. All data is represented as mean \pm SEM.

When the concentration is increased to 100 nM it appears that with increasing LP, there is an increase in particle number, this artefact may be due to saturation of the system, as this is reaching the upper limits for concentration in the FCS technique.

Finally, solution optimisation showed that, with increasing LP, there was an increase in molecular brightness. This observation is in agreement with the nature of the PCH analysis conducted, i.e. the higher the LP the larger the deviation of the super-Poissonian distribution as discussed in Chapter 2 (Section 2.6.2.6). The lower concentration of 0.1 nM and higher concentration of 100 nM did not follow this trend and showed a drop in molecular brightness at higher laser powers, this artefact may also be attributed to these concentrations reaching the higher and lower limits for the FCS technique.

From the Cy5mono data (Figure 5.7) and the data produced through the same measurements for RhB mono, RhB dimer, Cy5 dimer and Cy5 dual dimer, (data not shown), an optimal concentration of 10 nM and 50% LP was selected for future experiments, therefore all quoted values are at 10 nM and 50% LP unless otherwise stated.

5.3.2.2 FCS solution measurements

As with solution optimisation measurements (Section 5.3.2.1), measurements were performed for both RhB and Cy5 tagged monomeric and dimeric peptides, and conducted in HBSS/ 0.1 % BSA at RT (21 °C) over a range of concentrations (1-100 nM) at 50 % LP, as described in Chapter 2 (Section 2.4.2 and Section 2.4.2.2). All FCS based measurements are summarised in Table 5.1 below and FCS experimental set up parameters are summarised in Chapter 2 (Table 2.5). It should be noted that for each laser line used in these experiments the resultant confocal volume created differs in size, due to the optical properties of the wavelength of light used, thereby impacting on the interpretation of dwell times as discussed above (Section 5.1.4).

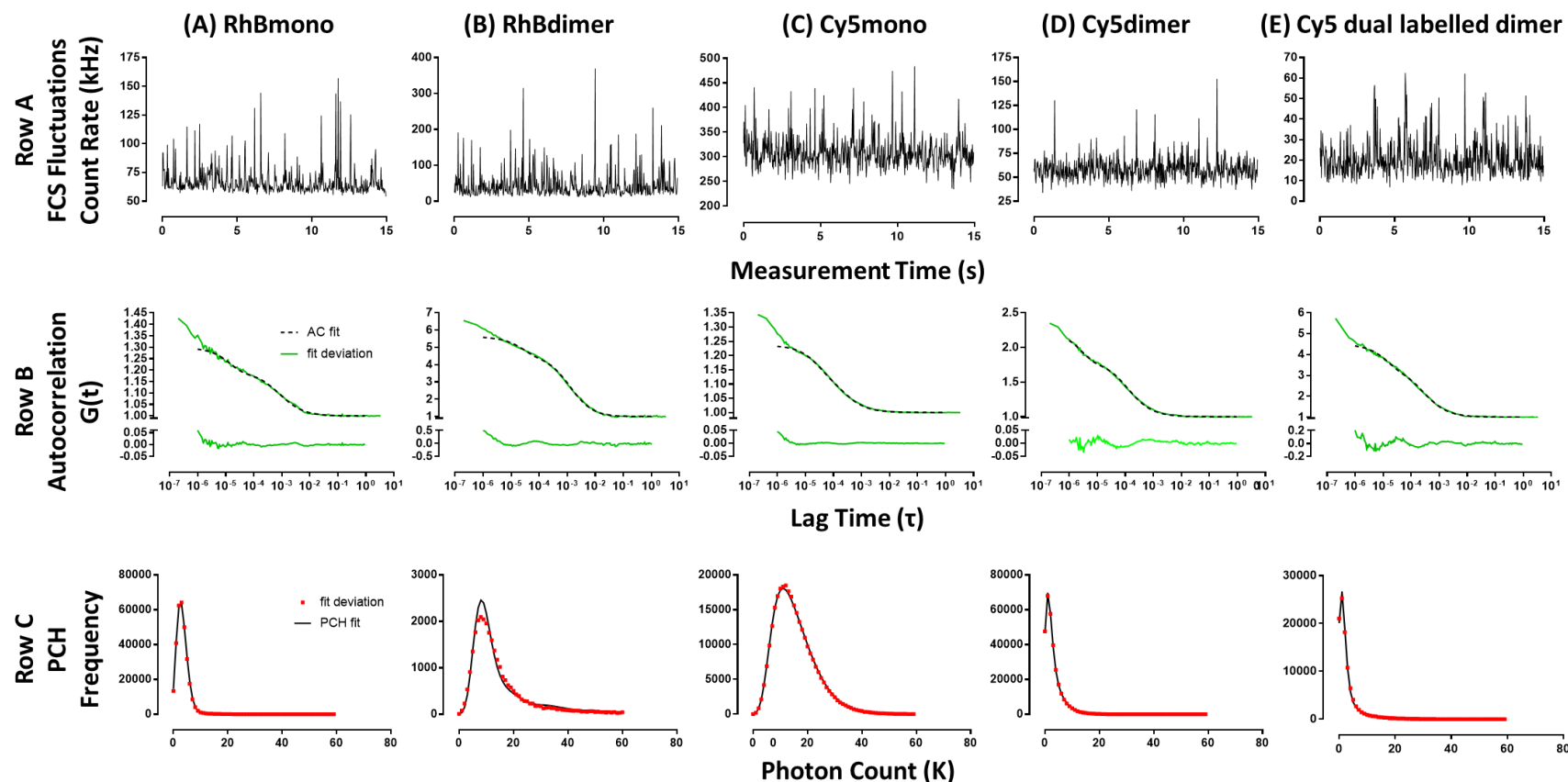


Figure 5.8 – Representative FCS traces for fluorescent peptides in solution. (Row A) shows the fluorescent fluctuations acquired during FCS measurements. (Row B) shows the corresponding autocorrelation curves produced through application of a 1x3D autocorrelation function, from which diffusion co-efficient and particle number is derived. (Row C) shows the corresponding PCH histograms, generated following a 1 component analysis, where RhBmono, Cy5mono and Cy5dimer were analysed with a 50 μ s bin time, RhBdimer a 500 μ s and Cy5dual dimer a 150 μ s bin time. All measurements represent 10 nM ligand taken at 50 % LP.

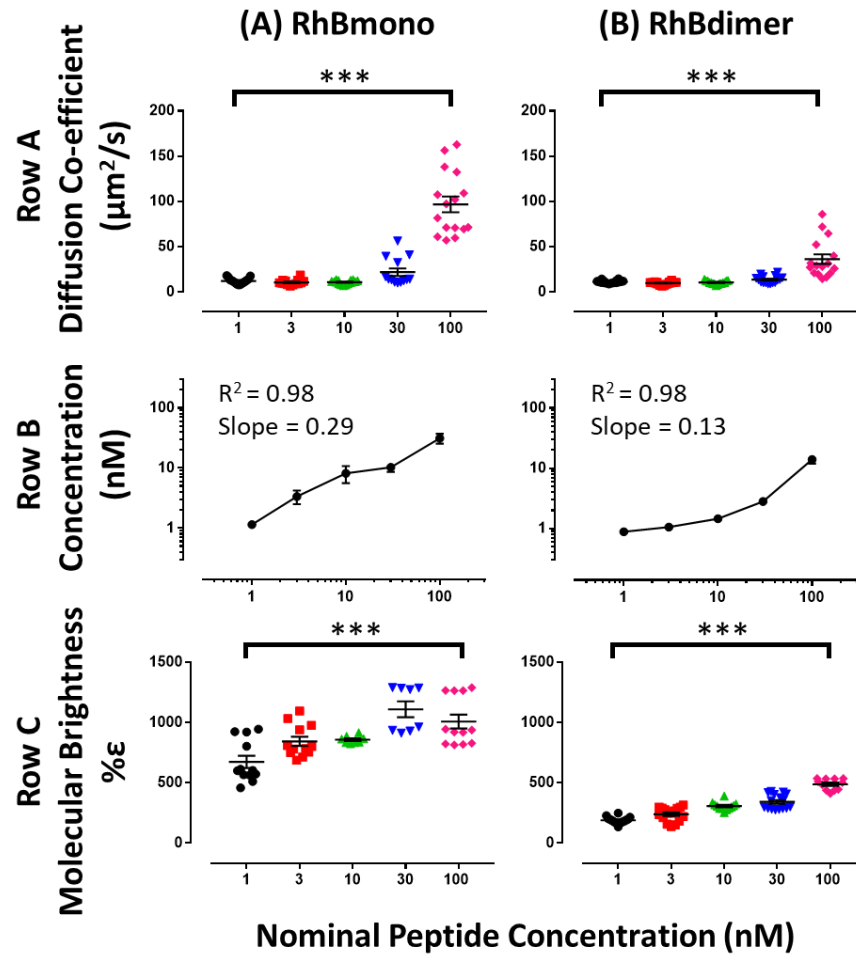


Figure 5.9 – Autocorrelation and PCH derived values of FCS solution measurements of RhB tagged peptides. (Row A) shows diffusion co-efficient ($\mu\text{m}^2/\text{s}$) in free solution (HBSS/ 0.1 % BSA) for each peptide, as indicated, determined by 1x3D autocorrelation analysis. (Row B) shows the PCH calculated concentration (nM) of each peptide present in solution, compared to the nominal concentration added. (Row C) shows the % molecular brightness (ϵ ; normalised as a percentage of calibration control) using a 1 component PCH analysis, where RhBmono was analysed using 50 μs bin time and RhB dimer a 500 μs , determined by the diffusion time calculated from autocorrelation analysis. Four FCS reads of 15 s were taken per experiment at 50 % LP and varying concentrations of compound, as indicated. (n=4). Data are represented as mean \pm SEM and significant differences are indicated by *** $p < 0.001$ following one-way ANOVA and Tukey's test, R^2 and slope values were calculated from linear regression plotted in GraphPad prism v7.

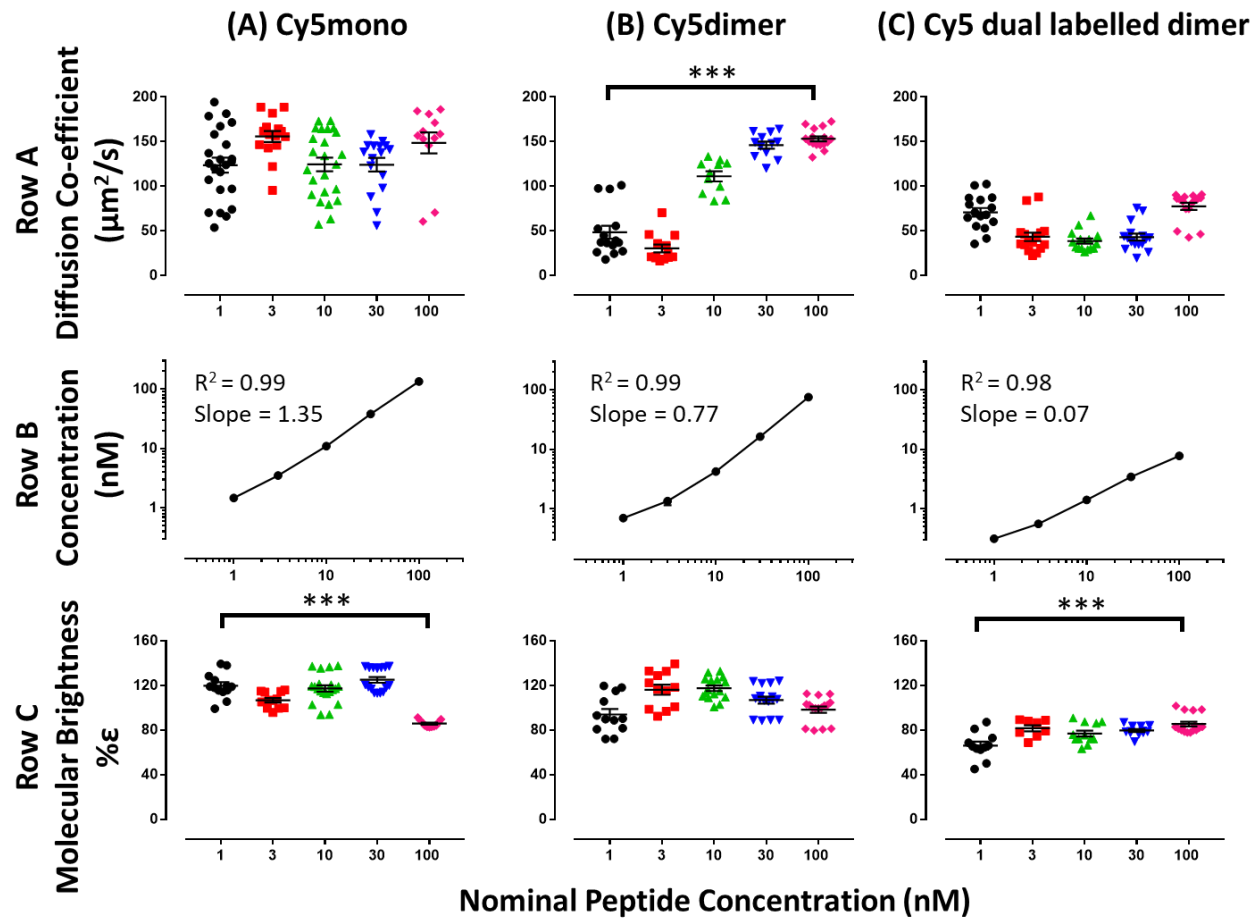


Figure 5.10 – Autocorrelation and PCH derived values of FCS solution measurements of Cy5 tagged peptides - (Row A) shows diffusion co-efficient ($\mu\text{m}^2/\text{s}$) in free solution (HBSS/ 0.1 % BSA) for each peptide as indicated, determined by 1x3D autocorrelation analysis. (Row B) shows the PCH calculated concentration (nM) of each peptide present in solution, compared to the nominal concentration added. (Row C) shows the % molecular brightness (ϵ ; normalised as a percentage of calibration control) using a 1 component PCH analysis where, Cy5mono and Cy5dimer were analysed with a 50 μs bin time and Cy5 dual dimer a 150 μs bin time, determined by the diffusion time calculated from autocorrelation analysis. Four FCS reads of 15 s were taken per experiment at 50 % LP and varying concentrations of compound, as indicated. (n=4). Data is represented as mean \pm SEM and significant differences are indicated by ***p<0.001 following one-way ANOVA and Tukey's test, R^2 and slope values were calculated from linear regression plotted in GraphPad prism v7.

Therefore the conversion of dwell time (τ_D) to the normalised measure of diffusion co-efficient (D), as described in Chapter 2 (Section 2.6.2; Table 5.1), is required to allow comparison of data sets; as such diffusion co-efficient is quoted unless otherwise stated. Example FCS recordings and autocorrelation analysis for all ligands from solution based experiments are illustrated in Figure 5.8. From the decay midpoint of the autocorrelation curve, the dwell time of the diffusing ligand in the confocal volume was calculated (Table 5.1), from which diffusion co-efficient (D) could be estimated (Figure 5.9 and Figure 5.10).

For Cy5 derivatives, D values ranged from 39-125 $\mu\text{m}^2/\text{s}$ (10 nM; Molecular mass (Mr) Cy5mono = 1859, Cy5dimer = 2991, Cy5 dual labelled dimer = 3628; Figure 5.10; Table 5.1) compared to the calibration fluorophore where $D = 329 \mu\text{m}^2/\text{s}$ (Cy5-NHS-Ester, Mr = 616). Differences in diffusion co-efficient between the Cy5 fluorescent derivate were therefore broadly consistent with predictions based on free diffusion and the hydrodynamic radius. In contrast, RhB derivatives showed much lower D compared to Cy5 counterparts, ranging from 10.4-10.8 $\mu\text{m}^2/\text{s}$ (10 nM; Mr RhBmono = 1815, RhBdimer = 2949; Figure 5.9 and Table 5.1), and the Rh6G calibration fluorophore where $D = 283 \mu\text{m}^2/\text{s}$ (Mr = 479).

Furthermore, RhBmono and RhBdimer demonstrated a significant increase in calculated concentration, but this did not correspond well with the theoretical concentration range of 1-30 nM (RhBmono $R^2 = 0.98$, slope = 0.29; RhBdimer $R^2 = 0.98$, slope = 0.13; Figure 5.9). In addition, a significant increase in molecular brightness was observed over this concentration range (**p<0.001 following one-way ANOVA and Tukey post-test), this observation, in combination with the calculated slope of the concentration curve suggests that these compounds aggregate in solution. In contrast, the observed and measured concentrations of Cy5mono and Cy5dimer corresponded closely across the theoretical concentration range of 1-30 nM concentrations (Cy5mono $R^2 = 0.99$, slope = 1.35; Cy5dimer $R^2 = 0.99$, slope = 0.77; Figure 5.10). In addition, there was no significant change in molecular

brightness observed over the same concentration range, suggesting non-aggregating behaviour in solution. A significant decrease in molecular brightness is observed at 100 nM Cy5mono, however this may be attributed to saturation of the systems photon detection ability and reaching the concentration limit of the FCS technique, as was previously observed in optimisation studies (Figure 5.7).

These initial solution experiments therefore demonstrated non-aggregating behaviour of the Cy5 tagged ligands because, in contrast to RhB derivatives, the free concentrations for these analogues closely matched that of the theoretical concentration and provided a good signal to noise for measurement. Hence, Cy5 derivatives were of particular interest in cell based FCS experiments as probes to investigate concentration dependent ligand binding to the Y₁R.

5.3.3 Optimisation of FCS for cell measurements of SNAP-Y₁R diffusion for SNAP surface fluorophore AF 488 and AF 647

Cell based FCS experiments were first optimised for measurement of receptor diffusion and molecular brightness in SNAP-Y₁R cells, using fluorescent receptors labelled with membrane impermeant SNAP fluorophores. Two SNAP labels were compared: SNAPsurface Alexa Fluor (AF) 488 (λ_{ex} 490 nm, λ_{em} 525 nm) was selected for compatibility with the confocal conditions (e.g. beam path and pinhole size) used for our previous measurements of Y₁R-GFP diffusion (Kilpatrick et al., 2012). In comparison SNAPsurface AF 647 was also selected for optimisation as AF 647 (λ_{ex} 650 nm; λ_{em} 665 nm) emits in a similar spectral range as the Cy5 label for the chosen fluorescent ligands (λ_{ex} 649 nm; λ_{em} 666 nm). This would allow FCS measurements of fluorescent ligand binding and directly labelled receptor diffusion to be compared under identical acquisition settings.

Measurements were conducted as described in Chapter 2 (Section 2.4.2 and 2.4.2.3). Cells were treated with 0.2 μM SNAPsurface AF 488 or AF 647 in

DMEM for 30 min at 37 °C. The cells were washed twice with HBSS/ 0.1 % BSA to remove free SNAP label from solution, followed by a further 30 min incubation at 37 °C with 1 μ M NPY or GR231118 in HBSS/ 0.1 % BSA. Following FCS calibration of the appropriate beam path (AF 488 = 488 argon laser excitation and BP530-610 emission collection; AF 647 = 633 HeNe laser excitation and LP650 filter emission collection; Table 2.5) the plate was mounted on to the stage and left to settle to RT (21 °C; 15 min). The plate was then aligned for FCS measurements to be taken from the cell membrane as previously described in Chapter 2 (Section 2.4.2 and 2.4.2.3; Kilpatrick et al., 2012). One 30 s FCS read with a 10 s pre-bleach was taken per cell, with measurements from at least 10 cells per well, at 50% LP.

Example FCS recordings and autocorrelation analysis for SNAP AF 488 and AF 647, \pm 1 μ M NPY or GR21118 are illustrated in Figure 5.11. From the decay midpoint of the autocorrelation curve, the dwell time of the diffusing receptor in the confocal volume was calculated (Table 5.1), from which diffusion coefficient (D) could be estimated (Figure 5.12).

The SNAP concentration of 0.2 μ M was selected based upon previous optimisation experiments, where varying concentration of SNAP were tested (0.1 μ M - 0.5 μ M; data not shown). This concentration was found to be optimal, as 100 % labelling of the receptor population was achieved and was consistent with the SNAP concentration used in all plate reader based assays. As with the solution based FCS, laser power optimisation was also conducted for SNAP AlexaFluor labels (25 %, 50% 75% and 100% LP; data not shown). It was determined that 50 % LP was optimal, where the photon counts per minute (cpm) was highest with no increase in dwell time, indicating limited photo-bleaching, whilst also producing enough photon counts to warrant appropriate application of autocorrelation and PCH analysis, without a decrease in D .

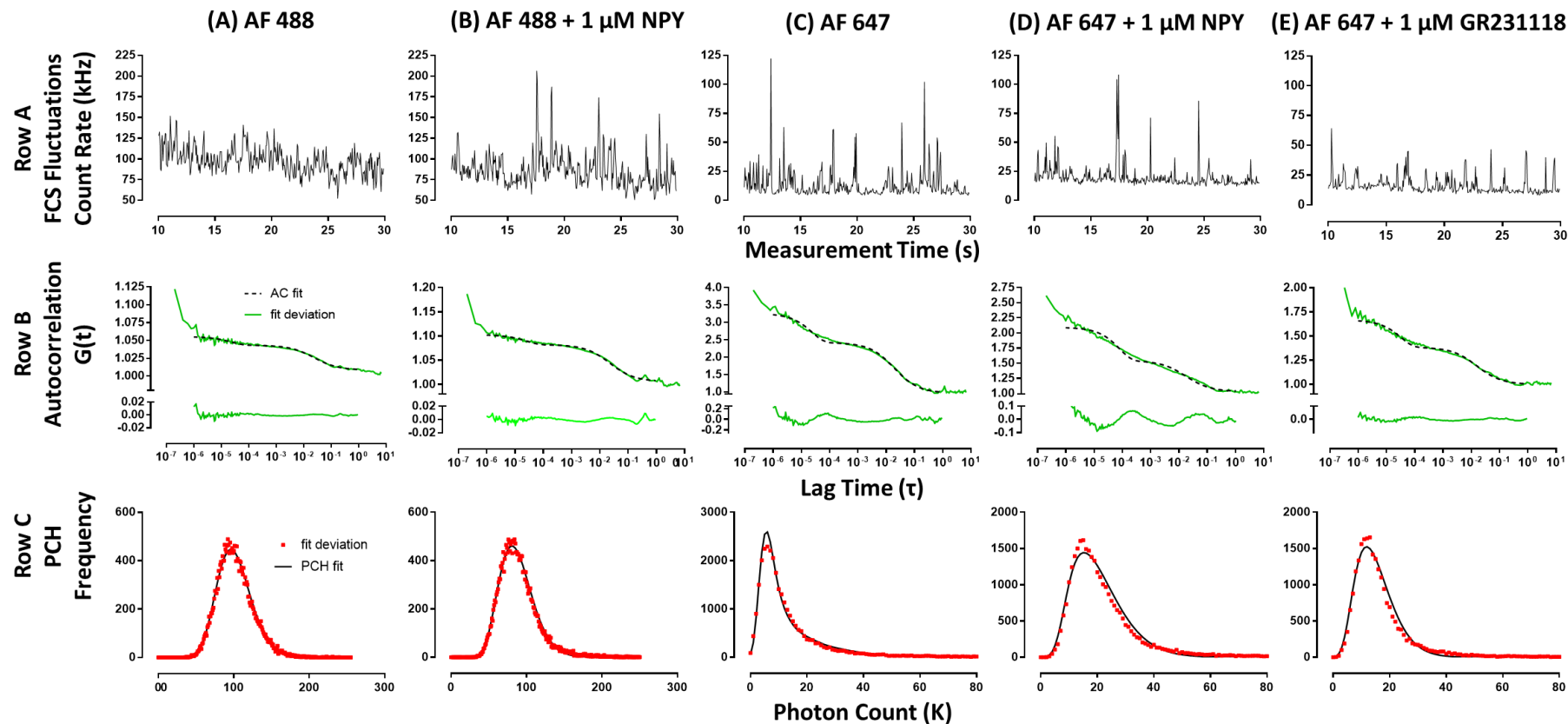


Figure 5.11 – Representative FCS traces for SNAP fluorophore optimisation before and after 1 μM NPY or GR231118 stimulation in SNAP-Y₁R cells. (Row A) shows the fluorescent fluctuations acquired during FCS measurements. (Row B) shows the corresponding autocorrelation curves produced through application of a 1x2D autoorrelation function, from which diffusion co-efficient and particle number is derived. (Row C) shows the corresponding PCH histogram following a 1 component analysis and 1 ms bin time. All measurements represent 10 nM ligand taken at 50% LP.

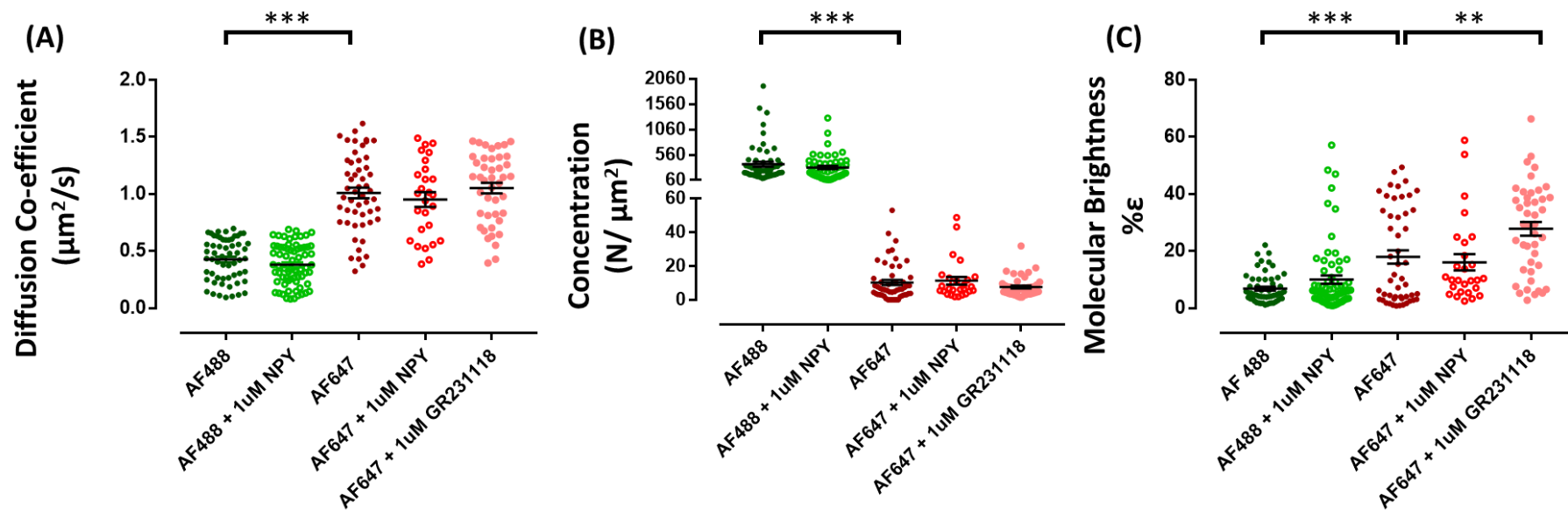


Figure 5.12– Optimisation of FCS system with the use of SNAP fluorophores before and after 1 μM NPY or GR231118 stimulation in SNAP- Y_1R cells for both AF 488 and AF 647 (0.2 μM , 30 min pre-treatment). Following a 1x2D autocorrelation fit, accounting for triplet state with a free offset, diffusion co-efficient (A; $\mu\text{m}^2/\text{s}$) for receptor-bound SNAP fluorophore, measured on the upper membrane of the cell was determined. (B) and (C) show the particle number ($\text{N}/\mu\text{m}^2$) determined through autocorrelation analysis and the molecular brightness (% ϵ ; normalised as a percentage of the calibration fluorophore) using a 1 component PCH analysis with a 1 ms bin time, respectively. One FCS read of 30 s with a 10 s pre-bleach was conducted per cell, at a LP of 50%. SNAP AF 488 was measured using 488 nm argon laser excitation with emission collection through BP530-610 filter sets, while AF 647 used 633 nm HeNe laser with excitation and LP650 filter emission collection. Data is represented as mean \pm SEM where individual data points represent FCS measurement of 1 cell, with a minimum of 10 cells per experiment, over 4 individual experiments. Significant differences are indicated by ** p < 0.01, *** p < 0.001 following one-way ANOVA and Tukey's post-test using GraphPad Prism v7.

Following measurement optimisation, analysis optimisation was also conducted. A 1 component 1x2D biophysical model and a 2 component 1x3D 1x2D model were applied to the same data in order to establish if a 2 component fit was required to account for unbound SNAP that would be present in solution. The application of both models showed that a 1x2D model (a single component model for one 2D component) was adequate, with little change in the χ^2 values (a measure of good fit) and other calculated parameters such as diffusion co-efficient and particle number. Similarly, a 1 component fit in PCH analysis also showed little change in molecular brightness when compared to a 2 component fit. PCH was further optimised by the application of several binning times ranging from 10 μ s-5 ms. It was determined that a 1 ms bin time was optimal for the SNAP labelled receptors as this was less than the average measured dwell time of labelled receptors (a parameter that should be considered when applying a bin time as previously discussed; Chapter 2, Section 2.6.2.6). and provided sufficient data points for accurate determination of molecular brightness.

The calculated D value of AF 647 labelled SNAP-Y₁R was significantly higher than that of AF 488 treated cells (Figure 5.12; Table 5.1). Similarly, the particle concentration in these cells was significantly lower than that in the same cells labelled with AF 488. This may be attributed to a lower labelling efficiency of AF 647, which had been previously reported (New England Biolabs reports a labelling efficiency of 95% and 90% for AF 488 and AF 647 under the same conditions, respectively). It was observed that, following 1 μ M NPY or GR231118 pre-treatment, AF 488 and AF 647 labelled Y₁R showed no change in D or particle number.

The molecular brightness was calculated using a 1 component PCH model and was normalised to the brightness of the calibration fluorophore (Cy5 or Rh6G) determined from the calibration reads conducted prior to experimentation on the same day, where the calibration fluorophore brightness was defined as 100 %. AF 488 labelled Y₁R showed no change in molecular brightness in the

presence or absence of 1 μ M NPY (Figure 5.12; Table 5.1). Similarly, AF 647 labelled receptors showed no change in molecular brightness following 1 μ M NPY. However, a significant increase in brightness was observed following 1 μ M GR231118 pre-treatment ($p < 0.01$ following one-way ANOVA and Tukey's post-test). Additionally, the range of data point distribution following 1 μ M GR231118 was much larger than that of AF 647 \pm 1 μ M NPY (interquartile range (IQR); AF 647; 25 % percentile = 3.2, 75 % percentile = 34.2; AF 647 + 1 μ M NPY; 25 % = 5.7, 75 % = 23.0; AF 647 + 1 μ M GR231118; 25 % = 13.4, 75 % = 38.8)

5.3.4 Receptor binding of monomeric and dimeric fluorescent ligands measured by FCS

Following the results of the solution based ligand measurements and the optimisation of the FCS system for cell reads, novel fluorescent ligand receptor binding to SNAP-Y₁R cells was investigated. These experiments were conducted in a similar manner to the SNAP optimisation experiments via the protocols set out in Chapter 2 (Section 2.4.2 and 2.4.2.4).

Cells were treated with varying concentrations of fluorescent peptide (Figure 5.13 and Figure 5.14) in HBSS/ 0.1 % BSA for 30 min at 37 °C. Following FCS calibration of the appropriate beam path as specified in Chapter 2 (Table 2.5) the plate was mounted on to the stage and left to settle to RT (21 °C; 15 min). The cells were washed twice before the plate was aligned for FCS measurements, taken from the cell membrane as previously described in Chapter 2 (Section 2.4.2.4; Kilpatrick et al., 2012). All measurements were taken within 30 min of HBSS /0.1 % BSA wash. One 30 s FCS read with a 10 s pre-bleach was taken per cell, with measurements from at least 10 cells per well, at 50 % LP.

With regards to receptor bound fluorescent ligand, we would expect to observe an increase in dwell time, represented as a decrease in diffusion co-efficient, when compared to ligand that is free to move in solution.

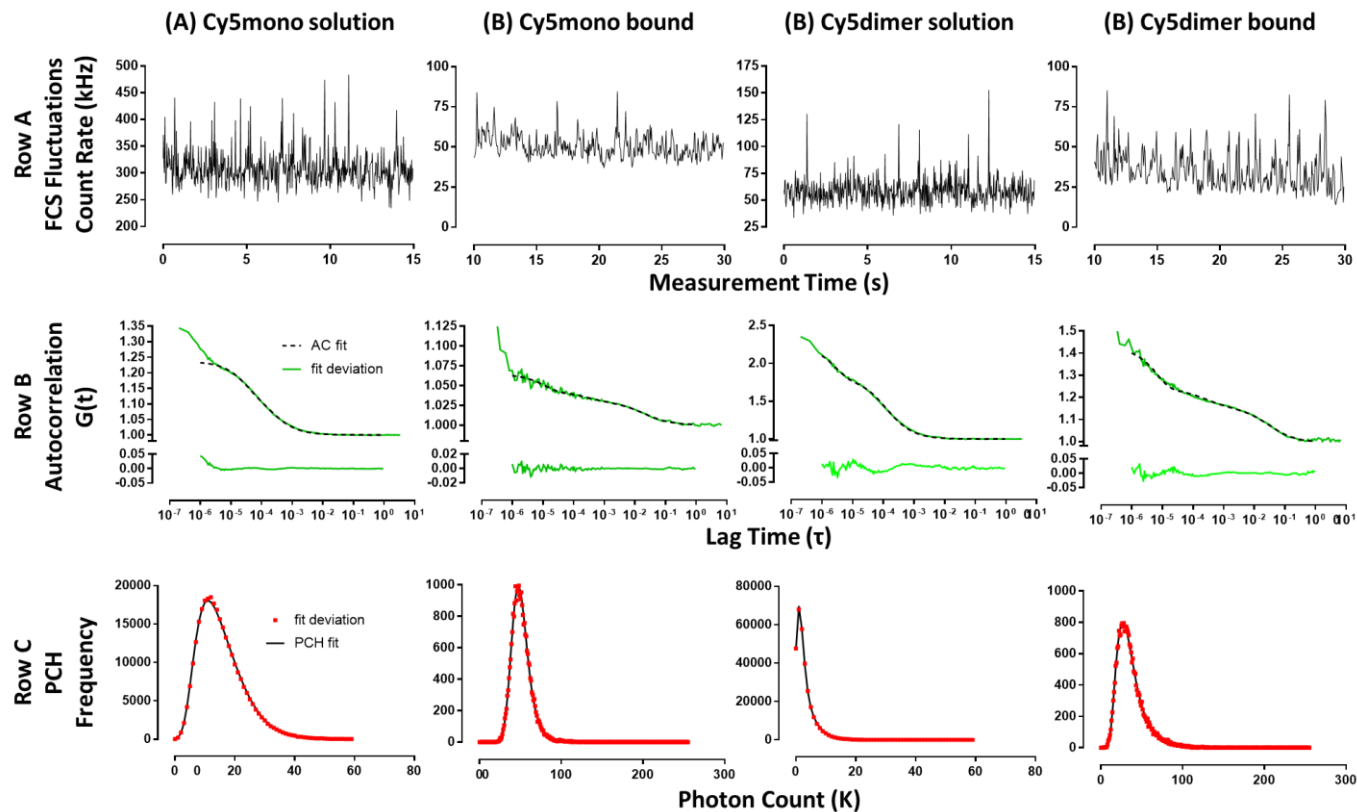


Figure 5.13– Representative FCS traces for fluorescent peptide treated SNAP-Y₁R cells in comparison to solution based measurements. Where (A) and (B) demonstrate analysis of solution based and receptor bound Cy5mono, respectively and (C) and (D) demonstrate analysis of solution based and receptor bound Cy5dimer, respectively. (Row A) shows the fluorescent fluctuations acquired during FCS measurements. (Row B) shows the corresponding autocorrelation curve produced through application of a 1x3D 1x2D autocorrelation function from which diffusion co-efficient and particle number is derived. (Row C) shows the corresponding PCH histogram following a 2 component analysis and 1 ms bin time. All measurements represent 10 nM ligand taken at 50% laser power.

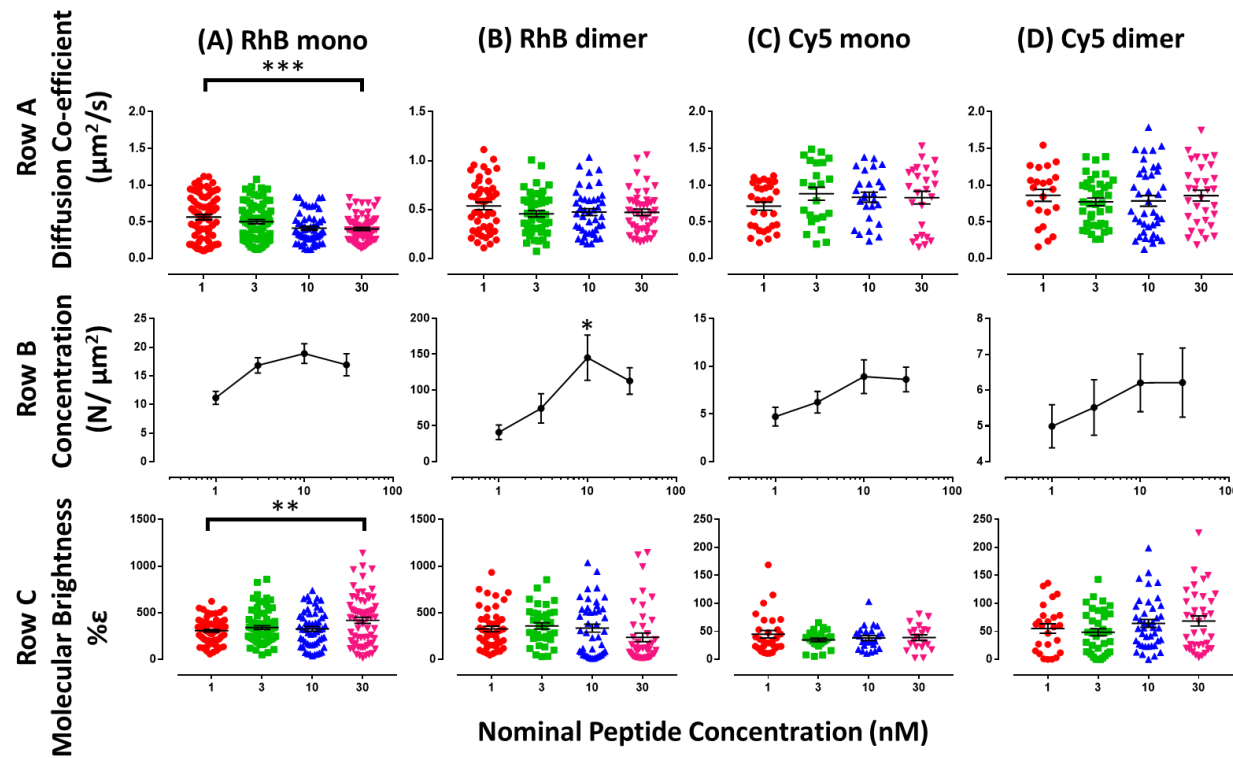


Figure 5.14 – Novel fluorescent peptides bind Y₁R based on FCS calculated diffusion time. (Row A) shows diffusion co-efficient ($\mu\text{m}^2/\text{s}$) of ligands when receptor bound, measured on the upper membrane of the cell following 30 min pre-treatment of ligand. *D* was determined by a 1x3D 1x2D autocorrelation fit where dwell time of the 3D component was fixed to that of free ligand in solution. (Row B) shows the autocorrelation calculated receptor-bound particle number ($\text{N}/\mu\text{m}^2$) at varying concentrations compared to the nominal concentration added. (Row C) shows the % molecular brightness using a 2 component PCH analysis with a 1 ms bin time. RhB compounds were measured using a 561 nm laser excitation with emission collection through LP580 filter sets, while Cy5 compounds used a 633 nm HeNe laser excitation and LP650 filter emission collection. Data is represented as mean \pm SEM where individual data points represents FCS measurement of 1 cell, with a minimum of 10 cells per experiment, over 4 individual experiments. Significant differences are indicated by * $p < 0.05$ ** $p < 0.01$ following one-way ANOVA and Tukey's post-test compared to 1 nM peptide.

This is attributed to the fact that, once bound to the 40kD receptor, the ligand will diffuse slower through the confocal volume because of the reduced mobility of the membrane bound receptor in 2D space, and the increased molecular weight of the receptor-ligand complex, as described above (Figure 5.2).

As with the previous FCS measurements, optimisations were conducted. It was found that washing of the cells before measurement reading was required as cell identification became difficult due to background fluorescence at higher concentrations. A 1x3D 1x2D 2 component autocorrelation model was used to account for the unbound ligand that was still present after washing where the 3D component dwell time was fixed to that of the free ligand (Table 5.1). A 2 component PCH fit was used with a 1 ms bin time for consistency with the chosen autocorrelation model and previous PCH bin times.

In addition, varying concentrations of ligand were used (1 nM-30 nM) in order to observe changes, as the proportional occupancy of the Y₁R changed. Where Cy5mono would result in 0-50 % occupancy of the receptors and Cy5dimer would occupy 50-100 % of the receptors, based on the calculated K_d of 30 nM and 1 nM for Cy5mono and Cy5dimer, respectively (Chapter 4; Section 4.3.1 and Section 5.3.1.1). For RhB labelled peptides the actual change in concentration in these experiments was limited due to the previously observed aggregation of the peptide in solution (Figure 5.9).

The calculated D values of the fluorescent peptides for component 2 (i.e. receptor bound ligand) ranged from 0.4-0.5 $\mu\text{m}^2/\text{s}$ for RhB tagged ligands, and both Cy5 ligands exhibited a D of 0.8 $\mu\text{m}^2/\text{s}$ (Figure 5.14 Row A; Table 5.1). These values were consistent with the D observed for AF 488 and AF 647 bound Y₁R, indicating ligand binding (Figure 5.12; Table 5.1). No significant difference in D was observed over the concentration range (1 nM-30 nM) for any of the ligands, except RhBmono, which exhibited a significant decrease in D at 30 nM compared to 1 nM peptide treatment ($p < 0.001$ following one-way ANOVA and

Tukey's post-test). Additionally, when Cy5mono and Cy5dimer were compared at 10 nM, no significant change in *D* was observed, similarly no change in *D* was observed at 10 nM RhBmono compared to 10 nM RhBdimer.

The particle concentration showed a significant increase ($p < 0.05$ following one-way ANOVA and Tukey's post-test) at 10 nM compared to 1 nM in RhBdimer (Figure 5.14, Row B). A comparison of the RhBmono and RhBdimer at 10 nM also showed a significant difference in particle number ($p < 0.01$ following one-way ANOVA and Tukey's post-test). No significant difference was observed at any of the concentrations in the Cy5 compounds or when Cy5mono was compared to Cy5dimer. Although no significant change in Cy5mono and Cy5dimer was observed, a trend of particle number increase similar to that of RhB compounds was observed indicating that particle concentration increased with free ligand concentration for all peptides.

The molecular brightness was also unaffected with increasing concentrations for RhBdimer and both of the Cy5 ligands (Figure 5.14, Row C). However, a significant increase in brightness was observed at 30 nM RhBmono ($p > 0.01$ following one-way ANOVA and Tukey's post-test) when compared to 1 nM RhBmono. As previously discussed, this increase in brightness maybe attributed to aggregation of the RhB tagged peptides (Section 5.3.2.2; Figure 5.9). Although no statistically significant difference was observed in the Cy5 tagged peptides the range of data points in Cy5dimer treated cells is larger at 30 nM than that observed in 30 nM Cy5mono treated cells (IQR of Cy5mono; 25 % percentile = 22.2, 75 % = 52.9; IQR of Cy5 dimer 25 % = 21.6, 75 % = 109.9). This is also reflected in RhB compounds where the RhBdimer shows a larger distribution of data points at 30 nM compared to RhBmono (IQR of RhBmono 25 % = 172.2, 75 % = 577.6; IQR of RhBdimer 25 % = 31.5, 75 % = 335.5). This observation is consistent with that of 1 μ M GR231118 treated SNAP AF 647 cells (Figure 5.12).

Table 5.1 - Summary of all FCS analyses in solution and SNAP-Y₁R HEK293 cell line. All values represent measurements at 10nM peptide. Solution reads were analysed using a 1x3D autocorrelation fit and a 1 comp PCH where bin time was 500 μ s for RhB dimer, 150 μ s for Cy5 dual dimer and 50 μ s all other ligands. SNAP-Y₁R optimisations were analysed using a 1x2D autocorrelation fit and a 1 comp PCH with a 1 ms bin time. Fluorescent ligand receptor binding was analysed using a 1x3D, 1x2D autocorrelation fit with fixed structural parameters and τ D1 as indicated below, fixed τ D1 values were determined from FCS reads for free ligand in solution. A 2 component PCH fit with a 1 ms bin time was applied. Molecular Brightness (ϵ) was normalised as a percentage of the calibration fluorophore, where the calibration fluorophore is 100%. All data presented as mean \pm SEM.

Condition	Diffusion time		Diffusion Co-efficient ($\mu\text{m}^2/\text{s}$)	Concentration (nM; N/ μm^2)	Molecular Brightness (% ϵ)	n
	τD1 (μs)	τD2 (ms)				
Calibration fluorophores						
Rhodamine 6G	40.2 \pm 1.1	∞	282.5 \pm 6.4	22.5 \pm 1.6 (nM)	100.0	16
Cy5 - NHS ester	51.6 \pm 15.3	∞	328.7 \pm 8.8	28.0 \pm 4.0 (nM)	100.0	28
Fluorescent ligand solution measurements (10nM)						
RhBmono	1037.1 \pm 58.6	∞	10.8 \pm 0.5	8.2 \pm 2.6 (nM)	858.0 \pm 11.0	16
RhBdimer	1060.2 \pm 52.7	∞	10.5 \pm 0.5	1.5 \pm 0.1 (nM)	307.8 \pm 9.9	15
Cy5mono	140.3 \pm 10.1	∞	124.5 \pm 7.5	11.0 \pm 1.3 (nM)	117.3 \pm 2.9	24
Cy5dimer	407.1 \pm 122.6	∞	111.1 \pm 5.6	4.3 \pm 0.6 (nM)	117.5 \pm 2.5	17
Cy5 dual dimer	423.3 \pm 26.5	∞	38.6 \pm 2.9	1.4 \pm 0.1 (nM)	76.8 \pm 2.6	15
SNAP labelled Y ₁ R \pm 1 μM NPY or GR231118 treatment						
Control AF 488	22292.13 \pm 2136.02	∞	0.43 \pm 0.02	373.43 \pm 47.69 (N/ μm^2)	6.85 \pm 0.68	58
AF 488+1 μM NPY	25249.96 \pm 2141.41	∞	0.38 \pm 0.02	308.46 \pm 34.24 (N/ μm^2)	10.01 \pm 1.45	71
Control AF 647	19162.53 \pm 1212.42	∞	1.01 \pm 0.05	10.29 \pm 1.56 (N/ μm^2)	17.94 \pm 2.34	52
AF 647+1 μM NPY	18720.03 \pm 1514.85	∞	0.95 \pm 0.06	11.28 \pm 2.25 (N/ μm^2)	16.07 \pm 2.86	27
AF 647+1 μM GR	16328.51 \pm 993.46	∞	1.05 \pm 0.05	7.60 \pm 0.89 (N/ μm^2)	27.81 \pm 2.40	43
Fluorescent ligand binding at Y ₁ R (10nM)						
RhBmono	1000-1300 (fixed)	34.25 \pm 0.25	0.41 \pm 0.03	18.91 \pm 1.73 (N/ μm^2)	327.75 \pm 25.38	56
RhBdimer	1500-2000 (fixed)	33.98 \pm 0.26	0.47 \pm 0.05	145.16 \pm 31.58 (N/ μm^2)	335.70 \pm 43.40	43
Cy5mono	200-250 (fixed)	21.86 \pm 0.26	0.83 \pm 0.07	8.93 \pm 1.77 (N/ μm^2)	38.21 \pm 4.30	26
Cy5dimer	250 (fixed)	29.19 \pm 0.30	0.78 \pm 0.07	6.20 \pm 0.81 (N/ μm^2)	64.26 \pm 7.07	42

5.4 Discussion

5.4.1 Summary of key findings

Previous chapters of this thesis and literature have highlighted the use and properties of dimeric and monomeric ligands in the generation of high affinity ligands for the Y₁R. This chapter aimed to expand the range of fluorescent antagonists for the investigation of the Y₁R to include the Cy5dimer and the Cy5 dual labelled dimer derivatives. We demonstrated that these showed equivalent high affinity and non-surmountable pharmacology as the parent compound, GR231118. These novel antagonists were then used in FCS experiments to explore the stoichiometry of Y₁R ligand binding using autocorrelation and PCH analysis, to provide evidence for a role of the dimeric ligand in Y₁R oligomerisation. For the Cy5mono derivative, the lack of change in molecular brightness of receptor bound particles over a range of free concentrations suggests single site, rather than multiple site occupancy of these receptors. However, we obtained evidence that high concentrations of unlabelled GR231118 or Cy5dimer peptides increased the overall oligomeric state of the Y₁R population

5.4.2 Novel fluorescent peptides act as Y₁R antagonists

A combination of saturation binding and β -arrestin2 recruitment assays demonstrated that novel peptide compounds, RhBmono, RhBdimer, Cy5mono, Cy5dimer and Cy5 dual labelled dimer act as high affinity antagonists at the Y₁R. The monomeric ligands, RhBmono and Cy5mono expressing similar, surmountable, antagonist behaviour to that of their parent compound, displaying K_d values in the high nanomolar range similar to BVD15 as previously reported (Balasubramaniam et al., 2001; Liu et al., 2016; Parker et al., 1998). This suggests that fluorophore labels conjugated at [Lys²] are well tolerated with no loss of affinity. This is in contrast to the previously reported loss of affinity when fluorophore conjugation was conducted at other positions such as [Lys⁴] (Liu et al., 2016; Mountford et al., 2014). The dimeric ligands RhBdimer and Cy5dimer also express a similarity to their parent ligand, GR231118, expressing a profile of non-surmountable antagonism at the Y₁R,

with K_d values in the nanomolar and sub-nanomolar range, as with GR231118 (Balasubramaniam et al., 2001; Daniels et al., 1995; Mountford et al., 2014; Parker et al., 1998). As with the difference between BVD15 and GR231118, the increase in affinity of Cy5mono to Cy5dimer for the Y_1R was >30 fold.

The antagonist nature of these ligands is reinforced through the cell surface distribution of Y_1R labelling and a lack of ligand associated internalisation. This quality is indicative of antagonist action and is a useful property in whole cell competition binding experiments when using imaging (Chapter 4). As such, these ligands may prove advantageous over NPY labelled analogues such as $[F^7, P^{34}]$ -NPY and $[Pra^4 (FGlc), F^7, P^{34}]$ -NPY which tend to be of lower affinity, millimolar range, and promote receptor internalisation (Ahrens et al., 2011; Hofmann et al., 2015).

The peptidic nature of these analogues may also prove to be advantageous in imaging based experiments because, although they express similar affinities to non-peptide fluorescent derivatives such as BIBO3304 and BIBP32226, these peptide ligands do not express the same level of lipophilicity and cell permeability, resulting in better observations of specific ligand binding in cell imaging compared to non-peptide counterparts (Keller et al., 2015, 2011). However, these non-peptide analogues are more selective for Y_1R versus other YR subtypes compared to the Cy5mono which expresses Y_4R affinity as an agonist (Liu et al., 2016). We would also predict that the Cy5dimer derivatives have agonist affinity at the Y_4R as GR231118 shows this behaviour (Parker et al., 1998).

5.4.3 Solution FCS indicates aggregation behaviours of RhB tagged peptides

FCS solution based measurements provided evidence that RhB tagged novel peptides, but not Cy5 derivatives, may aggregate in solution. While the relationship between predicted and FCS observed concentration was linear for Cy5 analogues (Figure 5.10), RhB compounds demonstrated a non-linear increase in FCS observed concentration compared to predicted (Figure 5.9).

One explanation for this aggregating behaviour may be due to dimer interfaces within the peptide residues. The concept of a dimeric interfaces within the NPY peptide family has previously been explored and it has been suggested that, in the absence of membrane, both PP and NPY can exist in a dimeric state in solution. It has been shown that a dimer interface occurs at the alpha helical segment of the PP-fold present in these peptides at residues 18-30 (Chapter 1, Section 1.1.1; Bader et al., 2001; Cowley et al., 1992; Germain et al., 2013). However, this PP fold is not present in the C-terminus replicated by these antagonist peptides, residues 28-36, so we would not expect this type of dimer behaviour in the analogues described. It had also been shown previously that the cyclic regions of peptides may undergo self-aggregation spontaneously, and assemble in many conformations in solution, to form 3D structures such as nanotubes (Silk et al., 2017).

A second explanation for this behaviour may be attributed to the presence of the chosen fluorophore, as the monomeric and dimeric counterpart compounds do not differ other than by their conjugated fluorophores. It is a known phenomenon that fluorophores can be prone to aggregation, due to the presence of charged functional groups within the compound or the presence of numerous aromatic groups which allow π -stacking interactions (a stabilising interaction common in compounds rich in aromatic groups; McGaughey et al., 1998; Paton and Goodman, 2009). Additionally, there is previous literature evidence that RhB may aggregate within aqueous environments (Karimi Goftar et al., 2014). There is also evidence that Rhodamine fluorophore derivatives such as Rh6G may also aggregate, resulting in poor emission and self-quenching (Lofaj et al., 2013; Martínez et al., 2005). Although it has also been reported that Cy5 dye can form aggregates (Kang et al., 2010), the behaviour of our Cy5-labelled peptides indicates this is less likely. It is also evident that this aggregation is fluorophore dependant as the peptide sequences are the same in Cy5 and RhB monomer and dimer counterparts.

From saturation binding experiments, it was found that the Cy5 dual labelled dimer derivative showed poor membrane binding distribution and a low signal to noise ratio. It was also found to display poor binding in FCS based ligand binding experiments. This may be attributed to the addition of the second Cy5 fluorophore resulting in obstructed receptor binding due to steric hindrance, which has previously been demonstrated to play a role in the effective application of fluorophores (Grigoryan et al., 2017; Lerner et al., 2016; Zhang et al., 2018). Additionally, poor membrane binding may have been observed due to self-quenching of the fluorophores which exist in close proximity. Self-quenching is a common phenomenon in the use of fluorescent species and occurs by a loss of fluorescence signal due to interactions between the fluorophore and the local molecular environment as discussed in Chapter 2 (Section 2.4; Briddon and Hill, 2007). Although undesired in some cases, it can also be employed in assays as a biological read out for protein interactions (Lippert et al., 2016; Zhang et al., 2018).

5.4.4 FCS demonstrates NPY treatment does not affect diffusion time of Y₁R in HEK293 cell membranes

The diffusion co-efficient of SNAP-Y₁R, measured by SNAP AF 488 labelling, was determined as 0.43 $\mu\text{m}^2/\text{s}$. This diffusion time was consistent with previous FCS measurements of Y₁R-GFP ($D = 0.22 \mu\text{m}^2/\text{s}$ in HEK293 cells; Kilpatrick et al., 2012). The average observed diffusion time of a receptor can vary between ~20 ms and 100 ms (Briddon and Hill, 2007), as such the measured value for SNAP AF 488 tagged receptors is within this range and is consistent with measured diffusion values for other receptors including; Adenosine A₁ and A₃ receptors ($D = 0.43 \mu\text{m}^2/\text{s}$ in CHO cells; $D = 0.12 \mu\text{m}^2/\text{s}$ in CHO cells, respectively; Briddon et al., 2004; Cordeaux et al., 2008), β_2 -AR-YFP receptors ($D = 0.74 \mu\text{m}^2/\text{s}$ in HEK293 cells; Herrick-Davis et al., 2013) and opioid D₁-YFP receptors ($D = 0.73 \mu\text{m}^2/\text{s}$ HEK293 cells; Herrick-Davis et al., 2013). The measured diffusion of the SNAP AF 488 tagged Y₁R is also consistent with the measured diffusion times obtained through different methods such as fluorescence recovery after bleaching (FRAP; $D = 0.013 \mu\text{m}^2/\text{s}$ in HEK 293 cells;

Kilpatrick et al., 2012). Therefore the diffusion co-efficient observed in SNAP AF 488 and AF 647 treated cells can be attributed to receptor diffusion.

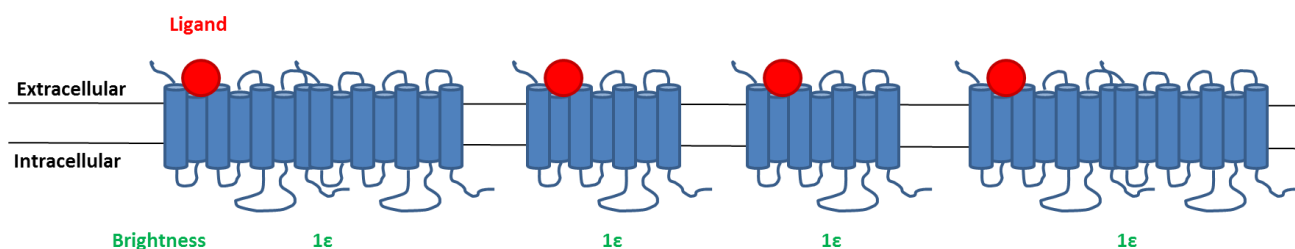
Addition of 1 μM NPY to AF 488 and AF 647 treated SNAP- Y_1R did not significantly change the diffusion co-efficient of the receptor. It has been shown in other investigations, on the adenosine A_3 receptor, for example, that agonist treatment has no effect on receptor diffusion (Cordeaux et al., 2008; Golebiewska et al., 2011). However, it has previously been shown, with data obtained through FCS on the Y_1R , that 100 nM NPY treatment slows the diffusion of a C-terminal GFP-tagged Y_1R (Kilpatrick et al., 2012). This observed decrease in diffusion co-efficient, i.e. increased dwell time, was attributed to clathrin mediated endocytosis and aggregation of receptor in clathrin coated pits. As aggregation into these pits results in slow moving receptors and, the measured diffusion time represents an average of the particle population passing through the volume, the result is an observed decrease in diffusion co-efficient. Although this difference in diffusion has been observed previously at the Y_1R , it may not have been observed here due to a range of factors. This may include the positioning of the N-terminal SNAP tag, as opposed to a C-terminal GFP tag. Both C- and N-terminal tagging have advantages and disadvantages (Böhme and Beck-Sickinger, 2009). N-terminal tagging of the receptor may result in negatively affecting the ligand binding pocket. Conversely, C-terminal tagging can disrupt the receptors ability to interact with the intracellular G-protein complex and associated proteins, resulting in the detriment of receptor signalling. Although no direct comparison of the effect of N-terminal versus C-terminal tagging has been conducted in FCS measured diffusion, previous studies of the adenosine A_3 receptor, by FCS, have shown a diffusion co-efficient of $0.105 \mu\text{m}^2/\text{s}$ for C-terminally tagged $\text{A}_3\text{-GFP}$ (Corriden et al., 2014). When compared to the diffusion co-efficient determined in non-tagged A_3 receptors, whose diffusion was measured through ligand binding, it was shown that two diffusing receptor populations were present, both of which expressed an increase in D (population one $D = 0.119 \mu\text{m}^2/\text{s}$; population two $D = 2.65 \mu\text{m}^2/\text{s}$; Cordeaux et al., 2008). These two observed

populations were attributed to membrane domain localisation for different receptor species. This principle may also be applied to the GFP tagged or SNAP tagged receptor, whereby they are localised to different microdomains within the membrane, thereby affecting the observed diffusion times (Briddon et al 2007). Therefore, it may be considered that the positioning of the tag could prove to be a contributing factor, potentially through altered membrane localisation or through altered interaction with the internal cell signalling complexes. Additionally, the N-terminal SNAP tag label is cell impermeable, as such only the receptors which originated on the cell surface are detected. However, in Y₁R-GFP cell lines the whole cell population of Y₁R is labelled, as such the distribution of the labelled receptors differs, contributing to the observed differences in diffusion co-efficient.

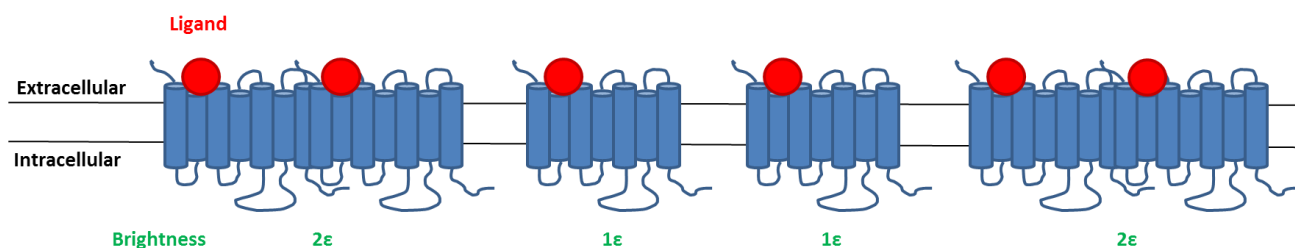
As previously mentioned (Section 5.3.2.1), D is a poor measure of oligomerisation due to the cubic relationship between mass and diffusion coefficient, where D halves as M_r increases 6 fold (Latunde-Dada et al., 2016). Therefore, a better indication of oligomerisation is the use of molecular brightness. As this is a stoichiometric measurement, the brightness of a fluorescent protein is directly proportional to the number of fluorescent proteins travelling together within the protein complex (Figure 5.15). As this is a relative measurement, that provides an ensemble average of the particles in the confocal volume, there is no way to determine a baseline state of the receptor complex, however changes in molecular brightness can indicate changes in receptor complexes when compared to a control, i.e. in response to NPY treatment. In addition, the brightness is rarely a direct integer multiple of monomer brightness, as not all receptors maybe present in aggregates, often resulting in the average brightness only changing by a fraction (Figure 5.15).

The application of PCH analysis as an indication of oligomeric receptor organisation has previously been used in studies of the 5-HT_{2C} receptor (Herrick-Davis et al., 2012).

(A) Model 1 – One binding site per receptor complex



(B) Model 2 – Multiple binding site per receptor complex



Model 1	Free conc	[Bound]	Brightness	Model 2	Free conc	[Bound]	Brightness
	Low	1x	1x		Low	1x	1x
	High	4x	1x		High	4x	1.5x

Figure 5.15 - Schematic representation of one site and multiple site binding in molecular brightness predictions. (A) Represents a one site-binding model, whereby increasing the concentration of free ligand would be predicted to result in increased bound particle concentration but brightness would remain constant. (B) Represents a multiple site-binding model, whereby increasing the concentration of free ligand would be predicted to result in an increase in both concentration and brightness. However, as the population of dimers is not homogenous the resultant measured brightness is not a direct doubling, and results in an observed brightness of 1.5x.

This study found that the molecular brightness of GFP tagged 5-HT_{2C} receptors was double that of GFP and YFP monomeric controls and equivalent to a dimeric GFP control, indicating that 5-HT_{2C} receptors exist as dimers at the plasma membrane. This method was later applied to β_2 -AR, muscarinic M₁ and M₂, and opioid D₁ receptors, with this study indicating that all of these GPCRs undergo homodimerisation to varying extents (Herrick-Davis et al., 2013).

The addition of 1 μ M NPY to SNAP-Y₁R cells did not affect the molecular brightness, indicating that there is no agonist induced change in oligomeric state of the receptors. This is in agreement with previous data obtained for Y₁R, in which homodimerisation was investigated through FRET, showing that the addition of varying concentration of NPY at varying incubation time points did not alter the, unknown, extent of the Y₁R oligomeric state (Dinger et al., 2003). This observation was also consistent with previous data obtained from FCS measurements on Y₁R-GFP (Kilpatrick et al., 2012), which indicated that an increase in brightness was due to the clustering of the receptor during endocytosis and not a change in oligomeric state confirmed as the increase in brightness was abolished in a non-internalising Y₁R-6A mutant.

5.4.5 Measurement of fluorescent ligand binding to the Y₁R by FCS

In this study we have demonstrated fluorescent ligand binding by FCS at the Y₁R. The diffusion co-efficient for RhBmono and RhBdimer bound receptors were 0.41 $\mu\text{m}^2/\text{s}$ and 0.47 $\mu\text{m}^2/\text{s}$, respectively. The D for Cy5mono and Cy5dimer ligands were 0.83 $\mu\text{m}^2/\text{s}$ and 0.78 $\mu\text{m}^2/\text{s}$, respectively. These D values were similar to that of SNAP labelled Y₁R (AF 488 = 0.43 $\mu\text{m}^2/\text{s}$; AF 647 = 1.01 $\mu\text{m}^2/\text{s}$).

The D values of Y₁R bound RhB and Cy5 compounds showed no significant difference when compared to irreversible AF 488 and AF 647 labelled Y₁R, respectively, indicating that the fluorescent ligands do not dissociate from the receptor as they traverse the confocal volume. Dissociation of the ligand would result in an artificially shortened dwell time and has previously been used as

an indicator of ligand dissociation from the adenosine A₃ receptor (Corriden et al., 2014). Indicating that both monomer and dimer ligands were stably bound, even after removal of free ligand by washing, for the duration of their passage as ligand-receptor complexes through the confocal volume. However, a significant difference between the *D* of RhBmono and RhBdimer was observed, indicating that the RhBdimer dissociates less readily than RhBmono from the Y₁R. This evidence of increase residence time for the RhBdimer was not present for the Cy5dimer.

5.4.6 Providing evidence for ligand-receptor stoichiometry, and promotion of Y₁R oligomers by dimer ligands

In fluorescent ligand binding studies we treated SNAP-Y₁R cells with varying concentrations of ligand (Section 5.3.4) with the expectation that this would vary the extent of receptor occupancy. Therefore the predicted effect of this, if the receptors are predominantly monomeric, would be that the brightness would not change with increasing concentration as there is only one binding site per particle. However, if the receptors were predominantly oligomeric then the ligand can occupy multiple binding sites with increasing concentration, thereby resulting in an increase in brightness with increased receptor occupancy (Figure 5.15). The culmination of data presented here, shows, that for the Cy5 ligands, the free concentration range can be varied by 30 fold and exhibits non-aggregating behaviour, as demonstrated through solution FCS measurement (Section 5.3.2.2), and as such can be used to predict changes in receptor occupancy. Fluorescent ligand binding of the Cy5 derivatives at the SNAP-Y₁R also suggest monomer and dimer ligands occupy the receptors at a single binding site with no change in molecular brightness comparatively. This would therefore suggest that the Y₁Rs are predominantly monomeric in HEK cells. This conclusion is consistent with recent BRET data surveying larger numbers of Class A GPCRs, including the Y₁R, suggesting that fewer than 20% of the 700 Class A GPCRs exist as homodimers and that the rest appear as monomeric, with the Y₁R shown to be monomeric (Felce et al., 2017).

Due to the nature of the FCS technique, it should be considered that ligands may be binding to a dimer or oligomer through negative cooperativity of the binding sites (i.e. binding at one site in a dimer prevent binding at a second site). Negative cooperativity has previously been shown to impact on the detection of receptor dimerisation, with its influence on ligand binding at the A₃ receptor (May et al., 2011), the family of glycoprotein hormone receptors (Urizar et al., 2005; Zoenen et al., 2012) and ECF receptors (Macdonald and Pike, 2008) having previously been investigated. This technique is also limited in terms of dynamic range, although it is a sensitive technique in its own right, allowing for molecular level measurements of fluorescent molecules, it is limited to a maximum free concentration of ~100 nM. Thereby the predicted occupancies of the Cy5mono (0-50 %) and Cy5dimer (50-100 %) are different due to their differing calculated K_d values. Additionally, the sensitivity of this technique means that even if receptors are present as dimers, the predicted doubling of brightness may be observed as a 1.5x change in brightness, or lower if the dimers population present is lower than 50%, due to the fact that the cell membrane is not a homogenous environment.

When we consider the SNAP AF treated Y₁R controls, 1 μM GR231118 treatment showed a significant increase in molecular brightness compared to untreated controls, indicating that this ligand may be promoting the formation of oligomeric states. Previous studies have suggested that GR231118 stimulates Y₁R internalisation (Pheng et al., 2003), thereby increasing brightness due to clustering in clathrin coated pits, as previously discussed for NPY treatment (Kilpatrick et al., 2012). However, this is not supported by imaging studies (Holliday et al., 2005), and observations in this thesis that show cell surface localisation of the fluorescent ligands. As the role of membrane micro-domains in GPCR cell signalling becoming an increasingly important factor (Briddon et al., 2018), it may be considered that dimer peptides stimulate receptor clustering of a different nature in compartments close to the plasma membrane. For example clustering of the muscarinic receptors has been shown to occur in caveolae (Dessy et al., 2000), and EGF receptors have

been shown to cluster in non-caveolae lipid rafts (Roepstorff et al., 2002). These findings thereby reconciling the findings of Pheng et al., (2003) and Holliday et al., (2005).

Alternatively, it may be considered that the dimer peptides directly span the receptors to increase oligomerisation. This mechanism has been suggested for other dimeric ligands, particularly for bivalent ligands. However, those ligands previously described expressed longer linkers between the pharmacophores (Arnatt and Zhang, 2014; Busnelli et al., 2016) in order to span the dimer (which can be estimated to be as small as 40Å, the diameter of the transmembrane core of GPCRs; Gurevich and Gurevich, 2008), and as such it is unlikely that the GR231118 dimer is large enough to span both binding sites at the same time, due to its small size (~49Å, assuming 3.5Å per amino acid; Biro, 2006). Constant dissociation and rebinding of the dimer ligand may also be considered as a possibility, however this mechanism of action is unlikely to result in the change in molecular brightness that is seen.

Finally, it may be possible that an increase in oligomerisation follows from the high affinity of the peptides and their effectiveness in promoting an inactive conformation of the receptor, i.e. acting as inverse agonists, and these inactive receptors are more prone to forming oligomeric complexes. It has previously been indicated that ligand induced dimerisation can occur in GPCRs, for example agonist induced dimerisation of the EGF and dopamine D₂ receptors (Kasai et al., 2017; Schlessinger, 2002). However, it has also been shown in δ -opioid receptors that agonist and inverse agonist treatment had no effect on oligomerisation state (McVey et al., 2001). In addition, the Y₁R has never been reported to expressing high constitutive activity that maybe affected by inverse agonist activation.

5.4.7 Final conclusions

We have generated novel monomeric and dimeric, high affinity Y₁R antagonist peptides as tools for the study of the YR family. We have demonstrated that

these ligands showed equivalent high affinity and non-surmountable pharmacology as their parent compounds exhibit. In addition, we have successfully employed the use of these ligands in the study of the oligomeric state of the Y₁R, through the application of FCS, combined with autocorrelation and PCH analysis. Resulting in the indication that high concentrations of dimer peptide increase the overall oligomeric state of the Y₁R population.

The future challenges of this study include gaining further evidence for an effect on oligomers by dimer peptides. This may be achieved through the possible application of BRET or FRET approaches. In addition, asserting that this effect is specific to dimers, as the monomer compounds were not explored at higher receptor occupancy concentrations. In addition, further exploration of the concept of inverse agonist activity of the dimer peptide maybe carried out. This may be conducted in systems that are capable of measuring constitutive activity of the Y₁R, and will explore whether this effect on oligomeric state causes the non-surmountable antagonism observed for the dimer peptide, or if it is a by-product of it.

Chapter 6

General discussion

"Yeah Boiiii!"

Laura Kilpatrick

6.1 General Discussion

Obesity has been increasing in prevalence since the early 1980s, and as such it poses a significant burden on health and healthcare across the globe (Inoue et al., 2018). The associated health risks of obesity encompass a wide range of illnesses including cardiovascular, metabolic and respiratory (Aronne, 2002). Therefore, obesity has a largely unmet clinical need for pharmacological intervention, through anti-obesity therapeutics that will help deliver long-term weight loss and maintained weight loss management safely.

The NPY family of GPCRs has been shown to contribute to the central control of feeding responses through the mediation of hyperphagia, lipogenesis and insulin resistance (Mercer et al., 2011; Shi and Baldock, 2012). The orexigenic activity of NPY is mediated through activation of the Y₁R and Y₅R in the central nervous system (CNS), and the satiety inducing activity of PYY and PP is mediated through activation of the Y₂R and Y₄R in the periphery (PNS). This family of receptors and peptides has therefore been targeted as a potential therapeutic route for the treatment of obesity. However, there has been limited development of clinically effective ligands towards this family of receptors. Small molecule subtype selective Y₁R and Y₅R antagonists show limited in vivo efficacy and there has been a lack of overall success in the development of small molecule Y₂R and Y₄R agonists, and several peptide ligands demonstrate limited selectivity between receptor subtypes (Brothers and Wahlestedt, 2010; Walther et al., 2011). Therefore, there is still scope for the development of more targeted drugs with increased affinity and selectivity at the YR family, which will aid in further elucidating the binding mode and mechanisms of action of ligands at these receptors.

The formation of YR dimers has also been suggested to play a role in this receptor family's regulation of appetite. In vitro, the Y₁R, Y₂R, Y₄R and Y₅R have all been shown to be capable of forming homodimers, and Y₁R/Y₅R has been demonstrated to form heterodimers (Berglund et al., 2003; Dinger et al., 2003; Gehlert et al., 2007). In vivo however, the evidence for Y₁R/Y₅R heterodimers

remains indirect, for example; immunohistochemistry studies implying co-expression of the Y₁R and Y₅R in paraventricular nuclei (PVN) cells (Gehlert et al., 2007; Wolak et al., 2003); and knock out studies in mice that suggest co-regulation of these subtypes in respect to feeding responses (Nguyen et al., 2012). There is evidence that heterodimers may selectively impact on ligand pharmacology, modifying the actions of small molecule Y₁R or Y₅R selective antagonists designed as appetite suppressants (Gehlert et al., 2007; Kilpatrick et al., 2015). However, the issue with recombinant systems, or constrained dimer studies, is that the extent and impact of oligomerisation may be affected by several factors, including receptor expression levels (Felce et al., 2017). The development of pharmacological agents that selectively target dimers would offer an opportunity to study their roles in native systems and offer the potential for this strategy to improve clinical efficacy and selectivity. Bivalent ligands, linking two orthosteric pharmacophores, provide a route that has been explored for both homodimer and heterodimer GPCR combinations (Chepurny et al., 2018; Glass et al., 2016), but often their actual mode of action at the target receptors remains unclear.

This thesis focused on the dimeric YR ligand GR231118, whose high affinity Y₁R antagonist pharmacology initially suggested a role for the bivalent structure, compared to monomer peptides based on the same pharmacophore. The purpose was to explore the mode of action of GR231118 related peptides at the Y₁R and Y₄R, and through the use of biophysical fluorescence imaging techniques such as FCS, the influence of such ligands on receptor oligomerisation. This was achieved through the initial production of GR231118 derivatives via the application of a novel solid phase peptide synthesis (SPPS) route (Mountford et al., 2014). Structure-activity relationships (SAR) for these novel peptides were then established as antagonists at the Y₁R, through the use of high content imaging based assays that allowed for the determination of functional and affinity data for these compounds. In addition, these assays allowed SAR comparisons between the Y₁R and Y₄R to establish compound selectivity at these receptors. The key findings of this thesis were the

identification of a novel, and Y₁R selective role, for [Tyr⁵] in receptor recognition and affinity for the GR231118 peptide, and evidence that GR231118, as a dimeric bivalent ligand, may promote receptor oligomerisation in vitro.

SAR studies showed that the size of the internal cycle structure within the GR231118 compound has an impact on receptor affinity. It was determined that the [Dap⁴]dimer analogue expressed the highest affinity at both the Y₁R and the Y₄R, and although larger ring sizes were better tolerated at the Y₄R, with preserved affinity and potency, the [Dap⁴]dimer ring structure was optimal. SAR studies also showed that selective alanine substitution of [Tyr⁵] in the second arm of GR231118 resulted in a substantive 10 fold, loss in Y₁R affinity, that was not observed at the Y₄R, suggesting a previously undetermined role for this residue, specific to Y₁R affinity. We have postulated that this residue stabilises ligand binding through interactions with the Y₁R at an independent site from the residue present in the first arm. This conclusion is supported by the known requirement for NPY [Tyr¹], at the NPY N-terminus, to be present in order to achieve high affinity Y₁R interaction, with the potential for [Tyr⁵] to mimic this interaction (Chapter 4). Confirmation of these findings may also be explored through the use of computational modelling studies. With the recently solved crystal structure of the Y₁R now available (Yang et al 2018), docking studies of GR231118 at the receptor may be conducted to investigate the details of this interaction further. These computational studies may then be used to direct receptor mutagenesis studies within the binding pocket of the Y₁R to aid in the identification of any potential residue interactions.

Our SAR data therefore indicates that the high affinity of GR231118 for the Y₁R relies on an extended binding surface using [Tyr⁵], rather than being an intrinsic property of the bivalent structure and replication of the core pharmacophore. Cyclic monomer derivatives of BVD15, that aimed to reproduce the ring moiety present in GR231118, did not display increased

affinity (Chapter 4). Potentially however, novel “monomeric” compounds that include both a ring and [Tyr⁵] may replicate the properties of GR231118 in a more compact peptide. This analysis illustrates that some properties of bivalent GPCR ligands may be derived from the linked moieties contributing to target receptor affinity, using secondary receptor interactions other than the “predicted” orthosteric site. This might be expected for GR231118 as an antiparallel cross-linked peptide. Although larger than its monomeric counterpart, and other small molecules, it is highly unlikely that this compound spans the distance between orthosteric sites of a dimer simultaneously, though mechanisms involving sequential rebinding of the dimer arms are possible (Chapter 5).

The chemical synthesis routes described in Chapter 3 were also used to increase the fluorescent ligand toolbox for the YR family, especially in developing high affinity, selective and mono-labelled fluorescent derivatives of GR231118. We achieved this through the production of novel Cy5 labelled GR231118 compounds, with the Cy5dimer expressing high affinity at the Y₁R and selectivity over the Y₄R, where it expresses moderate affinity. The advantages of fluorescent ligands in GPCR research has been recognised over the past ten years, and in particular has been spurred on by the development of fluorescent and bioluminescent plate reader technologies to assess ligand-receptor interaction in addition to spectroscopic and microscope based approaches (Sridharan et al., 2014). For example, the use of fluorescent ligands in combination with high content plate reader imaging in this thesis, developed saturation and competition binding assays that provided robust estimates of Y₁R and Y₄R affinity for both fluorescent and unlabelled ligands. As discussed throughout this thesis, the availability of ligands for the investigation of the YR family are limited, as such radiolabelled peptides are often employed. The most commonly available radiolabelled ligands for the YR family are the native peptides, e.g. [¹²⁵I]-PYY, [¹²⁵I]-NPY and [¹²⁵I]-PP, although [¹²⁵I]-GR231118 (Dumont and Quirion, 2000) and tritiated small molecule antagonists related to BIBP3226 and BIBO3304 have also been described (Doods et al., 1995; Keller

et al., 2015; Rudolf et al., 1994). Fluorophore conjugation has the potential to utilise a larger array of ligands including both peptides and small molecules. Other than eliminating radiation, more systematic use of fluorescent antagonist tracers (e.g. our Cy5 tagged BVD15 and GR231118 derivatives for the Y_1R) offers advantages over traditional radiolabelled agonists, as binding can be studied in live whole cells under physiological conditions, rather than in membrane preparations and assay buffers that stabilise a high affinity agonist bound receptor state. In our studies, this resulted in closer correspondence between the affinity estimates obtained and the properties of our ligands from functional data. Additionally, the use of antagonists limits the level of ligand-induced internalisation in cells, resulting in a more accurate representation of a system at equilibrium, a factor that is assumed for the determination of dissociation constants (Charlton and Vauquelin, 2010). In this respect, while we found Cy5-labelled BVD15 analogues were effective fluorescent ligands for both Y_1R and Y_4R binding studies, these analogues only have these preferred antagonist properties at the Y_1R , retaining agonist activity at Y_4R , and so, the ability to stimulate receptor internalisation (Liu et al., 2016; Chapter 4). Therefore, development of Y_4R antagonist ligands devoid of agonist activity, and subsequently associated labelled derivatives, remains a key goal in future.

In addition to the imaging approaches employed here, the use of additional assays such as time resolved - fluorescence resonance energy transfer (TR-FRET) or bioluminescence resonance energy transfer (BRET) would aid in further investigation and validation of this hypothesis. In both of these approaches, selectivity in detecting the ligand-receptor interaction is enhanced by labelling the receptors of interest with a donor fluorophore e.g. SNAP tag or luciferase. The proximity of fluorescent ligands with a suitable acceptor fluorophore is then detected by resonance energy transfer. Although they require modification of the receptor proteins, the key advantage of TR-FRET and BRET experiments, compared to high content imaging, is that they are readily adapted to a homogenous assay format which allows the recording of kinetic ligand association and dissociation data over time from a single

sample. This then enables straightforward analysis of the kinetics of ligand-receptor interactions, including the association rate and dissociation rate constants (Ergin et al., 2016; Sykes et al., 2017), as well as equilibrium measurements such as K_d . Increasingly, kinetic parameters are important components of SAR in drug discovery. For example, slow dissociating compounds may show an increasing duration of action at the target, and if antagonists, can produce non-surmountable effects. In this thesis, we consistently observed that GR231118 and other high affinity dimeric derivatives behaved as non-surmountable antagonists in Y_1R receptor functional assays, and interpreted this as a consequence of slowly reversible / irreversible binding over the time period of the assay. The synthesised derivatives described in this thesis are compatible with TR-FRET and Nano-BRET approaches, and their future optimisation to develop kinetic YR binding assays, will allow direct measurement of ligand k_{on} and k_{off} rates to confirm this interpretation.

This thesis also explored Y_1R dimerisation, and its regulation by ligand binding, through the application of fluorescence correlation spectroscopy (FCS) and photon counting histogram (PCH) analysis. As well as successfully monitoring interactions through changes in the diffusion co-efficient of the bound fluorescent ligand, these techniques provided a stoichiometric measure of ligand-receptor complex formation, through the determination of molecular brightness (Chapter 5). By comparing the behaviour of equivalent Cy5-tagged monomeric BVD15 and dimeric GR231118 derivatives, we were able to investigate the selective influence of the bitopic, dimeric ligand, GR231118, on receptor stoichiometry (Liu et al., 2016; Mountford et al., 2014; Chapter 3). These FCS experiments demonstrated that, following labelled or unlabelled GR231118 treatment, an increase in YR molecular brightness was observed. This observation is consistent with a greater proportion of oligomers. This increase in molecular brightness was not observed following NPY or monomeric ligand treatment and was not observed in previous studies following BIBO3304 treatment (Kilpatrick et al., 2012). These results indicated

that binding of the bitopic ligand GR231118 might promote receptor oligomer formation. It remains to be determined whether this derives from an intrinsic property of the bivalent dimer structure (with caveats as considered in the SAR section above), or if the formation of Y₁R oligomers is simply a more general consequence following occupancy of the Y₁R with a high affinity antagonist peptide. Thereby, resulting in stabilisation of an inactive receptor conformation as an inverse agonist.

FCS is a highly powerful and sensitive technique that allows investigation of the oligomeric state of receptors within a small area of the cell membrane. The observations made through FCS could be complemented through whole cell plate reader assays to detect receptor dimers using BRET or FRET or complementation based approaches (Dinger et al., 2003; Felce et al., 2017; Gehlert et al., 2007). The previously described bimolecular fluorescence complementation (BiFC) approach used to investigate YR dimers (Kilpatrick et al., 2015), constrains dimers irreversibly and is less suited as a dynamic measurement of dimer formation. However, more recent nanoluciferase complementation methods such as NanoBiT (Dixon et al., 2016), are reversible and use low affinity complementation fragments to more effectively reflect the dimer association and dissociation. Reversible luciferase complementation approaches in particular, would provide a higher throughput measure of ligand-stimulated Y₁R oligomerisation, which would enable the screening of multiple GR231118 and BVD15 analogues (e.g. alanine scan GR231118 mutants). It would also allow assessment of the concentration-dependence of the dimerisation effect, allowing effective comparison between monomeric and dimeric ligands. This would be effective validation to determine whether the bivalent properties of the GR231118 ligand are key to the production of these Y₁R oligomeric complexes or if other factors may be promoting this oligomeric state.

In addition to established techniques such as complementation, BRET and FRET, the use of more novel approaches such as the FKB12-rapamycin-FRB

system may also be employed to study both homo- and hetero- dimer systems (Banaszynski et al., 2005; Pollock and Clackson, 2002). This system employs the use of FKB12 and FRB fused receptor proteins, in which the FRB-FKB12 interaction is stabilised by rapamycin to generate protein-protein interactions. In theory, the system is also reversed by rapamycin washout (Rollins et al., 2000). This system has previously been employed successfully in the study of receptor tyrosine kinase dimers (Otto et al., 2001; Terrillon and Bouvier, 2004), as well as in the study of other cellular protein-protein interactions such as ubiquitination (Janse et al., 2004) and protein-protein interactions involved in cellular regulation pathways (Kohler and Bertozzi, 2003; Spencer et al., 1996). The use of a reversible, induced receptor dimer systems offers potential advantages in studying ligand-dimer pharmacology over techniques such as BiFC, which is inherently irreversible following the fragment association and maturation of the vYFP fluorophore (Kilpatrick et al., 2015). However, the rapamycin controlled system was investigated as a means to stabilise both Y₁R-arrestin and Y₁R dimer interaction in this project (data not shown), but inducible stabilisation of either complex was not achieved.

Our data clearly indicate that while GR231118 has effects on Y₁R oligomerisation, its high affinity as a Y₁R ligand does not appear to derive from its bivalency (Chapter 4) and selective interaction with a receptor dimer. Thus, in order to validate the role of YR dimers in native tissues and therefore their potential impact as therapeutic targets, the development of other dimer selective ligands is still required. These ligands will help determine if YR homo- and hetero- dimers have a physiological role in a native context, which remains an outstanding controversy in the GPCR dimer field in general. One route may be the development of bivalent ligands with spacers sufficient in size to link orthosteric sites simultaneously (Hubner et al., 2016). For some types of GPCR dimer, ligand selectivity might also be achieved in the future because the ligand influences allosteric communication between the receptor orthosteric sites. For example, this phenomenon has been observed at functionally constrained dopamine D₂ dimers, where binding of the bivalent ligand

SB269652 to one orthosteric ligand-binding site allows it to allosterically modulate the binding of dopamine to the second orthosteric site (Lane et al., 2013). It has also been suggested, and demonstrated in adenosine A₃ receptors, that alterations in dissociation rates from the orthosteric site may reflect dimer allosterism. Conformational changes in one receptor within the dimer complex occur in response to ligand binding at another, so that the second site effectively acts as an allosteric modulator through cooperative interactions (May et al., 2007; May et al 2011; Urizar et al 2005; Zoenen et al 2012). Evidence for allosteric communication between orthosteric binding sites, rather than indirect signalling crosstalk has been obtained in the constrained BiFC systems of Y₁R/Y₁R and Y₁R/Y₅R dimers (Kilpatrick et al., 2015) and this system, in conjunction with reversible techniques such as NanoBiT (Dixon et al., 2016) might be employed to further assess homodimer allosterism and cooperativity.

As well as the Y₁R/Y₅R dimer, other targeted combinations may also have future therapeutic benefit, for example the Y₂R/Y₄R receptors. However, targeting this combination of receptors proves difficult, as currently there is a lack of truly selective small molecule ligands for either receptor making it difficult to generate bivalent ligands, or investigate potential dimers to the same extent in vitro. There are indications that the introduction of β -amino acids may lead to the synthesis of compounds with high Y₄R selectivity in the future (Berlicki et al., 2013). The delineation of the relevance of the Y₄R mediated satiety effect is hampered by the lack of selective antagonists, though ligands with modest Y₄R antagonism have recently been described (Kuhn et al., 2016). A more general issue for satiety Y₂R/Y₄R ligands is that they need to be agonists, and hence may be prone to producing side effects such as nausea (as experienced with obinipitide), as well as subject to potential desensitisation of the response upon chronic use (Ouedraogo et al., 2008; Voisin et al., 2000).

It is worth considering a strategy, typified by the properties of GR231118, of a ligand targeted to both Y₁R/Y₄R as a dual antagonist-agonist therapeutic. Such ligands might have dual functionality at both receptor subtypes and so be able to suppress the NPY induced feeding response through Y₁R antagonism and activate PP induced satiety through Y₄R agonism, thereby providing potential for greater selectivity. In terms of pharmacological properties, GR231118 is suboptimal for this approach as it has relatively low affinity and low efficacy (compared to PP) as a Y₄R agonist, as established in our functional data by using β -arrestin2 signalling assays with low receptor reserve (Chapter 4). For such peptide ligands, routes of delivery, excluding oral, and pharmacokinetic aspects, must also be considered. As the Y₁R mediated response in feeding takes place within the brain, this drug, and other peptides that may be developed to target the YR family would need to be delivered across the blood brain barrier (BBB). Previous studies have indicated that delivery of peptides to the brain is certainly possible, with endogenous peptides able to cross the BBB, albeit at a low levels, as shown in the case of PYY and PP (Dumont et al., 2007; Stadlbauer et al., 2013). However, factors such as molecular weight, lipid solubility, protein binding and the charge of the molecule, affect the degree of uptake (Banks, 2015). Many strategies to circumvent the BBB have been proposed, such as direct administration to the brain, which carries inherent safety risks and is very unlikely when weight loss is the desired outcome. A second approach is the modification of molecules to enhance their diffusion across the BBB, however small modifications to the ligands can fundamentally affect the properties of the pharmacophore at the receptor, as evidenced through the recent study that investigated the polyethyleneglycol (PEG) conjugation of PP (Thieme et al., 2016). The use of non-invasive chaperone proteins has proven the most promising form of compound delivery across the BBB with the development of compounds such as Trojan horse antibodies via this method (Pardridge, 2002). Although still a developing technology the use of chaperones has helped to progress peptides and other biologic drug delivery to the brain, with a plethora of new BBB chaperone peptides emerging (Oller-Salvia et al., 2016).

The delivery of GR231118 to the Y₄R, or other drugs targeted towards the Y₂R and Y₄R receptors, may prove less challenging due to the peripheral vagal expression of these YR subtypes. However Y₂R and Y₄R are also thought to be expressed in the hypothalamus, as well as producing their responses through stimulating vagal afferent neurons (Abbott et al., 2005; Zhang et al., 1997), and so the issue of crossing the BBB is also apparent. The satiety effects of PYY₃₋₃₆ (Batterham 2007; Skibicka et al 2013), and clinical trials of the peptide TM30338 (obinipitide), targeted towards both Y₂R/Y₄R indicate that peripherally administered peptides may still have effects at centrally located hypothalamic Y₂R and Y₄R, and thus the issue of BBB penetration could be surmounted (Fulmer, 2008; Osherovich, 2009).

Other considerations in the use of peptide analogues include drug longevity, bioavailability and the route of administration. As discussed in Chapter 1, the delivery of peptides and other biologics, is often done through injection, due to the breakdown of the orally administered peptides through low pH denaturation in the stomach, enzymatic instability and low bioavailability. As peptides generally express a short half-life in the blood stream, delivery of the compounds must be done relatively quickly (Banks, 2015). Approaches have been developed in an attempt to extend the half-lives of peptide therapeutics, such as; identifying and eliminating enzymatic cleavage sites through amino acid substitution, and protecting these cleavage sites through enhancement of the secondary structure of the peptide, i.e. increased folding, which has been achieved through the insertion of lactam bridges or cyclisation of the peptide. The example of GR231118 illustrates the use of such bridges and cyclisation in an attempt to increase plasma half-life, though elimination is still rapid ($t_{1/2}$ = ~25 min; Serone et al., 2000), as well as removing the DPP IV N-terminal cleavage site that limits the lifetime and Y₁R selectivity of full length circulating PYY (Kushwaha et al., 2014). Additionally, the circulating protein albumin in the blood stream may be hijacked through peptide binding to increase the half-life of the peptide (Fosgerau and Hoffmann, 2015). However, peptides and other biologics are more commonly conjugated to carriers such as albumin or

PEG before injection (Thieme et al 2016). Conjugation to carriers increases molecular weight, reducing peptide renal filtration and elimination, and with an increase in plasma half-life, the therapeutic could be administered less frequently. This requirement may need to be balanced with a negative impact on access to the target site i.e. penetration through the blood brain barrier. Oral administration would prove the most desirable goal for peptide therapeutics, but due to the low bioavailability of the compounds, through degradation and associated physiological membrane barriers in the GI tract, further research will be required into the mechanisms that influence GI uptake, absorption and stabilisation of peptides against pH degradation (Tyagi et al., 2018). With such advancements in formulation chemistry, together with optimisation of Y₁R antagonist / Y₄R agonist pharmacodynamics, it is possible that future ligands, based on GR231118 as a template and tool compound, will lead to a successful approach in the pharmacological management of obesity.

Chapter 7

References

“Le Boschski!”

Matthew Styles

7.1 References

- Abbott, C.R., Monteiro, M., Small, C.J., Sajedi, A., Smith, K.L., Parkinson, J.R.C., Ghatei, M.A., Bloom, S.R., 2005. The inhibitory effects of peripheral administration of peptide YY3-36 and glucagon-like peptide-1 on food intake are attenuated by ablation of the vagal-brainstem-hypothalamic pathway. *Brain Res.* 1044, 127–131.
- Abdalla, M.M.I., 2017. Central and peripheral control of food intake. *Endocr. Regul.* 51, 52–70.
- Abot, A., Cani, P.D., Knauf, C., 2018. Impact of Intestinal Peptides on the Enteric Nervous System: Novel Approaches to Control Glucose Metabolism and Food Intake. *Front. Endocrinol. (Lausanne)*. 9, 1–8.
- Adrian, T.E., Bloom, S.R., Bryant, M.G., Polak, J.M., Heitz, P.H., Barnes, A.J., 1976. Distribution and release of human pancreatic polypeptide 940–944.
- Ahrens, V.M., Frank, R., Stadlbauer, S., Beck-Sickinger, A.G., Hey-Hawkins, E., 2011. Incorporation of ortho-carbaboranyl-N ϵ -modified L-lysine into neuropeptide Y receptor Y1- and Y2-selective analogues. *J. Med. Chem.* 54, 2368–77.
- Alam, U., Asghar, O., Azmi, S., Malik, R.A., 2014. General aspects of diabetes mellitus, 1st ed, *Handbook of Clinical Neurology*. Elsevier B.V.
- Albericio, F., Bofill, J.M., El-Faham, A., Kates, S.A., 1998. Use of onium salt-based coupling reagents in peptide synthesis. *J. Org. Chem.* 63, 9678–9683.
- Antal-Zimanyi, I., Bruce, M.A., LeBoulluec, K.L., Iben, L.G., Mattson, G.K., McGovern, R.T., Hogan, J.B., Leahy, C.L., Flowers, S.C., Stanley, J.A., Ortiz, A.A., Poindexter, G.S., 2008. Pharmacological characterization and appetite suppressive properties of BMS-193885, a novel and selective neuropeptide Y1 receptor antagonist. *Eur. J. Pharmacol.* 590, 224–232.
- Aponte, Y., Atasoy, D., Sternson, S.M., 2011. AGRP neurons are sufficient to orchestrate feeding behavior rapidly and without training. *Nat. Neurosci.* 14, 351–355.
- Arakaki, A.K.S., Pan, W.A., Trejo, J.A., 2018. GPCRs in cancer: Protease-activated receptors, endocytic adaptors and signaling. *Int. J. Mol. Sci.* 19, 1886–1910.
- Arnatt, C.K., Zhang, Y., 2014. Bivalent ligands targeting chemokine receptor dimerization: molecular design and functional studies. *Curr. Top. Med. Chem.* 14, 1606–18.
- Aronne, L.J., 2002. Classification of Obesity and Assessment of Obesity-Related Health Risks. *Obes. Res.* 10, 105S–115S.
- Aslanoglou, D., Alvarez-Curto, E., Marsango, S., Milligan, G., 2015. Distinct

- agonist regulation of muscarinic acetylcholine M2-M3 heteromers and their corresponding homomers. *J. Biol. Chem.* 290, 14785–14796.
- Atasoy, D., Nicholas Betley, J., Su, H.H., Sternson, S.M., 2012. Deconstruction of a neural circuit for hunger. *Nature* 488, 172–177.
- Azzi, M., Charest, P.G., Angers, S., Rousseau, G., Kohout, T., Bouvier, M., Piñeyro, G., 2003. Beta-arrestin-mediated activation of MAPK by inverse agonists reveals distinct active conformations for G protein-coupled receptors. *Proc. Natl. Acad. Sci. U. S. A.* 100, 11406–11.
- Babilon, S., Beck-sickinger, A.G., 2013. Towards improved receptor targeting : anterograde transport , internalization and postendocytic trafficking of neuropeptide Y receptors 394, 921–936.
- Bader, R., Bettio, A., Beck-Sickinger, A.G., Zerbe, O., 2001. Structure and dynamics of micelle-bound neuropeptide Y: comparison with unligated NPY and implications for receptor selection. *J. Mol. Biol.* 305, 307–29.
- Balaraman, G.S., Bhattacharya, S., Vaidehi, N., 2010. Structural insights into conformational stability of wild-type and mutant β 1-adrenergic receptor. *Biophys. J.* 99, 568–577.
- Balasubramaniam, A., 1997. Neuropeptide Y family of hormones: Receptor subtypes and antagonists. *Peptides*. 18, 445–457.
- Balasubramaniam, A., Dhawan, V.C., Mullins, D.E., Chance, W.T., Sheriff, S., Guzzi, M., Prabhakaran, M., Parker, E.M., 2001. Highly selective and potent neuropeptide Y (NPY) Y1 receptor antagonists based on [Pro(30), Tyr(32), Leu(34)]NPY(28-36)-NH₂ (BW1911U90). *J. Med. Chem.* 44, 1479–82.
- Balasubramaniam, A., Mullins, D.E., Lin, S., Zhai, W., Tao, Z., Dhawan, V.C., Guzzi, M., Knittel, J.J., Slack, K., Herzog, H., Parker, E.M., 2006. Neuropeptide Y (NPY) Y4 receptor selective agonists based on NPY(32-36): Development of an anorectic Y4 receptor selective agonist with picomolar affinity. *J. Med. Chem.* 49, 2661–2665.
- Ballesteros, J.A., Jensen, A.D., Liapakis, G., Rasmussen, S.G.F., Shi, L., Gether, U., Javitch, J.A., 2001. Activation of the β 2-Adrenergic Receptor Involves Disruption of an Ionic Lock between the Cytoplasmic Ends of Transmembrane Segments 3 and 6. *J. Biol. Chem.* 276, 29171–29177.
- Balthasar, N., Coppari, R., McMinn, J., Liu, S.M., Lee, C.E., Tang, V., Kenny, C.D., McGovern, R.A., Chua, S.C., Elmquist, J.K., Lowell, B.B., 2004. Leptin receptor signaling in POMC neurons is required for normal body weight homeostasis. *Neuron* 42, 983–991.
- Banaszynski, L.A., Liu, C.W., Wandless, T.J., 2005. Characterization of the FKBP.rapamycin.FRB ternary complex. *J. Am. Chem. Soc.* 127, 4715–21.
- Banks, W.A., 2002. Extent and Direction of Ghrelin Transport Across the Blood-Brain Barrier Is Determined by Its Unique Primary Structure. *J.*

Pharmacol. Exp. Ther. 302, 822–827.

Banks, W.A., 2015. Peptides and the blood-brain barrier. *Peptides* 72, 16–19.

Bard, J. a, Walker, M.W., Branchek, T.A., Weinshank, R.L., 1995. Cloning and functional expression of a human Y4 subtype receptor for pancreatic polypeptide, neuropeptide Y, and peptide YY. *J. Biol. Chem.* 270, 26762–5.

Bastien, M., Poirier, P., Lemieux, I., Després, J.P., 2014. Overview of epidemiology and contribution of obesity to cardiovascular disease. *Prog. Cardiovasc. Dis.* 56, 369–381.

Batterham, R.L., Cowley, M.A., Small, C.J., Herzog, H., Cohen, M.A., Dakin, C.L., Wren, A.M., Brynes, A.E., Low, M.J., Ghatei, M.A., Cone, R.D., Bloom, S.R., 2002. Gut hormone PYY(3-36) physiologically inhibits food intake. *Nature.* 418, 650–4.

Batterham, R.L., Ffytche, D.H., Rosenthal, J.M., Zelaya, F.O., Barker, G.J., Withers, D.J., Williams, S.C.R., 2007. PYY modulation of cortical and hypothalamic brain areas predicts feeding behaviour in humans. *Nature.* 450, 106–109.

Batterham, R.L., Le Roux, C.W., Cohen, M.A., Park, A.J., Ellis, S.M., Patterson, M., Frost, G.S., Ghatei, M.A., Bloom, S.R., 2003. Pancreatic polypeptide reduces appetite and food intake in humans. *J. Clin. Endocrinol. Metab.* 88, 3989–3992.

Beck-Sickinger, A.G., Jung, G., 1995. Structure - activity relationships of neuropeptide Y analogues with respect to Y1 and Y2 receptors. *Biopolymers.* 37, 123–142.

Beck-Sickinger, A.G., Wieland, H.A., Wittneben, H., Willim, K.D., Rudolf, K., Jung, G., 1994. Complete L-alanine scan of neuropeptide Y reveals ligands binding to Y1 and Y2 receptors with distinguished conformations. *Eur. J. Biochem.* 225, 947–958.

Behrendt, R., White, P., Offer, J., 2016. Advances in Fmoc solid-phase peptide synthesis. *J. Pept. Sci.* 22, 4–27.

Benovic, J.L., Strassert, R.H., Caront, M.G., Lefkowitz, R.J., 1986. j3-Adrenergic receptor kinase : Identification of a novel protein kinase that phosphorylates the agonist-occupied form of the receptor. *Proc Natl Acad Sci U.S.A.* 83, 2797–2801.

Benovic, J.L., Zastrow, M. Von, 2014. ScienceDirect Editorial overview : Cell regulation : The ins and outs of G protein-coupled receptors. *Curr. Opin. Cell Biol.* 27, v–vi.

Berglund, E.D., Liu, C., Sohn, J.W., Liu, T., Kim, M.H., Lee, C.E., Vianna, C.R., Williams, K.W., Xu, Y., Elmquist, J.K., 2013. Serotonin 2C receptors in pro-opiomelanocortin neurons regulate energy and glucose homeostasis. *J. Clin. Invest.* 123, 5061–5070.

- Berglund, E.D., Vianna, C.R., Donato, J., Kim, M.H., Chuang, J.C., Lee, C.E., Lauzon, D.A., Lin, P., Brule, L.J., Scott, M.M., Coppari, R., Elmquist, J.K., 2012. Direct leptin action on POMC neurons regulates glucose homeostasis and hepatic insulin sensitivity in mice. *J. Clin. Invest.* 122, 1000–1009.
- Berglund, M.M., Schober, D.A., Esterman, M.A., Gehlert, D.R., 2003. Neuropeptide Y Y4 Receptor Homodimers Dissociate upon Agonist Stimulation 307, 1120–1126.
- Bergonzelli, G.E., Pralong, F.P., Glauser, M., Cavadas, C., Grouzmann, E., Gaillard, R.C., 2001. Interplay between galanin and leptin in the hypothalamic control of feeding via corticotropin-releasing hormone and neuropeptide Y. *Diabetes* 50, 2666–2672.
- Berlicki, Ł., Kaske, M., Gutiérrez-Abad, R., Bernhardt, G., Illa, O., Ortuño, R.M., Cabrele, C., Buschauer, A., Reiser, O., 2013. Replacement of Thr32 and Gln34 in the C-terminal neuropeptide y fragment 25-36 by cis -cyclobutane and cis -cyclopentane β -amino acids shifts selectivity toward the Y4 receptor. *J. Med. Chem.* 56, 8422–8431.
- Bhardwaj, N.N., Wodajo, B., Gochipathala, K., Paul, D.P., Coustasse, A., Coustasse, A., 2017. Can mHealth Revolutionize the Way We Manage Adult Obesity? *Perspect. Heal. Inf. Manag.* 14, 1a.
- Bhattacharya, S., Hall, S.E., Vaidehi, N., 2008. Agonist-Induced Conformational Changes in Bovine Rhodopsin: Insight into Activation of G-Protein-Coupled Receptors. *J. Mol. Biol.* 382, 539–555.
- Bhushan, R.G., Sharma, S.K., Xie, Z., Daniels, D.J., Portoghesi, P.S., 2004. A bivalent ligand (KDN-21) reveals spinal δ and κ opioid receptors are organized as heterodimers that give rise to $\delta 1$ and $\delta 2$ phenotypes. Selective targeting of δ - κ heterodimers. *J. Med. Chem.* 47, 2969–2972.
- Biggar, K.K., Li, S.S.C., 2015. Non-histone protein methylation as a regulator of cellular signalling and function. *Nat. Rev. Mol. Cell Biol.* 16, 5–17.
- Binder, E.B., Kinkead, B., Owens, M.J., Nemeroff, C.B., 2001. Neurotensin and dopamine interactions. *Pharmacol. Rev.* 53, 453–486.
- Biro, J.C., 2006. Amino acid size, charge, hydropathy indices and matrices for protein structure analysis. *Theor. Biol. Med. Model.* 3, 1–12.
- Bjarnadóttir, T.K., Gloriam, D.E., Hellstrand, S.H., Kristiansson, H., Fredriksson, R., Schiöth, H.B., 2006. Comprehensive repertoire and phylogenetic analysis of the G protein-coupled receptors in human and mouse 88, 263–273.
- Blomqvist, A.G., Söderberg, C., Lundell, I., Milner, R.J., Larhammar, D., 1992. Strong evolutionary conservation of neuropeptide Y: sequences of chicken, goldfish, and *Torpedo marmorata* DNA clones. *Proc. Natl. Acad. Sci. U. S. A.* 89, 2350–4.

- Blundell, T.L., Pitts, J.E., Tickle, I.J., Wood, S.P., Wu, C.W., 1981. X-ray analysis (1.4-Å resolution) of avian pancreatic polypeptide: Small globular protein hormone. *Proc. Natl. Acad. Sci. U. S. A.* 78, 4175–9.
- Bodnar, R.J., 2018. Endogenous Opiates and Behavior: 2016. *Peptides* 101, 167–212.
- Boey, D., Lin, S., Enriquez, R.F., Lee, N.J., Slack, K., Couzens, M., Baldock, P.A., Herzog, H., Sainsbury, A., 2008. PYY transgenic mice are protected against diet-induced and genetic obesity. *Neuropeptides* 42, 19–30.
- Böhme, I., Beck-Sickinger, A.G., 2009. Illuminating the life of GPCRs. *Cell Commun. Signal.* 7, 1–22.
- Böhme, I., Stichel, J., Walther, C., Mörl, K., Beck-Sickinger, A.G., 2008. Agonist induced receptor internalization of neuropeptide Y receptor subtypes depends on third intracellular loop and C-terminus. *Cell. Signal.* 20, 1740–1749.
- Brain, S.D., Cox, H.M., 2006. Neuropeptides and their receptors: Innovative science providing novel therapeutic targets. *Br. J. Pharmacol.* 147, 202–211.
- Brauner-Osborne, H., Wellendorph, P., Jensen, A., 2007. Structure, Pharmacology and Therapeutic Prospects of Family C G-Protein Coupled Receptors. *Curr. Drug Targets* 8, 169–184.
- Briddon, S.J., Hill, S.J., 2007. Pharmacology under the microscope: the use of fluorescence correlation spectroscopy to determine the properties of ligand-receptor complexes. *Trends Pharmacol. Sci.* 28, 637–645.
- Briddon, S.J., Kilpatrick, L.E., Hill, S.J., 2018. Studying GPCR Pharmacology in Membrane Microdomains: Fluorescence Correlation Spectroscopy Comes of Age. *Trends Pharmacol. Sci.* 39, 158–174.
- Briddon, S.J., Middleton, R.J., Cordeaux, Y., Flavin, F.M., Weinstein, J.A., George, M.W., Kellam, B., Hill, S.J., 2004. Quantitative analysis of the formation and diffusion of A1-adenosine receptor-antagonist complexes in single living cells. *Proc. Natl. Acad. Sci. U. S. A.* 101, 4673–8.
- Broberger, C., Landry, M., Wong, H., Walsh, J.N., Hokfelt, T., 1997. Subtypes Y1 and Y2 of the neuropeptide Y receptor are respectively expressed in pro-opiomelanocortin- and neuropeptide-Y-containing neurons of the rat hypothalamic arcuate nucleus. *Neuroendocrinology* 66, 393–408.
- Brothers, S.P., Saldanha, S. a, Spicer, T.P., Cameron, M., Mercer, B. a, Chase, P., McDonald, P., Wahlestedt, C., Hodder, P.S., 2010. Selective and brain penetrant neuropeptide Y Y2 except against considered by whole-cell-high-throughput screening. *Mol. Pharmacol.* 77, 46–57.
- Brothers, S.P., Wahlestedt, C., 2010. Therapeutic potential of neuropeptide Y (NPY) receptor ligands. *EMBO Mol. Med.* 2, 429–39.

- Busnelli, M., Kleinau, G., Muttenthaler, M., Stoev, S., Manning, M., Bibic, L., Howell, L.A., McCormick, P.J., Di Lascio, S., Braida, D., Sala, M., Rovati, G.E., Bellini, T., Chini, B., 2016. Design and Characterization of Superpotent Bivalent Ligands Targeting Oxytocin Receptor Dimers via a Channel-Like Structure. *J. Med. Chem.* 59, 7152–7166.
- Cabrele, C., Beck-Sickinger, A.G., 2000. Molecular characterization of the ligand-receptor interaction of the neuropeptide Y family. *J. Pept. Sci.* 6, 97–122.
- Cabrele, C., Langer, M., Bader, R., Wieland, H.A., Doods, H.N., Zerbe, O., Beck-Sickinger, A.G., 2000. The first selective agonist for the neuropeptide YY5 receptor increases food intake in rats. *J. Biol. Chem.* 275, 36043–36048.
- Cahill, T.J., Thomsen, A.R.B., Tarrasch, J.T., Plouffe, B., Nguyen, A.H., Yang, F., Huang, L.-Y., Kahsai, A.W., Bassoni, D.L., Gavino, B.J., Lamerdin, J.E., Triest, S., Shukla, A.K., Berger, B., Little, J., Antar, A., Blanc, A., Qu, C.-X., Chen, X., Kawakami, K., Inoue, A., Aoki, J., Steyaert, J., Sun, J.-P., Bouvier, M., Skiniotis, G., Lefkowitz, R.J., 2017. Distinct conformations of GPCR- β -arrestin complexes mediate desensitization, signaling, and endocytosis. *Proc. Natl. Acad. Sci.* 114, 2562–2567.
- Carpenter, B., Nehmé, R., Warne, T., Leslie, A.G.W., Tate, C.G., 2017. Europe PMC Funders Group Structure of the adenosine A 2A receptor bound to an engineered G protein 536, 104–107.
- Carpino, L., Han, G., 1973. Correction. The 9-Fluorenylmethoxycarbonyl Amino-Protecting Group. *J. Org. Chem.* 38, 4218–4218.
- Carpino, L.A., 1987. The 9-Fluorenylmethoxycarbonyl Family of Base-Sensitive Amino-Protecting Groups. *Acc. Chem. Res.* 20, 401–407.
- Carpino, L.A., Han, G.Y., 1970. The 9-Fluorenylmethoxycarbonyl Function, a New Base-Sensitive Amino-Protecting Group. *J. Am. Chem. Soc.* 92, 5748–5749.
- Castan, I., Valet, P., Larrouy, D., Voisin, T., Remaury, A., Daviaud, D., Laburthe, M., Lafontan, M., 1993. Distribution of PYY receptors in human fat cells: an antilipolytic system alongside the alpha 2-adrenergic system. *Am. J. Physiol.* 265, E74-80.
- Castañeda, T.R., Tong, J., Datta, R., Culler, M., Tschöp, M.H., 2010. Ghrelin in the regulation of body weight and metabolism. *Front. Neuroendocrinol.* 31, 44–60.
- Chandarana, K., Drew, M.E., Emmanuel, J., Karra, E., Gelegen, C., Chan, P., Cron, N.J., Batterham, R.L., 2009. Subject Standardization, Acclimatization, and Sample Processing Affect Gut Hormone Levels and Appetite in Humans. *Gastroenterology* 136, 2115–2126.
- Chandrudu, S., Simerska, P., Toth, I., 2013. Chemical methods for peptide and protein production. *Molecules* 18, 4373–4388.

- Charlton, S.J., Vauquelin, G., 2010. Elusive equilibrium: The challenge of interpreting receptor pharmacology using calcium assays. *Br. J. Pharmacol.* 161, 1250–1265.
- Chen, Y., Müller, J.D., So, P.T., Gratton, E., 1999. The photon counting histogram in fluorescence fluctuation spectroscopy. *Biophys. J.* 77, 553–67.
- Cheng, Y., Prusoff, W.H., 1973. Relationship between the inhibition constant (K_1) and the concentration of inhibitor which causes 50 per cent inhibition (I_{50}) of an enzymatic reaction. *Biochem. Pharmacol.* 22, 3099–108.
- Chepurny, O.G., Bonaccorso, R.L., Leech, C.A., Wöllert, T., Langford, G.M., Schwede, F., Roth, C.L., Doyle, R.P., Holz, G.G., 2018. Chimeric peptide EP45 as a dual agonist at GLP-1 and NPY2R receptors. *Sci. Rep.* 8, 1–14.
- Cherezov, V., Rosenbaum, D.M., Hanson, M. a, Søren, G.F., Thian, F.S., Kobilka, T.S., Choi, H., Kuhn, P., Weis, I., Kobilka, B.K., Stevens, R.C., 2007. High resolution crystal structure of an engineered human beta2-adrenergic G protein-coupled receptor. *Science.* 318, 1258–1265.
- Chien, E.Y.T., Liu, W., Zhao, Q., Katritch, V., Han, G.W., Michael, a, Shi, L., Newman, A.H., Javitch, J. a, Cherezov, V., Stevens, R.C., 2011. Structure of the human dopamine D3 receptor in complex with a D2/D3 selective antagonist. *Science.* 330, 1091–1095.
- Chowdhury, T.A., Wright, R., Charlton, M., 2014. Insulin for the uninitiated. *Clin. Med. J. R. Coll. Physicians London* 14, 623–629.
- Cichocka, E., Wietchy, A., Nabrdalik, K., Gumprecht, J., 2016. Insulin therapy - new directions of research. *Endokrynol. Pol.* 67, 314–24.
- Clark, A.J., 1933. The Mode of Action of Drugs on Cells. *Nature* 132, 695–695.
- Cone, R.D., 2015. Melanocortin System 27, 736–749.
- Considine, R. V, Sinha, M.K., Heiman, M.L., Kriauciunas, A., Stephens, T.W., Nyce, M.R., Ohannesian, J.P., Marco, C.C., McKee, L.J., Bauer, T.L., 1996. Serum immunoreactive-leptin concentrations in normal-weight and obese humans. *N. Engl. J. Med.* 334, 292–5.
- Corbani, M., Marir, R., Trueba, M., Chafai, M., Vincent, A., Borie, A.M., Desarménien, M.G., Ueta, Y., Tomboly, C., Olma, A., Manning, M., Guillon, G., 2018. Neuroanatomical distribution and function of the vasopressin V1Breceptor in the rat brain deciphered using specific fluorescent ligands. *Gen. Comp. Endocrinol.* 258, 15–32.
- Cordeaux, Y., Briddon, S.J., Alexander, S.P.H., Kellam, B., Hill, S.J., 2008. Agonist-occupied A3 adenosine receptors exist within heterogeneous complexes in membrane microdomains of individual living cells. *FASEB J.* 22, 850–60.

- Corriden, R., Kilpatrick, L.E., Kellam, B., Briddon, S.J., Hill, S.J., 2014. Kinetic analysis of antagonist-occupied adenosine-A3 receptors within membrane microdomains of individual cells provides evidence of receptor dimerization and allostereism. *FASEB J.* 28, 4211–4222.
- Courcoulas, A.P., Yanovski, S.Z., Bonds, D., Eggerman, T.I., Horlick, M., Staten, M.A., Arterburn, D.E. 2014. Long-term outcomes of bariatric surgery: a National Institutes of Health symposium. *JAMA Surgery.* 149, 1323-9.
- Cowley, D.J., Hoflack, J.M., Pelton, J.T., Saudek, V., 1992. Structure of neuropeptide Y dimer in solution. *Eur. J. Biochem.* 205, 1099–106.
- Cowley, M.A., Smith, R.G., Diano, S., Tschöp, M., Pronchuk, N., Grove, K.L., Strasburger, C.J., Bidlingmaier, M., Esterman, M., Heiman, M.L., Garcia-Segura, L.M., Nillni, E.A., Mendez, P., Low, M.J., Sotonyi, P., Friedman, J.M., Liu, H., Pinto, S., Colmers, W.F., Cone, R.D., Horvath, T.L., 2003. The distribution and mechanism of action of ghrelin in the CNS demonstrates a novel hypothalamic circuit regulating energy homeostasis. *Neuron* 37, 649–661.
- Cox, H.M., 2007. Neuropeptide Y receptors; antiseecretory control of intestinal epithelial function. *Auton. Neurosci. Basic Clin.* 133, 76–85.
- Cox, H.M., Pollock, E.L., Tough, I.R., Herzog, H., 2001a. Multiple Y receptors mediate pancreatic polypeptide responses in mouse colon mucosa. *Peptides* 22, 445–452.
- Daniels, A.J., Matthews, J.E., Slepetis, R.J., Jansen, M., Viveros, O.H., Tadeballi, A., Harrington, W., Heyer, D., Landavazo, A., Leban, J.J., Spaltenstein, A., 1995. High-affinity neuropeptide Y receptor antagonists. *Proc. Natl. Acad. Sci. U. S. A.* 92, 9067–71.
- Dark, J., Pelz, K.M., 2008. NPY Y1 receptor antagonist prevents NPY-induced torpor-like hypothermia in cold-acclimated Siberian hamsters. *Am. J. Physiol. Regul. Integr. Comp. Physiol.* 294, R236-45.
- Date, Y., 2012. Ghrelin and the Vagus Nerve, 1st ed, Ghrelin. Elsevier Inc.
- Davey, A.E., Leach, K., Valant, C., Conigrave, A.D., Sexton, P.M., Christopoulos, A., 2012. Positive and negative allosteric modulators promote biased signaling at the calcium-sensing receptor. *Endocrinology* 153, 1232–1241.
- De Francesco, E.M., Sotgia, F., Clarke, R.B., Lisanti, M.P., Maggiolini, M., 2017. G Protein-Coupled Receptors at the Crossroad between Physiologic and Pathologic Angiogenesis: Old Paradigms and Emerging Concepts. *Int. J. Mol. Sci.* 18.
- Decressac, M., Barker, R.A., 2012. Neuropeptide Y and its role in CNS disease and repair. *Exp. Neurol.* 238, 265–272.
- Dessy, C., Kelly, R. a, Balligand, J.L., Feron, O., 2000. Dynamin mediates caveolar sequestration of muscarinic cholinergic receptors and

alteration in NO signaling. *EMBO J.* 19, 4272–4280.

- Di Marzo, V., Goparaju, S.K., Wang, L., Liu, J., Bátkai, S., Járαι, Z., Fezza, F., Miura, G.I., Palmiter, R.D., Sugiura, T., Kunos, G., 2001. Leptin-regulated endocannabinoids are involved in maintaining food intake. *Nature* 410, 822–825.
- Dias, S., Paredes, S., Ribeiro, L., 2018. Drugs Involved in Dyslipidemia and Obesity Treatment: Focus on Adipose Tissue. *Int. J. Endocrinol.* 2018, [eCollection].
- Diekmann, S., Hoischen, C., 2014. Biomolecular dynamics and binding studies in the living cell. *Phys. Life Rev.* 11, 1–30.
- Dijkman, P.M., Castell, O.K., Goddard, A.D., Munoz-Garcia, J.C., De Graaf, C., Wallace, M.I., Watts, A., 2018. Dynamic tuneable G protein-coupled receptor monomer-dimer populations. *Nat. Commun.* 9, 1710-1724
- Dinger, M.C., Bader, J.E., Kobor, A.D., Kretzschmar, A.K., Beck-Sickinger, A.G., 2003. Homodimerization of neuropeptide y receptors investigated by fluorescence resonance energy transfer in living cells. *J. Biol. Chem.* 278, 10562–71.
- Dixon, A.S., Schwinn, M.K., Hall, M.P., Zimmerman, K., Otto, P., Lubben, T.H., Butler, B.L., Binkowski, B.F., MacHleidt, T., Kirkland, T.A., Wood, M.G., Eggers, C.T., Encell, L.P., Wood, K. V., 2016. NanoLuc Complementation Reporter Optimized for Accurate Measurement of Protein Interactions in Cells. *ACS Chem. Biol.* 11, 400–408.
- Doods, H., Gaida, W., Wieland, H.A., Dollinger, H., Schnorrenberg, G., Esser, F., Engel, W., Eberlein, W., Rudolf, K., 1999. BII0246 : A selective and high affinity neuropeptide Y Y 2 receptor antagonist 1998–2000.
- Doods, H.N., Wienen, W., Entzeroth, M., Rudolf, K., Eberlein, W., Engel, W., Wieland, H.A., 1995. Pharmacological characterization of the selective nonpeptide neuropeptide Y Y1 receptor antagonist BIBP 3226. *J Pharmacol Exp Ther* 275, 136–142.
- Doré, A.S., Robertson, N., Errey, J.C., Ng, I., Hollenstein, K., Tehan, B., Hurrell, E., Bennett, K., Congreve, M., Magnani, F., Tate, C.G., Weir, M., Marshall, F.H., 2011. Structure of the adenosine A(2A) receptor in complex with ZM241385 and the xanthines XAC and caffeine. *Structure* 19, 1283–93.
- Dorsch, S., Klotz, K.-N., Engelhardt, S., Lohse, M.J., Bünemann, M., 2009. Analysis of receptor oligomerization by FRAP microscopy. *Nat. Methods* 6, 225–30.
- Draper-Joyce, C.J., Khoshouei, M., Thal, D.M., Liang, Y.-L., Nguyen, A.T.N., Furness, S.G.B., Venugopal, H., Baltos, J.-A., Plitzko, J.M., Danev, R., Baumeister, W., May, L.T., Wootten, D., Sexton, P.M., Glukhova, A., Christopoulos, A., 2018. Structure of the adenosine-bound human adenosine A1 receptor–Gi complex. *Nature* 558, 559–563.

- Dror, R.O., Arlow, D.H., Maragakis, P., Mildorf, T.J., Pan, A.C., Xu, H., Borhani, D.W., Shaw, D.E., 2011. Activation mechanism of the β_2 -adrenergic receptor. *Proc. Natl. Acad. Sci. USA* 108, 18684–18689.
- Dubinsky, M.C., Fleshner, P.P., 2003. Treatment of Crohn's Disease of Inflammatory, Stenotic, and Fistulizing Phenotypes. *Curr. Treat. Options Gastroenterol.* 6, 183–200.
- Duc, N.M., Kim, H.R., Chung, K.Y., 2015. Structural mechanism of G protein activation by G protein-coupled receptor. *Eur. J. Pharmacol.* 763, 214–222.
- Dumont, Y., Jacques, D., Bouchard, P., Quirion, R., 1998. Species differences in the expression and distribution of the neuropeptide Y Y1, Y2, Y4, and Y5 receptors in rodents, guinea pig, and primates brains. *J. Comp. Neurol.* 402, 372–384.
- Dumont, Y., Moyse, E., Fournier, A., Quirion, R., 2007. Distribution of peripherally injected peptide YY ([125I] PYY (3-36)) and pancreatic polypeptide ([125I] hPP) in the CNS: enrichment in the area postrema. *J. Mol. Neurosci.* 33, 294–304.
- Dumont, Y., Quirion, R., 2000. [125I]-GR231118: a high affinity radioligand to investigate neuropeptide Y Y1 and Y4 receptors. *Br. J. Pharmacol.* 129, 37–46.
- Edvinsson, L., Haanes, K.A., Warfvinge, K., Krause, D.N., 2018. CGRP as the target of new migraine therapies - successful translation from bench to clinic. *Nat. Rev. Neurol.* 14, 338–350.
- Eggeling, C., Widengren, J., Rigler, R., Seidel, C. a, 1998. Photobleaching of Fluorescent Dyes under Conditions Used for Single-Molecule Detection: Evidence of Two-Step Photolysis. *Anal. Chem.* 70, 2651–2659.
- Ekblad, E., Sundler, F., 2002. Distribution of pancreatic polypeptide and peptide YY. *Peptides* 23, 251–261.
- Elson, E.L., 2004. Quick tour of fluorescence correlation spectroscopy from its inception. *J. Biomed. Opt.* 9, 857–864.
- Erdélyi, M., Gogoll, A., 2002. Rapid Microwave-Assisted Solid Phase Peptide Synthesis. *Synthesis*. 11, 1592–1596.
- Ergin, E., Dogan, A., Parmaksız, M., Elcin, E., Elcin, Y.M., 2016. Time-Resolved Fluorescence Resonance Energy Transfer [TR-FRET] Assays for Biochemical Processes. *Current Pharmaceutical Biotechnology.* 17, 1-9.
- Erickson, J.C., Clegg, K.E., Palmiter, R.D., 1996. Sensitivity to leptin and susceptibility to seizures of mice lacking neuropeptide Y. *Nature* 381, 415-421
- Eriksson, H., Berglund, M.M., Holmberg, S.K., Kahl, U., Gehlert, D.R., Larhammar, D., 1998. The cloned guinea pig pancreatic polypeptide

receptor Y4 resembles more the human Y4 than does the rat Y4. *Regul. Pept.* 75–76, 29–37.

- Erondy, N., Gantz, I., Musser, B., Suryawanshi, S., Mallick, M., Addy, C., Cote, J., Bray, G., Fujioka, K., Bays, H., Hollander, P., Sanabria-Bohórquez, S.M., Eng, W., Långström, B., Hargreaves, R.J., Burns, H.D., Kanatani, A., Fukami, T., MacNeil, D.J., Gottesdiener, K.M., Amatruda, J.M., Kaufman, K.D., Heymsfield, S.B., 2006. Neuropeptide Y5 receptor antagonism does not induce clinically meaningful weight loss in overweight and obese adults. *Cell Metab.* 4, 275–82.
- Estes, A.M., Wong, Y.Y., Parker, M.S., Sallee, F.R., Balasubramaniam, A., Parker, S.L., 2008. Neuropeptide Y (NPY) Y2 receptors of rabbit kidney cortex are largely dimeric. *Regul. Pept.* 150, 88–94.
- Evron, T., Daigle, T.L., Caron, M.G., 2012. GRK2: multiple roles beyond G protein-coupled receptor desensitization. *Trends Pharmacol Sci.* 33, 154–164.
- Fan, Q.R., Hendrickson, W.A., 2005. Structure of human follicle-stimulating hormone in complex with its receptor. *Nature* 433, 269–277.
- Fang, P.-H., Yu, M., Ma, Y.-P., Li, J., Sui, Y.-M., Shi, M.-Y., 2011. Central nervous system regulation of food intake and energy expenditure: role of galanin-mediated feeding behavior. *Neurosci. Bull.* 27, 407–412.
- Farooqi, I.S., Keogh, J.M., Yeo, G.S.H., Lank, E.J., Cheetham, T., O’Rahilly, S., 2003. Clinical spectrum of obesity and mutations in the melanocortin 4 receptor gene. *N. Engl. J. Med.* 348, 1085–95.
- Farran, B., 2017. An update on the physiological and therapeutic relevance of GPCR oligomers. *Pharmacol. Res.* 117, 303–327.
- Feinstein, T.N., Wehbi, V.L., Ardura, J.A., Wheeler, D.S., Ferrandon, S., Gardella, T.J., Vilardaga, J., 2011. Retromer terminates the generation of cAMP by internalized PTH receptors. *Nat. Chem. Biol.* 7, 278–84.
- Felce, J.H., Latty, S.L., Knox, R.G., Mattick, S.R., Lui, Y., Lee, S.F., Klenerman, D., Davis, S.J., 2017. Receptor Quaternary Organization Explains G Protein-Coupled Receptor Family Structure. *Cell Rep.* 20, 2654–2665.
- Féférou, M., Nicolas, J.P., Rodriguez, M., Beauverger, P., Galizzi, J.P., Boutin, J.A., Duhault, J., 1999. NPY receptor subtype in the rabbit isolated ileum. *Br. J. Pharmacol.* 127, 795–801.
- Feng, W., Song, Z.H., 2003. Effects of D3.49A, R3.50A, and A6.34E mutations on ligand binding and activation of the cannabinoid-2 (CB2) receptor. *Biochem. Pharmacol.* 65, 1077–1085.
- Ferré, S., Casadó, V., Devi, L.A., Filizola, M., Jockers, R., Lohse, M.J., Milligan, G., Pin, J., 2014. G Protein – Coupled Receptor Oligomerization Revisited : Functional and Pharmacological Perspectives. 66, 413–434.

- Fertig, B.A., Baillie, G.S., 2018. PDE4-Mediated cAMP Signalling. *J. Cardiovasc. Dev. Dis.* 5, 8-22.
- Fetissov, S.O., Kopp, J., Hökfelt, T., 2004. Distribution of NPY receptors in the hypothalamus. *Neuropeptides* 38, 175–188.
- Foord, S.M., Bonner, T.O.M.I., Neubig, R.R., Rosser, E.M., Pin, J., Davenport, A.P., Spedding, M., Harmar, A.J., 2005. International Union of Pharmacology. XLVI. G Protein-Coupled Receptor List. *Pharmacol. Rev.* 57, 279–288.
- Fosgerau, K., Hoffmann, T., 2015. Peptide therapeutics: Current status and future directions. *Drug Discov. Today* 20, 122–128.
- Fredriksson, R., 2003. The G-Protein-Coupled Receptors in the Human Genome Form Five Main Families. Phylogenetic Analysis, Paralogon Groups, and Fingerprints. *Mol. Pharmacol.* 63, 1256–1272.
- Friedman, J.M., 2004. Modern science versus the stigma of obesity. *Nat. Med.* 10, 563–569.
- Fritze, O., Filipek, S., Kuksa, V., Palczewski, K., Hofmann, K.P., Ernst, O.P., 2003. Role of the conserved NPxxY(x)5,6F motif in the rhodopsin ground state and during activation. *Proc. Natl. Acad. Sci.* 100, 2290–2295.
- Fruitwala, S., El-Naccache, D.W., Chang, T.L., 2018. Multifaceted immune functions of human defensins and underlying mechanisms. *Semin. Cell Dev. Biol.* [Epub ahead of print].
- Fuhlendorff, J., Gether, U., Aakerlund, L., Langeland-Johansen, N., Thøgersen, H., Melberg, S.G., Olsen, U.B., Thastrup, O., Schwartz, T.W., 1990. [Leu31, Pro34]neuropeptide Y: a specific Y1 receptor agonist. *Proc. Natl. Acad. Sci. U. S. A.* 87, 182–6.
- Fulmer, T., 2008. A gut feeling. *Sci. Exch.* 1, 347.
- Gaddum, J., 1937. The quantitative effects of antagonistic drugs. *J. Physiol.* 89:, 7–9P.
- García-Nafria, J., Lee, Y., Bai, X., Carpenter, B., Tate, C.G., 2018a. Cryo-EM structure of the adenosine A2A receptor coupled to an engineered heterotrimeric G protein. *Elife.* 7, [eCollection].
- García-Nafria, J., Nehmé, R., Edwards, P.C., Tate, C.G., 2018b. Cryo-EM structure of the serotonin 5-HT1B receptor coupled to heterotrimeric Go. *Nature* 558, 620–623.
- Garg, S.K., Maurer, H., Reed, K., Selagamsetty, R., 2014. Diabetes and cancer: two diseases with obesity as a common risk factor. *Diabetes Obes Metab* 16, 97–110.
- Garzilli, I., Itzkovitz, S., 2018. Design principles of the paradoxical feedback between pancreatic alpha and beta cells. *Sci. Rep.* 8, 1–12.

- Gehlert, D.R., 1994. Subtypes of receptors for neuropeptide Y: implications for the targeting of therapeutics. *Life Sci.* 55, 551–62.
- Gehlert, D.R., Beavers, L.S., Johnson, D., Gackenheimer, S.L., Schober, D.A., Gadski, R.A., 1996a. Expression cloning of a human brain neuropeptide Y Y2 receptor. *Mol. Pharmacol.* 49, 224–8.
- Gehlert, D.R., Gackenheimer, S.L., Schober, D.A., Beavers, L., Gadski, R., Burnett, J.P., Mayne, N., Lundell, I., Larhammar, D., 1996b. The neuropeptide Y Y1 receptor selective radioligand, [125I][Leu31,Pro34]peptide YY, is also a high affinity radioligand for human pancreatic polypeptide 1 receptors. *Eur. J. Pharmacol.* 318, 485–90.
- Gehlert, D.R., Schober, D.A., Gackenheimer, S.L., Beavers, L., Gadski, R., Lundell, I., Larhammar, D., 1997. [125I]Leu31, Pro34-PYY is a high affinity radioligand for rat PP1/Y4 and Y1 receptors: Evidence for heterogeneity in pancreatic polypeptide receptors. *Peptides* 18, 397–401.
- Gehlert, D.R., Schober, D.A., Morin, M., Berglund, M.M., 2007. Co-expression of neuropeptide Y Y1 and Y5 receptors results in heterodimerization and altered functional properties. *Biochem. Pharmacol.* 74, 1652–64.
- George, M., Rajaram, M., Shanmugam, E., 2014. New and emerging drug molecules against obesity. *J. Cardiovasc. Pharmacol. Ther.* 19, 65–76.
- Gerald, C., Walker, M.W., Criscione, L., Gustafson, E.L., Batzl-Hartmann, C., Smith, K.E., Vaysse, P., Durkin, M.M., Laz, T.M., Linemeyer, D.L., Schaffhauser, A.O., Whitebread, S., Hofbauer, K.G., Taber, R.I., Branchek, T. a, Weinshank, R.L., 1996. A receptor subtype involved in neuropeptide-Y-induced food intake. *Nature.* 382, 168-171
- Gerald, C., Walker, M.W., Vaysse, P.J., He, C., Branchek, T. a, Weinshank, R.L., 1995. Expression cloning and pharmacological characterization of a human hippocampal neuropeptide Y/peptide YY Y2 receptor subtype. *J. Biol. Chem.* 270, 26758–61.
- Germain, N., Minnion, J.S., Tan, T., Shillito, J., Gibbard, C., Ghatei, M., Bloom, S., 2013. Analogs of pancreatic polypeptide and peptide YY with a locked PP-fold structure are biologically active. *Peptides* 39, 6–10.
- Gidon, A., Al-Bataineh, M.M., Jean-Alphonse, F.G., Stevenson, H.P., Watanabe, T., Louet, C., Khatri, A., Calero, G., Pastor-Soler, N.M., Gardella, T.J., Vilardaga, J.-P., 2014. Endosomal GPCR signaling turned off by negative feedback actions of PKA and v-ATPase. *Nat. Chem. Biol.* 10, 707–9.
- Glass, M., Govindpani, K., Furkert, D.P., Hurst, D.P., Reggio, P.H., Flanagan, J.U., 2016. One for the Price of Two—Are Bivalent Ligands Targeting Cannabinoid Receptor Dimers Capable of Simultaneously Binding to both Receptors? *Trends Pharmacol. Sci.* 37, 353–363.

- Glover, I.D., Barlow, D.J., Pitts, J.E., Wood, S.P., Tickle, I.J., Blundell, T.L., Tatemoto, K., Kimmel, J.R., Wollmer, A., Strassburger, W., 1984. Conformational studies on the pancreatic polypeptide hormone family. *Eur. J. Biochem.* 142, 379–85.
- Golebiewska, U., Johnston, J.M., Devi, L., Filizola, M., Scarlata, S., 2011. Differential response to morphine of the oligomeric state of μ -opioid in the presence of μ -opioid receptors. *Biochemistry* 50, 2829–2837.
- Gomes, I., Ayoub, M.A., Fujita, W., Jaeger, W.C., Pflieger, K.D.G., Devi, L.A., 2016. G Protein-Coupled Receptor Heteromers. *Annu. Rev. Pharmacol. Toxicol.* 56, 403–25.
- Goodman Jr, O.B., Krupnick, J.G., Santini, F., Gurevich, V. V, Penn, R.B., Gagnon, A.W., Keen, J.H., Benovic, J.L., 1996. β -Arrestin acts as a clathrin adaptor in endocytosis of the β 2-adrenergic receptor. *Nature* 383, 447.
- Grace, C.R.R., Perrin, M.H., DiGruccio, M.R., Miller, C.L., Rivier, J.E., Vale, W.W., Riek, R., 2004. NMR structure and peptide hormone binding site of the first extracellular domain of a type B1 G protein-coupled receptor. *Proc. Natl. Acad. Sci.* 101, 12836–12841.
- Grammatopoulos, D.K., 2017. Regulation of G-protein coupled receptor signalling underpinning neurobiology of mood disorders and depression. *Mol. Cell. Endocrinol.* 449, 82–89.
- Grandt, D., Dahms, P., Schimiczek, M., Eysselein, V.E., Reeve, J.R.J., Mentlein, R., 1993. [Proteolytic processing by dipeptidyl aminopeptidase IV generates receptor selectivity for peptide YY (PYY)]. *Med. Klin. (Munich)*. 88, 143–145.
- Granier, S., Manglik, A., Kruse, A.C., Kobilka, T.S., Thian, F.S., Weis, W.I., Kobilka, B.K., 2012. Structure of the δ -opioid receptor bound to naltrindole. *Nature* 485, 400.
- Greenway, F.L., Whitehouse, M.J., Guttadauria, M., Anderson, J.W., Atkinson, R.L., Fujioka, K., Gadde, K.M., Gupta, A.K., O’Neil, P., Schumacher, D., Smith, D., Dunayevich, E., Tollefson, G.D., Weber, E., Cowley, M.A., 2009. Rational design of a combination medication for the treatment of obesity. *Obesity* 17, 30–39.
- Gregor, P., Feng, Y., DeCarr, L.B., Cornfield, L.J., McCaleb, M.L., 1996. Molecular characterization of a second mouse pancreatic polypeptide receptor and its inactivated human homologue. *J. Biol. Chem.* 271, 27776–27781.
- Gregory, K.J., Dong, E.N., Meiler, J., Conn, P.J., 2011. Allosteric modulation of metabotropic glutamate receptors: Structural insights and therapeutic potential. *Neuropharmacology* 60, 66–81.
- Grigoryan, A., Eisenberg, A.S., Juszczak, L.J., 2017. PHOXI: A High Quantum Yield, Solvent-Sensitive Blue Fluorescent 5-Hydroxytryptophan

Derivative Synthesized within Ten Minutes under Aqueous, Ambient Conditions. *J. Phys. Chem. B* 121, 7256–7266.

- Gropp, E., Shanabrough, M., Borok, E., Xu, A.W., Janoschek, R., Buch, T., Plum, L., Balthasar, N., Hampel, B., Waisman, A., Barsh, G.S., Horvath, T.L., Brüning, J.C., 2005. Agouti-related peptide-expressing neurons are mandatory for feeding. *Nat. Neurosci.* 8, 1289–1291.
- Grundlingh, J., Dargan, P.I., El-Zanfaly, M., Wood, D.M., 2011. 2,4-Dinitrophenol (DNP): A Weight Loss Agent with Significant Acute Toxicity and Risk of Death. *J. Med. Toxicol.* 7, 205–212.
- Guérin, B., Ait-Mohand, S., Tremblay, M.C., Dumulon-Perreault, V., Fournier, P., Bénard, F., 2010a. Total solid-phase synthesis of NOTA-functionalized peptides for PET imaging. *Org. Lett.* 12, 280–283.
- Guérin, B., Dumulon-perreault, V., Tremblay, M., Ait-mohand, S., Fournier, P., Dubuc, C., Authier, S., Bénard, F., 2010b. Bioorganic & Medicinal Chemistry Letters [Lys (DOTA) 4] BVD15 , a novel and potent neuropeptide Y analog designed for Y 1 receptor-targeted breast tumor imaging. *Bioorg. Med. Chem. Lett.* 20, 950–953.
- Guo, W., Urizar, E., Kralikova, M., Mobarec, J.C., Shi, L., Filizola, M., Javitch, J.A., 2008. Dopamine D2 receptors form higher order oligomers at physiological expression levels. *EMBO J.* 27, 2293–304.
- Gurevich, V. V, Gurevich, E. V, 2008. How and why do GPCRs dimerize? *Trends Pharmacol. Sci.* 29, 234–40.
- Haga, K., Kruse, A.C.A., Asada, H., Yurugi-Kobayashi, T., Shiroishi, M., Zhang, C., Weis, W.I., Okada, T., Kobilka, B.K., Haga, T., Kobayashi, T., 2012. Structure of the human M2 muscarinic acetylcholine receptor bound to an antagonist. *Nature* 482, 547–551.
- Hagan, M.M., Rushing, P.A., Schwartz, M.W., Yagaloff, K.A., Burn, P., Woods, S.C., Seeley, R.J., 1999. Role of the CNS melanocortin system in the response to overfeeding. *J. Neurosci.* 19, 2362–7.
- Hanauer, S.B., 2003. Crohn's disease: Step up or top down therapy. *Bailliere's Best Pract. Res. Clin. Gastroenterol.* 17, 131–137.
- Hanson, M.A., Roth, C.B., Jo, E., Griffith, M.T., Scott, F.L., Reinhart, G., Desale, H., Clemons, B., Cahalan, S.M., Schuerer, S.C., Sanna, M.G., Han, G.W., Kuhn, P., Rosen, H., Stevens, R.C., 2012. Crystal structure of a lipid G protein-coupled receptor. *Science* 335, 851–5.
- Haupts, U., Maiti, S., Schwille, P., Webb, W.W., 1998. Dynamics of fluorescence fluctuations in green fluorescent protein observed by fluorescence correlation spectroscopy. *Proc. Natl. Acad. Sci. U. S. A.* 95, 13573–13578.
- Heisler, L.K., Lam, D.D., 2017. An appetite for life: brain regulation of hunger and satiety. *Curr. Opin. Pharmacol.* 37, 100–106.

- Herrick-Davis, K., Grinde, E., Cowan, A., Mazurkiewicz, J.E., 2013. Fluorescence correlation spectroscopy analysis of serotonin, adrenergic, muscarinic, and dopamine receptor dimerization: the oligomer number puzzle. *Mol. Pharmacol.* 84, 630–42.
- Herrick-Davis, K., Grinde, E., Lindsley, T., Cowan, A., Mazurkiewicz, J.E., 2012. Oligomer size of the serotonin 5-hydroxytryptamine 2C (5-HT_{2C}) receptor revealed by fluorescence correlation spectroscopy with photon counting histogram analysis: Evidence for homodimers without monomers or tetramers. *J. Biol. Chem.* 287, 23604–23614.
- Herzog, H., Hort, Y.J., Shine, J., Selbie, L.A., 1993. Molecular cloning, characterization, and localization of the human homolog to the reported bovine NPY Y3 receptor: lack of NPY binding and activation. *DNA Cell Biol.* 12, 465–471.
- Hill, A. V, 1910. The possible effects of the aggregation of the molecules of haemoglobin on its dissociation curve. *J. Physiol.* 40, iv-vii.
- Hill, A. V, 1909. The mode of action of nicotine and curari, determined by the form of the contraction curve and the method of temperature coefficients. *J. Physiol* 39, 361–373.
- Hinshaw, J.E., 2012. Neuro-cognitive Mechanism of Imagining Future and Its Role in Suicide. *Annu. Rev. Cell. Dev. Biol.* 16, 483–519.
- Hoffman, J.A., Chance, R.E., 1983. Crystallization of bovine pancreatic polypeptide. *Biochem. Biophys. Res. Commun.* 116, 830–5.
- Hofmann, S., Maschauer, S., Kuwert, T., Beck-Sickinger, A.G., Prante, O., 2015. Synthesis and in vitro and in vivo evaluation of an 18f-labeled neuropeptide y analogue for imaging of breast cancer by pet. *Mol. Pharm.* 12, 1121–1130.
- Holliday, N.D., Lam, C., Tough, I.R., Cox, H.M., 2005. Role of the C terminus in neuropeptide Y Y1 receptor desensitization and internalization. *Mol. Pharmacol.* 67, 655–64.
- Holst, J.J., 2004. On the physiology of GIP and GLP-1. *Horm. Metab. Res.* 36, 747–754.
- Home, P.D., 2015. Plasma insulin profiles after subcutaneous injection: How close can we get to physiology in people with diabetes? *Diabetes, Obes. Metab.* 17, 1011–1020.
- Hood, C.A., Fuentes, G., Patel, H., Page, K., Menakuru, M., Park, J.H., 2008. Fast conventional Fmoc solid-phase peptide synthesis with HCTU. *J. Pept. Sci.* 14, 97–101.
- Horsnell, H., Baldock, P.A., 2016. Osteoblastic Actions of the Neuropeptide Y System to Regulate Bone and Energy Homeostasis. *Curr. Osteoporos. Rep.* 14, 26–31.

- Hsieh, Y.S., Chen, P.N., Yu, C.H., Kuo, D.Y., 2014. Central dopamine action modulates neuropeptide-controlled appetite via the hypothalamic PI3K/NF- κ B-dependent mechanism. *Genes, Brain Behav.* 13, 784–793.
- Hu, G.M., Mai, T.L., Chen, C.M., 2017. Visualizing the GPCR Network: Classification and Evolution. *Sci. Rep.* 7, 1–15.
- Huang, B., Perroud, T.D., Zare, R.N., 2004. Photon counting histogram: One-photon excitation. *ChemPhysChem* 5, 1523–1531.
- Huang, J., Chen, S., Zhang, J.J., Huang, X., 2013. Crystal structure of oligomeric β 1-adrenergic G protein-coupled receptors in ligand-free basal state. *Nat. Struct. Mol. Biol.* 20, 419–25.
- Huber, T., Sakmar, T.P., 2014. Chemical biology methods for investigating G protein-coupled receptor signaling. *Chem. Biol.* 21, 1224–1237.
- Hubner, H., Schellhorn, T., Gienger, M., Schaab, C., Kaindl, J., Leeb, L., Clark, T., Moller, D., Gmeiner, P., 2016. Structure-guided development of heterodimer-selective GPCR ligands. *Nat. Commun.* 7, 1–12.
- Humphrey, S.J., James, D.E., Mann, M., 2015. Protein Phosphorylation: A Major Switch Mechanism for Metabolic Regulation. *Trends Endocrinol. Metab.* 26, 676–687.
- Hutchings, C.J., Koglin, M., Olson, W.C., Marshall, F.H., 2017. Opportunities for therapeutic antibodies directed at G-protein-coupled receptors. *Nat. Rev. Drug Discov.* 16, 787–810.
- Hyland, N.P., Cox, H.M., 2004. NPY-Like Peptides, Y Receptors and Gastrointestinal Function BT - Neuropeptide Y and Related Peptides. In: Michel, M.C. (Ed.), . Springer Berlin Heidelberg, Berlin, Heidelberg, pp. 389–408.
- Inoue, Y., Qin, B., Poti, J., Sokol, R., Gordon-Larsen, P., 2018. Epidemiology of Obesity in Adults: Latest Trends. *Current obesity reports.* 7, 276–288.
- Iwasaki, Y., Kakei, M., Nakabayashi, H., Ayush, E.A., Hirano-Kodaira, M., Maejima, Y., Yada, T., 2013. Pancreatic polypeptide and peptide YY3-36 induce Ca²⁺ signaling in nodose ganglion neurons. *Neuropeptides* 47, 19–23.
- Janse, D.M., Crosas, B., Finley, D., Church, G.M., 2004. Localization to the proteasome is sufficient for degradation. *J. Biol. Chem.* 279, 21415–21420.
- Jaradat, D.M.M., 2018. Thirteen decades of peptide synthesis: key developments in solid phase peptide synthesis and amide bond formation utilized in peptide ligation. *Amino Acids* 50, 39–68.
- Jazayeri, A., Rappas, M., Brown, A.J.H., Kean, J., Errey, J.C., Robertson, N.J., Fiez-Vandal, C., Andrews, S.P., Congreve, M., Bortolato, A., Mason, J.S., Baig, A.H., Teobald, I., Doré, A.S., Weir, M., Cooke, R.M., Marshall, F.H.,

2017. Crystal structure of the GLP-1 receptor bound to a peptide agonist. *Nature* 546, 254–258.
- Jesudason, D.R., Monteiro, M.P., McGowan, B.M.C., Neary, N.M., Park, A.J., Philippou, E., Small, C.J., Frost, G.S., Ghatei, M.A., Bloom, S.R., 2007. Low-dose pancreatic polypeptide inhibits food intake in man. *Br. J. Nutr.* 97, 426–429.
- Jin, X., Zhu, D.D., Chen, B.Z., Ashfaq, M., Guo, X.D., 2018. Insulin delivery systems combined with microneedle technology. *Adv. Drug Deliv. Rev.* 127, 119–137.
- Jois, S.D.S., Nagarajarao, L.M., Prabhakaran, M., Balasubramaniam, A., 2006. Modeling of neuropeptide receptors Y1, Y4, Y5, and docking studies with neuropeptide antagonist. *J. Biomol. Struct. Dyn.* 23, 497–508.
- Jordan, J., Astrup, A., Engeli, S., Narkiewicz, K., Day, W.W., Finer, N., 2014. Cardiovascular effects of phentermine and topiramate: A new drug combination for the treatment of obesity. *J. Hypertens.* 32, 1178–1188.
- Kaiser, A., Müller, P., Zellmann, T., Scheidt, H.A., Thomas, L., Bosse, M., Meier, R., Meiler, J., Huster, D., Beck-Sickinger, A.G., Schmidt, P., 2015. Unwinding of the C-Terminal Residues of Neuropeptide Y is critical for Y₂ Receptor Binding and Activation. *Angew. Chem. Int. Ed. Engl.* 54, 7446–9.
- Kamato, D., Mitra, P., Davis, F., Osman, N., Chaplin, R., Cabot, P.J., Afroz, R., Thomas, W., Zheng, W., Kaur, H., Brimble, M., Little, P.J., 2017. Gaq proteins: molecular pharmacology and therapeutic potential. *Cell. Mol. Life Sci.* 74, 1379–1390.
- Kanatani, a, Hata, M., Mashiko, S., Ishihara, a, Okamoto, O., Haga, Y., Ohe, T., Kanno, T., Murai, N., Ishii, Y., Fukuroda, T., Fukami, T., Ihara, M., 2001. A typical Y1 receptor regulates feeding behaviors: effects of a potent and selective Y1 antagonist, J-115814. *Mol. Pharmacol.* 59, 501–5.
- Kanatani, A., Kanno, T., Ishihara, A., Hata, M., Sakuraba, A., Tanaka, T., Tsuchiya, Y., Mase, T., Fukuroda, T., Fukami, T., Ihara, M., 1999. The novel neuropeptide YY1receptor antagonist J-104870: A potent feeding suppressant with oral bioavailability. *Biochem. Biophys. Res. Commun.* 266, 88–91.
- Kang, D.S., Tian, X., Benovic, J.L., 2014. Role of β -arrestins and arrestin domain-containing proteins in G protein-coupled receptor trafficking. *Curr. Opin. Cell Biol.* 27, 63–71.
- Kang, J., Kaczmarek, O., Liebscher, J., Dähne, L., 2010. Prevention of H-aggregates formation in Cy5 labeled macromolecules. *Int. J. Polym. Sci.* 2010, 1-7.
- Kanno, T., Kanatani, A., Keen, S.L.C., Arai-otsuki, S., Haga, Y., 2001. Different

- binding sites for the neuropeptide Y Y1 antagonists 1229U91 and J-104870 on human Y1 receptors 22, 405–413.
- Karimi Goftar, M., Moradi, K., Kor, N.M., 2014. Spectroscopic studies on aggregation phenomena of dyes. *Eur. J. Exp. Biol.* 4, 72–81.
- Kasai, R.S., Ito, S. V., Awane, R.M., Fujiwara, T.K., Kusumi, A., 2017. The Class-A GPCR Dopamine D2 Receptor Forms Transient Dimers Stabilized by Agonists: Detection by Single-Molecule Tracking. *Cell Biochem. Biophys.* 1–9.
- Kask, P., Palo, K., Ullmann, D., Gall, K., 1999. Fluorescence-intensity distribution analysis and its application in biomolecular detection technology. *Proc. Natl. Acad. Sci. U. S. A.* 96, 13756–13761.
- Katritch, V., Cherezov, V., Stevens, R.C., 2012. Diversity and modularity of G protein-coupled receptor structures. *Trends Pharmacol. Sci.* 33, 17–27.
- Katritch, V., Reynolds, K.A., Cherezov, V., Hanson, M.A., Roth, C.B., Yeager, M., Abagyan, R., 2010. Analysis of full and partial agonists binding to beta2-adrenergic receptor suggests a role of transmembrane helix V in agonist-specific conformational changes. *J. Mol. Recognit.* 22, 307–18.
- Keire, D.A., Mannon, P., Kobayashi, M., Walsh, J.H., Solomon, T.E., Reeve, J.R., 2000. Primary structures of PYY, [Pro34]PYY, and PYY-(3–36) confer different conformations and receptor selectivity. *Am. J. Physiol. Liver Physiol.* 279, G126–G131.
- Keller, M., Erdmann, D., Pop, N., Pluym, N., Teng, S., Bernhardt, G., Buschauer, A., 2011. Red-fluorescent argininamide-type NPY Y1 receptor antagonists as pharmacological tools. *Bioorg. Med. Chem.* 19, 2859–78.
- Keller, M., Kaske, M., Holzammer, T., Bernhardt, G., Buschauer, A., 2013. Dimeric argininamide-type neuropeptide y receptor antagonists: Chiral discrimination between Y1 and Y4 receptors. *Bioorganic Med. Chem.* 21, 6303–6322.
- Keller, M., Schindler, L., Bernhardt, G., Buschauer, A., 2015. Toward Labeled Argininamide-Type NPY Y1 Receptor Antagonists: Identification of a Favorable Propionylation Site in BIBO3304. *Arch. Pharm. (Weinheim)*. 348, 390–8.
- Kelly, E., Bailey, C.P., Henderson, G., 2008. Agonist-selective mechanisms of GPCR desensitization. *Br. J. Pharmacol.* 153, 379–388.
- Kenakin, T., Williams, M., 2014. Defining and characterizing drug/compound function. *Biochem. Pharmacol.* 87, 40–63.
- Kennedy, J.E., Marchese, A., 2015. Regulation of GPCR Trafficking by Ubiquitin. *Prog. Mol. Biol. Transl. Sci.* 132, 15–38.
- Kent, S.B.H., 1988. Chemical Synthesis of Peptides and Proteins, *Ann. Rev. Biochem.* 57, 957–989.

- Kermani, M., Eliassi, A., 2012. Gastric acid secretion induced by paraventricular nucleus microinjection of orexin A is mediated through activation of neuropeptide Yergic system. *Neuroscience* 226, 81–88.
- Kerppola, T.K., 2013. Design of fusion proteins for bimolecular fluorescence complementation (BiFC). *Cold Spring Harb. Protoc.* 2013, 714–8.
- Kilpatrick, L.E., Briddon, S.J., Hill, S.J., Holliday, N.D., 2010. Quantitative analysis of neuropeptide Y receptor association with β -arrestin2 measured by bimolecular fluorescence complementation. *Br. J. Pharmacol.* 160, 892–906.
- Kilpatrick, L.E., Briddon, S.J., Holliday, N.D., 2012. Fluorescence correlation spectroscopy, combined with bimolecular fluorescence complementation, reveals the effects of β -arrestin complexes and endocytic targeting on the membrane mobility of neuropeptide Y receptors. *Biochim. Biophys. Acta* 1823, 1068–81.
- Kilpatrick, L.E., Friedman-Ohana, R., Alcobia, D.C., Riching, K., Peach, C.J., Wheal, A.J., Briddon, S.J., Robers, M.B., Zimmerman, K., Machleidt, T., Wood, K. V., Woolard, J., Hill, S.J., 2017. Real-time analysis of the binding of fluorescent VEGF165a to VEGFR2 in living cells: Effect of receptor tyrosine kinase inhibitors and fate of internalized agonist-receptor complexes. *Biochem. Pharmacol.* 136, 62–75.
- Kilpatrick, L.E., Hill, S.J., 2016. The use of fluorescence correlation spectroscopy to characterize the molecular mobility of fluorescently labelled G protein-coupled receptors. *Biochem. Soc. Trans.* 44, 624–9.
- Kilpatrick, L.E., Humphrys, L.J., Holliday, N.D., 2015. A G Protein Coupled Receptor Dimer Imaging Assay Reveals Selectively Modified Pharmacology of Neuropeptide Y Y1 / Y5 Receptor Heterodimers. *Mol. Pharmacol.* 87, 718–732.
- Kim, J.-H., Cho, E.-Y., Min, C., Park, J.H., Kim, K.-M., 2008. Characterization of functional roles of DRY motif in the 2nd intracellular loop of dopamine D2 and D3 receptors. *Arch. Pharm. Res.* 31, 474–481.
- Kim, K.-H., Seong, B.L., 2001. Peptide amidation: Production of peptide hormones in vivo and in vitro. *Biotechnol. Bioprocess Eng.* 6, 244–251.
- Kishimoto, Y., 2006. Endogenous Cannabinoid Signaling through the CB1 Receptor Is Essential for Cerebellum-Dependent Discrete Motor Learning. *J. Neurosci.* 26, 8829–8837.
- Klok, M.D., Jakobsdottir, S., Drent, M.L., 2007. The role of leptin and ghrelin in the regulation of food intake and body weight in humans: A review. *Obes. Rev.* 8, 21–34.
- Kobilka, B.K., Deupi, X., 2007. Conformational complexity of G-protein-coupled receptors. *Trends Pharmacol. Sci.* 28, 397–406.
- Koegler, F.H., Enriori, P.J., Billes, S.K., Takahashi, D.L., Martin, M.S., Clark, R.L.,

- Evans, A.E., Grove, K.L., Cameron, J.L., Cowley, M. a., 2005. Peptide YY(3-36) inhibits morning, but not evening, food intake and decreases body weight in rhesus macaques. *Diabetes* 54, 3198–3204.
- Kohler, J.J., Bertozzi, C.R., 2003. Regulating cell surface glycosylation by small molecule control of enzyme localization. *Chem. Biol.* 10, 1303–11.
- Kojima, M., Hosoda, H., Date, Y., Nakazato, M., Matsuo, H., Kangawa, K., 1999. Ghrelin is a growth-hormone-releasing acylated peptide from stomach. *Nature* 402, 656–660.
- Kokare, D.M., Patole, A.M., Carta, A., Chopde, C.T., Subhedar, N.K., 2006. GABA receptors mediate orexin-A induced stimulation of food intake. *Neuropharmacology* 50, 16–24.
- Kola, B., Farkas, I., Christ-Crain, M., Wittmann, G., Lolli, F., Amin, F., Harvey-White, J., Liposits, Z., Kunos, G., Grossman, A.B., Fekete, C., Korbonits, M., 2008. The orexigenic effect of ghrelin is mediated through central activation of the endogenous cannabinoid system. *PLoS One*. 3, [eCollection]
- Koole, C., Pabreja, K., Savage, E.E., Wootten, D., Furness, S.G.B., Miller, L.J., Christopoulos, A., Sexton, P.M., 2013. Recent advances in understanding GLP-1R (glucagon-like peptide-1 receptor) function. *Biochem. Soc. Trans.* 41, 172–179.
- Kopinathan, A., Scammells, P.J., Lane, J.R., Capuano, B., 2016. Multivalent approaches and beyond: novel tools for the investigation of dopamine D2 receptor pharmacology. *Future Med. Chem.* 8, 1349–1372.
- Korczynska, M., Clark, M.J., Valant, C., Xu, J., Moo, E. Von, Albold, S., Weiss, D.R., Torosyan, H., Huang, W., Kruse, A.C., Lyda, B.R., May, L.T., Baltos, J.-A., Sexton, P.M., Kobilka, B.K., Christopoulos, A., Shoichet, B.K., Sunahara, R.K., 2018. Structure-based discovery of selective positive allosteric modulators of antagonists for the M₂ muscarinic acetylcholine receptor. *Proc. Natl. Acad. Sci.* 115, [Epub ahead of print].
- Kovac, S., Walker, M.C., 2013. Neuropeptides in epilepsy. *Neuropeptides* 47, 467–475.
- Kozer, N., Barua, D., Orchard, S., Nice, E.C., Burgess, A.W., Hlavacek, W.S., Clayton, A.H.A., 2013. Exploring higher-order EGFR oligomerisation and phosphorylation--a combined experimental and theoretical approach. *Mol. Biosyst.* 9, 1849–63.
- Krashes, M.J., Koda, S., Ye, C., Rogan, S.C., Adams, A.C., Cusher, D.S., Maratos-Flier, E., Roth, B.L., Lowell, B.B., 2011. Rapid, reversible activation of AgRP neurons drives feeding behavior in mice. *J. Clin. Invest.* 121, 1424–28.
- Kruse, A., Hu, J., Pan, A., Arlow, D., 2012. Structure and dynamics of the M3 muscarinic acetylcholine receptor. *Nature* 482, 552–556.

- Kuffer, A., Lakkaraju, A.K., Mogha, A., Petersen, S.C., Airich, K., Doucerain, C., Marpakwar, R., Bakirci, P., Senatore, A., Monnard, A., Schiavi, C., Nuvolone, M., Grosshans, B., Bassilana, F., Monk, K.R., Aguzzi, A., 2016. The prion protein is an agonistic ligand of the G protein-coupled receptor Gpr126/Adgrg6. *Nature* 536, 464–468.
- Kuhn, K.K., Ertl, T., Dukorn, S., Keller, M., Bernhardt, G., Reiser, O., Buschauer, A., 2016. High Affinity Agonists of the Neuropeptide Y (NPY) Y4 Receptor Derived from the C-Terminal Pentapeptide of Human Pancreatic Polypeptide (hPP): Synthesis, Stereochemical Discrimination, and Radiolabeling. *J. Med. Chem.* 59, 6045–6058.
- Kuhn, K.K., Littmann, T., Dukorn, S., Tanaka, M., Keller, M., Ozawa, T., Bernhardt, G., Buschauer, A., 2017. In Search of NPY Y4R Antagonists: Incorporation of Carbamoylated Arginine, Aza-Amino Acids, or d -Amino Acids into Oligopeptides Derived from the C-Termini of the Endogenous Agonists. *ACS Omega*. 2, 3616–3631.
- Kushwaha, R.N., Haq, W., Katti, S.B., 2014. Sixteen-years of clinically relevant dipeptidyl peptidase-IV (DPP-IV) inhibitors for treatment of type-2 diabetes: a perspective. *Curr. Med. Chem.* 21, 4013–4045.
- Lane, J.R., Sexton, P.M., Christopoulos, A., 2013. Bridging the gap: Bitopic ligands of G-protein-coupled receptors. *Trends Pharmacol. Sci.* 34, 59–66.
- Larhammar, D., 1996. Evolution of neuropeptide Y, peptide YY and pancreatic polypeptide. *Regul. Pept.* 62, 1–11.
- Larhammar, D., Blomqvist, A.G., Yee, F., Jazin, E., Yoo, H., Wahlested, C., 1992. Cloning and functional expression of a human neuropeptide Y/peptide YY receptor of the Y1 type. *J. Biol. Chem.* 267, 10935–10938.
- Larhammar, D., Salaneck, E., 2004. Molecular evolution of NPY receptor subtypes 38, 141–151.
- Larhammar, D., Wraith, A., Berglund, M.M., Holmberg, S.K.S., Lundell, I., 2001. Origins of the many NPY-family receptors in mammals. *Peptides* 22, 295–307.
- Latunde-Dada, S., Bott, R., Crozier, J., Trikeriotis, M., Leszczyszyn, O.I., Goodall, D., 2016. Rapid determination of hydrodynamic radii beyond the limits of Taylor dispersion. *J. Chromatogr. A* 1472, 66–73.
- Leban, J.J., Heyer, D., Landavazo, A., Matthews, J., Aulabaugh, A., Daniels, A.J., 1995. Novel modified carboxy terminal fragments of neuropeptide Y with high affinity for Y2-type receptors and potent functional antagonism at a Y1-type receptor. *J. Med. Chem.* 38, 1150–7.
- Lebon, G., Warne, T., Edwards, P.C., Bennett, K., Langmead, C.J., Leslie, A.G.W., Tate, C.G., 2011. Agonist-bound adenosine A2A receptor structures reveal common features of GPCR activation. *Nature* 474, 521–

5.

- Lee, S.M., Booe, J.M., Pioszak, A.A., 2015. Structural insights into ligand recognition and selectivity for classes A, B, and C GPCRs. *Eur. J. Pharmacol.* 763, 196–205.
- Lefkowitz, R.J., 2013. A brief history of G-protein coupled receptors (Nobel Lecture). *Angew. Chemie - Int. Ed.* 52, 6366–6378.
- Lerch, M., Gafner, V., Bader, R., Christen, B., Folkers, G., Zerbe, O., 2002. Bovine pancreatic polypeptide (bPP) undergoes significant changes in conformation and dynamics upon binding to DPC micelles. *J. Mol. Biol.* 322, 1117–1133.
- Lerch, M., Mayrhofer, M., Zerbe, O., 2004. Structural similarities of micelle-bound peptide YY (PYY) and neuropeptide Y (NPY) are related to their affinity profiles at the Y receptors. *J. Mol. Biol.* 339, 1153–1168.
- Lerner, E., Ploetz, E., Hohlbein, J., Cordes, T., Weiss, S., 2016. A Quantitative Theoretical Framework for Protein-Induced Fluorescence Enhancement-Förster-Type Resonance Energy Transfer (PIFE-FRET). *J. Phys. Chem. B* 120, 6401–6410.
- Li, J.B., Asakawa, A., Terashi, M., Cheng, K., Chaolu, H., Zoshiki, T., Ushikai, M., Sheriff, S., Balasubramaniam, A., Inui, A., 2010. Regulatory effects of Y4 receptor agonist (BVD-74D) on food intake. *Peptides* 31, 1706–1710.
- Li, W., Pang, I.H., Pacheco, M.T.F., Tian, H., 2018. Ligandomics: a paradigm shift in biological drug discovery. *Drug Discov. Today* 23, 636–643.
- Liang, Y.-L., Khoshouei, M., Deganutti, G., Glukhova, A., Koole, C., Peat, T.S., Radjainia, M., Plitzko, J.M., Baumeister, W., Miller, L.J., Hay, D.L., Christopoulos, A., Reynolds, C.A., Wootten, D., Sexton, P.M., 2018. Cryo-EM structure of the active, Gs-protein complexed, human CGRP receptor. *Nature*. 561, 492-497.
- Lindner, D., Stichel, J., Beck-Sickinger, A.G., 2008. Molecular recognition of the NPY hormone family by their receptors. *Nutrition* 24, 907–917.
- Lindner, D., Walther, C., Tennemann, A., Beck-Sickinger, A.G., 2009. Functional role of the extracellular N-terminal domain of neuropeptide Y subfamily receptors in membrane integration and agonist-stimulated internalization. *Cell. Signal.* 21, 61–68.
- Lipinski, C.A., 2004. Lead- and drug-like compounds: The rule-of-five revolution. *Drug Discov. Today Technol.* 1, 337–341.
- Lippert, L.G., Hallock, J.T., Dadosh, T., Diroll, B.T., Murray, C.B., Goldman, Y.E., 2016. NeutrAvidin Functionalization of CdSe/CdS Quantum Nanorods and Quantification of Biotin Binding Sites using Biotin-4-Fluorescein Fluorescence Quenching. *Bioconjug. Chem.* 27, 562–8.
- Liu, M., Richardson, R.R., Mountford, S.J., Zhang, L., Tempone, M.H., Herzog,

- H., Holliday, N.D., Thompson, P.E., 2016. Identification of a Cyanine-Dye Labeled Peptidic Ligand for Y₁ R and Y₄ R, Based upon the Neuropeptide Y C-Terminal Analogue, BVD-15. *Bioconjug. Chem.* 27, 2166–2175.
- Lofaj, M., Valent, I., Bujdák, J., 2013. Mechanism of rhodamine 6G molecular aggregation in montmorillonite colloid. *Cent. Eur. J. Chem.* 11, 1606–1619.
- Lohse, M.J., Nuber, S., Hoffmann, C., 2012. Fluorescence / Bioluminescence Resonance Energy Transfer Techniques to Study G-Protein-Coupled Receptor Activation and Signaling. *Pharmacol. Rev.* 64, 299–336.
- Lundberg, J.M., 1996. Pharmacology Nervous of Cotransmission in the Autonomic System : Integrative Aspects on Amines , Adenosine Amino Acids and Nitric Oxide. *Pharmacol. Rev.* 48, 113-178
- Lundberg, J.M., Franco-Cereceda, A., Hemsén, A., Lacroix, J.S., Pernow, J., 1990a. Pharmacology of noradrenaline and neuropeptide tyrosine (NPY)-mediated sympathetic cotransmission. *Fundam. Clin. Pharmacol.* 4, 373–391.
- Lundberg, J.M., Franco-Cereceda, A., Lacroix, J.S., Pernow, J., 1990b. Neuropeptide Y and sympathetic neurotransmission. *Ann. N. Y. Acad. Sci.* 611, 166–174.
- Lundell, I., Blomqvist, a G., Berglund, M.M., Schober, D. a, Johnson, D., Statnick, M. a, Gadski, R. a, Gehlert, D.R., Larhammar, D., 1995. Cloning of a human receptor of the npy receptor family with high-affinity for pancreatic-polypeptide and peptide yy. *J. Biol. Chem.* 270, 29123–29128.
- Luo, R., Jeong, S.-J., Jin, Z., Strokes, N., Li, S., Piao, X., 2011. G protein-coupled receptor 56 and collagen III, a receptor-ligand pair, regulates cortical development and lamination. *Proc. Natl. Acad. Sci.* 108, 12925–12930.
- Luquet, S., Perez, F.A., Hnasko, T.S., Palmiter, R.D., 2005. NPY / AgRP Neurons Are Essential for Feeding in Adult Mice but Can Be Ablated in Neonates. *Science.* 310, 683–686.
- Luttrell, L.M., 2005. Composition and Function of G Protein-Coupled Receptor Signosomes Controlling Mitogen-Activated Protein Kinase Activity. *J Mol Neurosci.* 26, 253-264.
- Luttrell, L.M., Gesty-Palmer, D., 2010. Beyond Desensitization : Physiological Relevance of Arrestin -Dependent Signaling. *Pharmacol. Rev.* 62, 305–330.
- Macdonald, J.L., Pike, L.J., 2008. Heterogeneity in EGF-binding affinities arises from negative cooperativity in an aggregating system. *Proc. Natl. Acad. Sci. U. S. A.* 105, 112–7.
- MacKerell, A.D., 1991. Molecular modeling and dynamics of biologically active peptides: application to neuropeptide Y. *Methods Enzymol.* 202,

- Maciejewski, M.L., Arterburn, D.E., Van Scoyoc, L., Smith, V.A., Yancy, W.S., Weidenbacher, H.J., Livingston, E.H., Olsen, M.K. 2016. Bariatric Surgery and Long-term Durability of Weight Loss. *JAMA Surgery*. 151, 1046-1055.
- Magde, D., Elson, E., Webb, W.W., 1972. Thermodynamic Fluctuations in a Reacting System—Measurement by Fluorescence Correlation Spectroscopy. *Phys. Rev. Lett.* 29, 705–708.
- Magde, D., Elson, E.L., Webb, W.W., 1974. Fluorescence correlation spectroscopy. II. An experimental realization. *Biopolymers* 13, 29–61.
- Mahoney, J.P., Sunahara, R.K., 2016. Mechanistic insights into GPCR – G protein interactions. *Curr. Opin. Struct. Biol.* 41, 247–254.
- Manglik, A., Kruse, A.C., Kobilka, T.S., Thian, F.S., Mathiesen, J.M., Sunahara, R.K., Pardo, L., Weis, W.I., Kobilka, B.K., Granier, S., 2012. Crystal structure of the μ -opioid receptor bound to a morphinan antagonist. *Nature* 485, 321-326.
- Marchese, A., Paing, M.M., Temple, B.R.S., Trejo, J., 2008. G protein-coupled receptor sorting to endosomes and lysosomes. *Annu. Rev. Pharmacol. Toxicol.* 48, 601–29.
- Martínez, V.M., Arbeloa, F.L., Prieto, J.B., Arbeloa, I.L., 2005. Characterization of rhodamine 6G aggregates intercalated in solid thin films of laponite clay. 2 fluorescence spectroscopy. *J. Phys. Chem. B* 109, 7443–7450.
- Matsumoto, M., Nomura, T., Momose, K., Ikeda, Y., Kondou, Y., Akiho, H., Togami, J., Kimura, Y., Okada, M., Yamaguchi, T., 1996. Inactivation of a novel neuropeptide Y/peptide YY receptor gene in primate species. *J. Biol. Chem.* 271, 27217–20.
- May, L.T., Bridge, L.J., Stoddart, L.A., Briddon, S.J., Hill, S.J., 2011. Allosteric interactions across native adenosine-A3 receptor homodimers: quantification using single-cell ligand-binding kinetics. *FASEB J.* 25, 3465–76.
- May, L.T., Leach, K., Sexton, P.M., Christopoulos, A., 2007. Allosteric Modulation of G Protein–Coupled Receptors. *Annu. Rev. Pharmacol. Toxicol.* 47, 1–51.
- McDermott, B.J., Millar, B.C., Piper, H.M., 1993. Cardiovascular effects of neuropeptide Y: receptor interactions and cellular mechanisms. *Cardiovasc. Res.* 27, 893–905.
- McGaughey, G.B., Gagné, M., Rappé, A.K., 1998. π -Stacking interactions. Alive and well in proteins. *J. Biol. Chem.* 273, 15458–63.
- McVey, M., Ramsay, D., Kellett, E., Rees, S., Wilson, S., Pope, A.J., Milligan, G., 2001. Monitoring Receptor Oligomerization Using Time-resolved Fluorescence Resonance Energy Transfer and Bioluminescence

- Resonance Energy Transfer. *J. Biol. Chem.* 276, 14092–14099.
- Medeiros, P.J., Al-Khazraji, B.K., Novielli, N.M., Postovit, L.M., Chambers, A.F., Jackson, D.N., 2011. Neuropeptide Y stimulates proliferation and migration in the 4T1 breast cancer cell line. *Int. J. Cancer* 131, 276–286.
- Mercer, R.E., Chee, M.J.S., Colmers, W.F., 2011. The role of NPY in hypothalamic mediated food intake. *Front. Neuroendocrinol.* 32, 398–415.
- Merrifield, R.B., 1963. Solid Phase Peptide Synthesis. I. The Synthesis of a Tetrapeptide. *J. Am. Chem. Soc.* 85, 2149–2154.
- Merten, N., Lindner, D., Rabe, N., Römpler, H., Mörl, K., Schöneberg, T., Beck-Sickinger, A.G., 2007. Receptor subtype-specific docking of Asp6.59 with C-terminal arginine residues in Y receptor ligands. *J. Biol. Chem.* 282, 7543–51.
- Michel, M.C., Beck-Sickinger, A., Cox, H., Doods, H.N., Herzog, H., Larhammar, D., Quirion, R., Schwartz, T., Westfall, T., 1998. XVI. International Union of Pharmacology recommendations for the nomenclature of neuropeptide Y, peptide YY, and pancreatic polypeptide receptors. *Pharmacol. Rev.* 50, 143–50.
- Middleton, R.J., Briddon, S.J., Cordeaux, Y., Yates, A.S., Dale, C.L., George, M.W., Baker, J.G., Hill, S.J., Kellam, B., 2007. New fluorescent adenosine A1-receptor agonists that allow quantification of ligand-receptor interactions in microdomains of single living cells. *J. Med. Chem.* 50, 782–793.
- Mishra, A.K., Dubey, V., Ghosh, A.R., 2016. Obesity: An overview of possible role(s) of gut hormones, lipid sensing and gut microbiota. *Metabolism.* 65, 48–65.
- Mitronova, G.Y., Lukinavičius, G., Butkevich, A.N., Kohl, T., Belov, V.N., Lehnart, S.E., Hell, S.W., 2017. High-Affinity Functional Fluorescent Ligands for Human β -Adrenoceptors. *Sci. Rep.* 7, 1–15.
- Mollereau, C., Gouardères, C., Dumont, Y., Kotani, M., Detheux, M., Doods, H., Parmentier, M., Quirion, R., Zajac, J.M., 2001. Agonist and antagonist activities on human NPFF2 receptors of the NPY ligands GR231118 and BIBP3226. *Br. J. Pharmacol.* 133, 1–4.
- Mollereau, C., Mazarguil, H., Marcus, D., Quelven, I., Kotani, M., Lannoy, V., Dumont, Y., Quirion, R., Detheux, M., Parmentier, M., Zajac, J.-M., 2002. Pharmacological characterization of human NPFF(1) and NPFF(2) receptors expressed in CHO cells by using NPY Y(1) receptor antagonists. *Eur. J. Pharmacol.* 451, 245–56.
- Montalbetti, C.A.G.N., Falque, V., 2005. Amide bond formation and peptide coupling. *Tetrahedron* 61, 10827–10852.
- Moody, T.W., Ramos-Alvarez, I., Jensen, R.T., 2018. Neuropeptide G protein-

- coupled receptors as oncotargets. *Front. Endocrinol. (Lausanne)*. 9, 1–11.
- Moore, C.A.C., Milano, S.K., Benovic, J.L., 2007. Regulation of Receptor Trafficking by GRKs and Arrestins. *Annu. Rev. Physiol.* 69, 451–482.
- Moreno, G., Perelló, M., Gaillard, R.C., Spinedi, E., 2005. Orexin a stimulates hypothalamic-pituitary-adrenal (HPA) axis function, but not food intake, in the absence of full hypothalamic NPY-ergic activity. *Endocrine* 26, 99–106.
- Morton, G.J., Cummings, D.E., Baskin, D.G., Barsh, G.S., Schwartz, M.W., 2006. Central nervous system control of food intake and body weight. *Nature* 443, 289–295.
- Mountford, S.J., Liu, M., Zhang, L., Groenen, M., Herzog, H., Holliday, N.D., Thompson, P.E., 2014. Synthetic routes to the Neuropeptide Y Y1 receptor antagonist 1229U91 and related analogues for SAR studies and cell-based imaging. *Org. Biomol. Chem.* 12, 3271–81.
- Mountjoy, K.G., 2015. Pro-Opiomelanocortin (POMC) Neurones, POMC-Derived Peptides, Melanocortin Receptors and Obesity: How Understanding of this System has Changed Over the Last Decade. *J. Neuroendocrinol.* 27, 406–418.
- Mousli, M., Trifilieff, A., Pelton, J.T., Gies, J.P., Landry, Y., 1995. Structural requirements for neuropeptide Y in mast cell and G protein activation. *Eur. J. Pharmacol.* 289, 125–133.
- Movafagh, S., Hobson, J.P., Spiegel, S., Kleinman, H.K., Zukowska, Z., 2006. Neuropeptide Y induces migration, proliferation, and tube formation of endothelial cells bimodally via Y1, Y2, and Y5 receptors. *FASEB J.* 20, 1924–1926.
- Müller, T.D., Nogueiras, R., Andermann, M.L., Andrews, Z.B., Anker, S.D., Argente, J., Batterham, R.L., Benoit, S.C., Bowers, C.Y., Broglio, F., Casanueva, F.F., D'Alessio, D., Depoortere, I., Geliebter, A., Ghigo, E., Cole, P.A., Cowley, M., Cummings, D.E., Dagher, A., Diano, S., Dickson, S.L., Diéguez, C., Granata, R., Grill, H.J., Grove, K., Habegger, K.M., Heppner, K., Heiman, M.L., Holsen, L., Holst, B., Inui, A., Jansson, J.O., Kirchner, H., Korbonits, M., Laferrère, B., LeRoux, C.W., Lopez, M., Morin, S., Nakazato, M., Nass, R., Perez-Tilve, D., Pfluger, P.T., Schwartz, T.W., Seeley, R.J., Sleeman, M., Sun, Y., Sussel, L., Tong, J., Thorner, M.O., van der Lely, A.J., van der Ploeg, L.H.T., Zigman, J.M., Kojima, M., Kangawa, K., Smith, R.G., Horvath, T., Tschöp, M.H., 2015. Ghrelin. *Mol. Metab.* 4, 437–460.
- Murphy, K.G., Bloom, S.R., 2006. Gut hormones and the regulation of energy homeostasis. *Nature* 444, 854–9.
- Nadolski, M.J., Linder, M.E., 2007. Protein lipidation. *FEBS J.* 274, 5202–5210.

- Narlawar, R., Lane, J.R., Doddareddy, M., Lin, J., Brussee, J., Ijzerman, A.P., 2010. Hybrid ortho/allosteric ligands for the adenosine A1 receptor. *J. Med. Chem.* 53, 3028–3037.
- Narumiya, S., Thumkeo, D., 2018. Rho signaling research: history, current status and future directions. *FEBS Lett.* 592, 1763–1776.
- Neary, M.T., Batterham, R.L., 2009. Gut hormones: Implications for the treatment of obesity. *Pharmacol. Ther.* 124, 44–56.
- Nedungadi, T.P., Briski, K.P., 2010. Effects of intracerebroventricular administration of the NPY-Y1 receptor antagonist, 1229U91, on hyperphagic and glycemic responses to acute and chronic intermediate insulin-induced hypoglycemia in female rats. *Regul. Pept.* 159, 14–18.
- Nguyen, A.D., Mitchell, N.F., Lin, S., Macia, L., Yulyaningsih, E., Baldock, P.A., Enriquez, R.F., Zhang, L., Shi, Y.-C., Zolotukhin, S., Herzog, H., Sainsbury, A., 2012. Y1 and Y5 receptors are both required for the regulation of food intake and energy homeostasis in mice. *PLoS One.* 7, [eCollection].
- Ni, Q., Mehta, S., Zhang, J., 2017. Live-cell imaging of cell signaling using genetically encoded fluorescent reporters. *FEBS J.* 285, 203–219.
- Nomura, W., Koseki, T., Ohashi, N., Mizuguchi, T., Tamamura, H., 2015. Trivalent ligands for CXCR4 bearing polyproline linkers show specific recognition for cells with increased CXCR4 expression. *Org. Biomol. Chem.* 13, 8734–8739.
- Nonaka, N., Shioda, S., Niehoff, M.L., Banks, W.A., 2003. Characterization of Blood-Brain Barrier Permeability to PYY 3 – 36 in the Mouse. *Pharmacology* 306, 948–953.
- Nutt, D.J., Lingford-Hughes, A., Erritzoe, D., Stokes, P.R.A., 2015. The dopamine theory of addiction: 40 years of highs and lows. *Nat. Rev. Neurosci.* 16, 305–312.
- Office for national statistics., 2017. NHS Digital, accessed 16th September 2018, <https://assets.publishing.service.gov.uk/government/uploads/system/uploads/attachment_data/file/613532/obes-phys-acti-diet-eng-2017-rep.pdf>
- Office for national statistics., 2018. NHS Digital, accessed 16th September 2018, <<https://files.digital.nhs.uk/publication/0/0/obes-phys-acti-diet-eng-2018-rep.pdf>>
- O’Hare, M.M., Tenmoku, S., Aakerlund, L., Hilsted, L., Johnsen, A., Schwartz, T.W., 1988. Neuropeptide Y in guinea pig, rabbit, rat and man. Identical amino acid sequence and oxidation of methionine-17. *Regul. Pept.* 20, 293–304.
- Oldham, W.M., Hamm, H.E., 2008. Heterotrimeric G protein activation by G-protein-coupled receptors. *Nat. Rev. Mol. Cell Biol.* 9, 60–71.

- Olesen, M. V., Christiansen, S.H., Gøtzsche, C.R., Holst, B., Kokaia, M., Woldbye, D.P.D., 2012. Y5 neuropeptide Y receptor overexpression in mice neither affects anxiety- and depression-like behaviours nor seizures but confers moderate hyperactivity. *Neuropeptides* 46, 71–79.
- Oller-Salvia, B., Sánchez-Navarro, M., Giral, E., Teixidó, M., 2016. Blood-brain barrier shuttle peptides: An emerging paradigm for brain delivery. *Chem. Soc. Rev.* 45, 4690–4707.
- Oo, C., Kalbag, S.S., 2016. Leveraging the attributes of biologics and small molecules, and releasing the bottlenecks: a new wave of revolution in drug development. *Expert Rev. Clin. Pharmacol.* 9, 747–749.
- Osherovich, L., 2009. Wising up to NPYs, SciBX: Science-Business eXchange.
- Otto, K.G., Jin, L., Spencer, D.M., Anthony Blau, C., 2001. Cell proliferation through forced engagement of c-Kit and Flt-3. *Blood* 97, 3662–3664.
- Ouakinin, S.R.S., Barreira, D.P., Gois, C.J., 2018. Depression and Obesity: Integrating the Role of Stress, Neuroendocrine Dysfunction and Inflammatory Pathways. *Front. Endocrinol. (Lausanne)*. 9, 1–7.
- Ouedraogo, M., Lecat, S., Rochdi, M.D., Hachet-Haas, M., Matthes, H., Gicquiaux, H., Verrier, S., Gaire, M., Glasser, N., Mély, Y., Takeda, K., Bouvier, M., Galzi, J.-L., Bucher, B., 2008. Distinct motifs of neuropeptide Y receptors differentially regulate trafficking and desensitization. *Traffic* 9, 305–24.
- Palczewski, K., Kumasaka, T., Hori, T., Behnke, C.A., Motoshima, H., Fox, B.A., Le Trong, I., Teller, D.C., Okada, T., Stenkamp, R.E., Yamamoto, M., Miyano, M., 2000. Crystal structure of rhodopsin: A G protein-coupled receptor. *Science* 289, 739–45.
- Palmiter, R.D., 2007. Is dopamine a physiologically relevant mediator of feeding behavior? *Trends Neurosci.* 30, 375–381.
- Panaro, B.L., Tough, I.R., Engelstoft, M.S., Matthews, R.T., Digby, G.J., Møller, C.L., Svendsen, B., Gribble, F., Reimann, F., Holst, J.J., Holst, B., Schwartz, T.W., Cox, H.M., Cone, R.D., 2014. The melanocortin-4 receptor is expressed in enteroendocrine L cells and regulates the release of peptide YY and glucagon-like peptide 1 in vivo. *Cell Metab.* 20, 1018–29.
- Pardridge, W.M., 2002. Drug and gene targeting to the brain with molecular trojan horses. *Nat. Rev. Drug Discov.* 1, 131.
- Park, J.H., Scheerer, P., Hofmann, K.P., Choe, H.-W., Ernst, O.P., 2008. Crystal structure of the ligand-free G-protein-coupled receptor opsin. *Nature* 454, 183–187.
- Park, S.H., Das, B.B., Casagrande, F., Tian, Y., Nothnagel, H.J., Chu, M., Kiefer, H., Maier, K., De Angelis, A.A., Marassi, F.M., Opella, S.J., 2012. Structure of the chemokine receptor CXCR1 in phospholipid bilayers. *Nature* 491, 779–83.

- Parker, E.M., Babij, C.K., Balasubramaniam, A., Burrier, R.E., Guzzi, M., Hamud, F., Mukhopadhyay, G., Rudinski, M.S., Tao, Z., Tice, M., Xia, L., Mullins, D.E., Salisbury, B.G., 1998. GR231118 (1229U91) and other analogues of the C-terminus of neuropeptide Y are potent neuropeptide Y Y1 receptor antagonists and neuropeptide Y Y4 receptor agonists. *Eur. J. Pharmacol.* 349, 97–105.
- Parker, E.M., Balasubramaniam, A., Guzzi, M., Mullins, D.E., Salisbury, B.G., Sheriff, S., Witten, M.B., Hwa, J.J., 2000. [D-Trp34] neuropeptide Y is a potent and selective neuropeptide Y Y5 receptor agonist with dramatic effects on food intake. *Peptides* 21, 393–399.
- Parker, S.L., Kane, J.K., Parker, M.S., Berglund, M.M., Lundell, I. a., Li, M.D., 2001. Cloned neuropeptide Y (NPY) Y1 and pancreatic polypeptide Y4 receptors expressed in Chinese hamster ovary cells show considerable agonist-driven internalization, in contrast to the NPY Y2 receptor. *Eur. J. Biochem.* 268, 877–886.
- Parker, S.L., Parker, M.S., Buschauer, A., Balasubramaniam, A., 2003. Ligand internalization by cloned neuropeptide Y Y 5 receptors excludes Y 2 and Y 4 receptor-selective peptides 474, 31–42.
- Parmar, V.K., Grinde, E., Mazurkiewicz, J.E., Herrick-Davis, K., 2017. Beta2-adrenergic receptor homodimers: Role of transmembrane domain 1 and helix 8 in dimerization and cell surface expression. *Biochim. Biophys. Acta - Biomembr.* 1859, 1445–1455.
- Parrado, C., Díaz-Cabiale, Z., García-Coronel, M., Agnati, L.F., Coveñas, R., Fuxe, K., Narváez, J.A., 2007. Region specific galanin receptor/neuropeptide Y Y1 receptor interactions in the tel- and diencephalon of the rat. Relevance for food consumption. *Neuropharmacology* 52, 684–692.
- Parrill, A.L., Lima, S., Spiegel, S., 2012. Structure of the first sphingosine 1-phosphate receptor. *Sci. Signal.* 5, 1–9.
- Patel, D., 2015. Pharmacotherapy for the management of obesity. *Metabolism.* 64, 1376–1385.
- Patel, D.K., Stanford, F.C., 2018. Safety and tolerability of new-generation anti-obesity medications: a narrative review. *Postgrad. Med.* 130, 173–182.
- Paton, R.S., Goodman, J.M., 2009. Hydrogen bonding and pi-stacking: how reliable are force fields? A critical evaluation of force field descriptions of nonbonded interactions. *J. Chem. Inf. Model.* 49, 944–55.
- Pavlos, N.J., Friedman, P.A., 2017. GPCR Signaling and Trafficking: The Long and Short of It. *Trends Endocrinol. Metab.* 28, 213–226.
- Paz-Filho, G.J. da, Volaco, A., Suplicy, H.L., Radominski, R.B., Boguszewski, C.L., 2009. Decrease in leptin production by the adipose tissue in obesity

associated with severe metabolic syndrome. *Arq. Bras. Endocrinol. Metabol.* 53, 1088–1095.

- Pearson, D.A., Blanchette, M., Baker, M. Lou, Guindon, C.A., 1989. Trialkylsilanes as scavengers for the trifluoroacetic acid deblocking of protecting groups in peptide synthesis. *Tetrahedron Lett.* 30, 2739–2742.
- Pedragosa-Badia, X., Sliwoski, G.R., Nguyen, E.D., Lindner, D., Stichel, J., Kaufmann, K.W., Meiler, J., Beck-Sickinger, A.G., 2014. Pancreatic polypeptide is recognized by two hydrophobic domains of the human Y4 receptor binding pocket. *J. Biol. Chem.* 289, 5846–5859.
- Peeters, M.C., van Westen, G.J.P., Guo, D., Wisse, L.E., Muller, C.E., Beukers, M.W., Ijzerman, A.P., 2011. GPCR structure and activation: an essential role for the first extracellular loop in activating the adenosine A2B receptor. *FASEB J. Off. Publ. Fed. Am. Soc. Exp. Biol.* 25, 632–643.
- Pheng, L.H., Dumont, Y., Fournier, A., Chabot, J.-G., Beaudet, A., Quirion, R., 2003. Agonist- and antagonist-induced sequestration/internalization of neuropeptide Y Y₁ receptors in HEK293 cells. *Br. J. Pharmacol.* 139, 695–704.
- Pierce, K.L., Premont, R.T., Lefkowitz, R.J., Hughes, T.H., 2002. Seven-transmembrane receptors 3. *Nat. Rev. Mol. Cell Biol.* 3, 639–650.
- Pleil, K.E., Rinker, J.A., Lowery-gionta, E.G., Mazzone, C.M., McCall, N.M., Kendra, A.M., Olson, D.P., Lowell, B.B., Grant, K.A., Thiele, T.E., Kash, T.L., 2015. NPY signaling inhibits extended amygdala CRF neurons to suppress binge alcohol drinking. *Nat. Publ. Gr.* 18, 545–552.
- Pollock, R., Clackson, T., 2002. Dimerizer-regulated gene expression. *Curr. Opin. Biotechnol.* 13, 459–67.
- Popova, N. V, Deyev, I.E., Petrenko, A.G., 2013. Clathrin-Mediated Endocytosis and Adaptor Proteins 5, 62–73.
- Portoghese, P.S., Lunzer, M.M., 2003. Identity of the putative δ 1-opioid receptor as a δ - κ heteromer in the mouse spinal cord. *Eur. J. Pharmacol.* 467, 233–234.
- Premont, R.T., Gainetdinov, R.R., 2007. Physiological Roles of G Protein – Coupled Receptor Kinases and Arrestins. *Annu. Rev. Physiol.* 69, 511–34.
- Raiborg, C., Stenmark, H., 2009. The ESCRT machinery in endosomal sorting of ubiquitylated membrane proteins. *Nature* 458, 445–452.
- Rajagopal, S., Shenoy, S.K., 2018. GPCR desensitization: Acute and prolonged phases. *Cell. Signal.* 41, 9–16.
- Rasmussen, S.G., Jensen, a D., Liapakis, G., Ghanouni, P., Javitch, J. a, Gether, U., 1999. Mutation of a highly conserved aspartic acid in the beta2 adrenergic receptor: constitutive activation, structural instability, and

- conformational rearrangement of transmembrane segment 6. *Mol. Pharmacol.* 56, 175–184.
- Rasmussen, S.G.F., Choi, H., Fung, J.J., Pardon, E., Chae, P.S., Devree, B.T., Rosenbaum, D.M., Thian, F.S., Kobilka, T.S., Schnapp, A., Konetzki, I., Sunahara, R.K., Samuel, H., Pautsch, A., Steyaert, J., Weis, W.I., Kobilka, B.K., 2011a. Tructure of a Nanobody-Stabilized Active State of the Beta2 Adrenoceptor. *Nature* 469, 175–80.
- Rasmussen, S.G.F., Choi, H., Rosenbaum, D.M., Kobilka, T.S., Thian, F.S., Edwards, P.C., Burghammer, M., Ratnala, V.R.P., Sanishvili, R., Fischetti, R.F., Schertler, G.F.X., Weis, W.I., Kobilka, B.K., 2007. Crystal structure of the human b 2 adrenergic G-protein-coupled receptor. *Nature.* 450, 383–388.
- Rasmussen, S.G.F., Devree, B.T., Zou, Y., Kruse, A.C., Chung, K.Y., Kobilka, T.S., Thian, F.S., Chae, P.S., Pardon, E., Calinski, D., Mathiesen, J.M., Shah, S.T.A., Lyons, J.A., 2011b. Crystal structure of the b 2 adrenergic receptor – Gs protein complex. *Nature* 477, 549–555.
- Rink, H., 1987. Solid-phase synthesis of protected peptide fragments using a trialkoxy-diphenyl-methylester resin. *Tetrahedron Lett.* 28, 3787–3790.
- Rodriguez, M., Audinot, V., Dromaint, S., Macia, C., Lamamy, V., Beauverger, P., Rique, H., Imbert, J., Nicolas, J.P., Boutin, J.A., Galizzi, J.P., 2003. Molecular identification of the long isoform of the human neuropeptide Y Y5 receptor and pharmacological comparison with the short Y5 receptor isoform. *Biochem. J.* 369, 667–673.
- Roepstorff, K., Thomsen, P., Sandvig, K., Van Deurs, B., 2002. Sequestration of epidermal growth factor receptors in non-caveolar lipid rafts inhibits ligand binding. *J. Biol. Chem.* 277, 18954–18960.
- Rogacki, M.K., Ottavia, G., J., T.S., Tianyi, L., Sunetra, B., Raphael, J., Huiying, Z., Vlad, R., Yu, M., Per, S., Daniel, G., L., W.D., Athanasios, S., R., S.A., Lars, T., Tijana, J.-T., Vladana, V., 2018. Dynamic lateral organization of opioid receptors (kappa, muwt and muN40D) in the plasma membrane at the nanoscale level. *Traffic*. [Epub ahead of print].
- Rollins, C.T., Rivera, V.M., Woolfson, D.N., Keenan, T., Hatada, M., Adams, S.E., Andrade, L.J., Yaeger, D., van Schravendijk, M.R., Holt, D.A., Gilman, M., Clackson, T., 2000. A ligand-reversible dimerization system for controlling protein-protein interactions. *Proc. Natl. Acad. Sci. U. S. A.* 97, 7096–101.
- Rose, P.M., Fernandes, P., Lynch, J.S., Frazier, S.T., Fisher, S.M., Kodukula, K., Kienzle, B., Seethala, R., 1995. Cloning and functional expression of a cDNA encoding a human type 2 neuropeptide Y receptor. *J. Biol. Chem.* 270, 29038.
- Rose, R.H., Briddon, S.J., Hill, S.J., 2012. A novel fluorescent histamine H(1) receptor antagonist demonstrates the advantage of using fluorescence

- correlation spectroscopy to study the binding of lipophilic ligands. *Br. J. Pharmacol.* 165, 1789–800.
- Rosenbaum, D.M., Cherezov, V., Hanson, M.A., Rasmussen, S.G.F., Thian, F.S., Kobilka, T.S., Choi, H., Yao, X., Weis, W.I., Stevens, R.C., Kobilka, B.K., 2007. GPCR engineering yields high-resolution structural insights into beta2-adrenergic receptor function. *Science* 318, 1266–73.
- Rovati, G.E., Capra, V., Shaw, V.S., Malik, R.U., Sivaramakrishnan, S., Neubig, R.R., 2017. The DRY motif and the four corners of the cubic ternary complex model. *Cell. Signal.* 35, 16–23.
- Rudolf, K., Eberlein, W., Engel, W., Wieland, H.A., Willim, K.D., Entzeroth, M., Wienen, W., Beck-Sickinger, A.G., Doods, H.N., 1994. The first highly potent and selective non-peptide neuropeptide Y Y1 receptor antagonist: BIBP3226. *Eur. J. Pharmacol.* 271, 5–7.
- Sabatino, G., Mulinacci, B., Alcaro, M.C., Chelli, M., Rovero, P., Papini, A.M., 2002. $N + Iq \sim N N^-$ --N. *Lett. Pept. Sci.* 9, 119–123.
- Saffarian, S., Li, Y., Elson, E.L., Pikey, L.J., 2007. Oligomerization of the EGF receptor investigated by live cell fluorescence intensity distribution analysis. *Biophys. J.* 93, 1021–1031.
- Sah, R., Balasubramaniam, A., Parker, M.S., Sallee, F., Parker, S.L., 2005. Neuropeptide Y as a partial agonist of the Y1 receptor. *Eur. J. Pharmacol.* 525, 60–68.
- Saito, T., Bunnett, N.W., 2005. Protease-activated receptors: regulation of neuronal function. *Neuromolecular Med.* 7, 79–99.
- Salama, I., Löber, S., Hübner, H., Gmeiner, P., 2014. Synthesis and binding profile of haloperidol-based bivalent ligands targeting dopamine D2-like receptors. *Bioorganic Med. Chem. Lett.* 24, 3753–3756.
- Santini, R., Griffith, M.C., Qi, M., 1998. A measure of solvent effects on swelling of resins for solid phase organic synthesis. *Tetrahedron Lett.* 39, 8951–8954.
- Santos, R., Ursu, O., Gaulton, A., Bento, A.P., Donadi, R.S., Bologa, C.G., Karlsson, A., Al-Lazikani, B., Hersey, A., Oprea, T.I., Overington, J.P., 2016. A comprehensive map of molecular drug targets. *Nat. Rev. Drug Discov.* 16, 19–34.
- Sato, N., Ogino, Y., Mashiko, S., Ando, M., 2009. Modulation of neuropeptide Y receptors for the treatment of obesity. *Expert Opin. Ther. Pat.* 19, 1401–1415.
- Sautel, M., Martinez, R., Munoz, M., Peitsch, M.C., Beck-Sickinger, A.G., Walker, P., 1995. Role of a hydrophobic pocket of the human Y1 neuropeptide Y receptor in ligand binding. *Mol. Cell. Endocrinol.* 112, 215–222.

- Sautel, M., Rudolf, K., Wittneben, H., Herzog, H., Martinez, R., Munoz, M., Eberlein, W., Engel, W., Walker, P., Beck-Sickinger, A.G., 1996. Neuropeptide Y and the nonpeptide antagonist BIBP 3226 share an overlapping binding site at the human Y1 receptor. *Mol. Pharmacol.* 50, 285–92.
- Scheer, A., Costa, T., Fanelli, F., Benedetti, P.G.D.E., Mhaouty-kodja, S., Abuin, L., Nenniger-tosato, M., Cotecchia, S., 2000. Mutational Analysis of the Highly Conserved Arginine within the Glu / Asp-Arg-Tyr Motif of the 1b - Adrenergic Receptor : Effects on Receptor Isomerization and Activation 231, 219–231.
- Schild, H.O., 1949. pAx and competitive drug antagonism. *Br. J. Pharmacol. Chemother.* 4, 277–280.
- Schiöth, H.B., Fredriksson, R., 2005. The GRAFS class I cation system of G-protein coupled receptors in comparative perspective 142, 94–101.
- Schlessinger, J., 2002. Ligand-induced, receptor-mediated dimerization and activation of EGF receptor. *Cell* 110, 669–672.
- Schober, D. a, Gackenhaimer, S.L., Heiman, M.L., Gehlert, D.R., 2000. Pharmacological characterization of (125)I-1229U91 binding to Y1 and Y4 neuropeptide Y/Peptide YY receptors. *J. Pharmacol. Exp. Ther.* 293, 275–80.
- Schubert, M., Stichel, J., Du, Y., Tough, I.R., Sliwoski, G., Meiler, J., Cox, H.M., Weaver, C.D., Beck-Sickinger, A.G., 2017. Identification and Characterization of the First Selective Y₄ Receptor Positive Allosteric Modulator. *J. Med. Chem.* 60, 7605-7612.
- Schwartz, M.W., Baskin, D.G., Bukowski, T.R., Kuijper, J.L., Foster, D., Lasser, G., Prunkard, D.E., Porte, D., Woods, S.C., Seeley, R.J., Weigle, D.S., 1996. Specificity of leptin action on elevated blood glucose levels and hypothalamic neuropeptide Y gene expression in ob/ob mice. *Diabetes* 45, 531–5.
- Schwartz, M.W., Seeley, R.J., Woods, S.C., Weigle, D.S., Campfield, L.A., Burn, P., Baskin, D.G., 1997. Leptin increases hypothalamic pro-opiomelanocortin mRNA expression in the rostral arcuate nucleus. *Diabetes* 46, 2119–23.
- Schwartz, T.W., 1983. Pancreatic Polypeptide: A Hormone Under Vagal Control. *Gastroenterology* 85, 1411–1425.
- Schwartz, T.W., Frimurer, T.M., Holst, B., Rosenkilde, M.M., Elling, C.E., 2006. Molecular Mechanism of 7Tm Receptor Activation—a Global Toggle Switch Model. *Annu. Rev. Pharmacol. Toxicol.* 46, 481–519.
- Schwille, P., Haustein, E., 2001. Fluorescence correlation spectroscopy. An introduction to its concepts and applications. *Biophys.* 1, 1–33 [eCollection]

- Schwille, P., Kummer, S., Heikal, A.A., Moerner, W.E., Webb, W.W., 2000. Fluorescence correlation spectroscopy reveals fast optical excitation-driven intramolecular dynamics of yellow fluorescent proteins. *Proc. Natl. Acad. Sci. U.S.A.* 97, 151–6.
- Scott, M.M., Williams, K.W., Rossi, J., Lee, C.E., Elmquist, J.K., 2011. Leptin receptor expression in hindbrain Glp-1 neurons regulates food intake and energy balance in mice. *J. Clin. Invest.* 121, 2413–21.
- Sebastiani, G., Ceccarelli, E., Castagna, M.G., Dotta, F., 2018. G-protein-coupled receptors (GPCRs) in the treatment of diabetes: Current view and future perspectives. *Best Pract. Res. Clin. Endocrinol. Metab.* 32, 201–213.
- Serone, A.P., Wright, C.E., Angus, J.A., 2000. Role of NPY Y1 receptors in cardiovascular control in the conscious rabbit. *J. Cardiovasc. Pharmacol.* 35, 315–321.
- Serrão, V.H.B., Silva, I.R., da Silva, M.T.A., Scortecchi, J.F., de Freitas Fernandes, A., Thiemann, O.H., 2018. The unique tRNA^{Sec} and its role in selenocysteine biosynthesis. *Amino Acids.* 50, 1145–1167.
- Shashkova, S., Leake, M.C., 2017. Single-molecule fluorescence microscopy review: shedding new light on old problems. *Biosci. Rep. [eCollection]*.
- Shi, Y., Baldock, P.A., 2012. Central and peripheral mechanisms of the NPY system in the regulation of bone and adipose tissue. *Bone* 50, 430–436.
- Shrivastava, A., Wang, S.H., Raju, N., Gierach, I., Ding, H., Tweedle, M.F., 2013. Heterobivalent dual-target probe for targeting GRP and Y1 receptors on tumor cells. *Bioorganic Med. Chem. Lett.* 23, 687–692.
- Siehl, S., 2007. G12/13-dependent signaling of G-protein-coupled receptors: Disease context and impact on drug discovery, Expert opinion on drug discovery. 2, 1591–1604.
- Silk, M.R., Newman, J., Ratcliffe, J.C., White, J.F., Caradoc-Davies, T., Price, J.R., Perrier, S., Thompson, P.E., Chalmers, D.K., 2017. Parallel and antiparallel cyclic d/l peptide nanotubes. *Chem. Commun.* 53, 6613–6616.
- Simons, M., Gordon, E., Claesson-Welsh, L., 2016. Mechanisms and regulation of endothelial VEGF receptor signalling. *Nat. Rev. Mol. Cell Biol.* 17, 611–625.
- Sipols, A.J., Baskin, D.G., Schwartz, M.W., 1995. Effect of Intracerebroventricular Insulin Infusion on Diabetic Hyperphagia and Hypothalamic Neuropeptide Gene Expression. *Diabetes* 44, 147–151.
- Sjödin, P., Holmberg, S.K.S., Akerberg, H., Berglund, M.M., Mohell, N., Larhammar, D., Åkerberg, H., 2006. Re-evaluation of receptor - ligand interactions of the human neuropeptide Y receptor Y1: a site-directed mutagenesis study. *Biochem. J.* 393, 161–169.

- Skibicka, K.P., Dickson, S.L., 2013. Enteroendocrine hormones - Central effects on behavior. *Curr. Opin. Pharmacol.* 13, 977–982.
- Sliwoski, G., Schubert, M., Stichel, J., Weaver, D., Beck-Sickinger, A.G., Meiler, J.M., 2016. Discovery of small-molecule modulators of the human Y4receptor. *PLoS One* 11, 1–13.
- Smith, J.S., Rajagopal, S., 2016. The β -Arrestins: Multifunctional regulators of G protein-coupled receptors. *J. Biol. Chem.* 291, 8969–8977.
- Smith, N.J., Milligan, G., 2010. Allostery at G protein-coupled receptor homo- and heteromers: uncharted pharmacological landscapes. *Pharmacol. Rev.* 62, 701–25.
- Sohn, J.W., 2015. Network of hypothalamic neurons that control appetite. *BMB Rep.* 48, 229–233.
- Söll, R.M., Dinger, M.C., Lundell, I., Larhammer, D., Beck-Sickinger, A.G., 2001. Novel analogues of neuropeptide Y with a preference for the Y1-receptor. *Eur. J. Biochem.* 268, 2828–37.
- Spencer, D.M., Belshaw, P.J., Chen, L., Ho, S.N., Randazzo, F., Crabtree, G.R., Schreiber, S.L., 1996. Functional analysis of Fas signaling in vivo using synthetic inducers of dimerization. *Curr. Biol.* 6, 839–47.
- Sridharan, R., Zuber, J., Connelly, S.M., Mathew, E., Dumont, M.E., 2014. Fluorescent approaches for understanding interactions of ligands with G protein coupled receptors. *Biochim. Biophys. Acta* 1838, 15–33.
- Srinivasan, S., Lubrano-berthelie, C., Govaerts, C., Picard, F., Santiago, P., Conklin, B.R., Vaisse, C., 2004. Constitutive activity of the melanocortin-4 receptor is maintained by its N-terminal domain and plays a role in energy homeostasis in humans. *J. Clin. Invest.* 114, 1158–64.
- Sriram, K., Insel, P.A., 2018. GPCRs as targets for approved drugs: How many targets and how many drugs? *Mol. Pharmacol.* [Epub ahead of print].
- Srivastava, A., Yano, J., Hirozane, Y., Kefala, G., Gruswitz, F., Snell, G., Lane, W., Ivetac, A., Aertgeerts, K., Nguyen, J., Jennings, A., Okada, K., 2014. High-resolution structure of the human GPR40 receptor bound to allosteric agonist TAK-875. *Nature* 513, 124–7.
- Stadlbauer, U., Arnold, M., Weber, E., Langhans, W., 2013. Possible mechanisms of circulating PYY-induced satiation in male rats. *Endocrinology* 154, 193–204.
- Stålberg, G., Ekselius, L., Lindström, L.H., Larhammar, D., Bodén, R., 2014. Neuropeptide Y, social function and long-term outcome in schizophrenia. *Schizophr. Res.* 156, 223–227.
- Stanley, B.G., Leibowitz, S.F., 1985. Neuropeptide Y injected in the paraventricular hypothalamus : A powerful stimulant of feeding behavior 82, 3940–3943.

- Stathopoulos, P., Papas, S., Tsikaris, V., 2006. C-terminal N-alkylated peptide amides resulting from the linker decomposition of the Rink amide resin. A new cleavage mixture prevents thier formation. *J. Pept. Sci.* 12, 227–232.
- Steegborn, C., 2014. Structure, mechanism, and regulation of soluble adenylyl cyclases - similarities and differences to transmembrane adenylyl cyclases. *Biochim. Biophys. Acta - Mol. Basis Dis.* 1842, 2535–2547.
- Steinfeld, T., Mammen, M., Smith, J.A.M., Wilson, R.D., Jasper, J.R., 2007. A Novel Multivalent Ligand That Bridges the Allosteric and Orthosteric Binding Sites of the M2 Muscarinic Receptor. *Mol. Pharmacol.* 72, 291–302.
- Stephens, T.W., Basinski, M., Bristow, P.K., Bue-Valleskey, J.M., Burgett, S.G., Craft, L., Hale, J., Hoffmann, J., Hsiung, H.M., Kriauciunas, A., 1995. The role of neuropeptide Y in the antiobesity action of the obese gene product. *Nature* 377, 530–2.
- Stephenson, R.P., 1956. A modification of receptor theory. *Br. J. Pharmacol. Chemother.* 11, 379–393.
- Stevens, R.C., Cherezov, V., Katritch, V., Abagyan, R., Kuhn, P., Rosen, H., Wüthrich, K., 2013. The GPCR Network: a large-scale collaboration to determine human GPCR structure and function. *Nat. Rev. Drug Discov.* 12, 25–34.
- Stoddart, L.A., Kilpatrick, L.E., Briddon, S.J., Hill, S.J., 2015. Probing the pharmacology of G protein-coupled receptors with fluorescent ligands. *Neuropharmacology.* 98, 48-57.
- Stott, L.A., Hall, D.A., Holliday, N.D., 2016. Unravelling intrinsic efficacy and ligand bias at G protein coupled receptors: A practical guide to assessing functional data. *Biochem. Pharmacol.* 101, 1–12.
- Stoveken, H.M., Larsen, S.D., Smrcka, A. V, Tall, G.G., 2018. Gedunin- and Khivorin-Derivatives are Small Molecule Partial Agonists for Adhesion G protein Coupled Receptors GPR56 / ADGRG1 and GPR114 / ADGRG5. *Mol. Pharmacol.*[Epub ahead of print].
- Strungs, E.G., Luttrell, L.M., 2014. Arrestin-dependent activation of ERK and Src family kinases. *Handb. Exp. Pharmacol.* 219, 225–257.
- Sun, Y., Wang, P., Zheng, H., Smith, R.G., 2004. Ghrelin stimulation of growth hormone release and appetite is mediated through the growth hormone secretagogue receptor. *Proc. Natl. Acad. Sci. U.S.A.* 101, 4679–84.
- Sykes, D.A., Moore, H., Stott, L., Holliday, N., Javitch, J.A., Robert Lane, J., Charlton, S.J., 2017. Extrapyramidal side effects of antipsychotics are linked to their association kinetics at dopamine D2receptors. *Nat. Commun.* 8, 1–11.
- Tabor, A., Weisenburger, S., Banerjee, A., Purkayastha, N., Kaindl, J.M.,

- Hübner, H., Wei, L., Grömer, T.W., Kornhuber, J., Tschammer, N., Birdsall, N.J.M., Mashanov, G.I., Sandoghdar, V., Gmeiner, P., 2016. Visualization and ligand-induced modulation of dopamine receptor dimerization at the single molecule level. *Sci. Rep.* 6, 1–16.
- Talsania, T., Anini, Y., Siu, S., Drucker, D.J., Brubaker, P.L., 2005. Peripheral exendin-4 and peptide YY3-36 synergistically reduce food intake through different mechanisms in mice. *Endocrinology* 146, 3748–3756.
- Tamura, Y., Hayashi, K., Omori, N., Nishiura, Y., Watanabe, K., Tanaka, N., Fujioka, M., Kouyama, N., Yukimasa, A., Tanaka, Y., Chiba, T., Tanioka, H., Nambu, H., Yukioka, H., Sato, H., Okuno, T., 2013. Identification of a novel benzimidazole derivative as a highly potent NPY Y5 receptor antagonist with an anti-obesity profile. *Bioorganic Med. Chem. Lett.* 23, 90–95.
- Tamura, Y., Omori, N., Kouyama, N., Nishiura, Y., Hayashi, K., Watanabe, K., Tanaka, Y., Chiba, T., Yukioka, H., Sato, H., Okuno, T., 2012. Identification of a novel and orally available benzimidazole derivative as an NPY Y5 receptor antagonist with in vivo efficacy. *Bioorganic Med. Chem. Lett.* 22, 6554–6558.
- Tanaka, T., Aoki, T., Nomura, W., Tamamura, H., 2017. Bivalent 14-mer peptide ligands of CXCR4 with polyproline linkers with anti-chemotactic activity against Jurkat cells. *J. Pept. Sci.* 23, 574–580.
- Tao, Y.-X., 2008. Constitutive activation of G protein-coupled receptors and diseases: insights into mechanisms of activation and therapeutics. *Pharmacology & therapeutics.* 120, 129-148.
- Tatemoto, K., 1982. Neuropeptide Y: complete amino acid sequence of the brain peptide. *Proc. Natl. Acad. Sci. U.S.A.* 79, 5485–9.
- Tatemoto, K., Carlquist, M., Mutt, V., 1982. Neuropeptide Y—a novel brain peptide with structural similarities to peptide YY and pancreatic polypeptide. *Nature* 296, 659–660.
- Tatemoto, K., Mutt, V., 1978. Chemical determination of polypeptide hormones. *Proc. Natl. Acad. Sci. U. S. A.* 75, 4115–9.
- Tatemoto, K., Mutt, V., 1980. Isolation of two novel candidate hormones using a chemical method for finding naturally occurring polypeptides. *Nature* 285, 417–418.
- Tehan, B.G., Bortolato, A., Blaney, F.E., Weir, M.P., Mason, J.S., 2014. Unifying Family A GPCR Theories of Activation. *Pharmacol. Ther.* 143, 51–60.
- Terrillon, S., Bouvier, M., 2004. Roles of G-protein-coupled receptor dimerization. *EMBO Rep.* 5, 30–4.
- Thal, D.M., Sun, B., Feng, D., Nawaratne, V., Leach, K., Felder, C.C., Bures, M.G., Evans, D.A., Weis, W.I., Bachhawat, P., Kobilka, T.S., Sexton, P.M., Kobilka, B.K., Christopoulos, A., 2016. Crystal structures of the M1 and

- M4 muscarinic acetylcholine receptors. *Nature* 531, 335–40.
- Thiele, T.E., Koh, M.T., Pedrazzini, T., 2002. Voluntary alcohol consumption is controlled via the neuropeptide Y Y1 receptor. *J. Neurosci.* 22, RC208.
- Thieme, V., Jolly, N., Madsen, A.N., Bellmann-Sickert, K., Schwartz, T.W., Holst, B., Cox, H.M., Beck-Sickinger, A.G., 2016. High molecular weight PEGylation of human pancreatic polypeptide at position 22 improves stability and reduces food intake in mice. *Br. J. Pharmacol.* 173, 3208–3221.
- Thomsen, W.J., Grottick, A.J., Menzaghi, F., Reyes-saldana, H., Espitia, S., Yuskin, D., Whelan, K., Martin, M., Morgan, M., Chen, W., Al-shamma, H., Smith, B., Chalmers, D., Behan, D., 2008. Lorcaserin, a Novel Selective Human 5-Hydroxytryptamine 2C Agonist : in Vitro and in Vivo Pharmacological Characterization. *J. Pharmacol. Exp. Ther.* 325, 577–587.
- Tilan, J., Kitlinska, J., 2016. Neuropeptide Y (NPY) in tumor growth and progression: Lessons learned from pediatric oncology. *Neuropeptides* 55, 55–66.
- Tong, Q., Ye, C.-P., Jones, J.E., Elmquist, J.K., Lowell, B.B., 2008. Synaptic release of GABA by AgRP neurons is required for normal regulation of energy balance. *Nat. Neurosci.* 11, 998–1000.
- Tough, I.R., Holliday, N.D., Cox, H.M., 2006. Y(4) receptors mediate the inhibitory responses of pancreatic polypeptide in human and mouse colon mucosa. *J. Pharmacol. Exp. Ther.* 319, 20–30.
- Trzaskowski, B., Latek, D., Yuan, S., Ghoshdastider, U., Debinski, a, Filipek, S., 2012. Action of molecular switches in GPCRs--theoretical and experimental studies. *Curr. Med. Chem.* 19, 1090–109.
- Tsvetanova, N.G., Irannejad, R., Von Zastrow, M., 2015. G protein-coupled receptor (GPCR) signaling via heterotrimeric G proteins from endosomes. *J. Biol. Chem.* 290, 6689–6696.
- Tuček, S., Michal, P., Vlachová, V., 2002. Modelling the consequences of receptor-G-protein promiscuity. *Trends Pharmacol. Sci.* 23, 171–176.
- Tyagi, P., Pechenov, S., Anand Subramony, J., 2018. Oral peptide delivery: Translational challenges due to physiological effects. *J. Control. Release* 287, 167-176.
- Uhlenbeck, O.C., Schrader, J.M., 2018. Evolutionary tuning impacts the design of bacterial tRNAs for the incorporation of unnatural amino acids by ribosomes. *Curr. Opin. Chem. Biol.* 46, 138–145.
- Unal, H., Jagannathan, R., Karnik, S.S., 2012. Mechanism of GPCR-Directed Autoantibodies in Diseases BT - Biochemical Roles of Eukaryotic Cell Surface Macromolecules. In: Sudhakaran, P.R., Surolia, A. (Eds.), . Springer New York, New York, NY, pp. 187–199.

- Urizar, E., Montanelli, L., Loy, T., Bonomi, M., Swillens, S., Gales, C., Bouvier, M., Smits, G., Vassart, G., Costagliola, S., 2005. Glycoprotein hormone receptors: Link between receptor homodimerization and negative cooperativity. *EMBO J.* 24, 1954–1964.
- Vagner, J., Xu, L., Handl, H.L., Josan, J.S., Morse, D.L., Mash, E.A., Gillies, R.J., Hruby, V.J., 2008. Heterobivalent ligands crosslink multiple cell-surface receptors: The human melanocortin-4 and δ -opioid receptors. *Angew. Chemie - Int. Ed.* 47, 1685–1688.
- Vaino, A.R., Janda, K.D., 2000. Solid-Phase Organic Synthesis: A Critical Understanding of the Resin [†]. *J. Comb. Chem.* 2, 579–596.
- Valeur, E., Bradley, M., 2009. Amide bond formation: beyond the myth of coupling reagents. *Chem Soc Rev* 38, 606–631.
- Van Bloemendaal, L., IJzerman, R.G., Ten Kulve, J.S., Barkhof, F., Konrad, R.J., Drent, M.L., Veltman, D.J., Diamant, M., 2014. GLP-1 receptor activation modulates appetite- and reward-related brain areas in humans. *Diabetes* 63, 4186–4196.
- van den Pol, A.N., Yao, Y., Fu, L., Foo, K., Huang, H., Coppari, R., Lowell, B.B., Broberger, C., 2009. Neuromedin B and gastrin-releasing peptide excite arcuate nucleus neuropeptide Y neurons in a novel transgenic mouse expressing strong Renilla green fluorescent protein in NPY neurons. *J. Neurosci.* 29, 4622–39.
- Vauquelin, G., Charlton, S.J., 2010. Long-lasting target binding and rebinding as mechanisms to prolong in vivo drug action. *Br. J. Pharmacol.* 161, 488–508.
- Venkatakrishnan, A.J., Deupi, X., Lebon, G., Tate, C.G., Schertler, G.F., Babu, M.M., 2013. Molecular signatures of G-protein-coupled receptors. *Nature* 494, 185.
- Veyrat-Durebex, C., Quirion, R., Ferland, G., Dumont, Y., Gaudreau, P., 2013. Aging and long-term caloric restriction regulate neuropeptide Y receptor subtype densities in the rat brain. *Neuropeptides* 47, 163–169.
- Voisin, T., Goumain, M., Lorinet, a M., Maoret, J.J., Laburthe, M., 2000. Functional and molecular properties of the human recombinant Y4 receptor: resistance to agonist-promoted desensitization. *J. Pharmacol. Exp. Ther.* 292, 638–646.
- Vu, T.K.H., Hung, D.T., Wheaton, V.I., Coughlin, S.R., 1991. Molecular cloning of a functional thrombin receptor reveals a novel proteolytic mechanism of receptor activation. *Cell* 64, 1057–1068.
- Wacker, D., Wang, S., McCorvy, J.D., Betz, R.M., Venkatakrishnan, A.J., Levit, A., Lansu, K., Schools, Z.L., Che, T., Nichols, D.E., Shoichet, B.K., Dror, R.O., Roth, B.L., 2017. Crystal Structure of an LSD-Bound Human Serotonin Receptor. *Cell* 168, 377–389.

- Wahlestedt, C., Hakanson, R., 1990. Norepinephrine vasoconstrictor and neuropeptide Y : cooperation in vivo and in vitro. *The American journal of physiology.* 258, 736–742.
- Walker, P., Munoz, M., Martinez, R., Peitsch, M.C., 1994. Acidic residues in extracellular loops of the human Y1 neuropeptide Y receptor are essential for ligand binding. *J. Biol. Chem.* 269, 2863–2869.
- Walther, C., Mörl, K., Beck-Sickinger, A.G., 2011. Neuropeptide Y receptors: ligand binding and trafficking suggest novel approaches in drug development. *J. Pept. Sci.* 17, 233–46.
- Walther, C., Nagel, S., Gimenez, L.E., Mörl, K., Gurevich, V. V., Beck-Sickinger, A.G., 2010. Ligand-induced internalization and recycling of the human neuropeptide Y2 receptor is regulated by its carboxyl-terminal tail. *J. Biol. Chem.* 285, 41578–41590.
- Wang, S.J., 2005. Activation of neuropeptide Y Y1 receptors inhibits glutamate release through reduction of voltage-dependent Ca²⁺-entry in the rat cerebral cortex nerve terminals: Suppression of this inhibitory effect by the protein kinase C-dependent facilitatory pathway. *Neuroscience* 134, 987–1000.
- Wanka, L., Babilon, S., Kaiser, A., Mörl, K., Beck-Sickinger, A.G., 2018. Different mode of arrestin-3 binding at the human Y1 and Y2 receptor. *Cell. Signal.* 50, 58–71.
- Ward, R.J., Pediani, J.D., Milligan, G., 2011. Heteromultimerization of cannabinoid CB 1 receptor and orexin OX 1 receptor generates a unique complex in which both protomers are regulated by orexin A. *J. Biol. Chem.* 286, 37414–37428.
- Warne, T., Moukhametzianov, R., Baker, J.G., Nehmé, R., Patricia, C., Leslie, A.G.W., Schertler, G.F.X., Tate, C.G., 2011. The structural basis for agonist and partial agonist action on a β 1 -adrenergic receptor. *Nature* 469, 241–244.
- Watts, A.O., Van Lipzig, M.M.H., Jaeger, W.C., Seeber, R.M., Van Zwam, M., Vinet, J., Van Der Lee, M.M.C., Siderius, M., Zaman, G.J.R., Boddeke, H.W.G.M., Smit, M.J., Pflieger, K.D.G., Leurs, R., Vischer, H.F., 2013. Identification and profiling of CXCR3-CXCR4 chemokine receptor heteromer complexes. *Br. J. Pharmacol.* 168, 1662–1674.
- Widdowson, P.S., 1993. Quantitative receptor autoradiography demonstrates a differential distribution of neuropeptide-Y Y1 and Y2 receptor subtypes in human and rat brain. *Brain Res.* 631, 27–38.
- Widengren, J., Chmyrov, A., Eggeling, C., Löffelholz, P., Ke, Seidel, C.A.M., 2007. Strategies to improve photostabilities in ultrasensitive fluorescence spectroscopy. *J. Phys. Chem.* 111, 429–440.
- Wieland, H.A., Engel, W., Eberlein, W., Rudolf, K., Doods, H.N., 1998. Subtype

- selectivity of the novel nonpeptide neuropeptide Y Y1 receptor antagonist BIBO 3304 and its effect on feeding in rodents. *Br. J. Pharmacol.* 125, 549–55.
- Williams, K.W., Margatho, L.O., Lee, C.E., Choi, M., Lee, S., Scott, M.M., Elias, C.F., Elmquist, J.K., 2010. Segregation of Acute Leptin and Insulin Effects in Distinct Populations of Arcuate Proopiomelanocortin Neurons. *J. Neurosci.* 30, 2472–2479.
- Wohland, T., Friedrich, K., Hovius, R., Vogel, H., 1999. Study of ligand-receptor interactions by fluorescence correlation spectroscopy with different fluorophores: Evidence that the homopentameric 5-hydroxytryptamine type 3(As) receptor binds only one ligand. *Biochemistry* 38, 8671–8681.
- Wolak, M.L., DeJoseph, M.R., Cator, A.D., Mokashi, A.S., Brownfield, M.S., Urban, J.H., 2003. Comparative distribution of neuropeptide Y Y1 and Y5 receptors in the rat brain by using immunohistochemistry. *J. Comp. Neurol.* 464, 285–311.
- Wood, J., Verma, D., Lach, G., Bonaventure, P., Herzog, H., Sperk, G., Tasan, R.O., 2016. Structure and function of the amygdaloid NPY system: NPY Y2 receptors regulate excitatory and inhibitory synaptic transmission in the centromedial amygdala. *Brain Struct. Funct.* 221, 3373–3391.
- Wood, S.P., Pitts, J.E., Blundell, T.L., Tickle, I.J., Jenkins, J.A., 1977. Purification, crystallisation and preliminary X-ray studies on avian pancreatic polypeptide. *Eur. J. Biochem.* 78, 119–26.
- Wootten, D., Christopoulos, A., Marti-Solano, M., Babu, M.M., Sexton, P.M., 2018. Mechanisms of signalling and biased agonism in G protein-coupled receptors. *Nat. Rev. Mol. Cell Biol.* 19, 638–653.
- Wraith, A., To, A., Chardon, P., Harbitz, I., Chowdhary, B.P., Andersson, L., Lundin, L., Larhammar, D., 2000. Evolution of the Neuropeptide Y Receptor Family : Gene and Chromosome Duplications Deduced from the Cloning and Mapping of the Five Receptor Subtype Genes in Pig. *Genome Research.* 3, 302–310.
- Wu, G., 2009. Amino acids: Metabolism, functions, and nutrition. *Amino Acids* 37, 1–17.
- Wu, H., Wacker, D., Mileni, M., Katritch, V., Han, G.W., Vardy, E., Liu, W., Thompson, A.A., Huang, X.-P., Carroll, F.I., Mascarella, S.W., Westkaemper, R.B., Mosier, P.D., Roth, B.L., Cherezov, V., Stevens, R.C., 2012. Structure of the human κ -opioid receptor in complex with JDTic. *Nature* 485, 327.
- Xu, B., Vasile, S., Ostergaard, S., Paulsson, J.F., Pruner, J., Aqvist, J., Wulff, B.S., Gutierrez-de-Teran, H., Larhammar, D., 2018. Binding mode of the peptide YY carboxyterminus to the human Y2 receptor. *Mol. Pharmacol.* [Epub ahead of print]

- Yan, H.A.I., Yang, J.I.E., Marasco, J., Yamaguchi, K., Brenner, S., Collins, F., Karbon, W., 1996. Cloning and functional expression of cDNAs encoding human and rat pancreatic polypeptide receptors. *Proc. Natl. Acad. Sci. USA.* 93, 4661–4665.
- Yang, Y., Atasoy, D., Su, H.H., Sternson, S.M., 2011. Hunger states switch a flip-flop memory circuit via a synaptic AMPK-dependent positive feedback loop. *Cell* 146, 992–1003.
- Yang, Y., Li, Q., He, Q., Han, J., Su, L., Wan, Y., 2018. Heteromerization of μ - opioid receptor and cholecystokinin B receptor through the third transmembrane domain of the μ - opioid receptor contributes to the anti- opioid effects of cholecystokinin octapeptide. *Exp Mol Med.* 50, 64-80
- Yang, Z., Han, S., Keller, M., Kaiser, A., Bender, B.J., Bosse, M., Burkert, K., Kögler, L.M., Wifling, D., Bernhardt, G., Plank, N., Littmann, T., Schmidt, P., Yi, C., Li, B., Ye, S., Zhang, R., Xu, B., Larhammar, D., Stevens, R.C., Huster, D., Meiler, J., Zhao, Q., Beck-Sickinger, A.G., Buschauer, A., Wu, B., 2018. Structural basis of ligand binding modes at the neuropeptide YY1 receptor. *Nature* 556, 520–524.
- Yaswen, L., Diehl, N., Brennan, M.B., Hochgeschwender, U., 1999. Obesity in the mouse model of pro-opiomelanocortin deficiency responds to peripheral melanocortin. *Nat. Med.* 5, 1066–1070.
- Yen, M., Ewald, M.B., 2012. Toxicity of weight loss agents. *J. Med. Toxicol.* 8, 145–52.
- Yin, W., Zhou, X.E., Yang, D., De Waal, P.W., Wang, M., Dai, A., Cai, X., Huang, C.Y., Liu, P., Wang, X., Yin, Y., Liu, B., Zhou, Y., Wang, J., Liu, H., Caffrey, M., Melcher, K., Xu, Y., Wang, M.W., Xu, H.E., Jiang, Y., 2018. Crystal structure of the human 5-HT_{1B}serotonin receptor bound to an inverse agonist. *Cell Discov.* 4, 12-25.
- Yulyaningsih, E., Zhang, L., Herzog, H., Sainsbury, A., 2011. NPY receptors as potential targets for anti-obesity drug development. *Br. J. Pharmacol.* 163, 1170–1202.
- Zacharko-Siembida, A., Valverde Piedra, J.L., Szymańczyk, S., Arciszewski, M.B., 2013. Immunolocalization of NOS, VIP, galanin and SP in the small intestine of suckling pigs treated with red kidney bean (*Phaseolus vulgaris*) lectin. *Acta Histochem.* 115, 219–225.
- Zemanová, L., Schenk, A., Hunt, N., Nienhaus, G.U., Heilker, R., 2004. Endothelin receptor in virus-like particles: Ligand binding observed by fluorescence fluctuation spectroscopy. *Biochemistry* 43, 9021–9028.
- Zeng, C.-M., Chen, Z., Fu, L., 2018. Frizzled Receptors as Potential Therapeutic Targets in Human Cancers. *Int. J. Mol. Sci.* 19, 1543.
- Zhan, C., Zhou, J., Feng, Q., Zhang, J. -e., Lin, S., Bao, J., Wu, P., Luo, M., 2013.

Acute and Long-Term Suppression of Feeding Behavior by POMC Neurons in the Brainstem and Hypothalamus, Respectively. *J. Neurosci.* 33, 3624–3632.

Zhang, C., Pan, J., Lin, K.-S., Dude, I., Lau, J., Zeisler, J., Merkens, H., Jenni, S., Guérin, B., Bénard, F., 2016. Targeting the Neuropeptide Y1 Receptor for Cancer Imaging by Positron Emission Tomography Using Novel Truncated Peptides. *Mol. Pharm.* 13, 3657–3664.

Zhang, X., Chytil, P., Etrych, T., Liu, W., Rodrigues, L., Winter, G., Filippov, S.K., Papadakis, C.M., 2018. Binding of HSA to Macromolecular pHMA Based Nanoparticles for Drug Delivery: An Investigation Using Fluorescence Methods. *Langmuir*. [Epub ahead of print]

Zhang, X., Shi, T., Holmberg, K., Landry, M., Huang, W., Xiao, H., Ju, G., Hökfelt, T., 1997. Expression and regulation of the neuropeptide Y Y2 receptor in sensory and autonomic ganglia. *Proc. Natl. Acad. Sci. U. S. A.* 94, 729–34.

Zhang, Y., Sun, B., Feng, D., Hu, H., Chu, M., Qui, Q., Tarrasch, J.T., Li, S., Sun Kobilka, T., Kobilka, B.K., Skiniotis, G., 2017. Cryo-EM structure of the activated GLP-1 receptor in complex with G protein. *Nature* 546, 248–253.

Zhao, F., Shen, T., Kaya, N., Lu, S., Cao, Y., Herness, S., 2005. Expression , physiological action , and coexpression patterns of neuropeptide Y in rat taste-bud cells. *Proc Natl Acad Sci U.S.A.* 102, 11100-11105.

Zheng, H., Townsend, R.L., Shin, A.C., Patterson, L.M., Phifer, C.B., Berthoud, H.R., 2010. High-fat intake induced by mu-opioid activation of the nucleus accumbens is inhibited by Y1R-blockade and MC3/4R-stimulation. *Brain Res.* 1350, 131–138.

Zhu, P., Sun, W., Zhang, C., Song, Z., Lin, S., 2016. The role of neuropeptide Y in the pathophysiology of atherosclerotic cardiovascular disease. *Int. J. Cardiol.* 220, 235–241.

Zoenen, M., Urizar, E., Swillens, S., Vassart, G., Costagliola, S., 2012. Evidence for activity-regulated hormone-binding cooperativity across glycoprotein hormone receptor homomers. *Nat. Commun.* 3, 1007-1016.

Zwanziger, D., Böhme, I., Lindner, D., Beck-Sickinger, A.G., 2009. First selective agonist of the neuropeptide Y1-receptor with reduced size. *J. Pept. Sci.* 15, 856–66.